Assessment of Wear and Corrosion at the Taper Junction of Modular Total Hip Replacements

A dissertation submitted to the University College London in fulfilment of the requirements for the degree of

Doctor of Philosophy

Anna Panagiotidou

Declarations

I hereby declare that the work in this thesis is my own, except in places where I have given due and clear recognition to collaboration made by others.

Anna Panagiotidou

Abstract

Assessment of Wear and Corrosion at the Taper Junction of Modular Total Hip Replacements
Doctor of Philosophy in Musculoskeletal Sciences
A. Panagiotidou, UCL, 2017

The concept of modularity in primary and revision total hip arthroplasty is well established. Whilst modern modular femoral components offer surgeons the flexibility to tailor the size, offset and biomaterials of the femoral head, neck and stem to the anatomy of the patients hip, they do present an additional interface and therefore a potential source of wear and corrosion. There is increasing global awareness of adverse reactions to metal debris and elevated serum metal ion concentrations following the use of third-generation modular metal-on-metal total hip arthroplasties. In some instances the high incidence of these complications can be attributed to corrosion at the head-neck interface.

In 2011 published clinical data highlighted the early revision rate of third-generation metal-on-metal modular hip replacements and consequently, in February 2012 the British Orthopaedic Association recommended that large head metal-on-metal hip replacements no longer be implanted. Although severe corrosion of the taper is identified most commonly in association with larger diameter femoral heads, there is emerging evidence of varying levels of corrosion observed in retrieved components with smaller diameter femoral heads and other material combinations such as metal on polyethylene and ceramic on polyethylene.

In my thesis a systematic retrieval analysis has been completed in order to understand the contribution of material wear at the modular junction compared to the wear at the bearing surface. Furthermore in-vitro dynamic experimental approaches were adopted utilising in-situ electrochemistry in order to investigate the factors that contribute to enhanced wear and corrosion at the head-neck junction and ultimately lead to the early failure of modular hip replacements.

Retrieval analysis of failed large head metal-on-metal prostheses (>36mm head diameter) indicated that about 1/3rd of total wear can be attributed to material loss at the taper junction. Experimental investigations indicated that neck taper rough surface finish and reduced engagement length contribute to enhanced fretting corrosion at the modular junction, a finding that points to concern associated with their current use in orthopaedics. Increased frictional torque and bending moment both of which can be associated with large diameter heads and high offsets may also increase the susceptibility of mechanically assisted crevice corrosion at the taper junction, an effect which may be diminished with the use of ceramic heads. Additionally it would appear that regardless of engagement length, surface roughness or material combination an assembly force of greater than 4kN reduces the amount of corrosion.

From the findings presented in this thesis all tapers tested exhibited evidence of mechanically assisted crevice corrosion. Although this may be unavoidable it may be reduced if certain parameters associated with implant design are taken into consideration during implant selection.

Acknowledgements

I must first thank my primary supervisor, Professor Gordon Blunn, for his continued support, encouragement and enthusiasm throughout my studies. His advice and guidance have been of vital importance to me in completing this work. I would also like to thank my secondary supervisor, Professor Fares Haddad who as my clinical director has allowed me time away from my clinical commitments to concentrate on my experiments; without which I would have not been able to complete my PhD.

I am deeply indebted to Orthopaedic Research UK who funded this work and I am grateful for their faith in my ability to complete this project.

I have relied heavily on Dr Jay Meswania for his continued support and I would also like to thank all the staff at John Scales Centre for Biomedical Engineering, particularly Mr Mark Harrison for all of his assistance.

A big thanks is owed to sister Valerie Johnson trauma co-ordinator at North Middlesex Hospital and Mr Mike Kurer for all of their support and assistance throughout the last year in completing my write up.

Finally I would like to thank my family. Without my parents' encouragement I would not have started this project and without their continued support I could not have finished it. In particular I would like to thank Ben whose patience and encouragement has been invaluable.

Contents

Figures

Tables

Abbreviations

ALTR	Adverse Local Tissue Reactions
ALVAL	Aseptic Lymphocytic Vasculitis Associated Lesions
AP	Anterior-Posterior
ARMD	Adverse Reaction to Metallic Debris
CE	Counter Electrode
Cl	Chloride
Cl^-	Chloride Ion
Co	Cobalt
CoCr	Cobalt Chromium
CoCrMo	Cobalt Chromium Molybdenum
CoNiCrMo	Cobalt Nickel Chromium Molybdenum
Cr	Chromium
CRM	Ceramic
Cr_2O_3	Chromium Oxide
CT	Computer Tomography
D	Displacement
DLC	Diamond Like Carbon

e^-	Electron
E_b	Critical Breakdown Potential
E_{corr}	Corrosion Potential
E_{pp}	Passivation Potential
E_r	Repassivation Potential
EDS	Energy Dispersive X-ray Spectroscopy
F_f	Friction
FEA	Finite Element Analysis
F_n	Normal Force
GPa	Gigapascals
H_2	Hydrogen
H^+	Hydrogen Ion
i_{cc}	Critical Current Potential
i_{corr}	Corrosion Current Density
ICPMS	Inductively Coupled Plasma Mass Spectrometry
i_p	Passive Current Density
LFA	Low Friction Arthroplasty
LH	Large Head
LH-MoM-THR	Large Head Metal-on-Metal Total Hip Replacement
M	Metal

MACC	Mechanically Assisted Crevice Corrosion
MARS	Metal Artifact Reduction Sequence
ML	Mediolateral
mL	Milliliters
Mn	Manganese
MoM	Metal-on-Metal
MoP	Metal-on-Polyethylene
MPa	Megapascals
MRI	Magnetic Resonance Imaging
NaCl	Sodium Chloride
O_2	Oxygen
OCC	Overall Current Change
OCP	Open Circuit Potential
OMFC	Overall Mean Fretting Current
OMC	Overall Mean Current
PBS	Phosphate Buffered Saline Solution
PMMA	Poly Methyl Methacrylate
PO_4	Phosphate
PO_4^{3-}	Phosphate
RE	Reference Electrode

SEM	Scanning Electron Microscopy
SCE	Saturated Calomel Electrode
SOP	Standard Operating Practise
SPSS	Statistical Package for the Social Sciences
SS	Stainless Steel
Ti	Titanium
TiO_2	Titanium Oxide
Ti-6Al-7Nb	Titanium Niobium Alloy
Ti-6Al-4V	Titanium Vanadium Alloy
THA	Total Hip Arthroplasty
THR	Total Hip Repalacement
UHMWPE	Ultra High Molecular Weight Polyethylene
WE	Working Electrode

Chapter 1 Introduction

1.1. Motivation for Research

Primary Total Hip replacement (THR) is recognized as one of the most successful surgical interventions of the twentieth-century. Since the early 1960s it has played an important role in alleviating pain and restoring mobility, primarily in patients with end-stage osteoarthritis of the hip (93%) but also in patients with fractures of the femoral neck (2%), avascular necrosis of the femoral head (2%), developmental dysplasia (2%) and inflammatory conditions (1%) (Bloomfield et al., 2014, Pivec et al., 2012). Over the years, THR has enjoyed increasing success and popularity; in 2012/2013, the National Joint Registry for England, Wales and Northern Ireland (NJR) recorded a total of 94,044 THRs, a 7.5% increase compared to the previous year (National Joint Registry, 2013), while in the United States it is estimated that THR will grow by 174%, from 208,600 in 2005 to 572,000 by the year 2030 (Kurtz et al., 2007).

Despite its popularity, the long term survivorship for some of the most widely used THR implants remains in the range of 85 – 90% at 10 years and 75 – 80% at 25 years, falling to 60-70% in patients under the age of 40 years (Berry et al., 2002, Sochart and Porter, 1997, Pivec et al., 2012).

More specifically, the 8th annual report of the National Joint Registry of England and Wales reported a 5-year revision rate of 6.96% for third generation metal on metal (MoM) total hip replacements. This compares to less than 3% for all other conventional hip replacements (Metal on Polyethylene (MoP), Ceramic on Ceramic (CoC) and Ceramic on Polyethylene (CoP)), and to 4.56% for MoM hip resurfacing (Smith et al., 2012b). A growing body of evidence have also shown that large head (>36 mm) MoM

total hip replacements (LH-MoM-THR) have higher revision rates than equivalently sized MoM resurfacings with a similar bearing surface design (Smith et al., 2012b, Langton et al., 2011, Australian Orthopaedic Association National Joint Replacement Registry, 2012). Consequently, in February 2012 the British Orthopaedic Association recommended that LH-MoM-THR no longer be implanted (Skinner et al., 2012).

An important difference between MoM resurfacing and LH-MoM-THR is the modular head-neck taper junction which has been shown to be susceptible to mechanically assisted crevice (MACC) and fretting corrosion, leading to the production of wear debris and metal ion release (Gilbert et al., 1994, Goldberg et al., 1997a). These by-products of MACC can migrate locally and systemically resulting in elevated serum metal ion levels thought to initiate a cascade of events leading to the presence of adverse local tissue reactions (ALTR) (Meyer et al., 2012, Cooper et al., 2012, Fricka et al., 2012). Evidence of corrosion around the head-neck interface has been identified in retrieval studies, indicating that the modular junction is a significant source of metal ion release (McCarthy et al., 1997, Collier et al., 1992a, Fricker and Shivanathan, 1990, Gilbert et al., 1993, Lieberman et al., 1994, Urban et al., 1997), and the effects of metallic wear debris have been well documented, with ALTR and systemic toxicity leading in some cases to pseudotumour formation, necrosis, osteolysis and ultimately implant failure (Cooper et al., 2012, Doorn et al., 1996, Maloney and Smith, 1996, Campbell et al., 2010, Jacobs et al., 1995, Goldberg et al., 2002).

Corrosion of the taper at the head-neck interface was first identified in THA retrievals by *Collier* (Collier et al., 1991) and was attributed to galvanically accelerated crevice corrosion, which was previously undetected by laboratory testing. At that time, its biological impact was poorly understood and seemed to be largely subclinical. This was until the introduction of third generation MoM THAs (LH-MoM-THR) whose unexpected high failures rates highlighted taper corrosion as a major focus of concern.

However, although taper corrosion was initially linked to modular MoM components or those with larger diameter femoral heads, the issue does not seem to be solely restricted to these components, as there is increasing evidence of taper corrosion with ALTR and elevated serum metal ions in modular MoP and modular CoP THAs (Rasquinha et al., 2006, Goldberg et al., 2002, Cooper et al., 2012, Kurtz et al., 2013, Whitehouse et al., 2015).

The concept of modularity in primary and revision total hip arthroplasties (THAs) is well established. Modern modular femoral components offer surgeons the flexibility to tailor the size, offset and biomaterials of the femoral head, neck and stem to the anatomy of the patient and the biomechanics of the hip (McCarthy et al., 1997), whilst reducing the size of the inventory required at operation. However, this provides the femoral component with an additional interface and a potential source of wear and corrosion. This has led to renewed interest and re-evaluation of modular junctions.

As younger, more active, patients are diagnosed with hip osteoarthritis, the limited lifespan of artificial joints is becoming more of a concern for the orthopaedic community. This changing demographic of patients undertaking THR surgery necessitates the search for improved prosthesis with the ultimate aim of achieving lifetime longevity (Kurtz et al., 2005). Therefore, improvement in wear characteristics is a major focus of orthopaedic research.

1.2. Hypothesis, Aims and Objectives

Although wear and corrosion at the head-neck modular junction has been identified in retrieval studies to be the source of wear debris and metal ion release, at the time of project conception there was very little clinical and academic evidence regarding the factors influencing the rates and mechanisms of corrosion at this interface. A number of factors have been proposed to affect the amount of corrosion and mechanical wear at

this junction. *Bolland* (Bolland et al., 2011) attributed this wear and corrosion to the high frictional torque associated with the large diameter heads, whereas *Langton* (Langton et al., 2012) attributed it to the high head offset (increased bending moment) associated with large heads.

Implant modularity has become one of the central design features of orthopaedic implants, however these tapers vary from company to company in terms of surface roughness, materials used, cone diameter, cone angles, tolerances and the surface area of the articulation. All of these factors associated with modularity have an important role to play in the performance of the prosthesis.

The aim of this thesis therefore, is to address implant and surgical technique related factors contributing to corrosion and wear at the modular taper junction of THRs so as to reduce the overall failure rate. As such, this thesis has three broad aims:

- **To investigate the material loss from the taper junction and compare it to that from the bearing surface of retrieved modular THRs.**
- **To delineate the factors which are critical in determining corrosion and wear at the taper junction.**
- **To determine the ideal parameters in order to create the "ultimate" taper junction.**

The hypothesis to be investigated is that the tapers of large metal heads contribute significantly to metal ion release and are susceptible to corrosion and wear which is associated with: 1) High Torque, 2) Increased Offset, 3) Surface Roughness and Area of the neck taper, 4) Taper Assembly, 5) Taper Material Composition.

A systematic investigation was therefore undertaken in order to understand the importance of MACC at the head-neck interface. Electrochemical analysis, surface

analysis and scanning electron microscopy (SEM) techniques were employed to investigate and quantify the influence of MACC on the mechanism and production of debris under in-vitro conditions.

1.3. Thesis Structure

Chapter 2 presents a comprehensive clinical and academic review relating to the evolution of THA design, the use of different biomaterials and the reasons that these implants fail prematurely.

Chapter 3 presents the general experimental methods and techniques utilised in order to investigate the degradation at the head-neck modular junction in both in-vitro experiments and retrieval analysis.

Chapter 4 investigates the material loss at the taper junction of retrieved LH-MoM-HRs in order to ascertain whether the volume of material loss from the taper is greater than that lost from the bearing surfaces and whether the volume of material loss from the junction correlates with blood metal ion levels.

Chapter 5 investigates the effect of high bending moment on fretting corrosion and wear at the modular head-neck taper junction of MoM THRs and compares the findings to the ones from retrieved LH-MoM-THR prostheses.

Chapter 6 investigates the effect of reduced contact area and increased surface roughness of the neck taper on the corrosion and wear at the modular taper junction of THRs.

Chapter 7 investigates the effect of increased frictional torque and bending moment on the fretting corrosion behaviour at the head-neck taper junction of MoM THAs of different material combinations.

Chapter 8 investigates how the assembly force affects the interface deformation and the fretting corrosion at the modular taper junction.

Chapter 9 presents a final discussion; highlighting the main findings, along with a comparison of recent clinical, retrieval and experimental studies. It also includes future work and overall conclusions.

Chapter 2 Literature Review: The Evolution of Joint Arthroplasty, Biomaterials, Tribology and Bio-Tribocorrosion

2.1. Introduction

Although corrosion and tribocorrosion of biomaterials has been discussed since the 1970s, information relating to the exact mechanism of localised corrosion of biomedical alloys and the potential implications still remains scarce. In light of this, the following literature review covers a large number of topics that are concerned with the science of joint replacement, metallurgy, wear, corrosion and tribocorrosion of alloys and articulations typically used for orthopaedic devices, focusing mainly at the head-neck modular interface.

2.2. The Hip Joint

2.2.1. Anatomy of the Hip

The hip joint is a "ball-and-socket" synovial joint comprised of the hemispherical head of the femur (ball) and the acetabulum (socket), a cup-shaped cavity located on the outside of the pelvis into which the ball-shaped head of femur fits in (Figure 2-1). The articular surface of the acetabulum is horseshoe shaped and is deficient inferiorly at the acetabular notch. The cavity itself is deepened by the presence of a fibrocartilaginous rim called the acetabular labrum. Of the inner surface of the acetabulum, only the most peripheral portion, i.e. the lunate-surface, is used in the articulation, while the central portion, the acetabular pit, accommodates the round ligament (ligament teres) extended between the acetabulum and the femoral head. The femoral head is round and in the

centre of the head there is a small depression called the fovea capitis femoris to which the round ligament is attached. The femoral head is supported by the anatomical neck which is situated at an angle of about 130° to the axis of the femoral shaft in the coronal plane. At the base of the neck there are two trochanters (the greater trochanter and the lesser trochanter), which form the points of attachment of periarticular muscles.

Hyaline cartilage lines both the acetabulum and the head of the femur with the exception of the acetabular fossa and the fovea capitis femoris, providing a smooth surface for the moving bones to glide past each other. Hyaline cartilage also acts as a flexible shock absorber to prevent collision of the bones during movement.

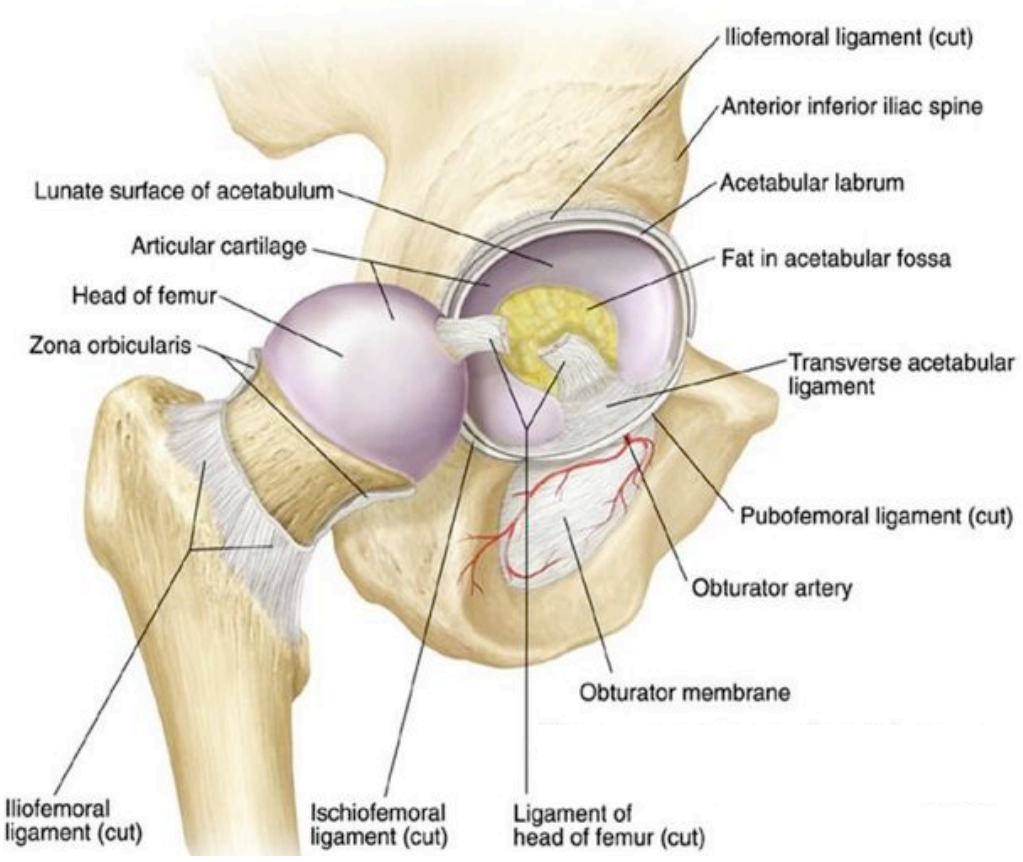

Figure 2-1: Anatomy of the normal hip joint.*

* Copyright © 2009 Wolters Kluwer Health | Lippincott Williams & Wilkins – Hip Joint

The hip joint is enclosed by a synovial membrane, which proximally inserts onto the edge of the acetabulum and onto the acetabular labrum and distally onto the intertrochanteric line (in front) and between the third medium and distal third of the femoral neck (behind). Three peripheral thickenings of the capsule form three important ligaments, which include the iliofemoral, the ischiofemoral and the pubofemoral ligaments. These contribute to the retention of the femur within the capsule.

2.2.2. Diseases of the Hip Joint

Arthritis comprises a group of conditions in which there is inflammation of the joints resulting in pain, stiffness, disability and deformity. In addition to the physical and psychological sequelae, arthritis is also associated with a large societal and economic burden(Chen et al., 2012, Gupta et al., 2005). It manifests itself as a degeneration of the tissues of the hip joint, including hyaline cartilage, fibrocartilage, bone, and synovium that ultimately lead to joint destruction. Hip arthritis can result from several different patterns of joint failure. The two main forms of arthritis include osteoarthritis and rheumatoid arthritis.

Osteoarthritis is a degenerative condition due mainly to accumulated wear of the joint. It is characterized by localised loss of articular cartilage, remodelling of adjacent bone with new bone formation (osteophyte) at the joint margins, subchondral bone sclerosis and thickening of the capsule. The Arthritis Research Council (UK) estimated in 2014 that at least 2.46 million people in England suffer from osteoarthritis of the hip (Arthritis Research UK, 2014).

Rheumatoid arthritis is an autoimmune inflammatory condition with widespread synovial joint involvement. It is the most common form of chronic polyarthritis, and although it is a systemic disease, it predominantly affects peripheral joints. Persistent

synovitis stretches supporting ligaments and thus reduces joint stability. Cartilage eventually degrades, leading to progressive destruction of the joint and ultimately in long-term morbidity and increased mortality.

Other conditions that may adversely affect the hip joint include other inflammatory arthropathies (psoriatic arthritis, spondyloarthropathies), developmental dysplasias (Legg-Calve-Perthes disease, slipped capital femoral epiphysis), trauma and avascular necrosis.

2.2.3. Operative and Non-Operative Management of Arthritis

Weight loss, exercise, pain relieving medication and corticosteroid injections are a number of non-operative management strategies designed with a view to optimizing joint physiology and joint integrity. To a certain extent they can be effective in relieving pain, restoring function and enhancing a patients' ability to live independently, even in the face of on-going joint destruction processes. However, these non-operative treatments do not address the underlying disease but rather treat the inflammation and side effects of the arthritis. Their purpose is to limit the patient's symptoms, not cure the underlying arthritis. Therefore, when non-operative measures fail, total hip replacement is the best choice.

In a total hip replacement (also called total hip arthroplasty), the damaged bone and cartilage is removed and replaced with prosthetic components. The ideal THR is one that re-creates a biomechanically normal hip joint, restoring, as best as possible, the individual's normal anatomy. It should allow full, pain-free activity and last the patient's life span without requiring any further interventions. In order to be able to achieve this, a number of criteria should be met. Firstly, reliable fixation and stability need to be

secured, along with appropriate stress transfer. Secondly, leg length and offset need to be restored and the normal orientation of the femoral stem and cup need to be recreated. Ultimately, improved abductor muscle strength, a greater range of movement and a reduced risk of postoperative complications can be accomplished (Bargar, 1989, Kowalczyk, 2001).

2.3. Total Hip Replacement

2.3.1. Evolution of the Total Hip Replacement

2.3.1.1. Early THR Designs

The current success of hip arthroplasty is the product of a century of evolution in science and surgical technique. The earliest recorded attempts at hip replacement occurred in Germany in 1891 when professor Themistocles Glück used ivory to replace femoral heads of patients whose hip joints had been destroyed by tuberculosis. In the late 19th / early 20th century, surgeons experimented with '*interposition arthroplasty*', which involved placing various tissues such as fascia lata, skin and pig bladders between the articulating surfaces of the arthritic hip. In 1912 Sir Robert Jones used a strip of gold foil as an interpositional layer to cover reconstructed femoral heads. In 1925 Dr Martin Smith-Petersen created the first '*mould arthroplasty*' out of glass, which consisted of a hollow hemisphere that could fit over the femoral head and provide a new smooth surface for movement.

The evolution of the hip replacement continued with the vitallium mould arthroplasty (1938) (Figure 2-2), the acetabular cup and femoral head resurfacing by Wiles (1938) (Figure 2-3) and the acrylic femoral head replacement by doctors Jean and Robert Judet (1940) (Figure 2-4).

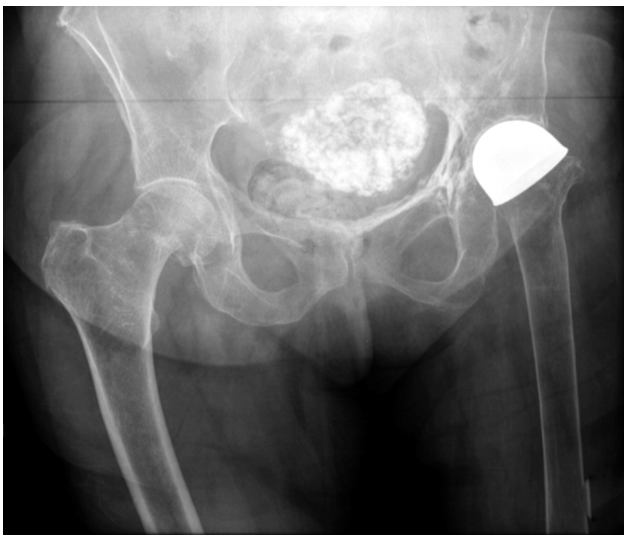

Figure 2-2: Anterioposterior pelvic radiograph depicting a left hip vitallium mould arthroplasty*.

Figure 2-3: Anterioposterior radiograph depicting a left acetabular cup and femoral head resurfacing by Wiles†.

* Image taken from J. F. Baker, M. H. Vioreanu, and H. A. Khan. Smith-Petersen Vitallium mould arthroplasty a 62 year follow up. J Bone Joint Surg Br. 2011 Sep; 93(9): 1285-6. Reproduced with permission and copyright © of the British Editorial Society of Bone and Joint Surgery

† Image taken from Learmonth ID, Gheduzzi, Vail TP. Clinical experience with metal-on-metal total joint replacements: indications and results. Proc. MechE Part H: J. Engineering in Medicine Vol. 220 p229-237. Reproduced with permission and copyright © of Proc. MechE Part H: J. Engineering in Medicine

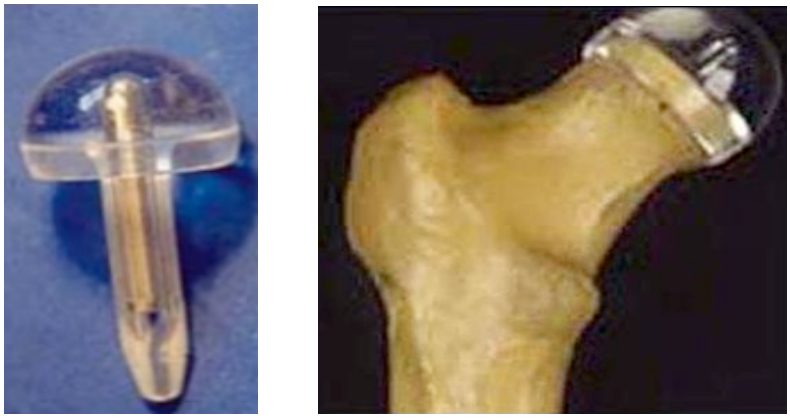

Figure 2-4: The Judet hemi hip acrylic arthroplasty featuring a distinctive flared collar below the head and a vertical intramedullary stem [*].

The first successful hip replacement was pioneered by Austin T. Moore (1940); he developed a metallic proximal femoral replacement using a stem to fix the prosthesis onto the femur. The revised prosthesis (1952), known as the Austin-Moore, is still in use today as a hemi-arthroplasty for the treatment of fractured neck of femur.

2.3.1.2. MoM THRs

Although hip joint replacements were being used in significant quantities since the 1940's the first designs that formed the basis of most modern hip devices were typified by the components developed in Red Hill by McKee & Farrar in the mid 1950's (Figure 2-5). These MoM devices with a large diameter head (35 – 40 mm) made of Cobalt-Chromium-Molybdenum alloy (CoCrMo) and articulating against a similar sized acetabular cup made of the same material. Similar devices were subsequently developed by Ring in 1962 (Figure 2-6), Muller in 1965 and by Scales and Wilson at Stanmore.

[*] Image taken from Judet J, Judet R. The use of an artificial femoral head for arthroplasty of the hip joint. J Bone Joint Surg Br 1950 (32) B: 166-173. Reproduced with permission and copyright © of the British Editorial Society of Bone and Joint Surgery.

Figure 2-5: The McKee & Farrar MoM monobloc hip replacement.*

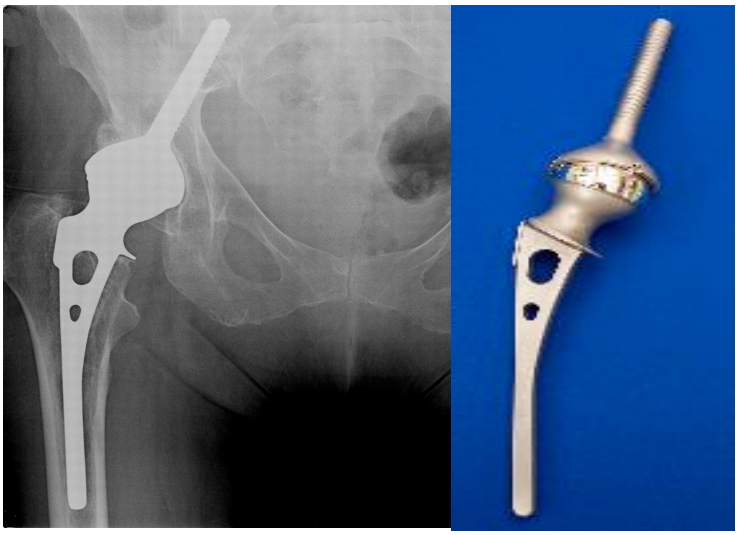

Figure 2-6: The Ring prosthesis, a large-bore monoblock MoM hip replacement.†

* Image taken with permission and copyright © of the Trends in biomaterials and artificial organs Jan 2005, Vol 19, pp15-26.

† Image taken with permission and copyright © of the Bone & Joint Journal Dec 1969, Vol 89-B, issue 5, pp586.

Although in the large part successful, acetabular component loosening and high frictional torque due to equatorial binding was a common problem leading to a decline in the use of such prostheses.

2.3.1.3. MoP THRs

Possibly the most significant advancement in THR surgery was developed by Sir John Charnley in 1962, who pioneered the '*low friction arthroplasty*' (LFA) by coupling a small metal femoral head with a thick high density polyethylene cup leading to reduced wear and better lubrication as well as popularizing the use of polymethyl-methacrylate (PMMA) bone cement leading to improved stability (Berry et al., 2002, Sochart and Porter, 1997, Wroblewski et al., 2009, Charnley, 1970). Initially Charnley used polytetrafluoroethylene but the material wore creating inflammation and was later replaced by polyethylene. From the early 1960s these metal-on-polyethylene (MoP) bearing prostheses using originally, 22.225 mm diameter stainless steel (SS) heads entered general widespread use with low wear rates being reported(Griffith et al., 1978) (Figure 2-7). Refinements of this initial design included heads of slightly larger diameter (28 – 32 mm) made of CoCrMo alloy and later on of Ceramic as well as the introduction of more advanced polyethylene called ultra high molecular weight polyethylene (UHMWP). Until the early 1990s this design remained essentially unaltered and had almost completely replaced other designs.

Figure 2-7: The Charnley MoP monobloc hip replacement.*

Although, predictions of wear-life on laboratory simulator tests suggested that these LFAs should have a satisfactory outcome for several decades, clinical experience showed average lifetimes of only 12-15 years, secondary to osteolysis of the bone adjacent to the femoral stem or the acetabular cup. Initially this phenomenon was attributed to the use of acrylic cement during fixation known as "cement disease". However, in due course it was recognized that such osteolytic reactions leading to implant loosening were linked to polyethylene wear debris (Willert and Semlitsch, 1977), susceptibility of gamma-irradiated polyethylene to oxidation (Sutula et al., 1995b) and the effect of roughened femoral heads (Fisher et al., 1995). This led to a renewed interest and the introduction of re-engineered MoM bearing surfaces from the early 1990s onwards.

* Image taken from Jackson J. Father of the modern hip replacement: Professor Sir John Charnley (1911–82). Journal of Medical Biography Volume 19 November 2011. Reproduced with permission and copyright © of the Journal of Medical Biography.

2.3.1.4. Renewed Interest in MoM THRs

First generation MoM THRs were initially abandoned due to concern over the high frictional torque produced by the large head causing increased wear and increased stresses on the acetabulum-bone interface often leading to "*equatorial binding*" resulting in cup loosening (Walker and Gold, 1971). However, some components had a relatively high level of survivorship. Long-term follow up studies of patients with McKee-Farrar implants showed outcomes comparable to established MoP THR, and revealed groups of patients who's implants had an 84% survivorship at 20 years and 74% at 28 years(August et al., 1986, Higuchi et al., 1997, Jacobsson et al., 1996, Visuri, 1987, Brown et al., 2002). Similarly long-term follow up of the Ring MoM prosthesis showed a survivorship of 95% at 15-16 years(Ring, 1989). In addition examination of retrieved MoM components exhibited low rates of linear and volumetric wear compared to MoP (Walker et al., 1974), (less than 8 μm/year) after 10-20 years(Semlitsch et al., 1989, Willert et al., 1996b). These low wear rates; also confirmed by other researchers (Schmidt et al., 1996, McKellop et al., 1996) led to the collaboration between Weber and Sulzer to develop a high carbon cobalt chromium wrought forged alloy bearing; the Metasul™(Zimmer, Warsaw, Indiana). The first Metasul™ MoM bearing prosthesis was implanted in 1988 and it is estimated that over 300 000 prostheses have been implanted worldwide with a survival rate of 94.4% at mean follow-up (12.3 years)(Saito et al., 2010).

2.3.1.5. MOM Resurfacing Arthroplasty

Recognising the potential value of the MoM technology, McMinn designed a new implant in the 1990s, the Birmingham Hip Resurfacing (BHR) prosthesis(McMinn et al., 1996). Traditional hip replacement designs consist of a cup shaped acetabular replacement articulating with a femoral component made up of a head and stem. This involves the removal of the femoral head and its replacement by a long, stemmed device

retaining very little of the femur. With the resurfacing procedure, however, just a few millimetres are removed from the two articulating surfaces of the hip making it a bone-preserving procedure because most of the joint is retained (Figure 2-8).

The femoral head is shaped to accept a low-wear metal sphere that matches the patient's anatomy (large in size >36 mm diameter) and the acetabular socket is then fitted with a corresponding metal cup (Figure 2-9).

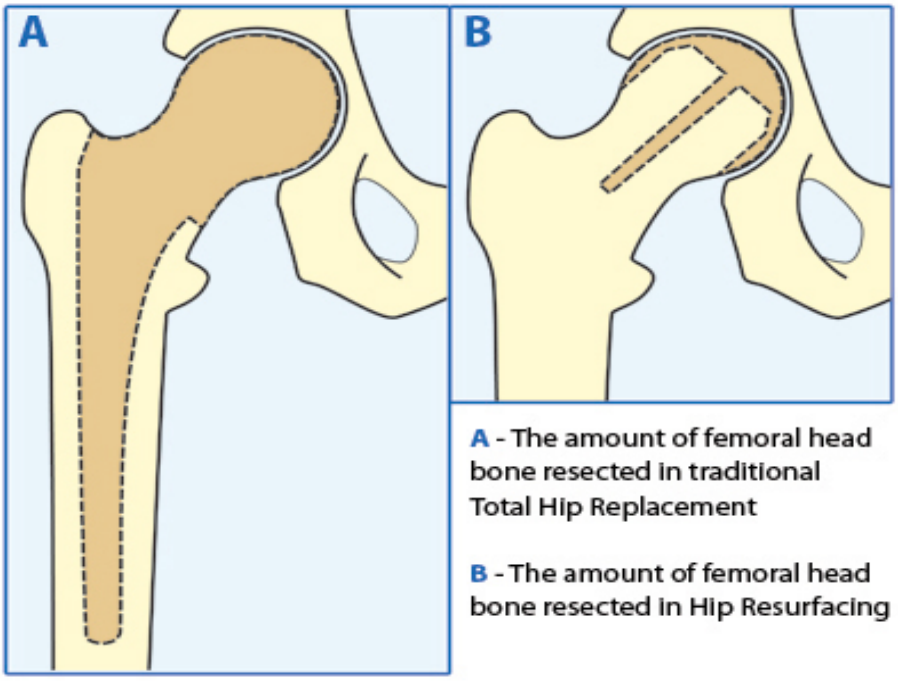

Figure 2-8: Femoral head resection comparison between a traditional THR and a Resurfacing. *

* Image taken from the McMinn Centre. Excellence in hips and knees. 25 Highfield Road Edgbaston Birmingham B15 3DP http://www.mcminncentre.co.uk.

Figure 2-9: Anterioposterior radiograph showing a BHR in situ and the prosthesis itself.[*]

This bone preservation seen with hip resurfacing allows for more bone to be retained in the femur. Should a femoral-side failure occur, the proximal femoral bone can be osteotomized and a conventional stemmed femoral prosthesis with a large femoral head to match the retained acetabular component be inserted. It also allows for the use of a much larger head (ball) size resulting in greater stability of the hip joint and a lower risk of dislocation. Also in theory they contribute to a greater range of motion. Due to these advantages hip resurfacings saw a tremendous increase in popularity, particularly amongst younger patients with higher activity levels and expectations.

2.3.1.6. Large Head MoM Modular THRs

In cases of failed resurfacing arthroplasty the acetabular component is usually well fixed and its revision may result in significant bone loss. Therefore, in 2003 modular CoCrMo large diameter femoral heads (>36mm diameter) were introduced as salvage implants that were compatible with standard stems in order to avoid acetabular cup revision

[*] Image taken from the McMinn Centre. Excellence in hips and knees. 25 Highfield Road Edgbaston Birmingham B15 3DP http://www.mcminncentre.co.uk.

(Gilbert et al., 2010). Large femoral head components experience a greater range of motion (Crowninshield et al., 2004) owing to the increased head diameter – neck thickness ratio (Figure 2-10) as well as a reduced risk of dislocation as a result of the increased distance required to dislodge them from the acetabular cup (Cuckler et al., 2004) (Figure 2-11).

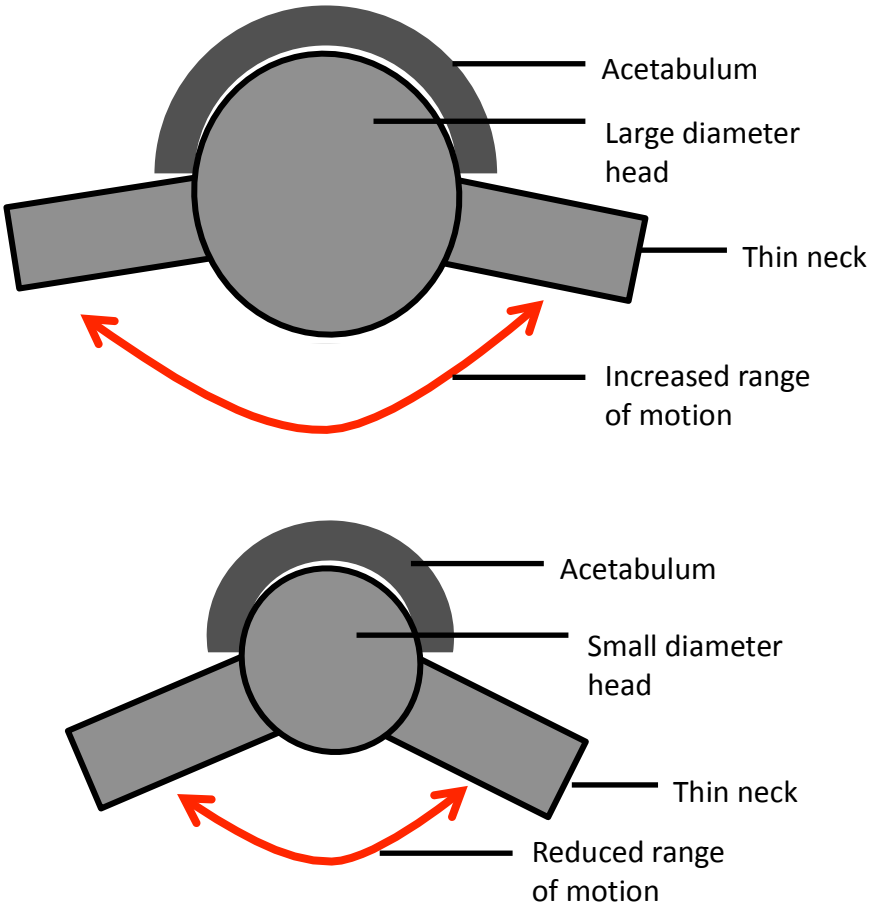

Figure 2-10: Diagram illustrating the increased range of motion owing to the increased head-neck ratio seen in large diameter heads compared to small diameter heads.

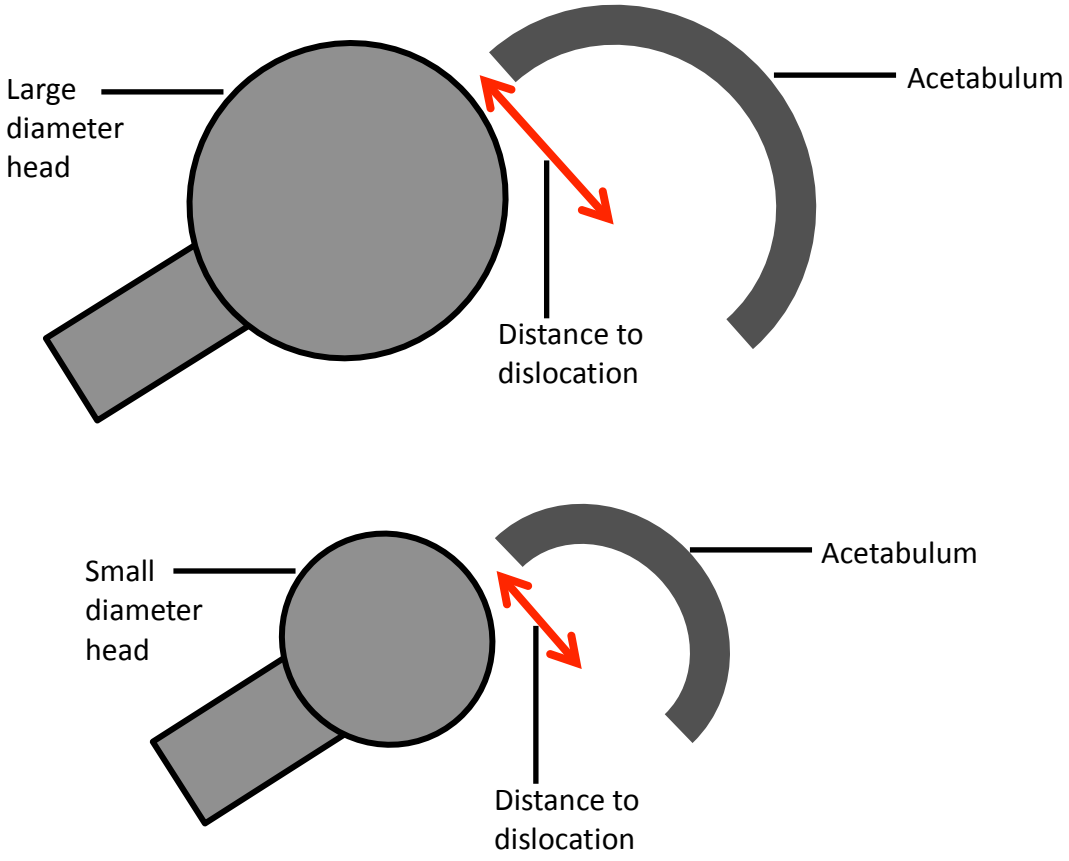

Figure 2-11: Diagram illustrating the increased distance that the prosthetic head must cover to come out of the cup and dislocate for a large diameter head compared to a small diameter head. This distance is proportional to the implant head, but also depends on the cup inclination.

Because of these key features large head MoM THRs and resurfacings became an attractive solution to the physical limitations of traditional MoP THR. The requirement for a relatively thin acetabular component in order to accommodate a large femoral head of near anatomical size limits the use of MoP since the high frictional torque produced by the large head would inevitably cause high wear of the polyethylene leading to accelerated failure.

Although large diameter modular femoral heads were initially introduced as a salvage procedure for failed resurfacings they were increasingly being used as primary hip

replacements instead of resurfacings for patients with poor quality femoral bone. Additionally, the advantages of modularity associated with the use of these large diameter modular MoM heads, increased their use in primary THA (Mertl et al., 2010) especially for younger active patients who stood to benefit the most.

2.3.1.7. Modular THRs

Early designs of THR were 'monobloc', with a one-piece femoral stem and head, whereas modern designs are modular with a range of heads, which can be attached once the stem has been implanted. Modularity of the head-neck junction was first introduced in the 1970s and was based on the adaptation of the Morse taper for use in orthopaedic surgery (Zweymüller et al., 1977, Weber et al., 1977). Morse tapers are one of the most widely used types in industry, and are particularly common on the shank of 'taper-shank' twist drills and machine reamers, in the spindles of industrial drill presses and in the tailstocks of lathes. Compared to orthopaedic tapers Morse tapers are much longer, smoother and have a much shallower angle.

The Morse taper is the brainchild of Stephen A. Morse. He first developed it in 1864 in order to reliably join two rotating machine components (Hernigou et al., 2013). Almost a century later, the introduction of ceramic in hip arthroplasty was the main drive for the orthopaedic industry to adopt the design. Initially, the fixation of the ceramic head on the metal stem was done with glue and subsequently by screwing the head on the stem, commonly leading to failure through fracture or separation of the components. These problems were solved when the Morse taper principle was used as a reliable means of fixing the ceramic head on the metal stem (Mittelmeier, 1984). Subsequently and under the generic term of Morse taper, this system was adapted for use with metal heads as well.

A typical modular implant uses the Morse taper principle, which is that of "the cone in the cone". It comprises a "male/female" junction; the "male" (or stem taper) is an extension of the femoral stem and the "female" (or head taper) is found on the head component (Figure 2-12). They are both uniformly tapered and machined to a desired surface roughness finish. When the head is tapped on the stem the connection allows for self-locking and resistance to multidirectional loading (Hallab et al., 2004). This results in stability in rotation, as well as in compression and tension.

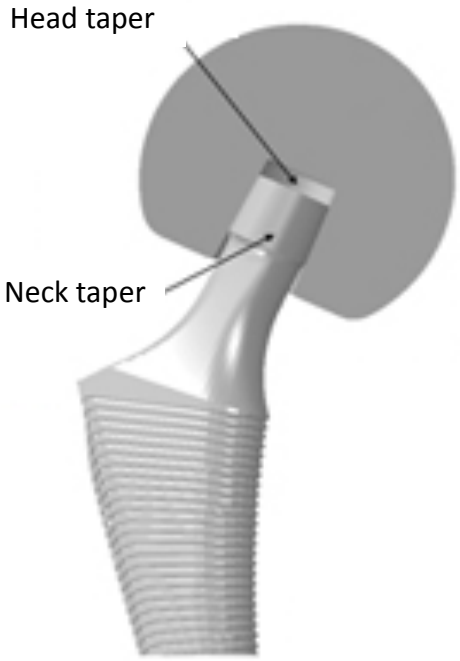

Figure 2-12: Diagram depicting a cross section of the taper junction - "female" (head taper) and "male" (stem taper).

Modularity offers a number of advantages in orthopaedic surgery. By allowing intra-operative selection of component size and type it provides the surgeon with the freedom to customise the prosthesis to individual patient parameters, whilst at the same time it reduces inventory and costs (Cook et al., 2013, Cameron, 1996). In doing so, discrepancies in leg length and femoral offset can be corrected in order to restore

desirable tissue tension, (Yerby et al., 1996). Larger head sizes, as well as improved tissue tension, enhance implant stability and reduce the risk of dislocation, while optimum femoral offset facilitates abductor tension and therefore function.

In addition, the modular nature of these implants enables selection of different materials for each component thus allowing the exploitation of their individual biomechanical properties for the benefit of the patient. This is exemplified by the frequent use of an uncemented titanium (Ti-6Al-4V) stem with a CoCrMo head. Ti-6Al-4V, has a Young's Modulus closer to that of bone making it the preferred material choice for the stem (Geetha et al., 2009) as it reduces the femoral susceptibility to 'stress-shielding'; a phenomenon whereby an implant with a Young's Modulus much higher than that of bone preferentially takes the stresses encountered during loading. This results in proximal bone loss secondary to the load being transferred preferentially through the distal part of the stem due to the relatively high stiffness of the implant compared to the surrounding bone. Titanium alloys are therefore preferred for cementless femoral stems due to their lower modulus compared with CoCrMo. On the other hand CoCrMo or ceramic materials are harder than Ti alloys and therefore more wear-resistant making them the preferred material choice for the bearing surface.

A further advantage of modular-type prostheses is that they can facilitate revision surgery. During isolated acetabular revisions the head can be removed to improve visibility and then replaced if still appropriate (Cameron, 1996). Equally, in situations of instability, a longer neck or larger head may be effective without the need for revision of a well-fixed stem (Jones et al., 2001) which avoids unnecessary damage to the femoral bone related to implant removal and replacement.

Today, the use of modular hip replacements is widespread. Old monoblock models, such as the Charnley (DePuy Orthopaedics, Warsaw, IN, USA) and Stanmore (Biomet, Warsaw, IN, USA), have now evolved to become modular systems, adapting to a market that almost exclusively produces modular components. As well as modular heads, some implants have been developed with modular necks or sleeve adapters e.g. Bioball (Lima Orthopaedics, Milano, Italy); which contribute to an additional modular interface. The benefits derived from the use of modular components have made these prostheses very popular, a fact reflected by the prevalent use of modular hip replacements as recorded by the National Joint Registry (National Joint Registry, 2013).

2.3.2. Theory Behind LH-MoM-THRs

Lubrication theory plays an important role in the successful performance of MoM bearings. Lubrication theory identifies three main regimes (Figure 2-13):

1. **Fluid-Film Lubrication.** This occurs between moving surfaces separated by interposed fluid thus solid-solid contact is avoided.
2. **Boundary Lubrication.** This occurs between moving surfaces that have direct asperity contact. In this mode of lubrication the load is carried by the surface asperities rather than by the lubricant.
3. **Mixed Lubrication.** This occurs when the load is partially supported by a combination of contact by the asperities (boundary lubrication) and by a fluid film that separates some, but not all, of the asperities of the interacting surfaces.

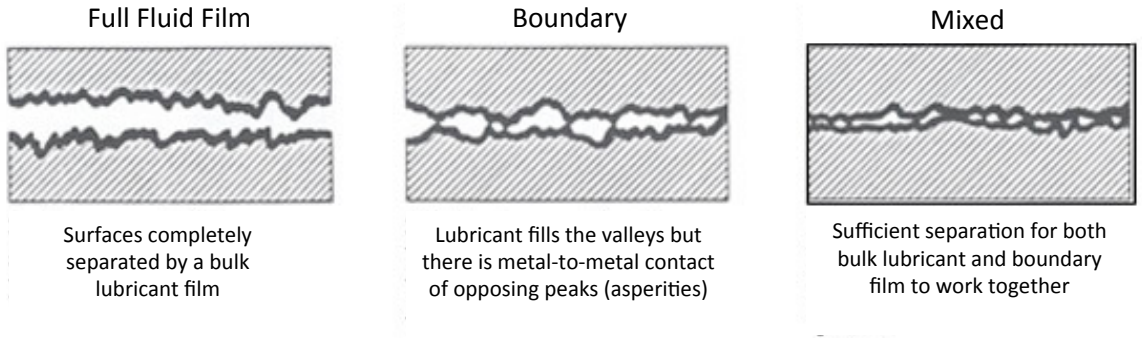

Figure 2-13: Diagram showing the different lubrication regimes.[*]

Although continuous fluid-film lubrication is required for the satisfactory performance of MoM bearings, the engineering materials available and the variable properties of lubricants render this very difficult. *Dowson* (Dowson et al., 2004) noted that actually MoM bearings operate under a mixed lubrication regime. However, optimisation of certain manufacturing parameters could elicit some of the benefits of full fluid-film whilst reducing the amount of wear as proposed by the lubrication theory adapted for hip joint replacement by *Jin* (Jin et al., 1996).

This work indicates that wear would be reduced if large diameter heads were utilised. Initially this seems to contradict the low friction arthroplasty principle proposed by *Charnley* (Charnley, 1979), stating that volumetric wear is directly proportional to the size of the femoral head. However, for MoM bearings the increased head diameter leads to increased sliding speeds in the mixed or fluid-film lubrication regime, which aids lubrication and reduces wear. Conversely MoP/CoP bearings operate in the boundary

[*] Image taken from ALS Tribology. Jonathan Sowers, CLS, Senior Diagnostician. *Esource.alstribology.com*

lubrication regime and as such the increased head diameter leads to reduced sliding speeds and therefore increased wear.

In addition LH-MoM hip simulator work by *Dowson* (Dowson et al., 2004), *Chan* (Chan et al., 1999a) and *Scholes* (Scholes et al., 2001) indicated how the amount of "running in" and "steady state" wear can be reduced by reducing the clearance between the femoral and acetabular components.

The effects of bearing surface roughness in LH-MoM components have been reported by *Chan* (Chan et al., 1999a) who concluded that, in line with lubrication theory, increased surface roughness is associated with higher wear rates.

2.3.3. Biomaterials

Biomaterials can be defined as materials that are intended to interact with human tissue and body fluids to treat, improve or replace anatomical elements of the human body (Mahyudin et al., 2016). The success of the biomaterials is mainly dependent on their biocompatibility, which refers to the tendency of these materials to remain biologically inert throughout the duration of their contact with the human body. The biocompatibility of a material is influenced by the hosts response induced by the material and the materials degradation by the host. Furthermore, in order for biomaterials to function adequately a number of fundamental mechanical and non-mechanical requirements must be fulfilled. These include: appropriate design, ability to be manufactured, mechanical stability and resistance to wear and corrosion and additionally special biomaterial properties such as elastic modulus, tensile strength, yield strength, fatigue resistance, creep, hardness and surface finish must be met (Patel and Gohil, 2012). The main biomaterials used in orthopaedic surgery are divided into two groups: Metals and Non-Metals.

The metallic implants that are widely used in orthopaedic joint replacement surgery are:

- Low carbon grade austenitic stainless steel (SS) – 316L
- Cobalt Chromium alloys
- Titanium alloys

The non-metallic implants that are extensively used in orthopaedic joint surgery are:

- Ultra High Molecular Weight Polyethylene (UHMWPE)
- Ceramics
- PMMA

A summary of the mechanical properties of the most common biomaterials in current orthopaedic use is shown in Table 2-1.

Material	Property/ Grade	Young's Modulus E(GPa)	Fatigue Limit S_{end}(MPa)	Ultimate Tensile Strength S_{UTS}(MPa)	Yield Strength S_y(MPa)	Hardness Hv
Stainless Steel	316L	190	260	500-800	195-685	199-225
CoCr Alloys	Cast CoCrMo	280	208-950	660	448-517	298
	Wrought CoCrMo	210-232	586-896	1000-1500	965-1606	280-445
Ti Alloy	Ti6Al4V	116	780-1050	860	795	349
Ceramic	Allumina	375	-	350	-	2000-3000
	Zirconia	150-199	-	200-495	-	1000-3000
Polymers	PMMA	1.8-3.3	19.3-38.5	77	-	10-22
	UHMWPE	0.9-2.7	-	53	17	62-66

Table 2-1: Comparison of mechanical properties of the most common biomaterials in current orthopaedic use.[*].

[*] Table taken from Aherwar A., Singh A.K., Patnaik A. Current and future biocompatibility aspects of biomaterials for hip prosthesis. Aims Bioengineering 2015 (3) 1: 23-43. Reproduced with permission and copyright © of the Aims Bioengineering journal.

2.3.3.1. Stainless Steel Alloys

The SS family is best described in reference to the metallurgical phases present in their microscopic structures and can be divided into: Austenitic, Ferritic, Martensitic and Duplex. Austenitic stainless steels constitute the largest family in terms of number of alloys and usage. They are essentially nonmagnetic and can be hardened at room temperature. They also exhibit superior corrosion resistance to the other families.

Today the primary SS alloy recommended for medical devise use is the 316L type. The main composition of 316L alloy is based on the very common 18-8 alloy, which typically contains 18% Cr (responsible for the creation of a thin Cr oxide (Cr_2O_3) protective film layer on its surface) and 8% Nickel (Ni), which contributes to the austenite phase formation in the alloy. Additionally though in order to increase its resistance to corrosion 316L alloy also contains 3% Molybdenum (Mo) and has a reduction in its carbon content by 0.03%. In order to maintain stability of the microstructure the addition of Ni is increased to 12%.

Austenitic stainless steel is reasonably strong, ductile and easily manufactured. As such it is widely used in traumatological devices such as fracture plates, screws and hip nails. However, its poor wear resistance and its susceptibility to crevice and fretting corrosion (Cottrell, 1995, Davis, 1998) limits its use in orthopaedic joint replacement surgery. At present, new austenitic stainless steel with high Cr content (over 20%), where Ni has been partially substituted by Manganese (Mn) and with a high Nitrogen content (between 0.3 and 0.4%), is being used in joint prosthesis. Nitrogen stabilizes the austenitic phase and induces an increase in both the corrosion resistance and the mechanical properties (yield stress) (Navarro et al., 2008).

2.3.3.2. Cobalt Chromium Alloys

Cobalt Chromium alloys have been used for many decades because they combine exceptional corrosion resistance in chloride environments with good wear resistance properties (Ramsden et al., 2007, Navarro et al., 2008, Alvarado et al., 2003). Their mechanical properties are also superior, most significantly they are resistant to fatigue and to cracking caused by corrosion. However, as is true of other alloys, cobalt based alloys may fail because of fatigue fracture (but less often than stainless steel stems). Cobalt Chromium alloys can be categorised into two types: CoCrMo alloy, (which is usually used to cast a product) and CoNiCrMo alloy, (which is usually wrought by hot forging). The abrasive wear properties of the wrought CoNiCrMo alloy are similar to the cast CoCrMo alloy (Chan et al., 1999b, Dowson et al., 2004) however, CoNiCrMo alloy is not recommended for the bearing surfaces of joint prosthesis because of its poor frictional properties with itself or other materials. These materials have a high elastic modulus (which is higher than that of cortical bone (Alvarado et al., 2003, Ramsden et al., 2007). On contact with bone, the metallic devices will take most of the load due to their high modulus, producing stress shielding in the adjacent bone. The lack of mechanical stimuli on the bone may induce its resorption that will lead to the eventual failure and loosening of the implant (Navarro et al., 2008).

2.3.3.3. Titanium Alloys

The most common Titanium (Ti) alloys used in biomedical applications are Ti-6Al-4V. Ti alloys offer excellent corrosion resistance due to a nano scale (10nm) Ti oxide (TiO_2) film formation on their surface. Their lower modulus of elasticity compared to CoCr and SS alloys also makes Ti alloys the material of choice for cementless femoral stems (Willert et al., 1996a). Although the mechanical properties of Ti alloys are regarded as being superior, when Ti is rubbed between itself or between other metals it suffers from severe

wear (Miller and Holladay, 1958). As such their application is avoided in areas where wear resistance is vital such as in the bearing surfaces (Nag et al., 2009). In addition *Navarro* and *Geetha* (Navarro et al., 2008, Geetha et al., 2009) have raised concerns regarding the long-term performance of Ti-6Al-4V due to the release of Aluminium and Vanadium both of which have been shown to be associated with Alzheimer disease and neuropathy.

2.3.3.4. UHMWPE

PE and more specifically UHMWPE are available at relatively low cost and easily processable. UHMWPE has been used in THA as bearing surface since the early 1960s mainly as the liner of the acetabular cups. The microstructural arrangement of UHMWPE provides high abrasion resistance, high impact strength, biocompatibility and excellent toughness in comparison with other polymeric materials (Fisher and Dowson, 1991, Sutula et al., 1995a). Initially however, it was shown that UHMWPE gamma-ray sterilization in air lead to oxidative aging of the PE and during the wear process this oxidation enhanced the production of the PE wear particles (Besong et al., 1998, Green et al., 1998) leading to wear-debris induced osteolysis (Ingham and Fisher, 1995). In the last 15 years improvements in the sterilization process of PE (performed in an inert atmosphere) and its storage in an oxygen free environment have shown increased resistance to oxidation and wear. In addition the wear resistance properties have been improved by increasing the crystalinity and cross linking density of UHMWPE (Endo et al., 2001). Crosslinking leads to the formation of a polymer in which chains are joined together to form a three-dimensional network structure (Sawatari and Mastuo, 1987, Houde and Schreiber, 1992) and thus, producing a more durable polymer matrix. This dense network of high molecular weight, improves impact strength, environmental stress crack resistance, creep and abrasion resistance without influencing tensile strength

and density to any appreciable extent (Tamboli et al., 2004). These cross-linked polymers are generally formed by generating free radicles using, excessive amounts of gamma irradiation. Depending on the type of cross-linked polyethylene the radiation dose is usually between 5-10 MRads, whereas 2.5 MRads are required to terminally sterilise implants. This high dose of radiation leads to the formation of free radicals in the material some of which combine to form cross-links. The residual free radicals, which would eventually lead to oxidative degradation, are removed by a heat treatment either by annealing at a temperature below meting point or just above the melting point. There are a number of variations of this technique leading to several different cross-linked PEs being available with each manufacturer claiming advantages and disadvantages depending on their method of production.

2.3.3.5. Ceramics

The ceramic materials used in orthopaedics today are formed by fusing microscopic grains of alumina (Al_2O_3) and/or Zirconia (ZrO_2) ceramic powder into a consolidated product. The applied manufacturing process (temperature, thermal step duration, powder purity, grain distribution and porosity) has a direct impact on the strength and biological properties of the ceramic components. The superior wear resistance of ceramic compared to metallic and other polymeric bearings (Hench and Wilson, 1993) is what inspired the increased interest in Ceramic on Ceramic (CoC) designs in hip arthroplasty during the 1990s (Boehler et al., 2000). However, low fracture toughness was one of the limiting properties of ceramic materials. Therefore, improvements in the material quality (by modification of the production processes and a reduction in the grain size) were employed, which have lead to an improvement in the overall strength of ceramic materials. Their good wear resistance is associated with their hardness and also with

their hydrophilic nature which can lead to the maintenance of fluid film lubrication for longer that with more hydrophobic surfaces such as cobalt chrome.

Alumina oxide has the longest history of successful use in hip articulations either in combination with UHMWPE or with itself (CoC) owing to its low friction and wear coefficients, corrosion resistance, good biocompatibility, high wear resistance and high strength. Zirconia oxide although softer than alumina, is stronger. This is because it is formed in a metastable state when mixed with Yttrium oxide. The metastable state maintains a phase structure under stress, which is slightly smaller than the natural phase. When the stress is increased due to the formation of a crack, a phase change occurs and a larger phase is formed compressing the crack tip resulting in a stronger material.

New ceramics known as delta ceramic are a combination of 1) alumina oxide which provide hardness, 2) Yttrium which stabilise zirconia thus, providing strength through the phase transformation mechanism and 3) plates of Chromium or Strontium which increase the surface area of grain boundaries making the material tougher by reducing crack propagation.

Oxidised Zirconium, which is marketed under the name Oxinium™ (Smith and Nephew Orthopaedics, Memphis, TN) is manufactured by heating Zirconium alloy in the presence of air. This process converts the surface to a black Zirconium oxide ceramic (~5μm thick). The Zirconium oxide provides increased scratch resistance and hip simulator studies have shown reduced UHMWPE wear when compared to a CoCr alloy femoral head (Bourne et al., 2005) without the increased risks of fracture associated with the Zirconium alloy substrate.

2.3.3.6. PMMA

Sir John Charnley pioneered PMMA bone cement, also known as "acrylic cement" in the 1960's as a method of fixation of the stem component within the femoral bone (Charnley, 1970) and by 2009, 53% of THRs carried out in the UK used PMMA bone cement in order to stabilize the femoral stem. PMMA is a versatile thermoplastic polymer and has the capacity to be polymerized at the time of surgery as a "filler" material for primary fixation of the prosthesis in total-hip insertion. It is prepared in situ by mixing a liquid monomer and a powdered polymer which produce an exothermic reaction at usually temperature of 48 – 56 °C in vivo. Manufacturers add initiators, accelerators, antibiotics and radiopacifiers to the powdered polymer to begin the polymerization process, reduce the risk of infection and increase radiographic visualization respectively (Duffy and Shafritz, 2011, Webb and Spencer, 2007). The monomer contains an inhibitor, which prevents polymerization. When used for primary fixation in total hip implantation, PMMA acts like grout and interdigitates between the bony trabeculae rather than adhering to bone or metal. When fully hardened PMMA, is strong but brittle. Its elastic modulus lies between 1– 4 GPa, which is close to that of cancellous (10 – 2,000 MPa) and cortical (10 – 20 GPa) bones and its viscoelastic properties demonstrate an increase in stiffness with higher rates of loading, as well as creep and stress relaxation, reaching its strongest point under compression (Wright and Maher, 2008, Mahyudin et al., 2016).

2.3.4. Tribology of MoM Bearings

Three distinct processes are involved in the degradation of metal-alloy implants; electrochemical dissolution, wear and a synergistic combination of the two.

2.3.4.1. Electrochemical Dissolution – Corrosion

Electrochemical dissolution applies to the process of corrosion, which is defined as the unwanted dissolution of a metal in an aqueous electrolyte resulting in its continued

degradation (Fontanna and Greene, 1967). There are two reactions occurring during the electrochemical degradation of a metal; the anodic reaction involving the removal of electrons from the metal atoms (oxidation) (Equation 1) and the cathodic reaction, which allows the electrons to be consumed by the oxidising agent (reduction) (Helson and Breme, 1998) (Equations 2-4).

(1) Anodic: $\mathbf{M \rightarrow M^{(n+)} + ne^-}$

The metal (M) has *n* valence electrons and can be considered as an array of ions. During oxidation at the anode the electrons are ejected leaving a positively charged metal ion (Equation 1). This leads to an increase in the potential difference between the metal and the electrolyte. This potential difference is called the electrode potential or, simply, the potential of the metal. As the metal remains in solution this potential becomes more positive as electrons are removed from the metal as part of the reduction reaction, which varies according to the chemistry of the electrolyte (Equations 2 to 4). In acid solutions, electrons can react with hydrogen ions, adsorbed on the metal surface from the solution, to produce hydrogen gas (Equation 2). In neutral solutions, the concentration of hydrogen ions is too low to allow reaction (Equation 2) to proceed at a significant rate, but electrons in the metal can react with oxygen molecules, adsorbed on the metal surface from air dissolved in the solution, to produce hydroxyl ions (Equation 3). Equally in acidic conditions cathodic reaction (Equation 4) will occur. It is these free electrons that account for the electrical conductivity of the metal (Stansbury and Buchanan, 2000).

(2) Cathodic for hydrogen-evolution: $\mathbf{2H^+ + 2e^- \rightarrow H_2}$
(3) Cathodic for oxygen-reduction in alkali solutions: $\mathbf{O_2 + 4e^- + 2H_2O \rightarrow 4OH^-}$
(4) Cathodic for oxygen-reduction in acidic solutions: $\mathbf{O_2 + 4H^+ + 4e^- \rightarrow 2H_2O}$

2.3.4.2. Passivity of Biomedical Alloys

Metallic alloys used in orthopaedics rely on a protective oxide layer, which forms spontaneously when the surface of the prosthesis reacts with oxygen. This passive film behaves as a kinetic barrier inhibiting further oxidation of the underlying thermodynamically reactive metal, thus keeping current flow and corrosion product release at a very low level (Yan et al., 2007, Y. Yan et al., 2007). Passive oxide film properties such as, low ionic conductivity, low chemical solubility, stability under a wide range of electrode potentials, high compressive strength and good adhesion to the underlying metal provide a barrier to the oxidation reaction of the metal surface (Brusic, 1972, Kruger, 1988, J.W. Schultze and Lohrengel, 2000). On CoCrMo the passive oxide film consists of two layers: an inner oxide layer and an outer hydroxide one and its thickness can range from 1 - 5nm depending on the metal, the electrolyte and the conditions under which the film was formed (Milosíev and Remskar, 2009, Hryniewicz et al., 2008, Kocija et al., 2004). In the absence of mechanical loading and underlying surface defects passive film breakdown occurs on a very small scale. However, in environments that contain aggressive anions such as chloride the passive film becomes unstable and susceptible to breakdown secondary to localised forms of corrosion such as pitting and crevice corrosion as well as mechanical events associated with tribology such as fretting and wear corrosion (Fontanna and Greene, 1967, Frankel, 1998).

2.3.4.3. Electrochemical Basis of Passivity

Electrochemical reactions involve the transfer of electrons and ions between the metal and the solution thus the rates are equivalent to electric currents (Scully and Taylor, 1987). The potential difference between the metal and the solution is what determines the rate of these reactions, consequently as the potential of the metal becomes more positive the anodic reaction increases whilst the cathodic reaction decrease. Similarly as

the potential of the metal becomes more negative the converse effect on reaction rate occurs. Therefore, by studying the relationship between potential and current (polarisation curve) we can predict the localised and general corrosion behaviour of passive metal alloys, known for undergoing active-passive transition. A representation of a polalisation curve for a passive metal is shown in Figure 2-14. It's a log current versus potential plot also know as an Evans or Tafel plot (Revie, 2000) and its obtained during potentiodynamic polarisation tests used to characterise passive metal alloy corrosion. From Figure 2-14, we see that moving in the anodic direction there is a region of active corrosion that occurs at a potential higher than the corrosion potential (E_{corr}). This continues until the potential reaches the passivation potential (E_{pp}) at which point any further increases in potential cause a decrease in the anodic current density. This current drop is characterised by the formation of a passive oxide film on the surface of the metal and the metal is said to be undergoing an active-passive transition. The current density passing through the passive film drops to a very low level and this is known as the passive current density (i_p). i_p is a measure of the protectiveness of the passive oxide film. During passivation the metal still corrodes but it does so at a lower rate. The current density at the E_{pp} is called the critical current density (i_{cc}) and it's a good indicator of the ease of passivation; the smaller the i_{cc} the easier is passivation. Eventually the current starts to increase again with increasing potential and this is due to localised breakdown of the oxide film. This occurs at a specific potential called the critical breakdown potential (E_b). The more positive the E_b is, the more stable the passive oxide film is. Beyond the breakdown potential (E_b) the material enters the transpassive region whereby the current starts to increase again with increasing potential and the material begins to corrode rapidly. Tafel extrapolation can be applied on the linear portions of a log current versus potential plot; the point at which they intersect represents the free

corrosion potential (E_{corr}) and the value of the corrosion current density (i_{corr}). At the E_{corr} the anodic and cathodic rates are exactly equal and can be used as a benchmark for comparison with the E_b such that the larger the difference between E_b and E_{corr} the greater the stability of the passive oxide film against localised corrosion.

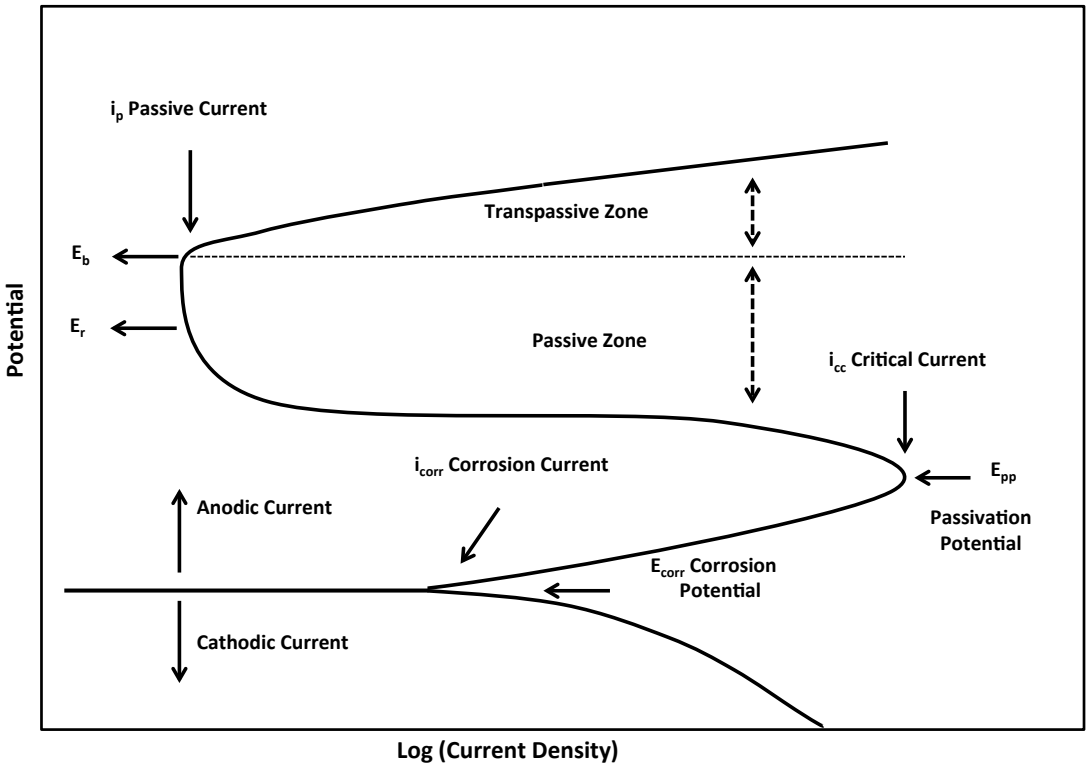

Figure 2-14: Typical Evan's plot for a passive metal*.

2.3.4.4. Types of Corrosion

Eight distinct forms of corrosion have been defined by Fontana (Fontanna and Greene, 1967) and these include: General corrosion, crevice corrosion, pitting corrosion, galvanic corrosion, intergranular corrosion, fretting corrosion, selective leaching and stress corrosion. This section will concentrate purely on electrochemical dissolution

* Image modified from Fraker, A. C., Corrosion of Metallic Implants and Prosthetic Devices, ASM Handbook, Vol. 13 Corrosion, 1987, pp1324-1335.

phenomena that are pertinent to the biomedical alloys currently used in orthopaedic implants.

2.3.4.5. General Corrosion

Uniform corrosion refers to the inevitable corrosion to which all metals immersed in electrolytic solutions are subjected to (Revie, 2000). In the case of metal alloys used for implants this process is very slow and visibly undetectable due to the high resistance these metals have against corrosion.

2.3.4.6. Crevice Corrosion

Crevice corrosion is a type of localised corrosion that can be found within crevices or at shielded surfaces where a stagnant fluid is present resulting in the localised breakdown of the surface passive oxide layer (ASTM, 2009). Once initiated crevice corrosion is autocatalytic in nature and can progress rapidly. At present there are several proposed models explaining the mechanisms involved in the initiation and propagation of crevice corrosion (Fontanna and Greene, 1967, Oldfield and Sutton, 1978, Oldfeild and Suttton, 1979, Pickering, 1990, Brigham, 1992, Sridhar and Dunn, 1997, Brossia and Kelly, 1999, Shaw et al., 1991).

The "Passive Dissolution Model" developed by Oldfield and Sutton used the Fontana and Greene mechanism as the foundation for building this computational model for crevice corrosion initiation. This model proposes the formation of an aggressive solution within the crevice through gradual acidification that ultimately results in the localised breakdown of the passive oxide film. Initially the anodic (Equation 1) and cathodic (Equation 3) reactions take place over the whole metal surface exposed to both the bulk and crevice electrolyte. The metal surface in contact with the bulk electrolyte has a constant supply of oxygen, however the restriction in the crevice region prevents

dissolved oxygen from entering, resulting in the depletion of oxygen within the crevice, which can no longer support the cathodic reaction. Outside the crevice the cathodic reaction continues as per normal whilst the anodic reaction ceases since it is concentrated in the crevice. This leads to an electrical charge imbalance between the positive metal ions in the crevice and the negative charge outside the crevice. Consequently negatively charged chloride and hydroxide ions that are small in size diffuse into the crevice to maintain charge conservation. With the chloride ions very small hydrogen ions migrate into the crevice; together they are responsible for decreasing the pH from values of 6 to 2-3 and thus increasing the corrosion rate within the crevice (Marlowe et al., 1997). Equations below show how metal chlorides form within the crevice and further react with water to produce metal hydroxides and hydrochloric acid.

(5) Metal Chloride formation: $\mathbf{M^{n+} + Cl^- \rightarrow MCl_n}$

(6) Metal Chloride hydrolysis: $\mathbf{MCl_n + nH_2O \rightarrow M(OH)_n + nHCl}$

In addition the dissociated chloride ions (equation 7) can further react with the metal ions from the continuous metal dissolution, thus repeating the reaction cycle. All these factors contribute to the continuous and gradual reduction of crevice electrolyte pH.

(7) Chloride ion dissociation: $\mathbf{HCl \rightarrow H^+ + Cl^-}$

Consequently the crevice electrolyte becomes aggressive enough to break down the passive oxide film locally and initiate crevice corrosion.

The "Thiosulphite Disproportionation" model was first proposed by Eklund (Eklund, 1976), who attributed crevice corrosion initiation at sulphide inclusions in the metal surface. This model was later supported by Alkire and Lott (Alkire and Lott, 1985, Laycock et al., 1997), their corrosion studies on steel showed that dissolution of

magnesium sulphate inclusions result in the formation of thiosulphate which also contributes to the film breakdown.

Pickering (Pickering, 1989) extended our understanding of crevice corrosion by introducing the "IR drop" model. This model focuses on the non-uniform electrode potential distribution between the outer surface of the crevice exposed to the bulk electrolyte and the inner surface of the crevice. As one moves into the crevice the voltage drop increases as the anodic current leaves the crevice. When this voltage drop becomes large enough it can force the local electrode potential from a passive region to an active one and therefore initiate corrosion (Pickering, 1995, Pickering, 1989).

2.3.4.7. Pitting Corrosion

Pitting corrosion is a form of localised corrosion that initiates on an open surface whilst crevice corrosion initiates at occluded sites. Although these closely related forms of localised corrosion differ in their initiation mechanism their propagation mechanism is similar, leading to the accelerated dissolution of the underlying metal. Over the years a number of mechanisms have been proposed for the initiation of pitting corrosion. These can be broadly categorised into three groups (Kruger, 1988, H.H., 1984, Frankel, 1998):

1) Passive film penetration

2) Passive film absorption

3) Passive film breakdown.

In the "passive film penetration" mechanism aggressive anions are transported through the oxide film to the underlying metal surface where aggressive dissolution of the metal/oxide interface is initiated (Kruger, 1988). Associated with this mechanism is the point defect model (Chao et al., 1981). This model describes point defects in an oxide

layer in the form of holes, metal vacancies and oxide vacancies that act as local anodes and initiate film breakdown. The "passive film absorption" mechanism developed by Uhlig (Uhlig, 1950), is based on the absorption of chloride and oxygen through the several monolayer-thick passive layer. It is believed that these absorbed species increase the local electric field strength that in turn reduces the thickness of the layers, eventually leading to the complete breakdown of the passive layer and the formation of pits. Lastly the "passive film breaking" mechanism considers the passive oxide film to be a dynamic system; in a continual state of breakdown and repair. It assumes that breakdown of he passive layer will always occur but will only lead to pitting when conditions allow for pit growth. According to *Sato* (Sato, 1971) an electrochemical breakdown of the passive film is initiated by a high electric field in the oxide and *Gavelle* (Galvele, 1989), suggested that a critical current density is required for the breakdown to stabilise. This mechanism fits with the dynamics of a corrosion reaction and also with the observation that some pits initiate and don't grow while others initiate late and grow.

It's important to note that these three mechanisms of pit initiation are not mutually exclusive. *Yu* (Yu et al., 2000) have shown evidence for both film penetration and film thinning for the pitting of aluminium in chloride solutions. Equally *Burstein and Mattin* (Burstein and Mattin, 1995) have shown that in the case of stainless steel a high chloride concentration is necessary to achieve the very high current density required for film breakdown and pit stabilisation, thus combining the mechanisms of film breaking and film penetration (Figure 2-15).

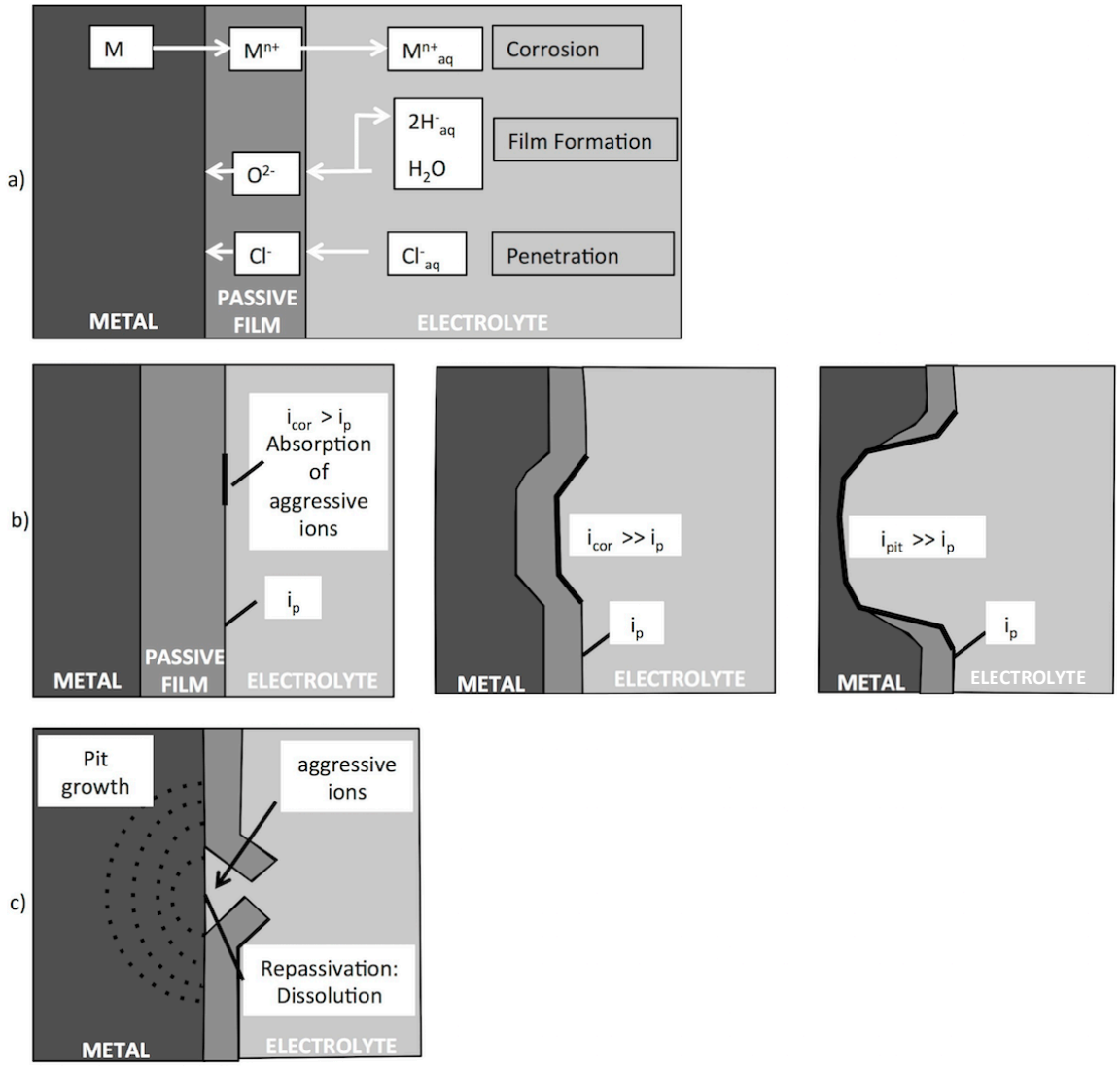

Figure 2-15: Schematic representation of pit initiation by a) penetration b) absorption and thinning and c) film breaking*.

2.3.4.8. Galvanic Corrosion

Galvanic corrosion is driven by the differences in electrochemical potentials of dissimilar metals in close proximity (Jacobs et al., 1998). The difference in potential results in an electron flow between the metals resulting in accelerated corrosion of the more

* Image taken from H.H. Strehblow, "Nucleation and Repassivation of Corrosion Pits for Pitting on Iron and Nickel," Werk. Korros., 27, 792 (1976) and Wiley-VCH Verlag GmbH, Weinheim, Germany.

susceptible alloy (anode) and protection of the other alloy (cathode) (Craig and Pohlman, 1987). Each alloy is ranked according to its tendency to corrode, thus the galvanic series can be used to predict galvanic relationships between metals and determine unsuitable combinations (Figure 2-16). A number of factors may influence galvanic corrosion such as local environment chemistry, proximity of the two dissimilar metals – the greater the proximity the greater the galvanic corrosion and the anode: cathode surface area ratio – a larger cathode area compared to a smaller anode area will produce higher local current densities at the anode and therefore greater corrosion (Helson and Breme, 1998).

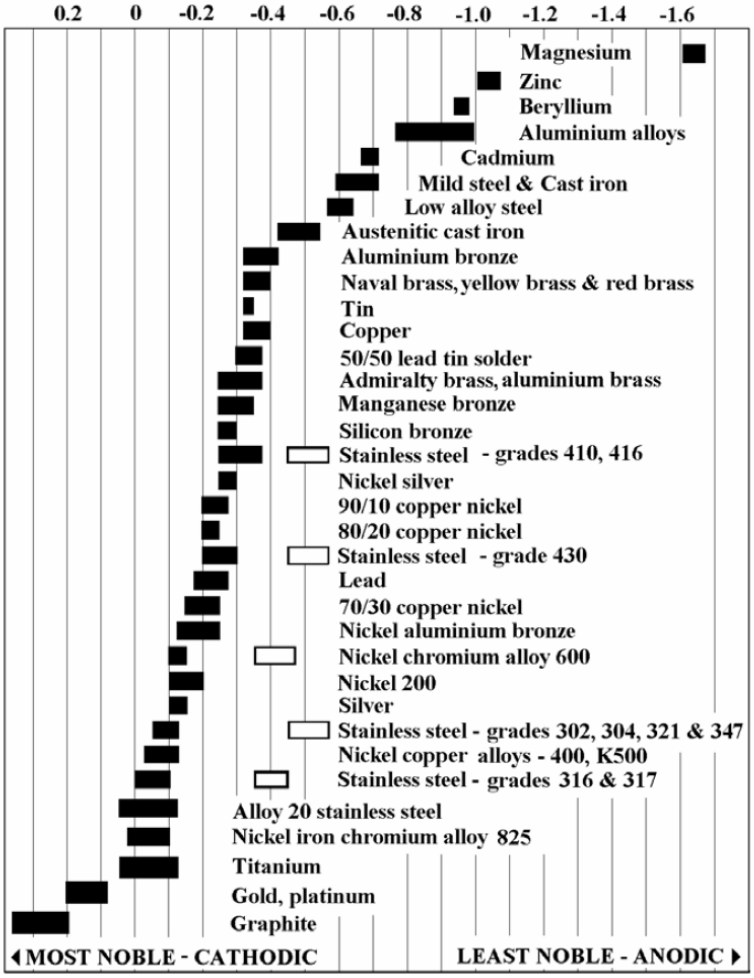

Figure 2-16: Galvanic series of various metals in salt water according to ASTM G82-98*.

* Image taken from the Stainless steel information centre. http://www.ssina.com/corrosion/galvanic.html

2.3.4.9. Intergranular Corrosion

Intergranular corrosion is the localised attack that occurs at or immediately adjacent to grain boundaries of an alloy. Metal alloys that are otherwise corrosion-resistant become susceptible to intergranular corrosion when the grain boundary becomes depleted of the corrosion-inhibiting element by a form of sensitisation. During sensitisation in biomedical alloys such as CoCrMo and stainless steel carbon diffuses to the grain boundaries where it combines with chromium to form chromium carbides, thus depleting chromium from the areas in and adjacent to the grain boundaries. A difference in electrode potential develops between the chromium-depleted areas and the bulk alloy allowing for localised corrosion (Fontanna and Greene, 1967, McCafferty).

2.3.4.10. Fretting Corrosion

Fretting corrosion is a synergistic combination of wear and corrosion of two materials in contact. It is defined as deterioration at the interface between contacting surfaces as a result of corrosion and micromotion between two surfaces (ASTM, 2009) . The movement required for disruption of the passive layer can be as little as 3 or 4 nm and is dependent on the contact load and frequency of movement (Craig and Pohlman, 1987).

2.3.4.11. Wear

The process of wear can be defined as the progressive loss of material from one or both of the surfaces during relative motion between them (Bhushan, 1999). Depending on the mechanical/chemical properties of the materials in contact, lubrication regime and sliding speed different mechanisms of wear may be observed. Wear mechanisms do not usually occur alone but two or three may occur at the same time or in sequence. Wear behaviour in MoM components consists of two time-based phases; "running-in" and "steady state". During the "running-in" phase, which, can last, for (0.5-2) x 10^6 cycles, conformity, topography and frictional compatibility of the metal surfaces are optimised

and it is characterised by a high wear rate. Transition to a "steady state" occurs when wear conditions are relatively constant and much lower, it usually lasts for (2-5) x 10^6. Once sufficient time passes fatigue will dominate (J.Williams, 1994). *Dowson's* review of "steady state" wear results following a number of hip simulator tests identified that oxide film thickness alone (excluding surface roughness) is an excellent predictor of long term performance of MoM components. With oxide film thicknesses ranging 12-20 nm the most dramatic reduction in wear rates (Dowson, 2003). The following section will concentrate on the most common types of wear encountered by biomedical orthopaedic implants.

2.3.4.12. Abrasive Wear

Abrasive wear results from a hard asperity damaging or ploughing the surface of a softer material, leading to the deformation and increase in surface roughness of the abraded area. It may occur when the harder surface cuts material from the softer surface creating abrasive particles (two-body abrasive wear) or when non-constrained debris particles are free to roll and slide between the 2 surfaces (three-body wear) (J.Williams, 1994).

2.3.4.13. Adhesive Wear

Adhesive wear works on the principle of plastic shearing of the tips of softer asperities leaving them adherent to the harder surface. Continuous motion leads to the subsequent detachment of these tips resulting in wear particle formation. Lubricants are often utilised to prevent wear, however when the lubrication film breaks down it brings the two surfaces into intimate contact, which is a prerequisite for adhesive wear (Affatab, 2012).

2.3.4.14. Erosive Wear

Erosive wear refers to the process of particle impingement, usually at high velocity on component surface resulting in material removal from that surface (Archarard, 1980). The severity of erosive wear is dependent on the material properties of the particles such as hardness, impact velocity, shape and impingement angle (Ombardi et al., 1989).

2.3.4.15. Fatigue Wear

Fatigue wear is associated with cyclic stress variations and therefore the lifetime of the material and outcome of the implant is dependent on the number of cycles. The repeated loading and unloading cycles to which the material is exposed leads to the formation of subsurface and surface cracks which eventually after a critical number of cycles will result in delamination and pit formation (Rowe, 1980).

2.3.4.16. Fretting Wear

Small-amplitude oscillatory movements usually less than tens of microns (Waterhouse, 1972) between two surfaces generate fretting wear. This mechanical action disrupts the passive oxide film from the metal substance exposing the unoxidised metal to the solution. Such films tend to repassivate (oxidise) in the presence of oxygen containing environment however, the film becomes disrupted again on the return path of the counter face and the cycle continues. Abrasive wear may follow secondary to disrupted film particle entrapment in the contact area (J.Williams, 1994).

2.3.4.17. Mechanically Assisted Crevice Corrosion

Mechanically assisted crevice corrosion (MACC) also referred to, as tribocorrosion is the term used to describe a conjoint failure mechanism encompassing mechanical processes and electrochemical processes. Mechanisms such as fretting corrosion, fretting-crevice corrosion, corrosion fatigue and stress assisted corrosion fall under this umbrella term.

Metallic biomaterials in use today are highly corrosion resistant due to the passive oxide film that forms spontaneously on their surface acting as a barrier to corrosion. However, mechanical disruption of the passive oxide film can lead to acceleration of corrosion processes on the surface of these metallic biomaterials. The rate and severity of such corrosion processes can be influenced by a number of factors including mechanical, electrochemical and environmental factors such as crevice geometry, local solution chemistry, material composition, load application, lubrication regime. An increase in corrosion rate is accompanied by changes in the stability of the passive oxide film, oxygen consumption, voltage shifts and reduction in pH all of which affect MACC further. The three main requirements for MACC are:

a) A metal alloy that is able to form a passive oxide film layer.
b) Disruption of the passive oxide film layer though a mechanical stress/abrasive process.
c) Aqueous electrolyte.

Additionally, in situations where restricted geometry limits fluid ingress as would be the case at the taper connection of modular joint replacement components, then crevice-like environments may form and predispose to aggressive and severe attack.

Using the head-neck taper junction of a modular total hip replacement as a model, the mechanism of MACC is as follows. Figure 2-17 represents a modular taper interface when cyclic bending is applied.

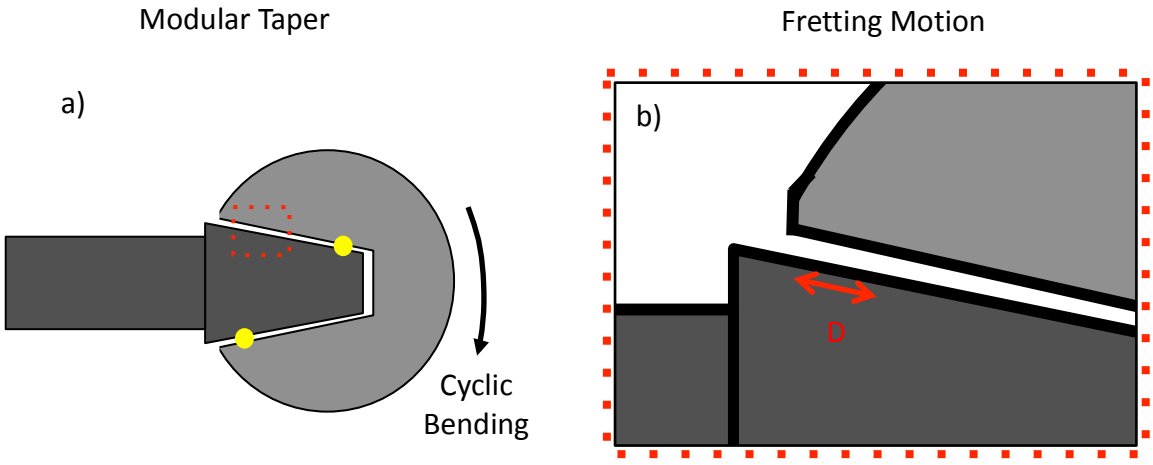

Figure 2-17: Schematic representation of the modular taper interface. a) Elastic strain associated with bending, in conjunction with rigidly connected contact point (yellow spheres) giving rise to elastically based displacements b) which depends on the bending stress, modulus and distance form the rigid contact*.

If we assume that that there are two points within the taper that are rigidly connected to the opposing surface (circular regions) then the elastic strain associated with cyclic bending will result in displacement (**D**). For typical tapers in use today this displacement has been calculated to be within the range of 20-40 µm (Gilbert, 2012). Elastic deformation therefore, can be solely responsible for fretting displacements without the need for rigid body displacement of the taper junction and its important to remember that flexural rigidity is a contributing factor to the extent of fretting displacement as it directly affects elastic deformation. For example, materials with a higher modulus such as CoCr alloys or larger diameter tapers will have less elastic-based fretting motion secondary to their higher flexural rigidity.

* Image modified from Gilbert, J.L. & Sachin, A.M. 2012. *Degradation of implant materials,* New York, Springer Science.

If we look closely at the taper interface, there is asperity to asperity contact taking place between the metal and the oxide surfaces (Figure 2-18) and within this asperity contact region there is enough space for crevice and solution ingress to develop.

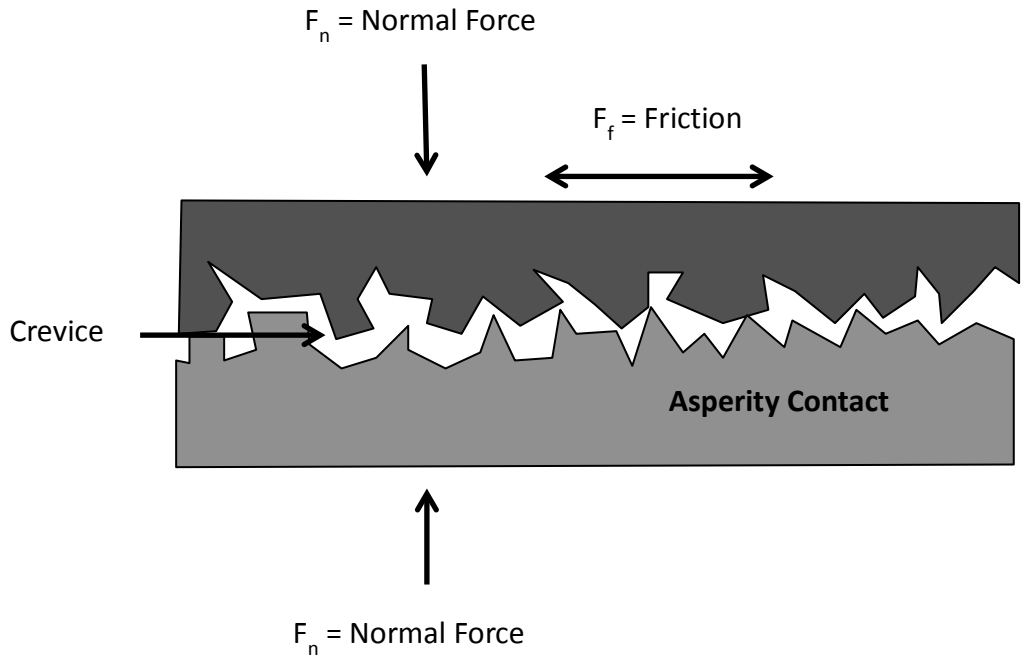

Figure 2-18: Schematic representation of the inner surface of the modular taper interface*.

During loading, mechanical processes including wear (fretting or otherwise), surface deformation or bulk deformation acting at this junction can result in the disruption of the passive oxide film and generation of oxide debris. A number of mechanical factors relating to oxide film stability have an impact on the mechanical disruption of this passive oxide film. These include; the hardening behaviour of the substrate and oxide layer; the oxide adherence to the substrate and the fracture strain/stress in the oxide film (resulting form the lattice mismatch between the oxide and the metal) (Gilbert, 2012). At this point it should also be noted that the fretting resistance of Ti alloy surfaces is

* Image modified from Gilbert, J.L. & Sachin, A.M. 2012. *Degradation of implant materials,* New York, Springer Science.

relatively poor compared to CoCr or SS alloys as its easier to abrade the oxide film off the Ti alloy compared to CoCr or SS alloy surfaces.

As the moving asperity is scraping oxide film from the metal surface, oxide debris is released resulting in two basic oxidation reactions. These include; the ion dissolution reaction (Equation 8), which releases metal ions into the crevice solution and the oxide film repassivation reaction (Equation 9), which generates the oxide, and releases hydrogen ions into the crevice solution (Figure 2-19).

(8) Metal dissolution: $\mathbf{M \rightarrow M^{(n+)} + ne^-}$

(9) Oxide film repassivation: $\mathbf{M + nH_2O \rightarrow MO_n + 2nH^+ + 2ne^-}$

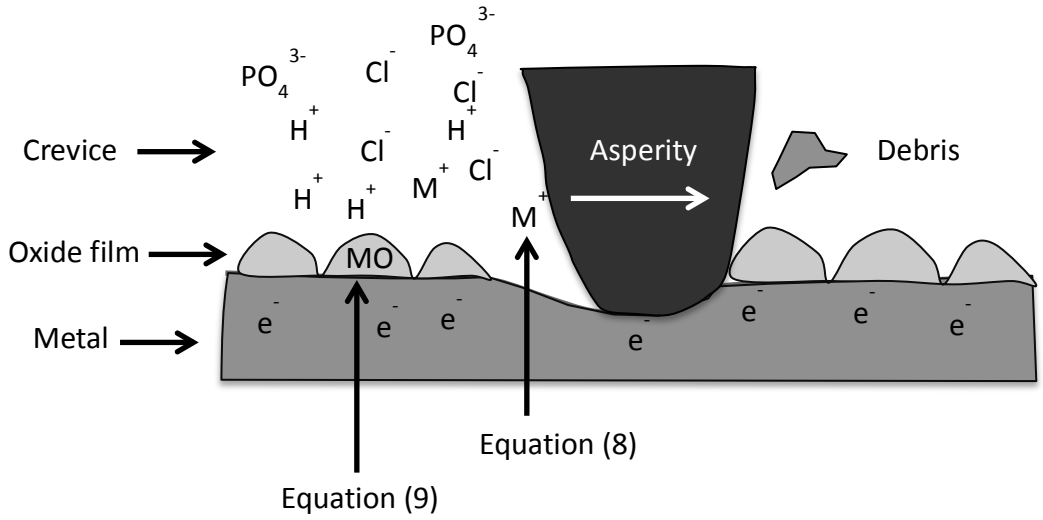

Figure 2-19: Schematic representation of an asperity moving across a metal-oxide surface – showing the formation of oxide debris and the electrochemical reactions leading to the reformation of the oxide layer and the dissolution of metal ions into the crevice solution*.

* Image modified from Gilbert, J.L. & Sachin, A.M. 2012. *Degradation of implant materials,* New York, Springer Science.

Both reactions generate an excess of electrons that remain for a period of time within the metal and their effect is to lower the overall potential of the metal being corroded. Electrons are consumed by reduction reactions (Equations 2-4) giving rise to a transient electric field that can propagate away from the surface. Additionally an influx of anions, primarily chloride (Cl^{-}) and phosphate (PO_4^{3-}) ions are drawn into the crevice solution, to balance the charge disparity and maintain, "charge neutrality". These reactions in combination with the generation of hydrogen ions (H^{+}) from the oxide film repassivation reaction result in a significant drop in the pH of the crevice solution. In the presence of crevice geometry with restricted fluid access (as is the case with head-neck taper junctions) this may result in a highly aggressive acidic solution and therefore, in a continuous corrosion process even after the fretting motion has ceased (Gilbert, 2012).

Oxide film repassivation shuts down the corrosion process and it normally occurs within milliseconds. However, electrochemical processes associated with repassivation that ultimately lead to pH changes and negative potential excursions result in an oxide film that is unstable and one that will not reform once abraded (Goldberg, 2004, Goldberg et al., 1997a, Venugopalan et al., 2000). Under these conditions the underlying metal will continue to actively corrode even after the mechanical stimulus is removed (Gilbert et al., 2009b). However as long as metallic biomaterials experience stresses, abrasion, crevices and biological fluids, corrosion processes will continue to be a significant issue. In the biological system therefore, biotribocorrosion is the term given to the process of corrosion assisted by mechanical wear and influenced by the surrounding biological environment.

2.3.4.18. Testing of Mechanically Assisted Crevice Corrosion

In order to investigate the processes taking place during MACC a number of tests have been developed. These tests simulate the *in-vivo* loading and electrochemical

environments modular hip connections are subjected to and measure corrosion using a three-cell electrode system whereby a Counter Electrode (CE) is used to polarize an electrochemical cell and current/potential of the test sample (Working Electrode, WE) is measured against that of a Reference Electrode (RE) (Goldberg and Gilbert, 2003, Zhu and Windler, 2003, ASTM F897, 1998, ASTM, 2009). The Open-Circuit Potential (OCP) of the cell, is the sample's rest potential and when monitored over time it gives an indication of the sample's corrosive nature (Mroczkowski et al., 2006, Goldberg and Gilbert, 2003). Although electrochemical methods provide useful comparative measures of an implants susceptibility to corrosion, they are limited in that they cannot provide absolute measures of corrosion non-the less they are able to provide some insight into the MACC processes occurring at the modular tapers.

Pitting can be electrochemically induced in a potentiodynamic cyclic polarization test (pitting scan), whereby an implant is subjected to a stepwise increase in anodic potential and the current is measured. Initially, at low potentials, anodic polarization results in a modest increase in current until the pitting potential is reached producing a sharp increase when pits are formed. The implant is further anodically polarized beyond the pitting potential before the potential is reversed in the cathodic direction. If the implant has undergone pitting, a hysteresis loop is seen whereby the cathodic curve crosses the anodic curve (ASTM, 2004). The point at which the cathodic curve crosses the linear segment of the anodic curve represents the protection potential (Khan et al., 1996). The area of the hysteresis loop seen indicates the amount of pitting corrosion that has taken place.

The "Scratch Test" method looks at the effects of contact stress and potential on the abrasion behaviour of oxide-film covered alloys (ASTM F897, 1998) (Goldberg and Gilbert, 2004, Goldberg et al., 1997b). This test involves the application of a scratch of

known length on the surface of a potentiostatically held passive metal immersed in a physiological solution. The transient current associated with oxide film disruption can then be monitored under varied conditions (e.g. varied load at a fixed potential and varied potential at a fixed load). The main limitation of the "Scratch Test" is the rate of scratching which may not be high enough to fully abrade the surface before repassivation takes place, hence underestimating current densities. However used as a comparative means the "Scratch Test" can systematically assess MACC by evaluating mechanical, electrical and chemical aspects of the corrosion process.

"*In-Vitro* Fretting Corrosion Test" method is another testing method used to evaluate modular connections (Goldberg and Gilbert, 2003, Fleming et al., 1994, Brown et al., 1997). This test isolates the modular taper junction (where fretting crevice corrosion occurs) from the rest of the component. Using the three-cell electrode system the electrochemical response to cyclic mechanical loading can be monitored whilst the sample is immersed in a physiological solution. These monitored current and potential changes can determine the mechanical conditions whereby fretting crevice corrosion takes place. Fretting currents are sharp changes in the measured current caused by mechanical disruption of the passivation layer. During sinusoidal cyclic loading of a modular implant, the monitored current observed is in phase with the loading cycle. The peak-trough current range indicates the magnitude of fretting taking place (Goldberg and Gilbert, 2003). During potentiostatic tests, a gradual increase in the average current over a period of cyclic loading indicates that there is increasing disruption of the passivation layer, which is a vital prerequisite to corrosion. On the other hand, a gradual decrease in current indicates that the modular interface has become less susceptible to corrosion following cyclic loading.

Further details regarding electrochemical potentiostatic and potentiodynamic tests will be provided in Chapter 3.

2.3.5. Clinical Context of Corrosion

Although the process of corrosion occurs in all passivating alloys used in orthopaedics, the main reason why corrosion in modular tapers was not identified before their introduction is because mechanical loading was not included as part of their testing process. The high cyclic mechanical loads/stresses these devices are subjected to (which can be several times the weight of the patient at 1-2 million cycles/year) influence the electrochemical driving forces of corrosion through oxide disruption processes. Therefore, much of what we know about in-vivo corrosion of metallic biomaterials comes from retrieved studies of modular THRs in the presence of mechanical factors. It is now well recognized that modular junctions are often a focus area for MACC, a term used to describe all mechanisms that combine mechanical factors and electrochemical factors that ultimately increase the rate of corrosion. This includes processes such as wear, fretting, crevice and galvanic corrosion that eventually lead to the failure of materials and release of particles into the effective joint space (Kop et al., 2012, Kop and Swarts, 2009).

Early reports of corrosion affecting modular implants demonstrated that evidence of crevice corrosion was present in every alloy combination however it seemed to be more prevalent in mixed alloy combinations (Levine and Staehle, 1977). This notion was further supported by retrieval work looking at combinations were Ti-6Al-4V stems were used with CoCrMo heads (Cook et al., 1994a, Collier et al., 1991, Collier et al., 1992b). Indeed, Collier et al. (1992) postulated that in mixed alloy systems, the "galvanic

stimulus accelerated the rate of crevice corrosion" in a time-dependent fashion (Figure 2-20).

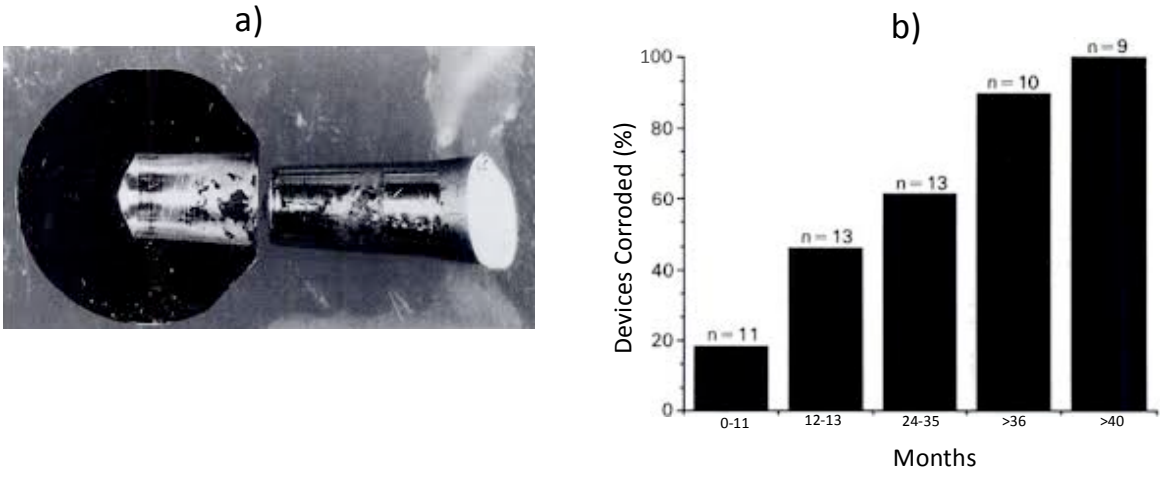

Figure 2-20: a) Dismantled retrieved prosthesis following 28 months of implantation comprising of a Co-alloy head taper (cut in half) and a Ti- alloy stem taper (rotated 180^0) to show matching corroded taper surfaces (x1.25). b) Bar graph showing the relationship between the percentage of corroded mixed-alloy prostheses and time of implantation [*].

Despite the growing consensus that the presence of dissimilar metals enhanced the rate at which corrosion occurred other retrieval studies around the same time began to show that corrosion within these modular interfaces was not limited to dissimilar metal combinations (Bauer et al., 1992, Gilbert et al., 1993, Matheisen et al., 1991). Analysis of 108 modular THRs revealed evidence of wear and corrosion in 7% of similar metal and 34.5% of mixed metal implants following 25 months of implantation (Cook et al., 1994b). This wear and corrosion seen was attributed to a combination of fretting, crevice and galvanic corrosion. It was hypothesised that the fretting (micromotion at interfaces) led to the breakdown of the passive oxide film on the surface of the alloy, making it more

[*] Image taken from Collier, J.P. Surprenant, V.A. Jensen, R.E. Mayor, M.B. Surprenant, H.P. Corrosion between the components of modular femoral hip prostheses. J. Bone Joint Surg (Br) 1992 Vol 74. Issue 4 p511-517. Reproduced with permission and copyright © of J. Bone Joint Surg (Br)

susceptible to crevice and galvanic corrosion (Gilbert JL and Sachin, 2012). The importance of fretting corrosion and its role in initiating corrosion and accelerating crevice corrosion at the head-neck modular interface was also evidenced in a retrieval study by Brown et al. (1995) who looked at 79 retrieved modular THRs and evaluated the incidence and nature of corrosion using SEM (Brown et al., 1995). In their 1991 paper, Collier et al. discussed the possibility of fluid infiltration into the crevice formed between the head taper and the neck taper, and its potential as a corrosion site if "sufficiently narrow to maintain a stagnant zone" (Collier et al., 1991). With corrosion, the oxygen within the stagnant area of fluid on the surface of the metal would become depleted, and as a result the crevice fluid would contain an excess of positively charged metal ions. Negatively charged chloride ions would migrate into the fluid and the resulting hydrochloric acid and low pH exacerbate focal corrosion by beginning to dissolve the metal and more of its passive film. Gilbert et al. (1993) looked at the head-neck interface of 148 retrieved modular THRs of similar and mixed alloy combinations and identified evidence of fretting and crevice corrosion in 16-35% of prostheses (Gilbert et al., 1993). Their findings suggested that the restricted crevice conditions seen at the taper interface in conjunction with mechanical factors such as cyclic loading and fretting could lead to the repetitive fracture and abrasion of the protective passive oxide film on the surface of the metal alloy and ultimately affect the mechanical integrity of the implant (Figure 2-21). Fretting involves more severe mechanical damage to the metal surface with deep surface asperities beyond the passive layer providing further isolated electrochemical environments for pitting corrosion to occur. Once fretting has been initiated, the corrosion processes may continue in the absence of loading (Goldberg and Gilbert, 2003).

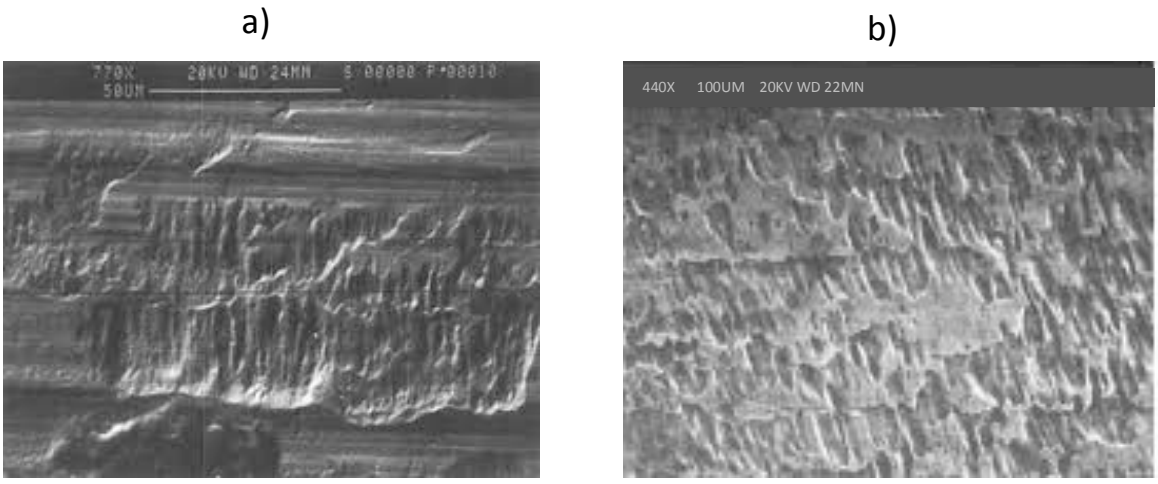

Figure 2-21: a) SEM image of Co-alloy head taper from same metal alloy prosthesis showing the presence of fretting attack. The fretting pattern is seen to be perpendicular to the machining scratches, which run horizontally and is caused by small-scale cyclic motion of the head relative to the neck. b) SEM image of a Ti-alloy neck taper from mixed metal alloy prosthesis showing corrosive attack of the Ti alloy. The orientation of the attack is perpendicular to the remnant machine scratches seen to be running horizontally suggestive of the possible influence of motion along the neck taper*.

Modular junctions are designed to be free of movement in-vivo, and indeed the success of a self-locking taper is influenced by the design of the taper, particularly the taper angle, the roughness, and the mating materials between the "head" and "neck" components (Figure 2-22). However, taper tolerances in terms of cone diameter, cone angles and surface roughness allow for a degree of fretting, of the head taper relative to the neck during cyclic loading, leading to further acceleration of crevice corrosion.

* Image taken from Gilbert, J.L. Buckley, C.A. Jacobs, J.J. In vivo corrosion of modular hip prosthesis components in mixed and similar metal combinations. The effect of crevice, stress, motion, and alloy coupling. J. Biomed Mat Res. 1993 Vol 27. Issue 12 p1533-1544. Reproduced with permission and copyright © of J. Biomed Mat Res.

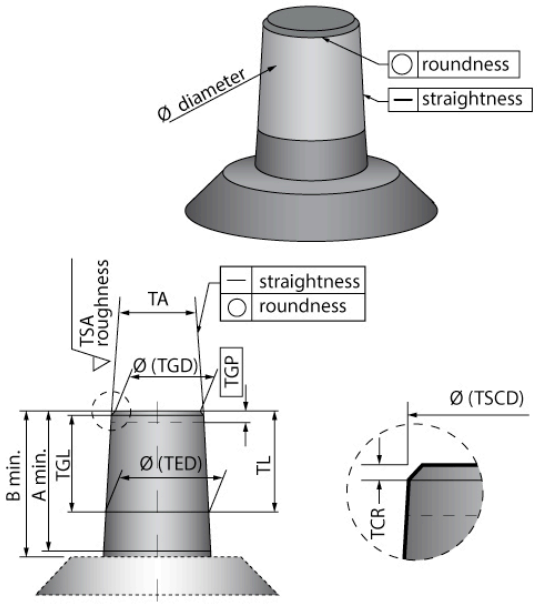

Abbreviation	Description
TGP	Taper gage plane
TGD	Taper gage diameter
TA	Taper angle
TL	Taper length
TCR	Taper chamfer/radius
TSR	Taper surface roughness
TS	Taper straightness
TR	Taper roundness
TGL	Taper gage length
TED	Taper end diameter
TSCD	Taper sharp corner diameter

Figure 2-22: Characteristics of a neck taper*.

In the last two decades, manufactures have been altering femoral neck tapers from 11/13 to 12/14 to 14/16 (Figure 2-23) with the 12/14 taper being the most popular.

Figure 2-23: Image depicting different taper designs by manufacturers†.

* Image taken from Scheuber L, Usbeck S, Petkow F. The Neck Taper in Hip Arthroplasty-What does the surgeon have to consider? CeramTec Publication, CeraNews 1/2014 © of CeramTec.
† Image taken from McTighe T, Brazil D, Clarke I, Keppler L, Keggi J, Tkach T, McPherson E Metallic Modular Taper Junctions in Total Hip Arthroplasty. Recostructive review 2012. Vol2 No. 2 © of Reconstructive review.

However, within commercially available hip systems from the same or different manufacturer taper angles, component tolerances and sizes differ (Figure 2-24).

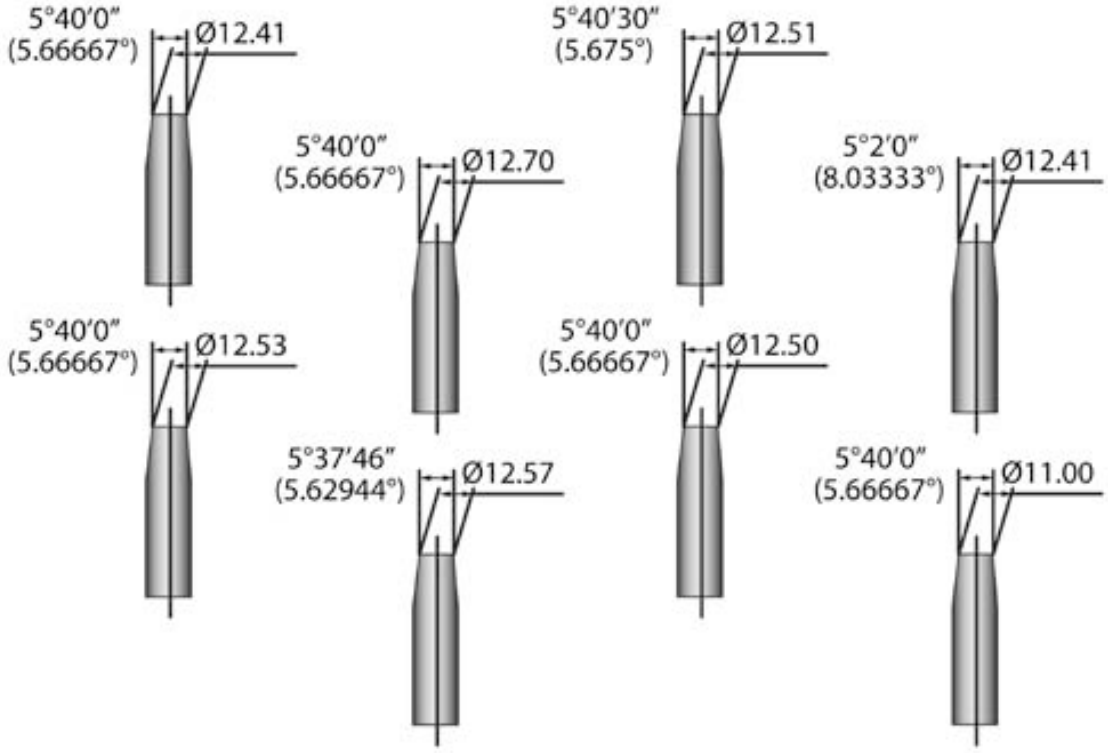

Figure 2-24: Different designs of 12/14 neck tapers*.

Shareef and Levine (1996) explored the effect of manufacturing tolerances on the degree of micromotion, finding that generally "the magnitude of micromotion at various interfaces increased between 4 and 16% with increasing values of angle tolerance" (Shareef and Levine, 1996). Recent studies of retrieved tapers show evidence of etching and delamination at these interfaces, suggesting some microscopic movement at the interface (Rodrigues et al., 2009). Furthermore, corrosion at the interface may lead to

* Image taken from Scheuber L, Usbeck S, Petkow F. The Neck Taper in Hip Arthroplasty-What does the surgeon have to consider? CeramTec Publication, CeraNews 1/2014 © of CeramTec.

increased instability and micromotion, making them further susceptible to abrasive wear (Meyer et al., 2012). Various cases of spontaneous dissociation of the head–neck junction have been recently noted in the literature in association with corrosion at the interface (Talmo et al., 2014). Although manufacturing tolerances were tightened following identification of severe corrosion and wear with the use of large-diameter heads, they still remain an issue.

Recent retrieval studies have focused on the modular head-neck junction of LH-MoM-THRs and have shown unexpectedly high levels of corrosion relative to conventional THRs (Bolland et al., 2011, Langton et al., 2011, Langton et al., 2012, Nassif et al., 2014). The identification of a significant amount of metal debris arising from the modular head–neck interface of LH-MoM-THR has led to increased interest in the effect of the size of the femoral head. *Dyrkacz* (Dyrkacz et al., 2013) recently described a series of retrieved LH-MoM-THRs and noted that larger heads (> 36 mm) had more corrosive damage at the modular junction than smaller (28 mm) heads. They suggested that larger heads create greater torque, which is transmitted to the head-neck interface, leading to increased micromotion, deterioration of the protective oxide film and MACC. Most recently the use of large diameter femoral heads in conjunction with crossed-linked polyethylene has shown similar effects. *Cooper* (Cooper et al., 2012) investigated patients who underwent revision for corrosion at the modular head-neck interface of MoP THAs. The high torque generated at the bearing surface is not only a function of large head size but may also be associated with edge loading, the mal-alignment of components (Morlock et al., 2008, Lavigne et al., 2011) and poor lubrication. In an *in vitro* study *Bishop* (Bishop et al., 2013) showed a twofold increase in friction moments for metal bearings, which translates to a joint friction moment of 11.8 Nm for a 48 mm diameter head in dry conditions compared with one of 7 Nm, which is adequately lubricated. Another factor

that may be enhancing micromotion at the taper interface of LH-MoM-THRs is the generation of a high bending moment at the modular junction. An increased bending moment may be associated with a varus stem and an inappropriate relationship between the centre of the femoral head and its modular junction. The latter may be associated with 'overstuffing' of the joint or if a large femoral head is used and the femoral taper is not centrally placed (Langton et al., 2012).

Retrieval analysis has concluded that corrosion at the taper interface is due to a mixture of different modes of failure. As it is often difficult to differentiate between them they are now generally known as MACC. The process of MACC leads to the production of wear debris and metal ion release (Gilbert et al., 1994, Goldberg et al., 1997a). These by-products of MACC can migrate locally and systemically resulting in elevated serum metal ion levels thought to initiate a cascade of events leading to the presence of adverse local tissue reactions (Fricka et al., 2012, Meyer et al., 2012, Cooper et al., 2012) systemic toxicity, muscle atrophy, the development of pseudotumours and osteolysis (Doorn et al., 1996, Campbell et al., 2010, Donell et al., 2010). These effects are all frequently identified as causes for failure and revision of MoM hip replacements (Cooper et al., 2012, Bolland et al., 2011, Polyzois et al., 2012, Jacobs et al., 1995).

2.3.6. Local and Systemic Consequences of Corrosion

The products of corrosion generated at the head-neck interface vary in size from < 1 to 500 micrometres (Jacobs et al., 1995). Most particulate debris is < 5 micrometres in size, plate-shaped and similar, regardless of the material combination used (Jacobs et al., 1995, Urban et al., 1997). The most abundant particles produced are chromium orthophosphate and mixed oxides, as well as chlorides of chromium, molybdenum and Ti (Jacobs et al., 1995). The biological response to these corrosion products is similar to

that produced by bearing surface metal debris (Cooper et al., 2012), but there is evidence suggesting that they may be more biologically active, possibly as a result of higher concentrations of ionised particles (Langton et al., 2013). They trigger an immune response comprising macrophages, giant cells and lymphocytes, leading to localised soft-tissue ARMD (adverse reaction to metallic debris) (Figure 2-25) and periarticular osteolysis (Bauer et al., 2014) (Figure 2-26). Many have classified the physiological response as a characteristic Type IV Hypersensitivity reaction; leading to subsequent osteolysis and in some cases the formation of pseudotumours (Malviya and Holland, 2009, Goldberg et al., 2002, Cooper et al., 2012) (Figure 2-27). High levels of metal ions, released by corrosion of surfaces and particulate debris, can be detected in blood and urine while the toxic effects may be seen systemically (Urban et al., 1994, Polyzois et al., 2012, Jacobs et al., 1995).

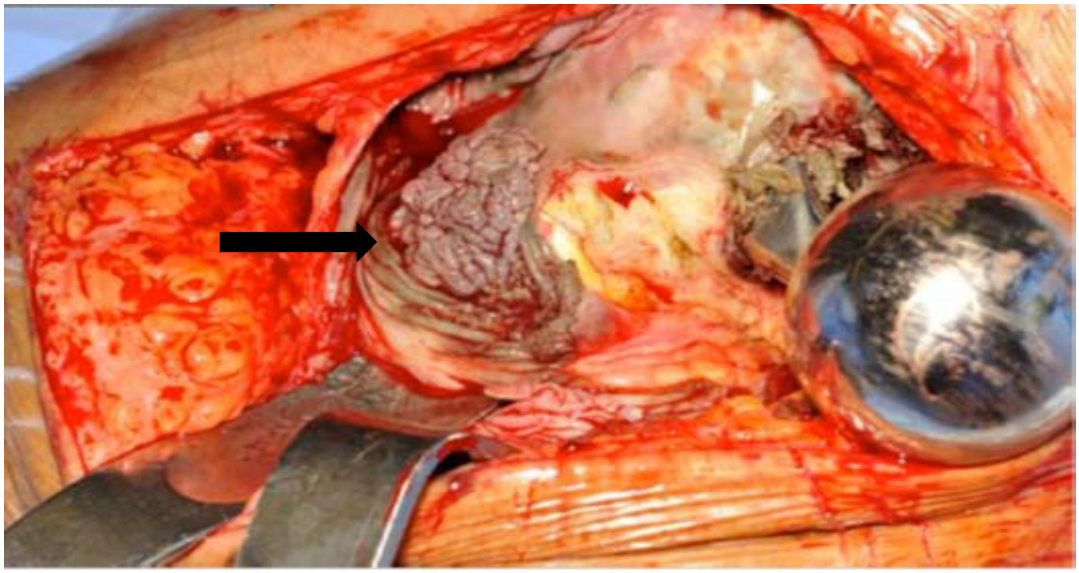

Figure 2-25: Mass of necrotic tissue (arrow) identified at the time of revision surgery around the proximal femur associated with ARDM*.

* Image taken from McTighe T, Brazil D, Clarke I, Keppler L, Keggi J, Tkach T, McPherson E Metallic Modular Taper Junctions in Total Hip Arthroplasty. Recostructive review 2012. Vol2 No. 2 © of Reconstructive review.

Figure 2-26: Lateral radiograph of a MoM THR demonstrating progressive proximal osteolysis (arrow)*.

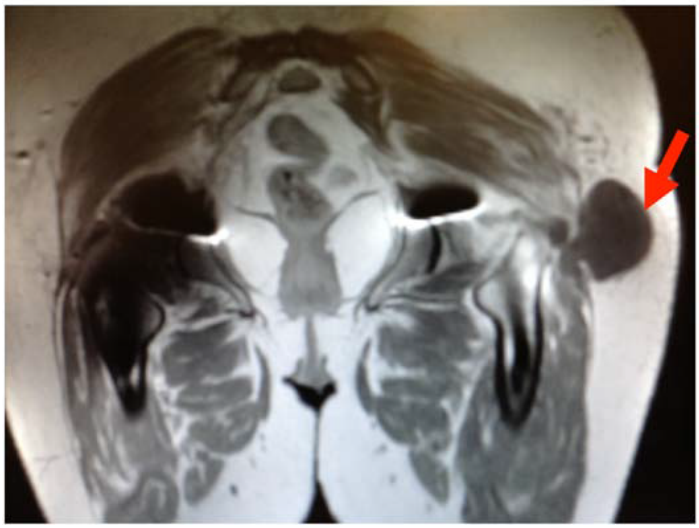

Figure 2-27: Magnetic resonance image depicting a pseudotumour (arrow) adjacent to a MoM hip prosthesis originating from the abductor muscles†.

* Image taken from McTighe T, Brazil D, Clarke I, Keppler L, Keggi J, Tkach T, McPherson E Metallic Modular Taper Junctions in Total Hip Arthroplasty. Recostructive review 2012. Vol2 No. 2 © of Reconstructive review. Courtesy of Mr. A. JohnMB BS, FRCS, FRCS, UniversityHospital of Wales

† Image taken from McTighe T, Brazil D, Clarke I, Keppler L, Keggi J, Tkach T, McPherson E Metallic Modular Taper Junctions in Total Hip Arthroplasty. Recostructive review 2012. Vol2 No. 2 © of Reconstructive review. Courtecy of E. Smith.

There is concern regarding the systemic distribution of submicrometer-sized particulate debris and metal ions, which have been discovered in organs such as the liver, spleen, abdominal lymph nodes and placenta of patients with THAs (Urban et al., 2000, Ziaee et al., 2007). The potential for carcinogenicity has been demonstrated (Dunstan et al., 2008). Nevertheless, population-based studies are yet to establish a causal association with any malignancy (Nyrén et al., 1995, Smith et al., 2012a). Cobalt toxicity is an extremely rare phenomenon associated with THA (Mao et al., 2011).

2.3.7. Summary of Literature Review

There has been widespread concern about the adverse soft-tissue reactions after MoM total THRs (Crowninshield et al., 2004 , Langton et al., 2010, Langton et al., 2013). These changes have been described by various authors as pseudotumours, aseptic lymphocytic vasculitis-associated lesions (ALVAL) and metallosis (Haddad et al., 2011, MHRA, 2012). Due to their widespread use, most of these adverse incidents were associated with resurfacing hip replacements, however a number of research studies indicated that LH-MoM-THRs were of even greater concern.

The 8th Annual report of the National Joint Registry for England and Wales revealed that LH-MoM-THRs had the highest failure rate of all hip replacement procedures (Smith et al., 2012b). An important difference between MoM resurfacing and LH-MoM-THR is the modular head-neck taper junction which has been shown to be susceptible to MACC and fretting corrosion, leading to the production of wear debris and metal ion release (Gilbert et al., 1994, Goldberg et al., 1997a). However, although taper corrosion was initially linked to modular MoM components or those with larger diameter femoral heads, the issue did not seem to be solely restricted to these components with recent evidence of taper corrosion with ALTR and elevated serum metal ions in modular MoP

and modular CoP THAs (Rasquinha et al., 2006, Goldberg et al., 2002, Cooper et al., 2012, Kurtz et al., 2013, Whitehouse et al., 2015).

Although retrieval studies have identified the head-neck modular junction as a significant source of wear debris and metal ion release, to date few studies have investigated the factors that contribute to wear and corrosion at the taper junction. It is important to gain a full and in depth understanding of the factors that are critical in determining corrosion and wear at the taper junction in order to identify the ideal parameters and create the 'ultimate' taper junction.

Chapter 3 Methodology and Surface Analysis Techniques

3.1. Introduction

This chapter outlines the main experimental procedures used to quantify the effect of MACC at the head-neck modular junction under experimental conditions and to validate and relate these measurements to fretting corrosion seen with in vivo retrievals and autopsy specimens. In order to do this the morphology of the surfaces, which are associated with MACC are assessed and measured. In vitro simulator tests are carried out, which attempt to replicate MACC and the morphology of the taper surface and the amount of material loss are validated against these measurements. Methods of sample preparation, electrochemical measurements and surface analysis of the taper junction are covered by this chapter, such methods will be used throughout my thesis in order to measure, describe and quantify MACC.

3.2. Experimental Materials

3.2.1. Components Tested

Throughout the study a combination of head and neck taper components were utilised, varying from in house manufactured head/neck tapers (coupons), brand new implants from well known manufacturers and retrieved prostheses that had been in situ for at least 12 months.

3.2.1.1. Head and Neck Taper Coupons

In this study, two commonly used biomaterial alloys were utilised to manufacture the head and neck taper coupons. Wrought CoCrMo (ASTM F1537, 2011) and Ti-6Al-4V (ASTM F136, 2013) alloys were purchased from Firth Rixson Metals Limited (Sheffield,

S35 9XH, UK) and Sundvik Bioline UK (Sheffield, S20, 1DJ, UK) respectively and their chemical composition is shown in Table 3-1.

	Chemical Composition (% wt.)							
	C	**Mn**	**Cr**	**Fe**	**Mo**	**Ni**	**Co**	**Si**
Wrought CoCrMo	0.047	0.76	27.60	0.50	5.51	0.40	Balance	**0.71**

	C	**Ti**	**Al**	**Fe**	**V**	**N**	**O**	**H**
Wrought Ti-6Al-4V	0.015	Balance	6.10	0.13	4.00	0.008	0.106	0.004

Table 3-1: Chemical composition of alloys tested in this study.

All head and neck tapers were manufactured to a single specification using conventional machine centre with a constant cutting speed. The R_z and R_a values for each component were assessed using a Talyrond 365 (Taylor Hobson, Leicester, UK) roundness-measuring instrument. Average roughness R_a is the arithmetical mean of the absolute values of the profile deviations from the mean line. The R_z value is the highest peak to valley value measured within each cut-off distance and is averaged over five consecutive cut-off values (ISO/CD 4287, 1997). The recommendation by CeramTec (Ceramtec Ltd Baden-Württemberg, 73207, Germany) for neck taper surface roughness to be used with a ceramic head is between 6µm and 20µm, and the majority of manufacturers have adopted this range for use with metal heads.

In order to capture the extreme ends of the range, neck tapers were divided into two groups: 1) 'Smooth' surface finish with an R_z range of 3-6µm and 2) 'Rough' surface finish with an R_z range of 16-20µm. The average R_z value of the smooth neck tapers used was 3.82µm, and for the rough neck tapers this was 16.58µm. The average R_a value of

the smooth and rough neck tapers was 0.81µm and 4.14µm, respectively. All neck taper coupons had a 12/14 taper with a cone angle between 5° 37′ 30″ to 5° 42′ 30″. A further division relating to the taper surface area in contact resulted in two additional groups: 1) tapers with full length taper contact were termed 'Standard' neck tapers and 2) tapers with reduced length taper contact were termed 'Short' neck tapers. Figure 3-1 illustrates the taper angles and locking zones along the tapers, the reference diameters of the head and neck tapers are not the same size and they are referenced at two separate points along the taper axis. What this means is that the taper engages much deeper in relation to the 12mm dimension mentioned. In fact, when fully impacted the large diameter of the short taper sits approximately 3.2mm inside the female bore which is reduced by 0.5mm due to the small chamfer in the female bore. Therefore, the total engagement length is 14.7mm and 12.0mm for standard and short tapers respectively. This results in just over 18% difference in the amount of taper engaged. The neck taper coupons were made from both wrought CoCrMo (ASTM F1537, 2011) and Ti-6Al-4V (ASTM F136, 2013) alloys.

All head coupons had a 12/14 taper with a cone angle 5° 43′ 30′′ and were made from wrought CoCrMo alloy (ASTM F1537, 2011) with smooth taper finishes (R_a and R_z values 0.58 and 2.8µm respectively). They were modified to incorporate serrations onto the bearing surfaces for reasons later explained.

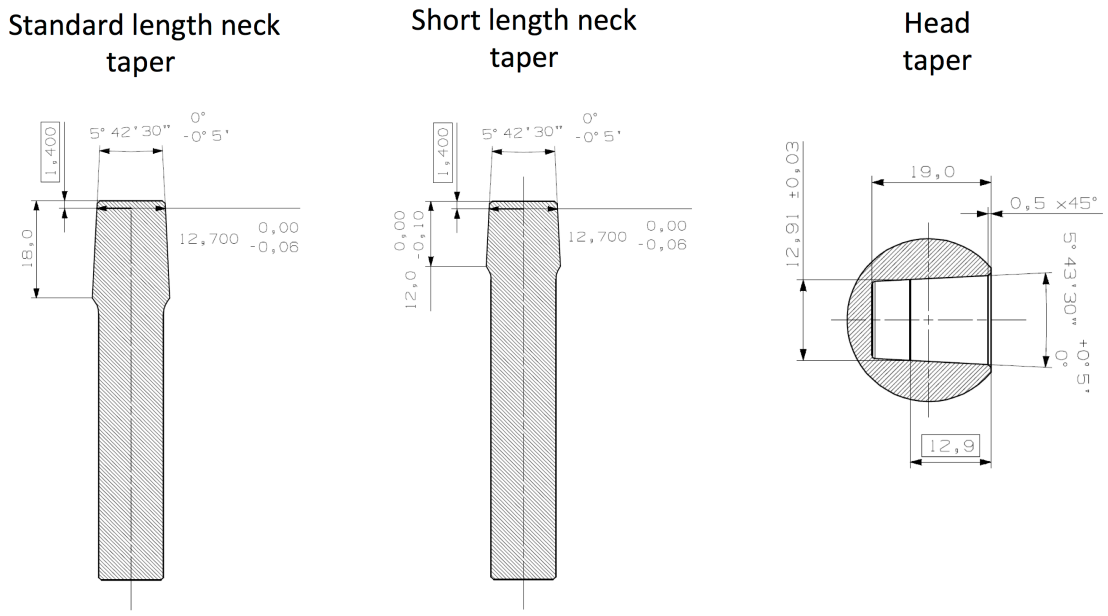

Figure 3-1: Diagram illustrating dimensions for the standard length neck taper, short length neck taper and head taper used in the study.

3.2.1.2. Implants

Brand new implants from well known manufacturers utilised in this study for in-vitro hip simulation testing included: '*Metasul*' CoCrMo femoral heads (Zimmer, Inc. Warsaw, Indiana) (36mm and 28mm diameter), '*Endo Head*' CoCrMo femoral head (Medacta International SA, Strada Regina, Castle San Pietro, CH-6874) (40mm diameter), '*Biolox Delta*' ceramic femoral heads (Ceramtec Ltd Baden-Württemberg, 73207, Germany) (28mm diameter), '*CPT*' CoCrMo and CLS Spotorno Ti-6Al-4V stems (Zimmer, Inc Warsaw, Indiana) and '*QADRA-S*' Ti-6Al-7Nb (titanium niobium alloy) stems (Medacta International SA, Strada Regina, Castle San Pietro, CH-6874). All heads had a smooth finished 12/14 taper with a cone angle 5° 43' 30'' and a variable neck offset which will be addressed in each relevant chapter. The head diameter variability will also be addressed in each relevant chapter. All stems had a 12/14 taper, 0 offset and a neck angle of 135°. Taper details of the implants tested are given in Table 3-2.

	Implant	Material Composition	12/14 taper	Diameter (mm)	Cone Angle (degrees)	Offset	Neck Angle (degrees)
Head Taper	Metasul	CoCrMo	✓	28	5°43′30′′	+8	-
	Metasul LDH	CoCrMo	✓	36	5°43′30′′	Zero	-
	Endo Head	CoCrMo	✓	40	5°43′30′′	+10.5	-
	Biolox Delta	82%$Al2O_3$, 17%ZrO_2, 1%SrO	✓	28	5°43′30′′	Zero	-
Neck Taper	CPT	CoCrMo	✓	-	5°42′30′′	Zero	135°
	CLS Sportono	Ti6Al4V	✓	-	5°38′30′′	Zero	135°
	QADRA-S	Ti6Al7Nb	✓	-	5°42′30′′	Zero	135°

Table 3-2: Brand new implants from well known manufacturers used in in-vitro hip simulation testing.

3.2.1.3. Retrievals

Retrieval analysis included the first 110 consecutive LH-MoM-THR cases referred to our retrieval laboratory that met our inclusion criteria. To be included, patients must have undergone full pre-clinical assessment, to include Co and Cr blood ion measurement, computer tomography (CT) or plain X-ray imaging to measure cup position, and metal artifact reduction sequence (MARS) magnetic resonance imaging (MRI) to assess the soft tissues. Sufficient clinical data were required to diagnose the reason for revision according to categories used by the National Joint Registry of England and Wales (National Joint Registry, 2013). For purposes of blood metal ion analysis, we required that all prostheses were unilateral. To reduce the confounding effect of bedding-in wear at the bearing surfaces, all implants were in situ for 12 months. Finally only arthroplasties using monoblock cup with a large diameter (>36mm) were included. The

laboratory operates with the approval of the Human Tissue Authority and the local institutional ethical committee. Components were collected from 34 surgeons from 24 hospitals in the UK. Patient demographic data and component details for the 110 cases are given in Table 3-3. The cup and head components were collected in all cases; however, we received only 36 femoral stems, as in most cases the surgeon did not remove a well-fixed undamaged femoral stem. 31 stems were Ti alloy and 5 stems were CoCrMo alloy (Matthies et al., 2013).

	Number	Mean	Median	Range
Gender (male:female)	52:68	—	—	—
Age at primary surgery (years)	—	53.5	55.0	36.0–82.0
Time to revision (months)	—	44.2	45.5	12.0–85.0
Femoral head diameter (mm)	—	46.2	47.0	38.0–60.0
Angle of acetbular inclination (°)	—	43.8	43.0	9.0–66.0
Angle of acetbular version (°)	—	12.5	11.0	29.0 to 57.0
Whole blood cobalt (ppb)	—	19.5	7.6	0.6–237.0
Whole blood chromium (ppb)	—	10.8	3.0	0.4–111.0
Bearing design				
Adept	10	—	—	—
ASR XL	40	—	—	—
Birmingham hip	22	—	—	—
Cormet	8	—	—	—
Durom	12	—	—	—
M2A-Magnum	18	—	—	—
Stem design				
CLS[b]	5	—	—	—
Corail[b]	36	—	—	—
CPCS[a]	7	—	—	—
CPT[a]	6	—	—	—
C-Stem	13	—	—	—
Freeman	6	—	—	—
Taperloc[b]	16	—	—	—
Zweymuller[b]	21	—	—	—

[a]Stem material: cobalt–chrome alloy (Co:Cr:Mo). [b]Stem material: titanium alloy (TiAl6:V4).

Table 3-3: Overview of the patient demographic and component details.*

3.2.2. Machinery

"Talyrond 365": Taylor Rank Hobson Talyrond 365 computer-controlled radial and longitudinal measuring machine (Taylor Hobson, Leicester, UK) was used to measure volume of material loss and characterise the surface finish of head and neck tapers.

* Table taken form Matthies AK, Racasan R, Bills P, Blunt L, Cro S, Panagiotidou A, Blunn G, Skinner J, Hart AJ. Material loass at the taper junction of retrieved large head metal-on-metal total hip replacements. J. Orthop Res. 2013 Nov;31(11):1677-85. Reproduced with permission and copyright © of J. Orthop Res.

"Coordinate Measuring Machine": Zeiss Prismo (Carl Zeiss, Ltd., Rugby, UK) coordinate measuring machine was used to measure the volume of material loss from the bearing surfaces of retrieval components.

"Materials testing machine": Instron Hydraulic tension/compression single-station testing machine (Max load 50kN) (Instron, Norwood, MA, USA) was used to assemble components according to the ASTM F2009 standard at a loading rate of 0.05 mm/s.

"Taper testing machine": A purpose-built 6-station 10kN hydraulic tension/compression testing machine (R.D.P.-Howden, Warwickshire, United Kingdom), capable of producing sinusoidal cyclical loads, was used to apply load during testing.

"Diamond saw" WELL model 3241 exact diamond-bladed bone cutting saw (Harley Instruments, Pune 411009, India). The saw cuts by moving a wire coated with abrasive diamond particles through a sample. A single strand of wire is used, fastened at each end, with a reciprocal movement. In this way, wire welds are avoided eliminating a weak point in the wire and giving smoother cut surfaces. A fine setting to within 10 microns is within its capabilities.

"Scanning Electron Microscope": JEOL JSM-6480LV high-performance (JEOL Inc, CA, USA), Variable Pressure Analytical Scanning Electron Microscope with a high resolution of 3.0nm, along with EDS (Energy Dispersive System) and EBSD (Electron Backscatter Diffraction) using the Oxford Link system.

"Energy Dispersive X-ray Spectroscopy" (EDS): EDS is an analytical technique employed for the chemical characterization of a sample, used in conjunction with SEM. The fundamental principle behind the chemical characterization is the fact that each element has a unique atomic structure. A high-energy beam of charged particles such as

electrons can excite an electron in an orbital shell in the atom, which causes it to move into another orbital shell releasing X-rays of a characteristic energy that can be detected by an energy dispersive spectrometer. This energy is characteristic of the specific element, thus allowing its recognition.

"Stereo microscope": Leitz MZ10 (Leitz, Wetzlar, Germany). Up to 40x magnification utilized for microscopic inspection of corrosion of the surface of retrieval head and neck tapers.

"High-power light microscope": Bruker Contour GT-I 3D Microscopy (Tucson, AZ, USA). Max scan range up to 10nm. Vertical resolution <0.01nm and step height accuracy 8nm and greater. Analysis performed on Vision64 Analysis Software on Windows 7 64-bit OS.

3.2.3. Electrodes and Analysis Software

Throughout the study a 3-cell electrochemical cell was utilized to characterize corrosion at the head neck taper junction and electrochemical measurements were conducted using the Metrohm Autolab PGSTAT 101 multi-channel modular potentiostat/galvanostat (Metrohm Autolab B.V. Rucorn, England) and recorded and analyzed with the aid of the NOVA Software supplied by the same company with all the relevant updates. The following electrode arrangement was adopted:

"Working Electrode (WE)": The working electrode in all experiments was the isolated taper junction (specimen).

"Calomel Reference electrode (RE)": Hg/Hg_2Cl_2 Hanna ® reference electrode for ISE and titration HI-5412 (Hanna instruments, Woonsochet, Rhode Island, USA).

"Platinum/Counter electrode (CE)": Metrohm platinum sheet electrode (Metrohm Autolab B.V. Rucorn, England).

3.3. Component Preparation

3.3.1. Coupon and Implant Head and Neck Taper Analysis

Prior to the start of the study the surface profiles of the head and neck tapers (for both coupons and implants tested) were measured using a computer controlled radial and longitudinal measuring machine (Talyrond 365). The Talyrond 365 is a roundness instrument specifically designed for measurement of circular and cylindrical components. The head and neck tapers were mounted, using custom fixtures, on a rotating air spindle (maximum run out of 20 nm) and were centered and leveled with respect to the spindle axis, allowing vertical measurement traces coincident to the taper axis. A 5-micron diamond stylus collected 180 linear surface profiles (spaced 2° apart), which, were combined into a rectangular surface contour map, and analyzed using a Matlab (Mathworks, Inc., Natick, MA) program to produce a 360° representative volumetric measurement for each individual taper (Figure 3-2).

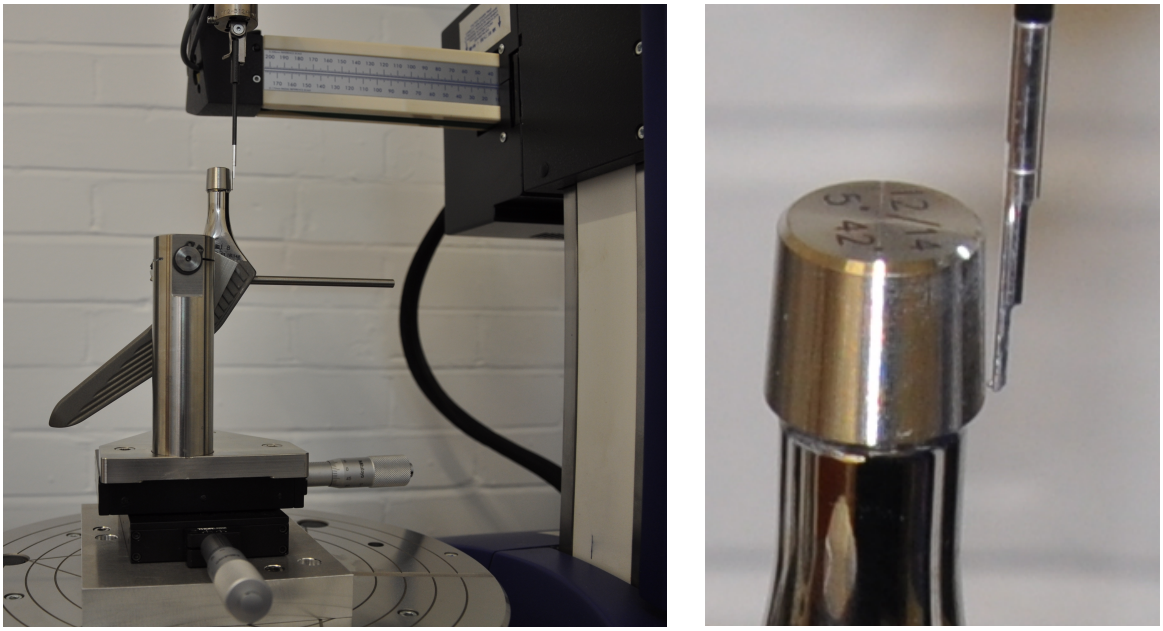

Figure 3-2: Linear profile measurement for surface analysis of neck taper using Talyrond 365.

Each individual taper's pre-test baseline volumetric measurement could then be compared to its post-test volumetric measurement in order to provide an accurate volumetric wear reading (overall volumetric wear sensitivity of 2 mm^3), thus eliminating manufacturing tolerance variability. In addition the Talyrond 365 assessed the taper surface roughness and measured the R_z and R_a values for each head and neck component (surface roughness measurements sensitivity of 1 µm) (as described in section 3.2.1.1). These measurements were used to ensure that the component's surface roughness fell within appropriate tolerances and provided a baseline for later analysis when comparing pre and post-test surface roughness measurements (Figure 3-3).

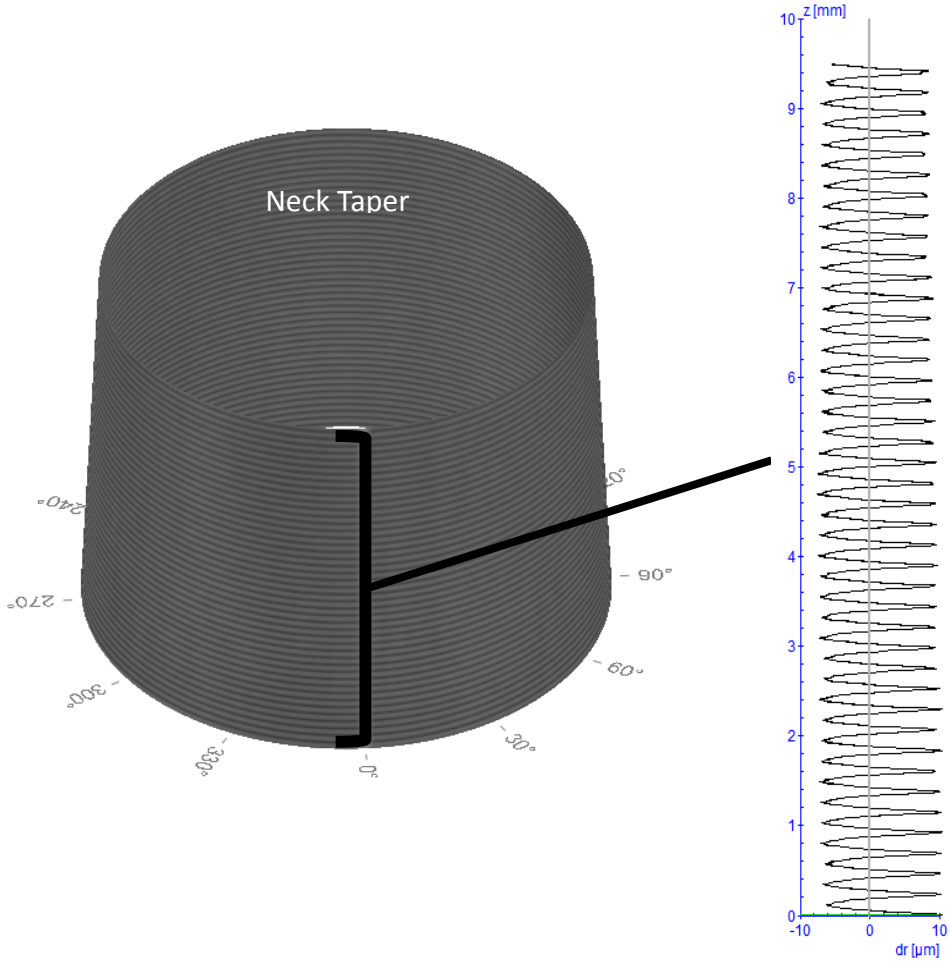

Figure 3-3: Analysis of a single linear profile measurement of a neck taper at 0 degrees showing the surface roughness using Talyrond 365.

Before the start of any surface analysis testing the neck and head tapers were marked for orientation purposes. The markings did not interfere with the taper surface and consisted of two lines, one on the stem of the neck taper and another on the outer rim of the head taper. These markings corresponded to the starting point for each set of surface measurements (i.e. 0° of the surface profile measurements) thus allowing direct pre- and post-test comparison. In addition, during assembly of the head onto the neck the two marking would align and the components would be positioned within the experimental fixture with the markings facing superiorly (always the same orientation). Consequently areas of greater stress within the 4 quadrants of the taper (superior-anterior superior-posterior, inferior-anterior and inferior-posterior) in relation to the load application could be identified during post-test surface profile analysis (Figure 3-4) with further diagrammatic explanations to follow in chapters 6 and 7.

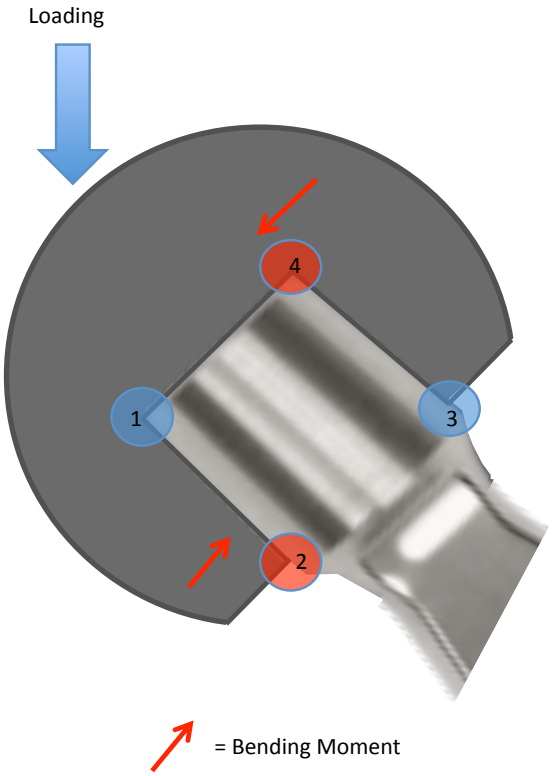

Figure 3-4: Diagrammatic representation of the 4 taper quadrants under stress in relation to the load application.

3.3.2. Retrieval Head and Neck Taper Analysis

Head and neck taper surfaces of retrieved components were also measured using the Talyrond 365 roundness instrument. The head and neck components were mounted on a rotating air spindle and a series of surface linear profiles were taken in the same way as described in section 3.3.1. However calculation of the volume of material loss was more difficult since the original taper volume measurement was not available. For the head taper retrieval once the surface contour map was generated using the method described in 3.3.1 the data were leveled through manual selection of part of the taper that was considered to be the unworn reference surface (Figure 3-5). The surfaces were then digitally regenerated and the volume of material loss calculated using a generated Abbott-Firestone curve. The same method could not be used to calculate the volume loss from the neck taper as in the majority of cases the entire surface of the neck taper engages with the head taper and so a true reference surface is unavailable. For the neck taper therefore, individual areas of material loss were isolated and assessed to give localized volumes of material loss, which were then summed to give the total volume of material loss. A separate Matlab based program was used to calculate the volume of material loss, for which it was required to filter the measured machine-threaded surface texture from the measurement.

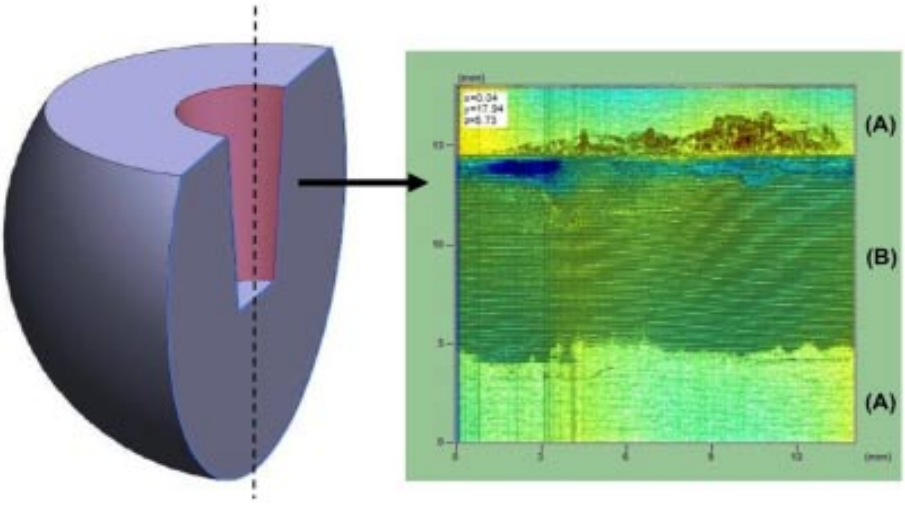

Figure 3-5: Schematic demonstrating the method and analysis of taper surface measurement. The regions labeled (A) represent unworn areas of the head taper. The worn area of the head taper, labeled (B), represents the area engaged with the male taper. *

3.3.3. Retrieval Bearing Surface Analysis

The volume of material loss from the bearing surfaces was measured using a Zeiss Prismo coordinate measuring machine. Measurements were conducted using a 2 mm ruby stylus moving at 3 mm/s using a previously described protocol optimized for accuracy and measurement certainty (Bills et al., 2012). Each surface was digitized using 400 polar scan lines, giving an angular point spacing of 0.9° and a linear point pitch of 0.1 mm. The number of data points obtained for each component was up to 300,000 depending on component diameter and angular coverage. The data were analyzed using an intelligent iterative least square fitting operation. This involved removal of the worn area from the analysis, and the data refitted using the residual area. The data were segmented so that only the unworn geometry was used. This was optimized through use of a fitting algorithm such that the surface fitting standard deviation was minimized (Bills et al., 2012). This method is robust against phenomena such as edge wear, which can adversely affect the resulting wear measurement (Bills et

* Image taken from Matthies AK, Racasan R, Bills P, Blunt L, Cro S, Panagiotidou A, Blunn G, Skinner J, Hart AJ. Material loass at the taper junction of retrieved large head metal-on-metal total hip replacements. J. Orthop Res. 2013 Nov;31(11):1677-85. Reproduced with permission and copyright © of J. Orthop Res.

al., 2012), and allows for accurate repeatable determination of unworn geometry, thus allowing direct determination of linear and volumetric wear and accurate mapping of the material loss distribution. A limitation of this method is that the femoral heads are assumed spherical, therefore it's not accounting for any potential manufacturing form errors. Form error is not determinable ex vivo due to component wear (Bills et al., 2012).

3.3.4. Component Passivation

Prior to the start of each test, all head and neck taper coupons were passivated through immersion in 20% nitric acid for 30 minutes as per ASTM F86-13 (ASTM F86-13, 2013).

3.3.5. Component Cleaning

3.3.5.1. Coupon Tapers and Implant Tapers

Following surface measurements and prior to passivation, the head and neck tapers (coupons and implants) were cleaned in an ultrasonic bath with 10% solution of Decon 90 for 30 minutes, after which, they were rinsed under tap water. Finally they were subjected to further cleaning with distilled water for 30 minutes and then with methylated spirit for another 30 minutes. All cleaned samples were then passivated as described above. Each sample was then placed in an individual polyurethane bag and sealed to avoid further contamination. Upon testing, samples were handled carefully with latex free gloves to prevent contamination of the metallic surfaces.

3.3.5.2. Retrieval Tapers and Head Bearing Surface

It is well understood that any aggressive cleaning process on retrieved implants may damage the corroded or worn surface and may change the texture. Therefore, a gentle cleaning process was used whereby all retrieved implants were soaked in formal-saline for a minimum of 24 hours and then rinsed under running tap water for 30 minutes to remove any loose contamination and some of the body fluid. The implants were then rinsed in distilled water and allowed to dry in air before placing them in individual

plastic containers. Prior to inspection the taper surfaces were gently wiped with a clean swab doused with distilled water, followed by a swab doused with methylated spirit. This was repeated until no further visual contamination was removed from the surface.

3.3.6. Assembly

Following cleaning, components were allowed to dry in air before assembly. *Rehmer* (Rehmer et al., 2012) observed a similar relationship between dynamic and quasi-static assembly procedures therefore, components were assembled according to the ASTM F2009 (ASTM F2009, 2011) standard at a loading rate of 0.05 mm/s in a materials testing machine (Figure 3-6) to allow for reproducibility throughout the study. The maximal load used for assembly was 2kN as per ASTM F2009, unless otherwise dictated by the experimental protocol.

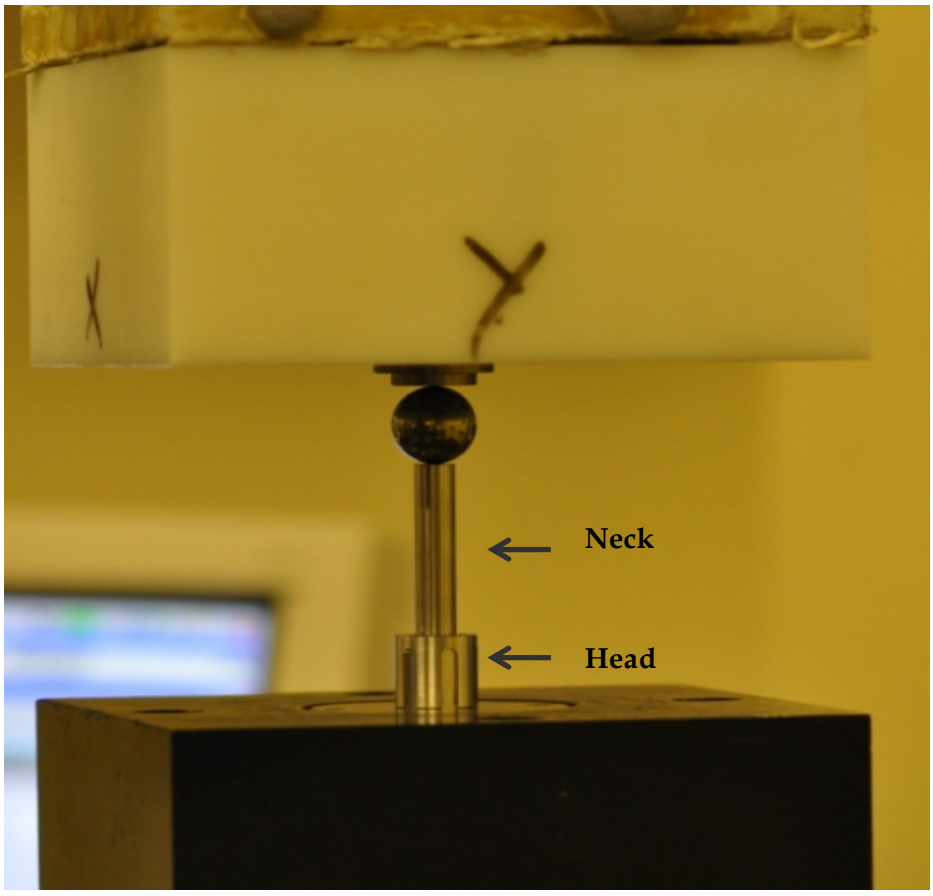

Figure 3-6: Photograph of assembly of components with a rate of axial loading of 0.05 mm/s using an Instron Hydraulic tension/compression single-station testing machine.

3.4. Experimental Set-Up

3.4.1. Mechanical Load Testing

The loading set-up was constructed based on ASTM F1875 – 98 (2014) *'Standard Practice for Fretting Corrosion Testing of Modular Implant Interfaces: Hip Femoral Head- Bore and Cone Taper Interface'* (ASTM F1875-98(2014), 2014), which provides a set of guidelines for the construction of test procedures to evaluate the relative difference in fretting corrosion between different implant designs. The tests are not intended to give an absolute quantitative evaluation of design performance for a particular implant, however are useful for comparative studies. The ASTM F1875 – 98 Standard describes 2 methods for fretting corrosion testing; *Method I* - An anatomical orientation and *Method II* – An inverted orientation. Both of these orientations can be used provided that the load is applied between the centre of the head and stem tip giving an overall result for a given head/stem system. However, as stated in the standard, there are concerns about bearing surface wear between the head and the low friction load applicator, which might influence the result and therefore would require isolation from the electrolyte without interfering with the bearing/articular motion. Also, we anticipated that the manufacturing tolerances and the variations in contact topology of the taper between different components/batches/manufacturers would significantly affect the amount of corrosion potentials produced at the interface which would require a large number of test samples in order to gain a meaningful result.

To overcome both of these issues the ASTM test *Method I* was modified by rigidly fixing the femoral head in a holder so that the wear from the bearing surface would not be an issue and the load would be applied either through the centre of the head or offset relative to the centre of head and depending on the plane of off-set producing either torque or increased bending moment or components of both at the taper interface. This

technique allowed application of different amounts of torque and bending moments without disturbing each assembly thus maintaining the taper interface conditions constant showing real effects of the changes in torque and bending moments. Since in clinical practice torque generated by the articular friction is directly related to the joint force at the bearing surface this test method closely resembled the actual clinical conditions.

Examples of the experimental set up used in the anatomical configuration as per the ASTM F1875 – 98 Standard modified *Method I* for implant tapers and coupon tapers are shown in Figures 3-7 and 3-8 respectively. The stem was held in a fixture constructed from polyoxymethylene (Delrin, DuPont, Parkersburg, West Virginia). A cylinder chamber was reamed within the Delrin block to accommodate the stem. The stem was potted within the cylindrical chamber at 10° of adduction off the vertical axis and cemented using PMMA bone cement (Simplex, Stryker, 2825 Airview Boulevard Kalamazoo, MI 49002 USA). The cylindrical chamber had vertical serrations as well as 3 screw fixed stoppers on its inner surface to facilitated interdigitation and prevent rotation of the cement mantle with the fixture. The fixture for the head component was also constructed from polyoxymethylene and the head was cemented into a cylindrical chamber on the Delrin block at an anatomical angle of 45° (Figure 3-9). An exchangeable superior plate with a machined indentation or crater to accommodate a ball joint for transfer of load from the loading apparatus was fitted on top of the head fixture.

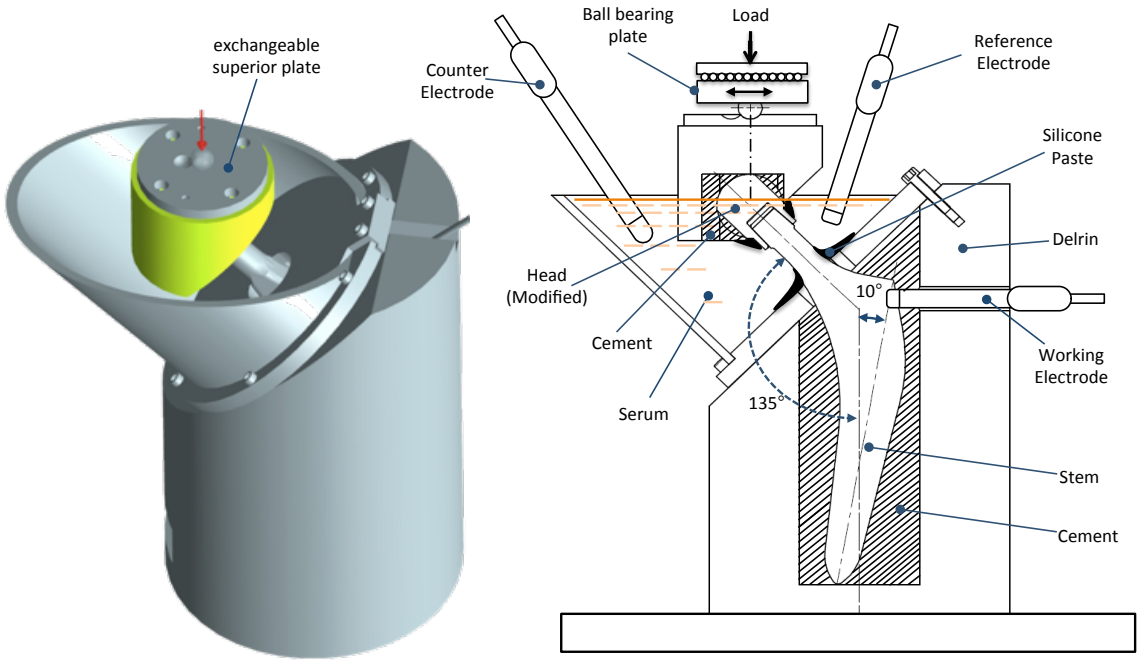

Figure 3-7: Diagrams illustrating the basic design used for measuring fretting current during mechanical loading (modified *Method I* of the ASTM F1875 – 98 standard) for implant tapers.

Similarly to the stem-fixture the head fixture also included vertical serrations and a screw fixed stopper on its inner surface. The geometry of the setup was designed to simulate in-vivo hip joint geometry and typical femoral stem design for THR. The head-neck angle was 135°. A Perspex electrochemical cell was constructed around the fixture to house the lubrication, with its base fitting at the top of the stem Delrin block thus ensuring the fluid would surround the modular head/neck interface. In order to prevent the passage of test fluid into potential crevices, the cement–head interface and the stem-cement-perspex interface were sealed using commercially available Silicone paste (RTV 3535 blue and white), which polymerizes on mixing to form a watertight seal (Figure 3-7).

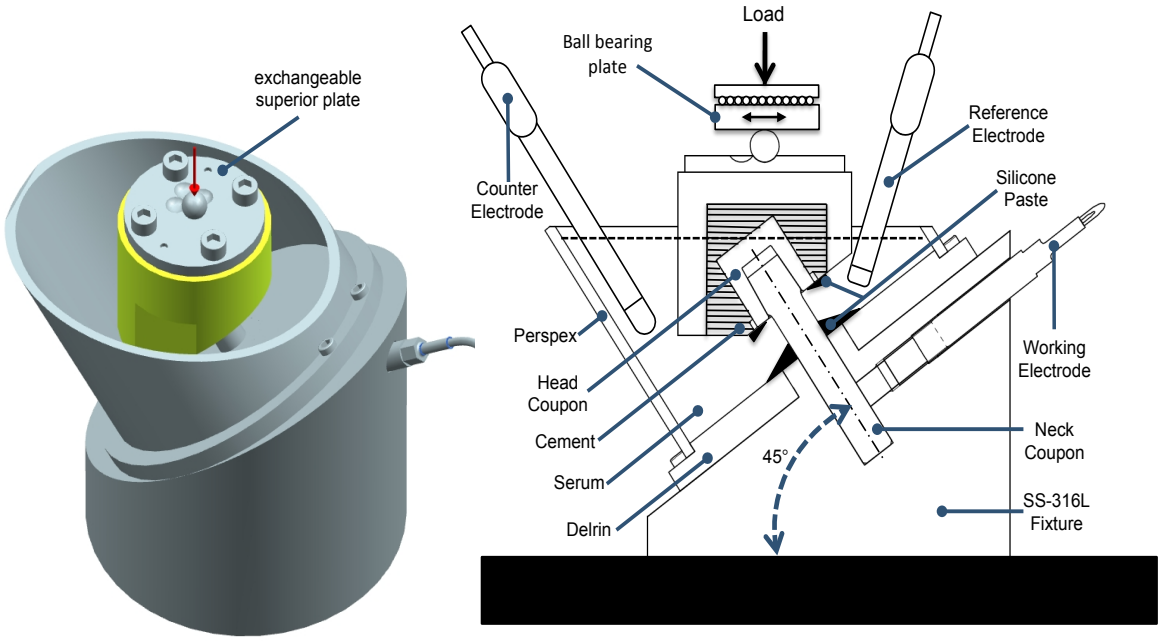

Figure 3-8: Diagrams illustrating the basic design used for measuring fretting current during mechanical loading (modified *Method I* of the ASTM F1875 – 98 standard) for coupon tapers.

The experimental design set up for mechanical load testing of coupon tapers was essentially the same as the one for the implant tapers (described above) with the only difference being in the design of the neck coupon fixture. A precisely reamed tunnel though a Ti alloy block was designed to accommodate the neck coupon shaft with minimal clearance therefore minimizing motion at the interface. A titanium block was used instead of Delrin since it was considered that the contact pressure generated between the coupon and the base fixture would be too high for a Delrin block to sustain without wear and deformation which could lead to further complications. The additional interface generated between the Ti alloy block and the metal coupon body was sealed using commercially available Silicone paste (RTV 3535 blue and white) electrically isolating it from the fluid. The head neck angle was 45° and approximately 28.5 mm of neck length for the coupon was exposed to the fluid, which is comparable neck length of a standard hip stem. A separate tunnel was reamed in order to

accommodate the lead for the working electrode. The Perspex chamber was set on top of the metal block and the coupon-metal block-Perspex interface was sealed using Silicone paste (Figure 3-8).

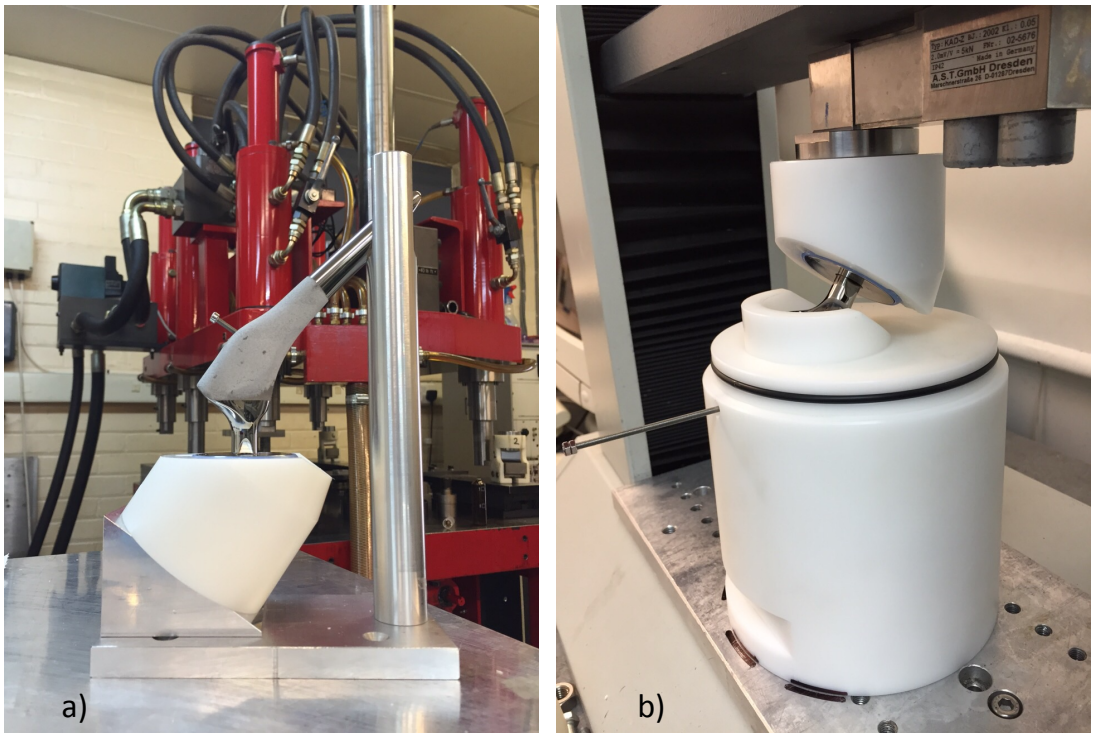

Figure 3-9: Photographs illustrating a) cementing of the head at 45° within the head fixture (following assembly of the head onto the stem as per the ASTM F2009 Standard) and b) cementing the stem within the stem fixture.

A purpose-built implant fatigue-testing machine (manufactured by R.D.P. Howden, Warwickshire, United Kingdom), capable of producing sinusoidal cyclical loads, was used to apply load during testing. Six double acting, equal area actuators are fitted to the crosshead with their piston rods extending through into the test area. A differential pressure transducer was fitted to produce a signal proportional to load and a separate bench mounted cabinet contained all control and monitoring modules necessary to operate the actuators with load or displacement as the controlling factor and computer software to apply waveforms. The loads produced by the fatigue-testing

machine were calibrated before use throughout its range up to 5 kN by following a standard operating practise (SOP). This was done using calibrated load cells that produce an electrical output via a transducer when a force is applied. The electrical output was measured in volts and had a linear relationship with the force applied. Increasing load on the machines actuator was used to generate voltage readings on the load cell (via a calibrated multimeter) and these were compared to the potentiometer readings on the instrument itself. The calibration was checked at the end of the test. The samples were loaded for a variable number of cycles depending on each test specification with a sinusoidal cyclical load between 200 N and 2300 N at a frequency of 3Hz unless otherwise specified by each test protocol. The load was transferred to the fixture via a ball joint, with the ball engaging into the superior crater on the fixture thereby maintaining the axial load at a constant offset. A ball bearing plate was utilized to prevent the transfer of potentially damaging lateral forces onto the machine.

Throughout testing, components were immersed in 200mL of 10% bovine calf serum (Seralab Inc. sterile filtered newborn bovine calf serum) diluted with phosphate buffered 0.9% Sodium Chloride (NaCl) saline (PBS) solution with a pH of 7.4. 1 in 1000 concentration of Sodium Azide was added as a preservative. All tests were conducted at room temperature (20° C ± 1° C) in an air-conditioned temperature-controlled room.

3.4.2. Electrochemical Testing

All electrochemical tests involved the use of a Metrohm Autolab PGSTAT 101 multi-channel modular potentiostat/galvanostat for the measurement and control of currents and potentials including resting currents and potentials (open-circuit), potentiostatic and potentiodynamic (pitting) tests. The main potentiostat unit consisted of six individual potentiostat's that enabled it to run six independent tests simultaneously. The results were recorded and analysed with the aid of the NOVA Software supplied by the same

company (Metrohm Autolab B.V. Runcorn, England) with all the relevant updates included. As is standard practice internationally for corrosion measurements, the system connected to a three-electrode system. The counter electrode (CE) supplied current to the cell and polarized the working electrode (WE) (taper junction). Since the voltage across these two electrodes was not relative (due to the reactions not being in equilibrium and each having an overpotential (Scully and Taylor, 1987)), a reference electrode (RE) was employed in order to make a relative measurement of the potential of the sample.

Following assembly of the test cell, external clamps were used to hold the RE and CE in position: their tips were immersed in test fluid at a constant position within the cell. The RE was held with the tip 2 mm from the head/stem interface, thereby minimising the electrochemical impedance of the fluid medium and allowing for more accurate readings. The CE tip was held at a fixed position towards the periphery of the cell. The WE lead was directly connected to the stem or neck coupon taper. All three electrodes were connected to the computer-controlled potentiostat to take electrochemical measurements (Figure 3-10). Three types of electrochemical tests were performed on the samples in an attempt to further investigate the observed damage to the tapered interface.

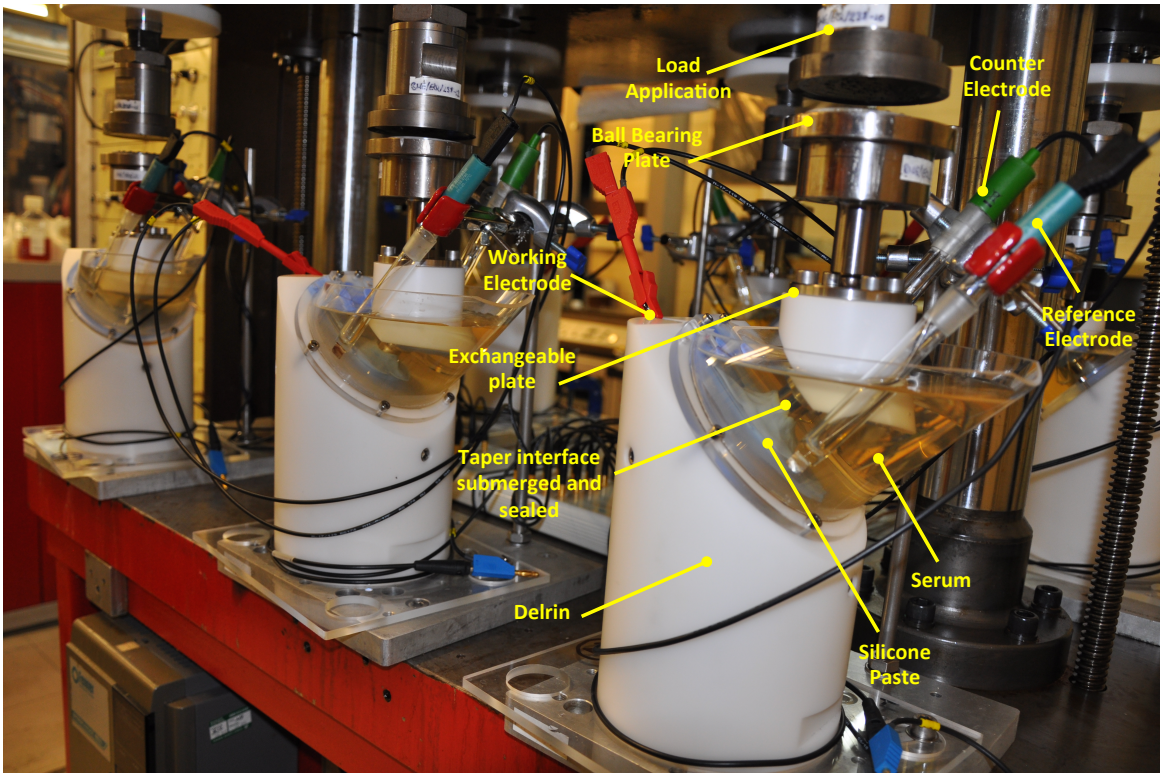

Figure 3-10: Photograph illustrating the final set up mounted onto the fatigue-testing machine.

3.4.2.1. Open Circuit Potential (OCP)

Initial open circuit potential (OCP) tests would record the sample's rest values of current and potential. During OCP measurements the samples were isolated from the potentiostat so that no current/potential was induced. The recorded potentials during OCP measurements were a recording of the potential difference that was spontaneously established between the WE and the RE. The OCP was therefore a measurement of a material's corrosion potential and thus, reflects the galvanic coupling between the two metal components (i.e. head and stem). The rest potential of a specimen would reduce if corrosion was occurring and would increase again to its resting value when repassivating. According to the ASTM F2129-08 '*Standard test method for conducting cyclic potentiodynamic polarization measurements to determine the corrosion susceptibility of small implant devices*' (ASTM F2129-08) and the ASTM G5-94(2004) '*Standard reference test*

method for making potentiostatic and potentiodynamic anodic polarization measurements' (ASTM G5–94, 2004) each sample's OCP (rest potential) was recorded for 1 h or, until the rest potential stabilized to a rate of change less than 3 mV/min.

3.4.2.2. Potentiodynamic Cyclic Polarisation Tests

Potentiodynamic polarisation tests (pitting scans) rely on the change in potential of the WE in order to initiate and propagate the mechanisms of localised crevice corrosion. Potentiodynamic tests were performed after the samples had been immersed for 1 hour to allow a steady rest potential to be obtained. Using the three-cell electrode system the computer-controlled potentiostat would shift the potential of the specimen (WE) at a rate of 5mv/sec starting at a cathodic potential of OCP-250mV to an anodic potential limit of 1V before reversing the potential at the same rate down to 0 mV. The resultant logarithmic polarization curve with the current density (A/cm^2) on the *x*-axis versus Potential (V) on the *y*-axis was then analysed to compare results between different implant and loading conditions. The rise in potential instigated the breakdown of the passive layer and was characterised by the point at which a rapid increase in the current was seen; known as the breakdown potential (E_b). When the implant had undergone pitting, a hysteresis loop was seen as the area formed by the cathodic curve crossing the anodic curve (ASTM G5–94, 2004). E_r represented the repassivation potential or protection potential and was seen as the point of crossover between the anodic and cathodic scans once the potential was reversed (Khan et al., 1996). The degree of observed hysteresis indicated the specimen's affinity to undergo pitting corrosion and the difference between E_b and E_r (ΔE) was used as an indicator of the propagation of localised crevice corrosion. Figure 3-11 shows an example of a potentiodynamic cyclic polarisation test (also refer back to Figure 2-14).

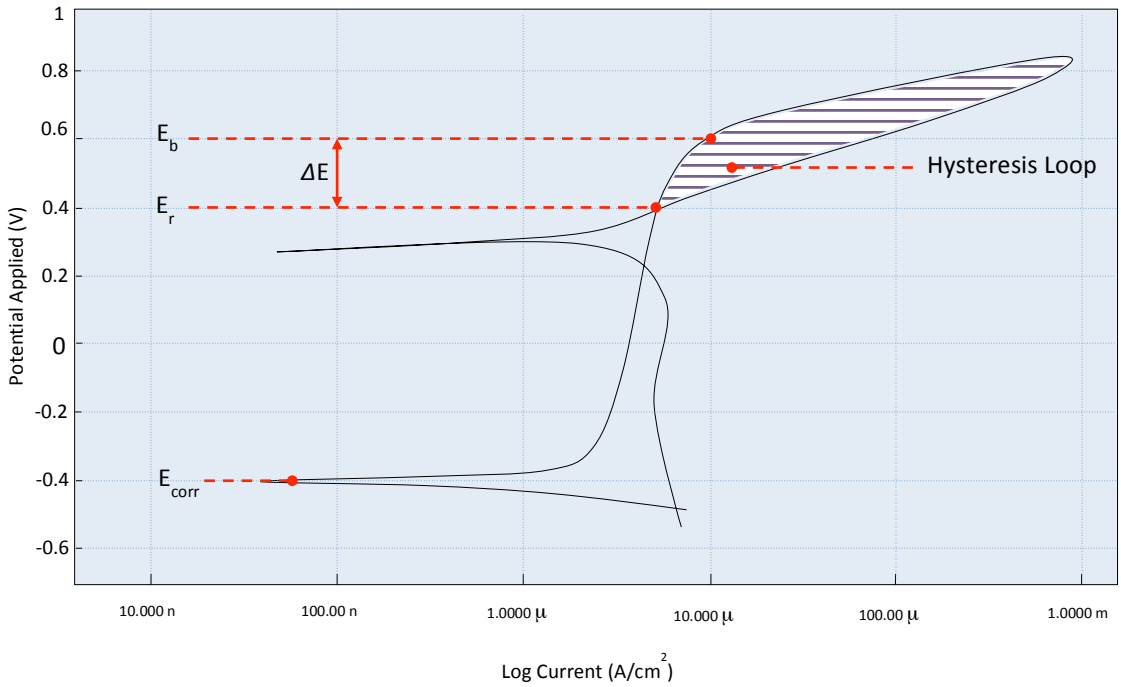

Figure 3-11: An example of a potentiodynamic (pitting) scan of CoCr head and Ti neck taper.

3.4.2.3. Potentiostatic Tests

In potentiostatic tests the specimen (WE) was held at a specified potential imposed by the three cell electrode set up and the resultant current flowing from the WE to the CE was measured as a function of time to follow the evolution of the electrochemical kinetics of the involved reactions. This technique was synchronised with the loading output of the mechanical loading test to evaluate how the current varied per cycle, thus, allowing observation of fretting/tribocorrosion occurring at taper junctions. An implant alloy will spontaneously form a protective oxide layer on its surface acting as a semiconductor in the circuit and therefore, when this layer is damaged or removed (e.g. during mechanical loading), a spike in the current is observed (Figure 3-12). It is hypothesized that within each load cycle during the upward load gradient the passive film at the taper interface is gradually damaged allowing for an increase in potential between the two components; this is caused by the fractured passive film and is

conventionally termed as 'depassivation'. Likewise during the downward load gradient, almost instantaneous passivation occurs at the taper interface causing a decrease in potential between the two components; this is caused by the healing of passive film and is conventionally termed as 'repassivation'. This process appears to be instantaneous however, if more sensitive equipment were used one would expect to see a delay in response of the repassivation process. As a result, cyclic loading results in a sinusoidal waveform of current.

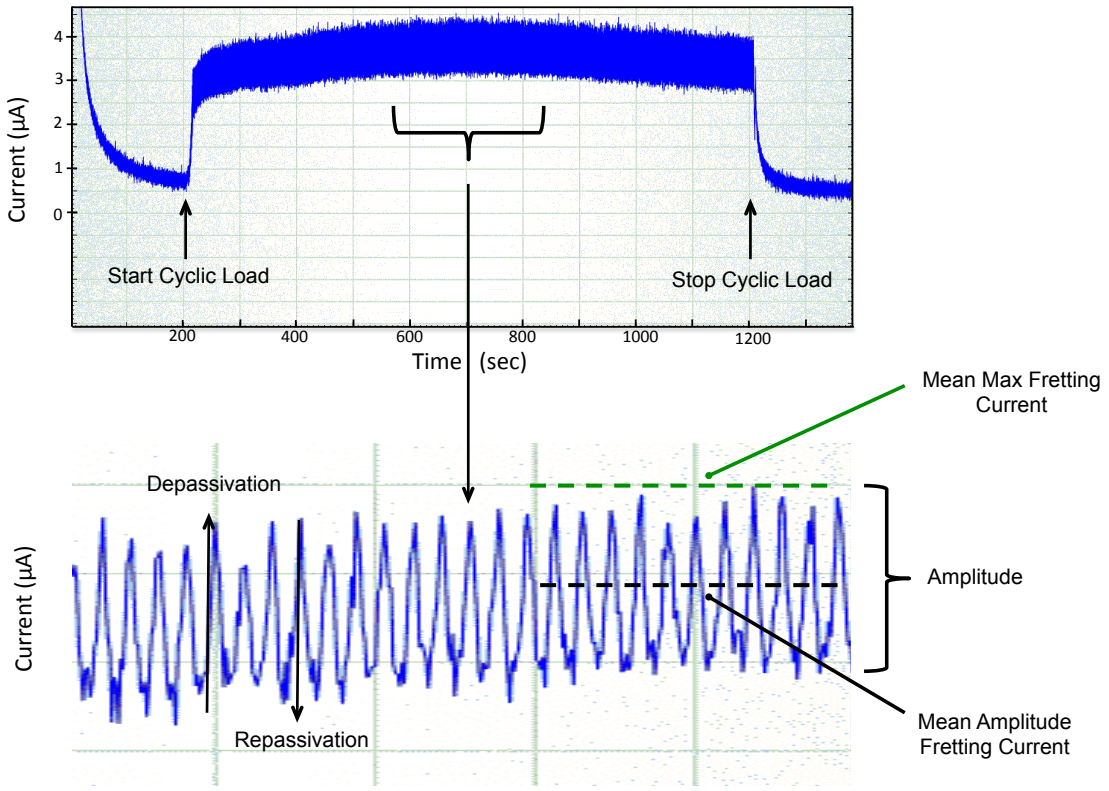

Figure 3-12: Graphs showing typical measurements of the corrosion current with a cyclical load. Note the line in the uppermost chart is broad and represents a series of peaks and troughs shown in the expanded lower chart. The amplitude of the line changes with each load and the determination of the mean amplitude and the mean maximum current that was used to measure the fretting corrosion current. Each peak represents the application of load; at that point fracturing of the passive oxide film that covers the tapers occurs (depassivation), enabling current to flow across the interface. Each trough corresponds to the load being removed; at that point the oxide film reforms (repassivation) and current does not flow freely across the interface.

According to ASTM G5-94(2004) potentiostatic fretting tests should be conducted at +50mV above the measured E_{corr} (i.e. above the OCP) (ASTM G5–94, 2004). During preliminary tests, there was little/no observable change in the current behavior when loading was started at OCP +50 mV and therefore we decided to perform potentiostatic scans at OCP +200mV, which was far below the pitting potential and protection potentials observed in the potentiodynamic cyclic polarization scans for the same implants/coupons.

3.4.2.4. Basic Electrochemical Preliminary Protocol

Below is a description of the protocol used for short term loading tests that provided quantitative measures of fretting corrosion rates and compared the effects of design variables of bore (head) and cone (neck) components.

1. Each electrochemical cell was filled with 200mL of the pre-titrated test fluid (fluid level just above the modular head-neck junction).
2. The specimen was initially unloaded.
3. OCP was monitored for 1 hour and observed to settle to a steady potential.
4. A potentiodynamic cyclic polarisation scan was performed at a rate of 5mv/sec starting at a cathodic potential of OCP-250mV to an anodic potential limit of 1V before reversing the potential at the same rate down to 0mV.
5. OCP was again allowed to settle for 1 hour.
6. Sinusoidal load applied at load and frequency specified per each experiment was commenced.
7. A potentiostatic scan was performed at potential; OCP +200mV for 1400 seconds.

8. Sinusoidal load was initiated 200 seconds into the potentiostatic scan and terminated 1200 seconds into the scan giving sufficient time for the current to settle pre & post loading (Figure 3-12).
9. The specimen was then unloaded.
10. OCP was again allowed to settle for 1 hour.
11. A post-cyclic loading potentiodynamic cyclic polarisation scan was performed using the same parameters described in step (4).
12. Fluid was removed and the test cell was washed out.
13. The above procedure was repeated under different loading conditions depending on the experiment set up.

The protocol described above, was extrapolated to involve long term tests over 5 million and 10 million cycles which will be described in their appropriate chapters. However the basic step sequence is as follows:

1. Each electrochemical cell was filled with 200mL of the pre-titrated test fluid (fluid level just above the modular head-neck junction).
2. The specimen was initially unloaded.
3. OCP was monitored for 1 hour and observed to settle to a steady potential.
4. Sinusoidal load applied at load and frequency specified per each experiment was commenced.

5. After 1000 cycles a potentiostatic scan was performed at potential; OCP +200mV measuring the fretting current at the start of the sinusoidal load.

6. The implants then continued to be loaded for 1 million cycles without any applied potential.

7. At the end of the 1 million cycles a potentiostatic scan was performed at potential; OCP +200mV for 1000 cycles.

8. Each 1 million cycles at 3 HZ took 4 days to complete. The test fluid was topped up to the same starting level during these 4 days. At the end of each 1 million cycles and after the fretting current was recorded for 1000 cycles the load was briefly stopped for the 200mL of the test fluid to be changed and then the sinusoidal load was restarted.

9. This procedure was repeated at every 1 million cycles up to and including 5 or 10 million cycles.

3.4.2.5. Control Test to Ensure Silicone Sealant's Electrochemical Inertness

A control experiment was performed to ensure that the Silicone sealant was electrochemically inert and would therefore not contribute to any electrical activity within the test cell. A beaker containing 200ml of 10% bovine calf serum (Seralab Inc. sterile filtered newborn bovine calf serum) diluted with phosphate buffered 0.9% Sodium Chloride (NaCl) saline (PBS) solution with a pH of 7.4 was used as a test cell. The RE was a saturated calomel electrode; CE and WE were both platinum filament electrodes. The difference in potential between CE and WE should therefore be zero or close to zero. OCP was then monitored over a 2-hour period. At approximately 1 hour when OCP was observed to settle, 2g of cross-linked Silicone paste was inserted into the test cell to determine whether this would cause any change in the OCP. The Autolab

Nova software was used to plot OCP vs. time to give a visual representation of the data. Figure 3-13 demonstrates the lack of electrochemical activity of the Silicone sealant used in the experimental set-up. It shows a typical graph of OCP settling over time to a steady potential. The silicone paste was inserted at 9700 seconds once the OCP was seen to have settled. The resultant trajectory of the graph was unaffected by the addition of silicone paste into the cell, therefore providing evidence for the electrochemical inertness of the sealant. Therefore, it would be unlikely that any variability in the results would be secondary the Silicone sealant itself or to different quantities of Silicone paste used which, never exceeded 2g in weight.

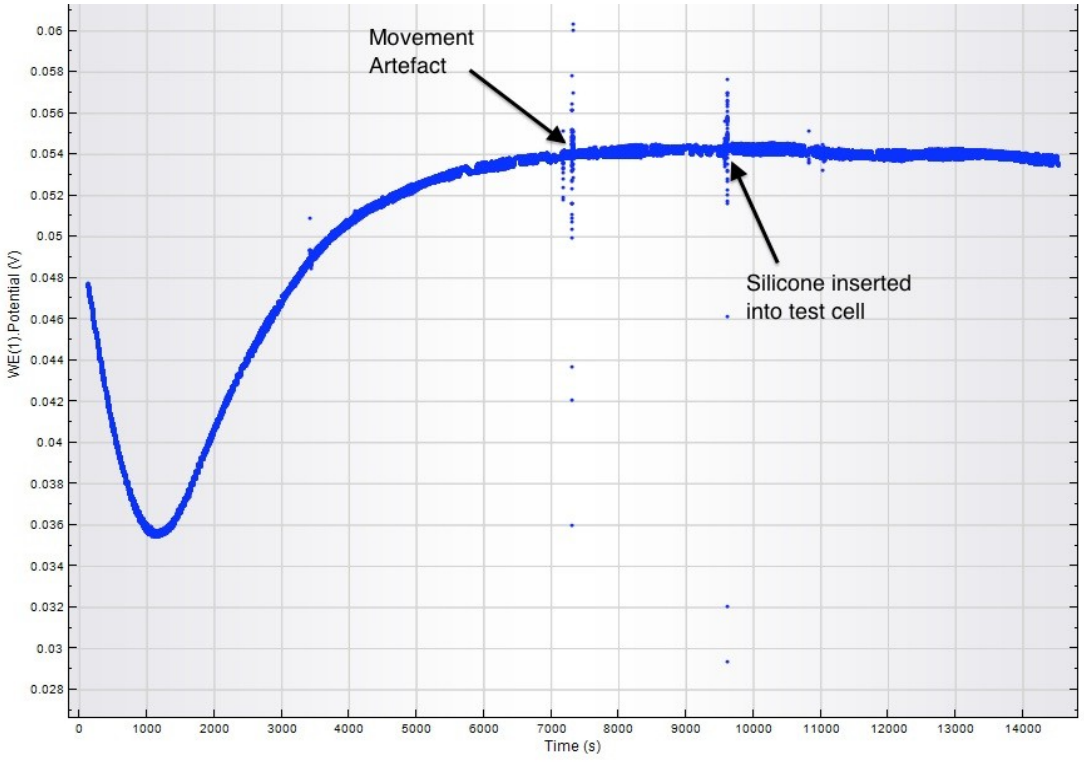

Figure 3-13: Control experiment showing the point of insertion of the silicone paste and how the OCP is unaffected by its insertion.

Chapter 4 Material Loss from Retrieved LH-MoM-THRs: Taper Junction *vs* Bearing Surface

4.1. Introduction

[*] The 8th Annual report of the National Joint Registry for England and Wales revealed that LH-MoM-THRs had the highest failure rate of all hip replacement procedures; with a reported 5 year revision rate of 6.96% which compared to <3% for all other conventional hip replacements (MoP, CoC, CoP) and 4.56% for large head MoM hip resurfacings (Smith et al., 2012b). A growing body of evidence shows that LH-MoM-THRs (>36 mm) have higher revision rates than equivalently sized MoM resurfacings with a similar bearing surface design (Smith et al., 2012b, Australian Orthopaedic Association National Joint Replacement Registry, 2012, Langton et al., 2011). For example the ASR XL THR (DePuy Orthopaedics, Warsaw, IN, USA) has a higher revision rate than the ASR hip resurfacing (DePuy Orthopaedics, Warsaw, IN, USA), with reported 5-year revision rates of 21.9% and 13.8%, respectively (Langton et al., 2011). Similar results have also been shown for the Birmingham Hip Resurfacing THR (Malviya et al., 2011). Consequently in February of 2012 the British Orthopaedic Society recommended that LH-MoM-THRs no longer be implanted (Skinner et al., 2012).

As mentioned previously in the literature review an important difference between MoM resurfacing and LH-MoM-THR is the modular head-neck junction, which provides an additional source of metal debris either as result of mechanical wear, corrosion, or a combination of both (Gilbert et al., 1994, Goldberg et al., 1997a).

[*] This chapter (Material Loss at the Taper Junction of Retrieved Large Head Metal-on-Metal Total Hip Replacements) was published in the Journal of Orthopaedic Research in June 2013.

It has therefore, been speculated that material loss, either as corrosion or wear, at the head-neck taper junction is implicated in the high revision rates reported for LH-MoM-THRs (Smith et al., 2012b). Whilst numerous qualitative studies of corrosion at the taper junction of different types of total hip replacement exist (Goldberg et al., 2002, Lindgreen et al., 2011, Huber et al., 2009), including one reporting on evidence of corrosion at the junction in up to 95% of large head MoM retrievals (Fricka et al., 2012) at the start of this study only two were identified to quantify the volume of material loss from the head-neck taper junction of LH-MoM-THRs (Langton et al., 2012, Bolland et al., 2011). Additionally the clinical significance of material loss at the taper junction remained unclear, with one previous retrieval study (Matthies et al., 2011) showing no difference in blood metal ion levels between patients with failing LH-MoM-THRs and MoM hip resurfacings whilst, other studies reported on higher blood metal ion levels in patients with well performing LH- MoM-THR when compared to hip MoM hip resurfacings (Garbuz et al., 2010, Beaule et al., 2011).

The aims of this chapter therefore were to:

1) Undertake a comprehensive measure of the volume of material loss from the taper junctions and compare it to the volume of material loss from the bearing surface of over 100 retrievals.

2) Correlate the volume of material loss from the taper junction to the blood metals ion levels.

3) Investigate whether the volume of material loss from the taper junction is higher in cases associated with a diagnosis of a pseudotumour.

4.2. Materials and Methods

4.2.1. Patients and Components

This was a retrospective study of prospectively collected data from the first 110 consecutive LH-MoM-THR cases referred to our retrieval laboratory that met our inclusion criteria. Details regarding implant selection and patient demographics are given in Chapter 3 under the section 3.2.1.3 titled *Retrievals.*

4.2.2. Pre-Revision Clinical Assessment

Prior to revision all patients had undergone clinical examination and either CT or plain radiograph assessment of the hip. All had MARS MRI scanning to assess the soft tissues and blood sampling to measure whole blood cobalt and chromium ion levels using inductively coupled plasma mass spectrometry (ICPMS). We defined a pseudotumour as a sterile (non- infected) cystic or solid inflammatory mass in the soft tissues surrounding the joint (Matthies et al., 2012). If present, the lesion was characterized according to a previously described method (Matthies et al., 2012).

The reasons for revision were diagnosed using published criteria (Matthies et al., 2012, Hart et al., 2012). The presence of a cystic soft tissue mass is not synonymous with revision (Kwon et al., 2011), and so the presence of pseudotumour was not deemed a "reason for revision." The reasons for revision were: unexplained pain (77), aseptic femoral loosening (12), aseptic acetabular loosening (8), component misalignment (4), infection (4), component mismatch (2), fracture (2), and one case following fracture of the stem–neck.

4.2.3. Visual Inspection of Components

All components were visually inspected prior to measurement of material loss from the bearing and taper surfaces. We noted any evidence of surface damage, wear, and corrosion.

4.2.4. Assessment of Corrosion of the Head and Neck Taper Surfaces

Both head and neck taper surfaces were inspected macroscopically and then viewed (up to 40x) using a stereo-microscope (Leitz MZ10; Leitz, Wetzlar, Germany) to assess for corrosion. Corrosion was scored using a published method (Goldberg et al., 2002) and all taper surfaces were scored by a single author blinded to all other data using a 4-tiered classification (Table 4-1).

Severity	Score	Grading Criteria
None	I	No visible evidence of corrosion
Mild	II	<30% taper surface discoloured
Moderate	III	>30% taper discoloured
		<10% taper discoloured in black corrosive debris
Severe	IV	>10% taper surface discoloured in black corrosive debris

Table 4-1: Criteria used to classify corrosion of the retrieval taper surfaces.

4.2.5. Measurement of Retrieval Head and Neck Taper Surfaces

The method is described in Chapter 3 section 3.3.2 titled *Retrieval Head and Neck Taper Surface Analysis.*

4.2.6. Measurement of Retrieval Bearing Surfaces

The method is described in Chapter 3 section 3.3.3 titled *Retrieval Bearing Surface Analysis.*

4.2.7. Statistical Methods

All univariate distributions were assessed for normality using the Shapiro–Wilk test. Blood metal ion levels and surface measurement data were not normally distributed, so the Wilcoxon signed-rank test was used to compare the median surface measurements and cobalt and chromium ion levels. Spearman's correlation coefficient (r) was used to quantify the strength of the relationships between the taper surface and bearing surface measurements. Multiple linear regression models were used to explore the multivariable associations between metal ion levels and the taper and bearing surface measurements. Tests for interactions between taper and bearing surface measurements were performed to assess whether the relationships with metal ion levels were independent of each other. Similarly, multivariable analysis was used to determine differences in bearing and taper surface material loss according to the presence/absence of pseudotumour. This accounted for interaction between variables. All analyses were performed using Stata/IC version 12.1 (StataCorp, College Station, TX); $p < 0.05$ was considered significant.

4.3. Results

The appearance of the taper junction was variable but in the worst cases the taper on the CoCr head showed evidence of MACC. In these retrievals MACC, was associated with deposition of corrosion products which was often seen just outside the taper contact region and with an imprinting effect whereby, a series of circumferential grooves dissimilar to the original CoCr surface finish were seen (Figure 4-1). These

circumferential grooves were seen on the surface of the head taper where it was in contact with the neck taper. On the linear surface profile measurements these grooves appeared to have the same pitch as those of the neck taper surface (Figure 4-2) and were clearly associated with material loss. Looking at a map of the CoCr alloy head taper contact area generated during volumetric analysis these grooves were often seen to be distributed over the entire taper or were seen to be associated with one area of high material loss (Figure 4-3).

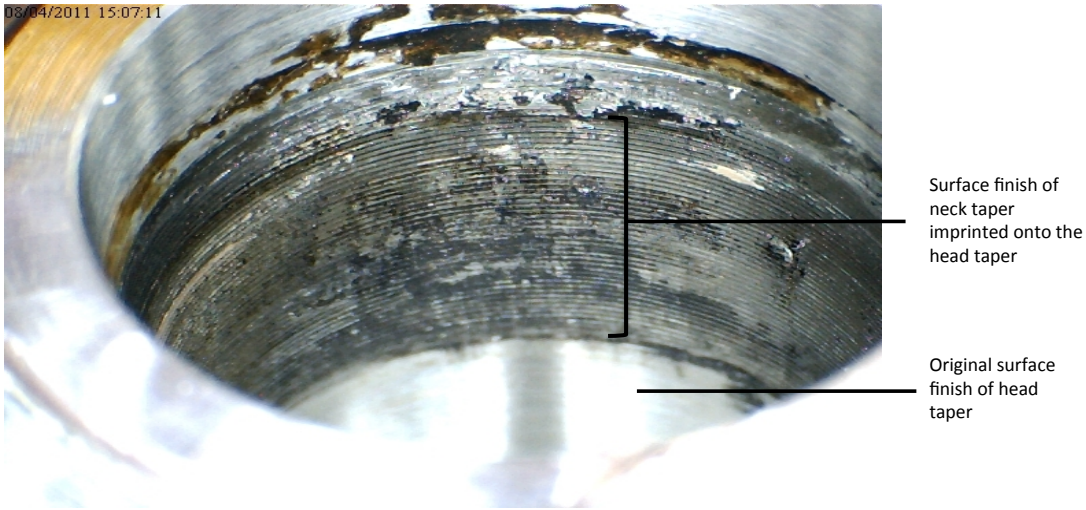

Figure 4-1: Photograph of a retrieval head taper showing the original surface markings of the head taper and the imprinted surface markings of the neck taper onto the head taper.

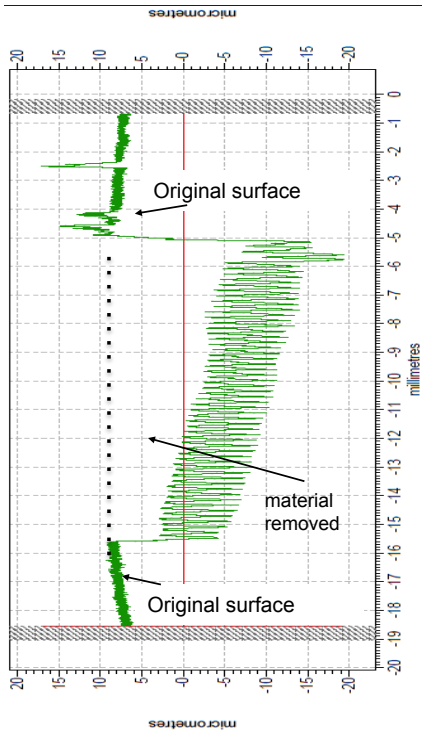

Figure 4-2: Linear profile surface analysis of a retrieval head taper, showing the material loss of the head taper and the imprinting effect of the neck taper onto the head taper surface in contact.

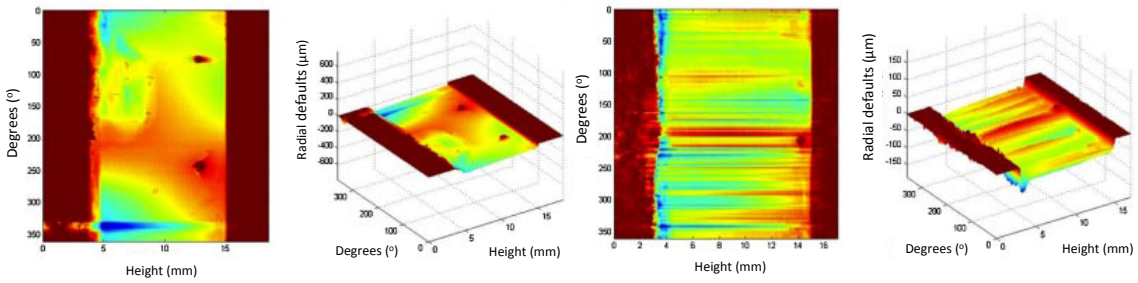

(a) Asymmetric pattern of material loss (b) Axisymmetric pattern of material loss

Figure 4-3: Typical taper surface measurements demonstrating (a) asymmetric (19.4 mm^3), and (b) axisymmetric (17mm^3) patterns of material loss.

Corrosion was found at the head taper surface in 99 out of 110 cases: according to the Goldberg score (Table 4-1), 29 were classified as mild, 40 as moderate, and 30 as severe. Of the 36 neck taper surfaces, 6 demonstrated corrosion, all mild. A strong correlation existed between corrosion score and the volume of material loss at the head taper (r =

0.94, 95% CI = 0.91–0.96, $p < 0.001$). A similarly strong correlation occurred between corrosion score and the volume of material loss at the neck taper ($r = 0.72$, 95% CI = 0.44–0.87, $p < 0.001$). Given the strength of these relationships, only volumetric data are reported for the remainder of the results. The presence of significant retrieval damage (deep scratches) was noted on 21 of the 36 neck tapers. A summary of the surface measurement data is given in Table 4-2.

	Cup Bearing Surface (n=110)		**Head Bearing Surface (n=110)**		**Head Taper Surface (n=110)**		**Neck Taper Surface (n=36)**	
	Volume (mm^3)	Rate (mm^3/year)	Volume (mm^3)	Rate (mm^3/year)	Volume (mm^3)	Rate (mm^3/year)	Volume (mm^3)	Rate (mm^3/year)
Mean	9.04	2.56	11.62	3.10	3.60	0.85	0.34	0.12
Median	1.94	0.62	3.44	1.31	2.02	0.54	0.29	0.08
Range	0.06-194.8	0.04-39.62	0.11-228.3	0.06-45.66	0-25.19	0-4.29	0-0.83	0-0.36

Table 4-2: Summary of the volumetric material loss from the bearing and taper surfaces.

The median volume (2.02 mm^3) of material lost from the head taper surface was significantly less than the median volume of material lost from the femoral head bearing surface (3.44 mm^3, $p < 0.001$), but not different to that from the acetabular bearing surface (1.94 mm^3, $p = 0.55$). For the 36 neck tapers, the volume of material loss was negligible (<1 mm^3) in all cases. The median volume (0.29 mm^3) was significantly less than that lost from the head taper and the head and acetabular bearing surfaces (all $p < 0.001$). Comparison of the taper and bearing surface data is shown in Figure 4-4.

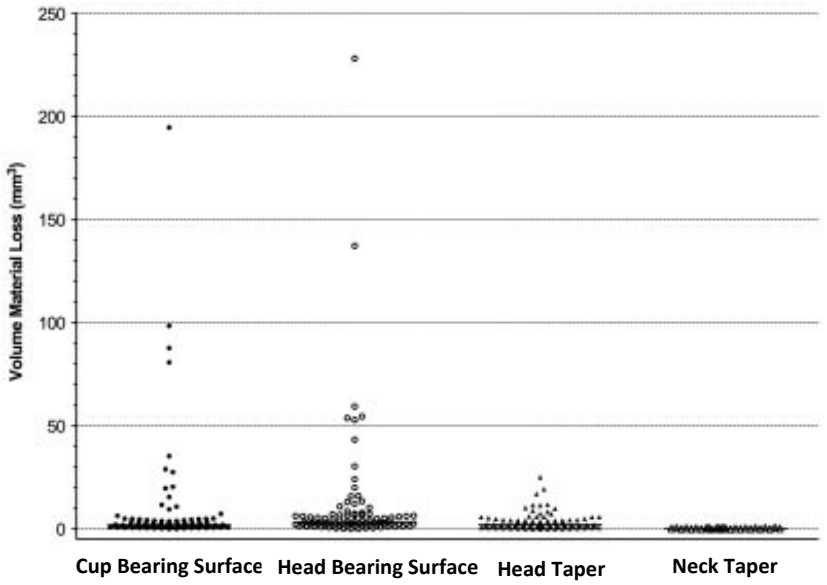

Figure 4-4: Graph comparing volumetric material loss of the bearing and taper surfaces.

Material loss from the head taper was greater than that from the combined bearing surfaces in only 23% of the cases. A weak but significant positive correlation existed between the volume of material loss from the head taper and that from the head-bearing surface (r = 0.25, 95% CI = 0.05–0.44, p = 0.017). The correlation between volume loss from the head taper and that from the acetabular bearing surface (r = 0.17, 95% CI = - 0.04–0.36, p = 0.12) was not significant (Figure 4-5). A moderate significant correlation existed between the volume of material loss from the neck and head tapers (r = 0.42, 95% CI = 0.01–0.72, p = 0.04).

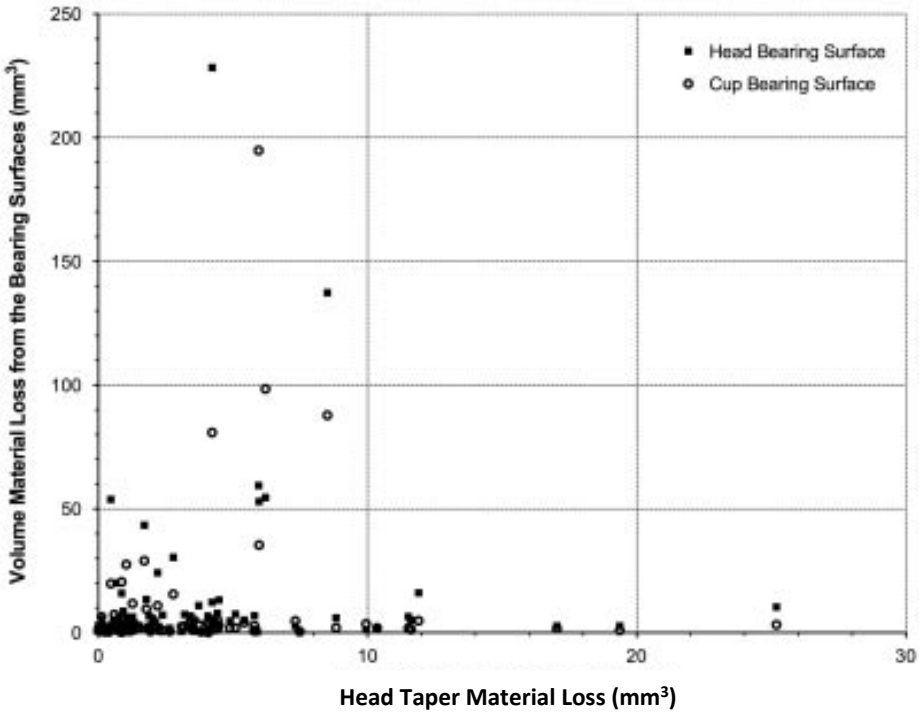

Figure 4-5: Scatter plot showing the correlations between the volume of material loss from the head taper and the bearing surfaces.

No significant correlations existed between the volume of material loss from the neck taper and that from the head (r = 0.03, 95% CI = - 0.45 to 0.40, p = 0.90) and acetabular bearing surfaces (r = 0.17, 95% CI = - 0.27 to 0.55, p = 0.43). The median Co level of 7.6 ppb (parts per billion) was significantly higher than the median Cr level of 3.0 ppb ($p < 0.0001$); (Figure 4-6).

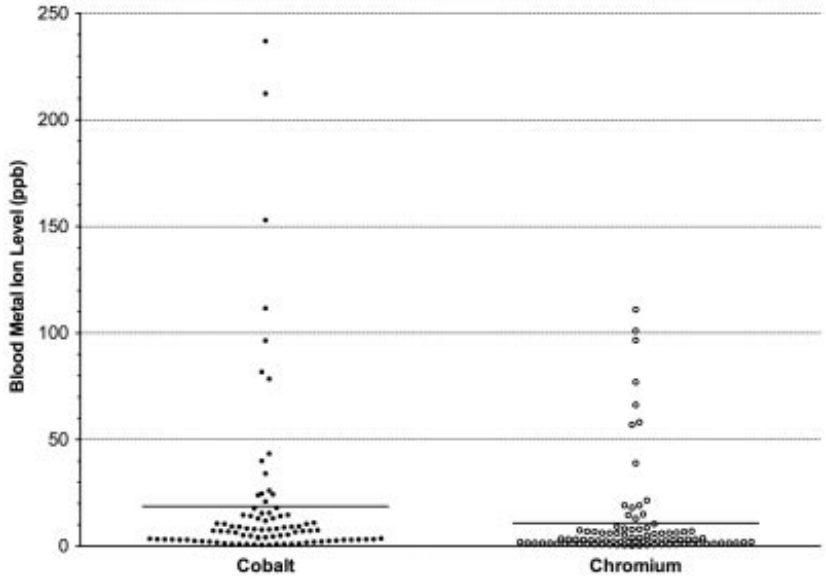

Figure 4-6: Comparison of whole blood Co and Cr ion levels measured in ppb (parts per billion).

Univariable analysis showed that a weak but significant positive correlation existed between the volume of material loss from the head taper and Co levels (r = 0.29, 95% CI = 0.09–0.47, p = 0.01); however, no significant correlation was found with Cr levels (r = 0.19, 95% CI = - 0.02 to 0.38, p = 0.08). No significant correlations existed between the neck taper volume loss and either Co (r = 0.41, 95% CI = - 0.10 to 0.75, p = 0.10), or Cr (r = 0.47, 95% CI = - 0.03 to 0.78, p = 0.06) levels. Conversely, univariable analysis showed that the volume of material loss from the femoral bearing was significantly correlated with both Co (r = 0.40, 95% CI = 0.21–0.56, p < 0.001) and Cr levels (r = 0.41, 95% CI = 0.22–0.57, p < 0.001). Similarly, the acetabular bearing volume loss was significantly correlated with Co (r = 0.39, 95% CI = 0.20–0.55, p < 0.001), and Cr (r = 0.37, 95% CI = 0.18–0.54, p < 0.001) levels (Figures 4-7 and 4-8).

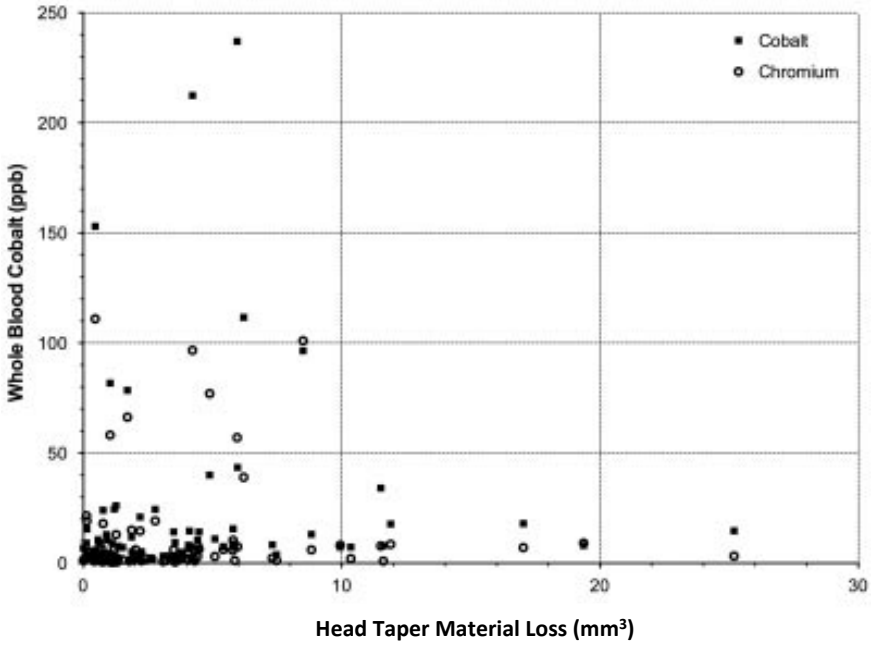

Figure 4-7: Scatter plot showing the correlation between whole blood metal ion levels and the volume of material loss from the head taper measured in ppb (parts per billion).

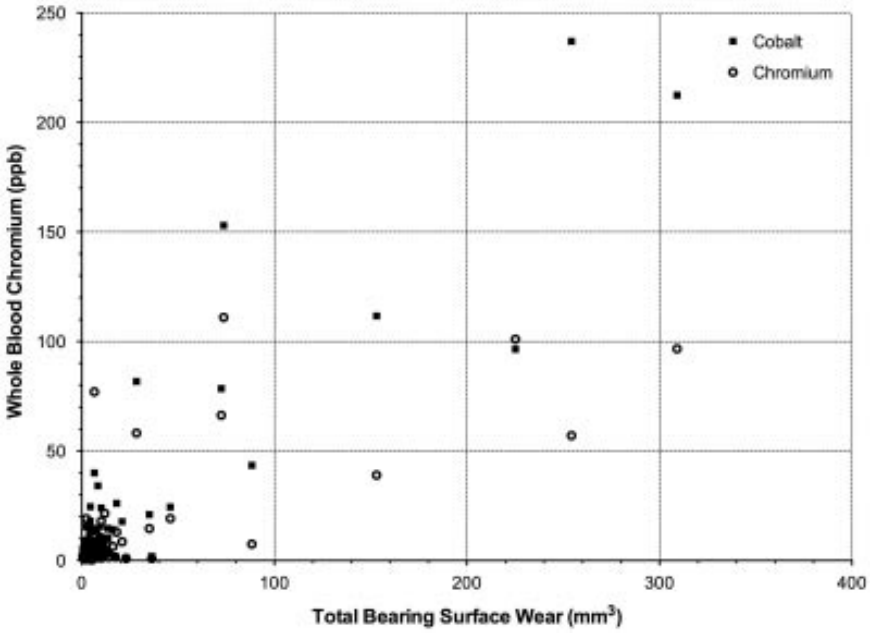

Figure 4-8: Scatter plot showing the correlation between whole blood metal ion levels and bearing surface wear volumes measured in ppb (parts per billion).

Further multiple linear regression analysis, adjusted for both femoral head and acetabular bearing surface wear, confirmed the absence of any significant correlations between the volume of material lost at the head taper and either Co ($p = 0.18$) or Cr ($p = 0.60$) levels. Furthermore, there was no evidence of any significant interactions between the volumes of material lost at the head taper and bearing surfaces. Full results of the multiple regression analyses are given in Tables 4-3 and 4-4, showing bearing surface material loss as the only independent predictor of blood metal ion levels.

	95% Confidence Interval	p-Value
Cup bearing surface material loss	0.27 to 0.76	<0.001
Head bearing surface material loss	- 0.04 to 0.46	0.098
Head taper surface material loss	- 0.07 to 0.36	0.177

When adjusted for the other sources of material loss, wear of the cup bearing surface was the only significant predictor of cobalt ion levels.

Table 4-3: Results of the multiple linear regressions model describing the relationship between material loss and whole blood cobalt ion levels.

	95% Confidence Interval	p-Value
Cup bearing surface material loss	0.16 to 0.68	0.002
Head bearing surface material loss	0.01 to 0.53	0.042
Head taper surface material loss	- 0.17 to 0.29	0.598

When adjusted for the other sources of material loss, wear of the cup and head bearing surfaces were the only significant predictors of cobalt ion levels.

Table 4-4: Results of the multiple linear regressions model describing the relationship between material loss and whole blood chromium ion levels.

Too few cases of neck tapers existed to perform meaningful multivariable statistics. Pseudotumours were found in 69 out of 110 cases (62.7%); 68 were cystic and 1 solid. Univariable analysis showed that cases with pseudotumour were associated with

significantly higher median volumes of material loss at the acetabular cup and head bearing surfaces and the head taper surface, but not the neck taper (Table 4-5).

	Bearing Surface Material Loss (mm^3)				**Taper Surface Material Loss (mm^3)**			
	Cup (n=110)		Head (n=110)		Head Taper (n=110)		Neck Taper (n=36)	
	Pseudo tumour	No Pseudo tumour	Pseudo tumour	No Pseudo tumour	Pseudo tumour	No Pseudo tumour	Pseudo tumour	No Pseudo tumour
Median	2.55	1.13	4.49	2.20	3.15	1.20	0.35	0.34
Mean	12.18	3.17	14.90	5.50	4.18	2.51	0.32	0.36
Range	0.11-194.8	0.06-20.46	0.11-228.3	0.12-53.85	0-25.19	0-10.36	0-0.62	0-0.83

Univariable analysis showed that head and cup bearing surface material loss and head taper surface material loss were significantly higher in cases associated with pseudotumour (all $p<0.05$). Increased material loss at the neck taper surface was not significantly associated with pseudotumour ($p=0.446$).

Table 4-5: Comparison of material loss according to the presence or absence of pseudotumour on MARS-MRI scans.

However, after adjustment for the volume of material loss at each of the other surfaces (accounting for possible interactions), neither the material losses at either bearing surface or at the head taper were significantly associated with the presence of pseudotumour. Increased total bearing surface material loss was associated with increased odds of pseudotumour presence, but when adjusted for head taper material loss this relationship became insignificant ($p = 0.142$). Full results of the multiple linear regression analysis for pseudotumour are given in Table 4-6.

	95% Confidence Interval	p-Value
Cup bearing surface material loss	- 0.13 to 1.32	0.109
Head bearing surface material loss	- 1.90 to 0.14	0.092
Head taper surface material loss	- 1.59 to 0.51	0.315

When adjusted for the other sources of material loss, neither increased material loss from the cup or head bearing surfaces or increased material loss from the head taper surface was significantly associated with the presence of pseudotumour.

Table 4-6: Results of the multiple linear regression models describing the relationship between material loss and the presence/absence of pseudotumour.

Again, too few cases of neck tapers existed to perform meaningful multivariable statistics. None of the clinical and design variables (Table 3-3) were significantly associated with higher taper material loss. There were no differences between prosthesis design (manufacturer) and no difference between similar and mixed-alloy head–neck combinations.

4.4. Discussion

4.4.1. Summary of Results

This study has demonstrated that material loss from the head taper is of similar magnitude to that of the bearing surfaces (although it is still the predominant source of implant derived metal debris in less than a third of failed LH-MoM-THRs). Additionally it has shown that in patients with failing LH-MoM-THRs, high taper material loss is difficult to detect using blood metal ion levels and furthermore, pseudotumours are not more likely to occur in cases with higher volumes of taper material loss. Thus, this study has provided clinically relevant findings and has contributed to the understanding of the failure mechanisms of LH-MoM-THRs.

Whilst the head–neck taper junction is clearly an important source of implant-derived material in LH-MoM-THRs, it is difficult to explain the higher revision rates of these devices compared to MoM hip resurfacing through a dose-response reaction alone. However, it may be that additional material from the stem (either cobalt-chrome or titanium) may contribute to failure or that the material lost from the taper junction may be more potent than the particulate debris released from the bearing surfaces.

This study reports on data from a large series of explanted LH-MoM-THRs of several designs, and has shown a wide variation in the volume of taper material loss. A previous study by *Langton* (Langton et al., 2012), looked at only one design, the ASR XL and proposed a predominantly mechanical mechanism to explain the variation in taper material loss in which the combination of a large head, short taper length and a low stem-shaft angle provide a lever-arm sufficient to cause high volumes of localized wear at the taper junction. The authors suggested that corrosion occurred secondary to a mechanical process (Langton et al., 2012). Whilst it is likely that material loss at the taper junction is multi-modal and in some cases mechanical wear may be the dominant process, this study suggests that corrosion is likely to be the principle source of implant-derived material. Corrosion of the head taper was virtually universal (99 of 110 cases), and the presence of "imprinting" of the neck taper thread onto the head taper surface is highly suggestive of galvanic corrosion, a process by which material is lost preferentially from the head taper (Figures 4-1 and 4-2). This is supported by data from the 36 retrieved stems in the study; whereby the neck tapers all had negligible material loss (<1 mm^3) and only six of the taper surfaces demonstrated any evidence of corrosion (and all only mild). Furthermore, the morphology of the neck taper surface measurement profiles was rarely consistent with a mechanical process. In most cases an axisymmetric pattern of regular and uniform circumferential groves associated with material on the head taper

was observed (Figure 4-3). This likely represents uniform loss or transfer of material, supporting a mechanism involving corrosion rather than wear. In contrast, increased local contact pressures would result in localized areas of increased material loss. It is doubtful that the appearance of a wear scar generated through high bending moments as indicated by Langton et al. (2012) would have a regular appearance of material loss as I have reported on in this section of my thesis.

This data supports a mechanism whereby the volume of material loss at the taper junction is only weakly associated with elevated metal ion levels and soft tissue reactions. This may be explained if we consider the nature of the loss of material from the taper. Material loss at the taper due to corrosion will be associated with a release of ions into solution whereas material loss at the bearing surfaces generated by wear results in the release of debris where the metallic constituents (ions) are locked into the wear particles and have a reduced biological effect. Loss of material from the taper may be a more potent stimulator of inflammation than particulate debris from the bearing surfaces. This may then help explain the higher revision rates of LH-MoM-THR compared to MoM hip resurfacing. The volumetric material loss measurements of this study compare well with those reported by *Langton* (Langton et al., 2012) for the ASR XL; who reported rates of material loss at the taper junction from 0.46 to 82.5 mm^3 per year. The slightly higher volumes may be explained by the inclusion of only one design that is recognized to have the poorest performance (Australian Orthopaedic Association National Joint Replacement Registry, 2012, National Joint Registry, 2012). Differences in measurement technique and analysis may also account for some variation and is likely to provide ongoing problems comparing data between studies.

The results of my study may provide important information for clinical surveillance of patients with LH-MoM-THRs, showing that the volume of material loss from the head

taper is of a similar magnitude to the loss from each of the bearing surfaces. However, this was not reflected in the blood Co and Cr ion levels measured prior to revision surgery. Similar to the trend observed for MoM hip resurfacing, in our group of retrieved MoM total hip replacements, bearing surface wear volumes were strongly correlated with blood metal ion levels. In contrast, the volumes lost from the CoCr tapers were only weakly correlated with ion levels. This supports the theory that material loss from the taper junction is the predominant source of implant derived debris in few cases (less than a third), and in the majority of cases an increased potency of a low volume of ionic material is likely to be responsible for failure. Another explanation for the higher revision rates of LH-MoM-THR is that these implants are subject to a higher total volume of material loss; a combination of material loss from the bearing and taper surfaces. However, the evidence is unclear given that previous studies showed an equally high occurrence of pseudotumours (and revisions) in both low wearing and high-wearing MoM hip replacements (Matthies et al., 2012, Hart et al., 2012), furthermore, in this study a substantial number of cases with pseudotumour had low volumes of material loss at the bearing and taper surfaces. While the role of taper material loss remains unclear, high taper material loss is likely to present clinically in a variety of ways, not merely adverse soft tissue reactions.

The potency and importance of metal ions released from the taper junction has been previously recognised. Adverse local tissue reactions resulting from corrosion of the modular head-neck taper of metal-on-polyethylene total hip prostheses have been reported (Cooper et al., 2012). These reactions appear to be quite similar to those reported in patients with MoM bearing surfaces. Serum metal levels were abnormal in every case, with an elevation of cobalt levels that was differentially higher than that of chromium levels.

4.4.2. Study Limitations

As with all work on retrievals, there are several limitations. Only 36 neck tapers were analyzed, as in the majority of cases the revising surgeon did not remove a well-fixed femoral stem. Also, we did not assess the stem itself as a potential source of material loss. Data for the neck tapers were excluded from multivariable regression analyses. However, emphasis should be given to the fact that in the available cases material loss from the neck taper was negligible and therefore omission is unlikely to have affected the results. Another limitation is the lack of Ti ion measurement. Titanium ion release from mixed-alloy MoM total hip replacements is of unknown clinical significance; future studies and follow-up of these patients may incorporate this measurement.

4.4.3. Conclusions and Further Work

In conclusion, though a significant volume of material is released at the taper junction, the failure mechanism of these implants remains unclear. It appears unlikely to be a simple dose-response relationship. The results of this study are suggestive of the mechanism of material loss to be predominantly corrosion. Ionic debris is likely to be a more potent inflammatory stimulator compared to particulate debris released from the bearing surface, and this may explain the differences in revision rates between resurfacing and LH-MoM-THRs. Of clinical importance is the lack of a significant correlation between taper material loss and either blood metal ion levels or the incidence of pseudotumours. This has implications for the clinical surveillance of all patients with LH-MoM-THRs.

The purpose of this study was not to identify surgical and design factors responsible for increased taper material loss. This will be investigated in the next chapters, which will concentrate on the taper design factors responsible for increased taper material loss.

Variables such as increased bending moment, torque, material combination; surface roughness and surface area will be investigated in terms of their effect on the fretting corrosion at the taper junction.

Chapter 5 Taper Junction MACC Findings: Retrieved LH-MoM-THR vs. In-Vitro MoM THRs (simulating high bending moment)

5.1. Introduction

Many recent retrieval studies have focused on the modular head-neck taper junction of LH-MoM-HR (Bolland et al., 2011, Langton et al., 2012, Nassif et al., 2014) and various clinical and laboratory studies have shown that increasing the size of the head leads to increasing corrosion at the head-neck interface with greater ALTR and elevated metal ion levels in the blood (Dyrkacz et al., 2013, Malviya et al., 2011, Smith et al., 2014). A well-described observation has been the production of significant metal debris at the head-neck taper interface (Matthies et al., 2013, Langton et al., 2012). Although the clinical significance of metal debris is not entirely clear as concluded by my previous study described in Chapter 4 (Matthies et al., 2013), the effects of such metal debris in general, have frequently been identified as causes for failure and revision of not only MoM but also MoP hip replacements indicating the importance of taper corrosion (Cooper et al., 2012, Polyzois et al., 2012, Bolland et al., 2011, Jacobs, 1998, Whitehouse et al., 2015). *Cooper* et al., 2012 investigated patients who underwent revision for corrosion at the modular head-neck interface of large head MoP THAs and concluded that patients presented with pain or swelling around the hip with serum cobalt levels that were typically more elevated than serum chromium levels. In addition large soft tissue masses and surrounding tissue damage were visible with corrosion at the femoral head-neck interface.

Identification of significant amounts of metal debris arising from the modular head-neck interface of retrieved LH-MoM-THRs lead to the increased interest in the potential causative effect on MACC at the taper junction of the size of the head. Dyrkacz et al. (2013) reported on a series of retrieved modular hip prostheses and identified the larger heads (36 mm) as having more corrosion damage than smaller, 28 mm heads (Dyrkacz et al., 2013). However, although taper corrosion was initially linked to large head modular MoM components, the issue did not seem to be solely restricted to these components with recent evidence of taper corrosion with ALTR and elevated serum metal ions in modular MoP and modular CoP THAs (Rasquinha et al., 2006, Goldberg et al., 2002, Cooper et al., 2012, Kurtz et al., 2013, Whitehouse et al., 2015). In addition, a recent systematic review of all cases revised for symptomatic taper corrosion, Carli et al. (2015) found that the median head size was 46 mm for MoM and 36 mm for MoP components (Carli et al., 2015, Osman et al., 2016) .

Following the inspection of retrieved LH-MoM-THRs, Langton et al. (2012) reported on the pattern of material loss to be maximal on the neck taper on the opposite side of the head taper suggestive of a bending moment effect at the modular junction (Langton et al., 2012). This pattern of wear is suggestive of mediolateral toggling and its magnitude is directly related to the head-neck offset with macroscopic fretting having been demonstrated to increase in magnitude as the femoral head-neck offset is increased (Brown et al., 1995, Higgs et al., 2013). This finding is also supported by finite element analysis (FEA) (Donaldson et al., 2014a). Higher bending moments at the modular head-neck junction can be the result of increased head-neck offset, increased bearing diameter (Figure 5-1), increasingly varus neck shaft angle (Langton et al., 2012) and heavier more active patients (due to the increased force going through the taper).

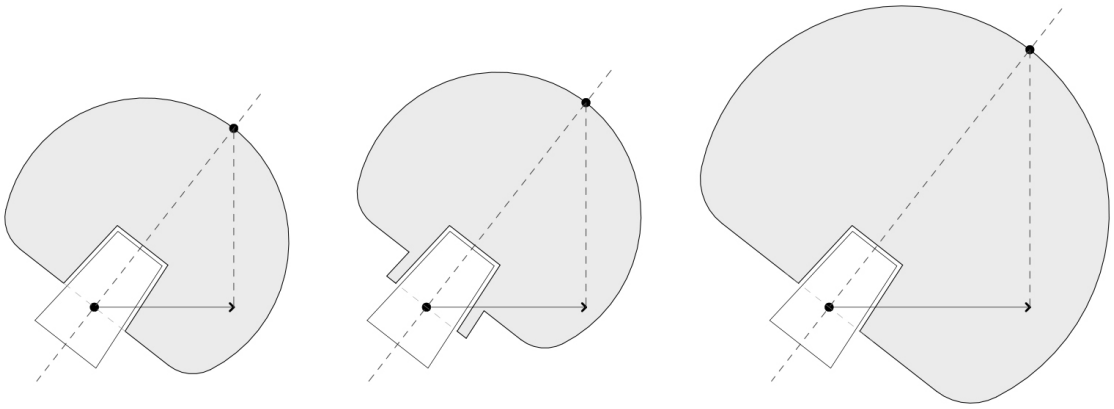

Figure 5-1: A diagrammatic representation of the effect of increased head offset and increased bearing diameter on the lever arm (horizontal arrow); the latter increases on both occasions.

Hence, a high bending moment may influence any taper junction where such conditions are created, with wide-reaching repercussions in the overall THR design.

The aim of this chapter was to investigate the effect of high bending moment on fretting corrosion and wear at the head-neck taper junction of in-vitro tested MoM THRs and to compare the pattern of wear seen to that of retrieved LH-MoM-THRs.

The objective was to perform long term (10 million cycles) in-vitro tests with high bending moment on implants provided by a well-known manufacturer, periodically analyse their electrochemical behaviour and assess their surface topography and wear and to compare findings from the in-vitro tests to the observed morphology of the taper junction from retrieved LH-MoM-THR prostheses.

5.2. Materials and Methods

5.2.1. Components

5.2.1.1. Implants

The in-vitro experiment comprised of six brand new '*Endo Head*' CoCrMo femoral heads and six '*QADRA-S*' Ti-6Al-7Nb stems; all provided by Medacta (Medacta International SA, Strada Regina, Castle San Pietro, CH-6874). All heads had a 40mm diameter with a smooth finished 12/14 taper; a cone angle of 5° 43' 30'' and high offset (+10.5mm) in order to replicate the high bending moment conditions, representative of a LH-MoM-THR. All stems had a 12/14 taper, 0 offset and a neck angle of 135°. Further details regarding the implants used can be found in Chapter 3 under section 3.2.1.2, titled *Implants* and in Table 3-2.

5.2.1.2. Retrievals

Five LH-MoM-THR retrieved prostheses were investigated. The prostheses were from cases referred to the LIRC and met the Centre's inclusion criteria (for further details refer to Chapter 3, section 3.2.1.3, titled *Retrievals)*. For the purposes of this study and to achieve better uniformity in the group, the prostheses were specified further to have been in situ for 3-5 years; moreover, cases of revision due to fracture, infection and component mismatch were excluded. Both stems and their corresponding heads had to be available for the retrievals to be included in the study. All the femoral heads were made of CoCrMo and had been used in combination with Ti-6Al-4V stems (Table 5-1).

Case	Gender	Manufacturer	Head design	Stem design	In situ (months)	Head size (mm)
1	Male	DePuy	ASR XL	Corail	40	50
2	Female	Smith and Nephew	BHR	Synergy	60	54
3	Female	DePuy	ASR XL	Corail	45	46
4	Female	Biomet	M2A	Taperlock	39	44
5	Male	Biomet	M2A	Taperlock	56	48

Table 5-1: Patient demographics and retrieval component details.

5.2.2. Pre-Test Implant Surface Analysis

Prior to the start of the study the surface profiles of the head and neck taper implants were measured using a computer-controlled radial and longitudinal measuring machine (Talyrond 365) as described in Chapter 3, section 3.3.1, titled *Coupon and Implant Head and Neck Taper Analysis* (Figure 3-2). Initial measurements were therefore taken to ensure that the surface roughness fell within appropriate tolerances whilst providing baseline measurements for later analysis.

5.2.3. Pre-Test Cleaning and Assembly

Following surface measurements the implants were cleaned and assembled as described in Chapter 3 sections 3.3.5 and 3.3.6, titled *Component Cleaning and Assembly* respectively.

5.2.4. Mechanical Load Testing and Electrochemical Testing

The six implant assemblies were placed into their fixtures and then mounted onto a purpose-built implant fatigue-testing machine (manufactured by R.D.P. Howden, Warwickshire, United Kingdom), used to apply load during testing (for a detailed description refer to Chapter 3, section 3.4.1, titled *Mechanical Load Testing)*. Examples of the modified experimental set up used in the anatomical configuration as per the ASTM

F1875 – 98 Standard modified *Method I* for implant tapers are shown in Figures 3-7 and 3-10 respectively. The implants were then sinusoidally loaded at 300 to 2300N for 10 million cycles, at 3Hz. Every 1 million cycles the fretting current was measured for 1000 cycles as described in Chapter 3, section 3.4.2.

The protocol described below was used for long term loading tests to provide quantitative measures of fretting corrosion rates at the implant taper interface over 10 million cycles:

1. Each electrochemical cell was filled with 200mL of the pre-titrated test fluid (fluid level just above the modular head-neck junction).
2. The specimen was initially unloaded.
3. OCP was monitored for 1 hour and observed to settle to a steady potential.
4. Sinusoidal load applied at 300 to 2300N at 3Hz was commenced.
5. After 1000 cycles a potentiostatic scan was performed at potential; OCP +200mV measuring the fretting current at the start of the sinusoidal load.
6. The implants then continued to be loaded for 1 million cycles without any applied potential.
7. At the end of the 1 million cycles a potentiostatic scan was performed at potential; OCP +200mV for 1000 cycles (whilst the implants continued to be sinusoidally loaded). Sampling rate of 48 data points per second. With the test running at 3Hz this equates to 16 data points per cycle.
8. Each 1 million cycles at 3 HZ took 4 days to complete. The test fluid was topped up to the same starting level during these 4 days. At the end of each 1

million cycles and after the fretting current was recorded for 1000 cycles the load was briefly stopped for the 200mL of the test fluid to be changed and then the sinusoidal load was restarted.

9. This procedure was repeated at every 1 million cycles up to and including 10 million cycles. In total the experiment took 40 days to complete.

5.2.5. Post-Test Implant Surface Analysis

Upon completion of the 10 million cycles the implants were pulled apart and disassembled. Note, that in subsequent chapters the components were disassembled by sectioning the taper junction in the sagittal plane and then gently peeling the two surfaces apart thus, preventing further potential damage/deformation caused by the shear effect of a pulling force. In this chapter however the in-vitro taper junctions were disassembled by a pulling force (not measured) similar to the way the retrieval tapers were disengaged in-vivo, thus creating a like for like comparison. The surface profiles of the head and neck tapers were measured using the Talyrond 365. The head tapers were then sectioned in the sagittal plane using a diamond-coated saw and both head and neck tapers were assessed using SEM. EDS was used to measure the elemental composition of any corrosion products that were seen on the taper junction.

5.2.6. Retrieval Analysis

All the retrieved components were visually inspected for macroscopic evidence of corrosion using the Goldberg score as described in Chapter 4 section 4.2.4. Surface profile analysis of the retrieval head and neck tapers was performed using the method described in Chapter 3, section 3.3.2, titled *Retrieval Head and Neck Taper Surface Analysis.* The head tapers were then sectioned in the sagittal plane using a diamond-coated saw and both head and neck tapers were assessed using EDS and SEM.

5.2.7. Statistical Methods

A Shapiro-Wilk test for normality found the data to be non-parametric. A comparison was made using a Mann-Whitney U-test to determine any statistically significant differences ($p=<0.05$) in the fretting currents during the 10 million cycles. All analyses were performed using Statistical package for the social sciences (SPSS) Statistics version 22 (Armonk, NY: IBM Corp.)

5.3. Results

5.3.1. Electrochemical Testing

A typical trace of the measured fretting current and an explanation of how the mean fretting current and mean amplitude current were calculated are shown in Figures 5-2 and 3-12.

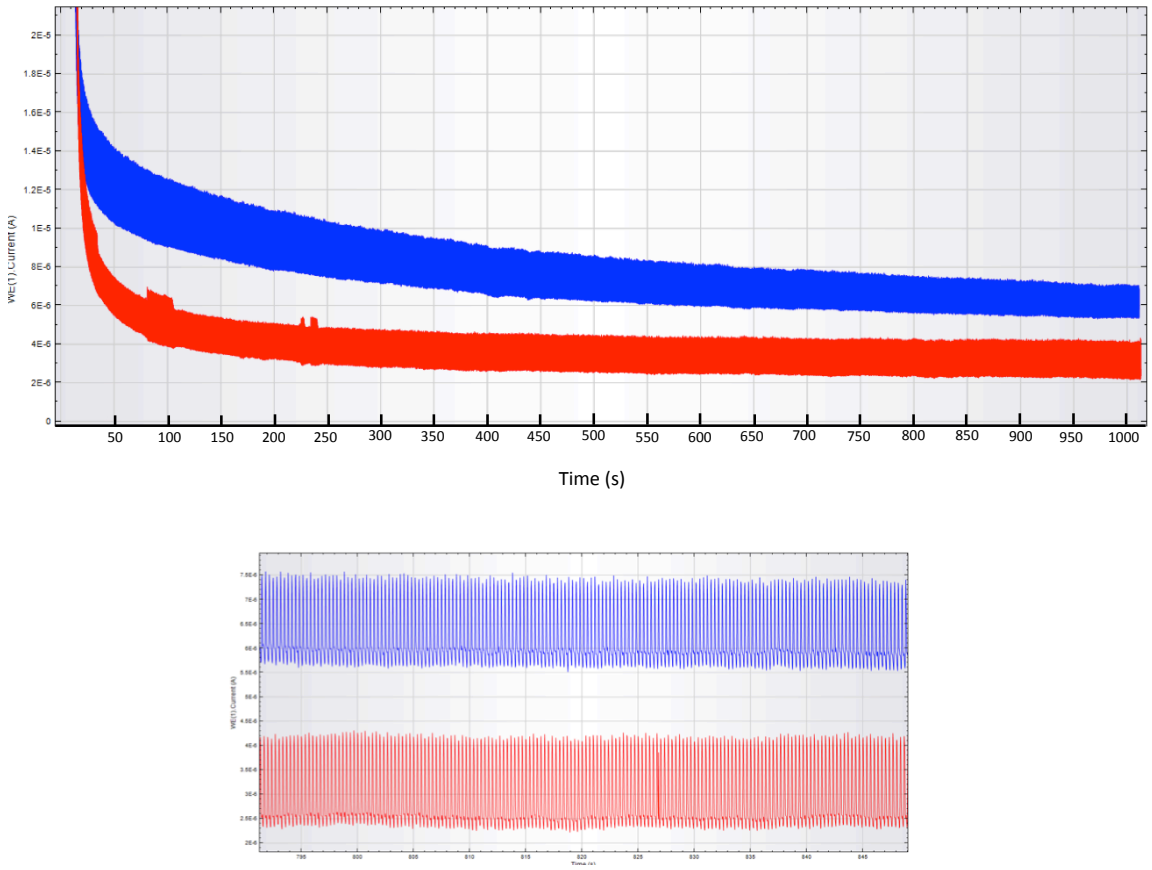

Figure 5-2: Graph showing individual fretting current readings over 1000 cycles for a single implant at 1 million (Blue) and at 2 million (Red) cycles. Note the lines in the uppermost chart are broad and represent a series of peaks and troughs shown in the expanded lower chart (also refer to figure 3-12).

The results obtained through this process were analyzed and the means of the maximum fretting current along with the mean amplitude current at every stage of the experiment are depicted in Figures 5-3, 5-4 and Table 5-2.

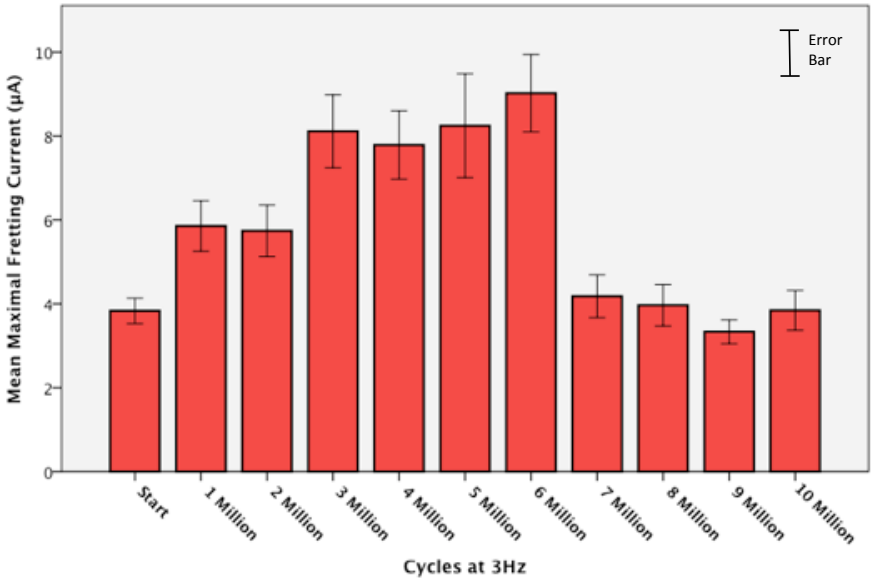

Figure 5-3: Mean Maximal Fretting Current (µA) at the beginning and every 1 million cycles.

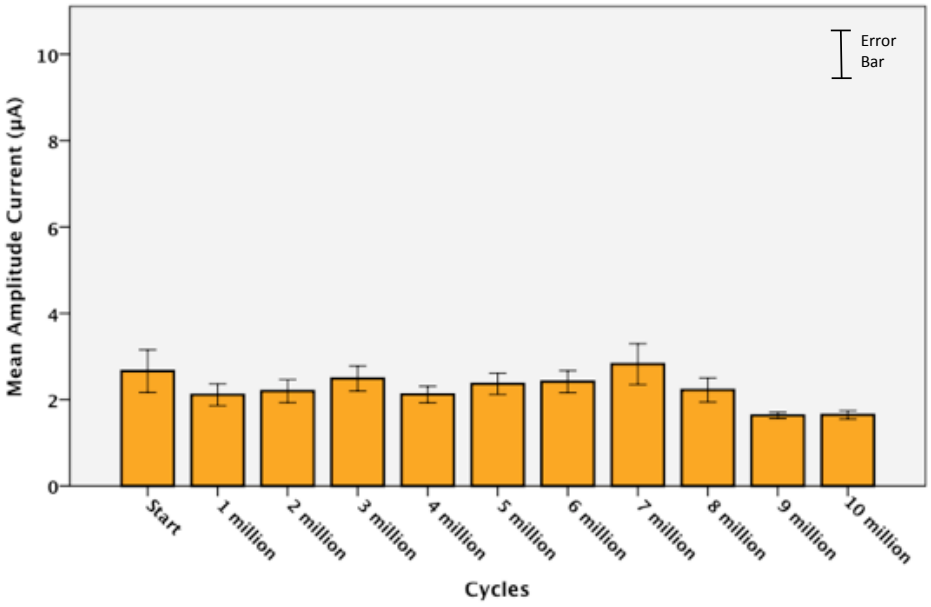

Figure 5-4: Mean Amplitude Current (µA) at the beginning and every 1 million cycles.

Cycles Completed	Mean Current (± Standard Deviation) - Average of n=6	
	Max Fretting Current (μA)	Current Amplitude (μA)
Start	**3.83** (±1.18)	**2.65** (±2.56)
1 million	**5.85** (±2.88)	**2.11** (±1.27)
2 million	**5.74** (±3.20)	**2.19** (±1.47)
3 million	**8.11** (±4.5)	**2.48** (±1.60)
4 million	**7.78** (±4.06)	**2.12** (±0.95)
5 million	**8.24** (±4.71)	**2.37** (±1.15)
6 million	**9.02** (±4.09)	**2.41** (±1.31)
7 million	**4.81** (±2.43)	**2.82** (±2.26)
8 million	**3.96** (±2.43)	**2.22** (±1.50)
9 million	**3.33** (±1.48)	**1.63** (±0.38)
10 million	**3.85** (±2.44)	**1.65** (±0.47)

Table 5-2: Results of the Mean maximum fretting and amplitude currents (μA).

Whilst the mean amplitude current is the same from start to 3 million cycles the mean maximal fretting current increases from time zero to 3 million cycles. The reasons for this are unclear but it could be associated with the recruitment of additional surface area as the taper junction '*beds in*'. It is possible that the local conditions allowed for micromotion at the start of the test with higher fretting currents recorded until deformation at the head-neck interface resulted in a better interlock, returning to a more 'stable' condition with smaller fretting currents. There is a significant increase in the fretting current from zero to 6 million cycles with a reduction in this current between 6 and 7 million cycles. There is no significant difference in the fretting current at 10 million

cycles and the fretting current measured at the start of the test. The statistical significance for these changes can be seen on Table 5-3.

Variable	**Combination Compared, "A vs. B" (n=6 for each)**	**Difference in average means, B – A (p-value)**	
		Max Fretting Current (μA)	Amplitude Current (μA)
Number of Cycles	Start **vs.** 1 million	**+2.02** (<0.001)	**-**
	Start **vs.** 6 million	**+5.19** (<0.001)	-
	6 million **vs.** 7 million	**-4.21** (<0.001)	-
	Start **vs.** 7 million	**+0.98** (NS -0.869)	-
	Start **vs.** 10 million	**+0.02** (NS - 0.402)	**-1.00** (0.036)

Table 5-3: The main changes in the fretting current and amplitude and their statistical significance using Mann-Whitney U test.

It is worth noting that the standard deviation for these means are very similar and this does appear to occur in all six implants. The mean amplitude of the current is similar for these six implants across the 10 million cycles however, in chapter 7 where the parameters such as torque and bending have been increased there seems to be a concomitant increase in both the mean maximal fretting current and in the mean amplitude of the current.

5.3.2. Surface Profile Analysis

5.3.2.1. In-Vitro Implants post 10 million Cycles

Examination of the in-vitro head taper showed the development of imprinting similar to that found in retrieval head tapers (Figure 5-5). The original surface profile of the head taper was evident outside the region where there was contact with the neck taper.

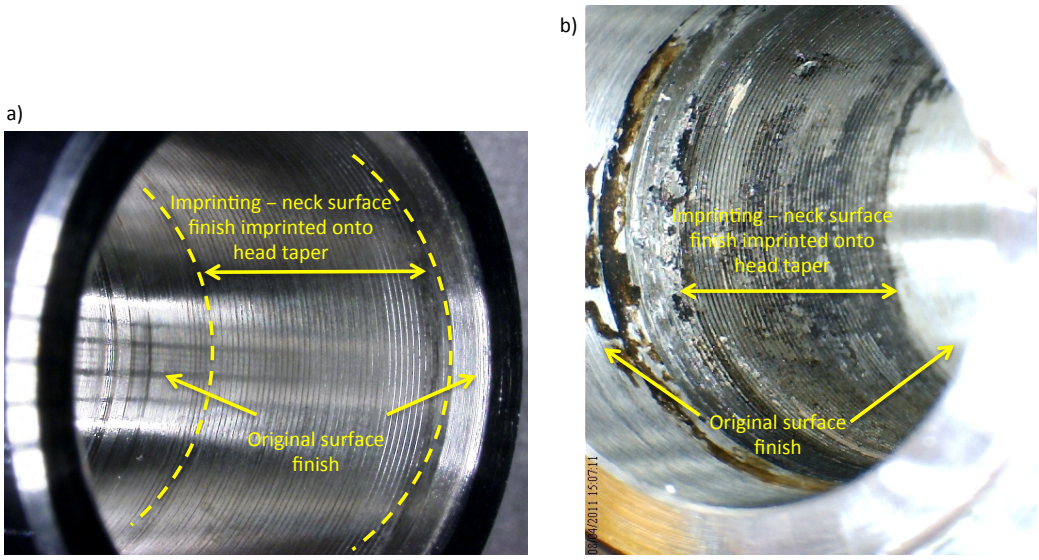

Figure 5-5: a) Photograph of an in-vitro head taper after 10 million cycles showing imprinting at the head-neck interface and the original surface markings of the head taper where it was not in contact with the neck taper. b) Photograph of a retrieval head taper also showing evidence of imprinting (magnification x15).

Imprinting was evident as the generation of coarser circumferential ridges in the region where the two tapers were in contact. Closer examination of the in-vitro head taper showed that in between these ridges the original machine markings could be identified (Figure 5-6).

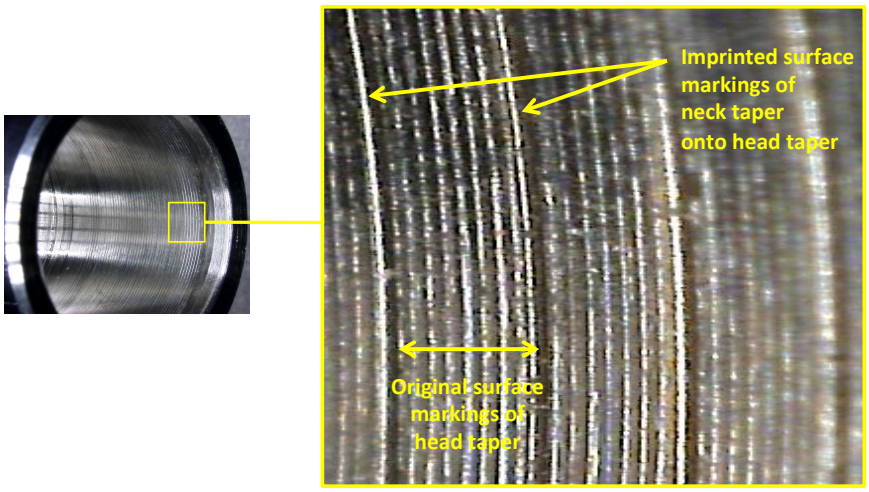

Figure 5-6: Photograph of an in-vitro head taper after 10 million cycles showing the original surface markings of the head taper that can be seen in between the imprinting markings of the neck taper (magnification x30).

The ridges associated with imprinting had the same periodicity as the surface ridges on the neck taper (Figures 5-7).

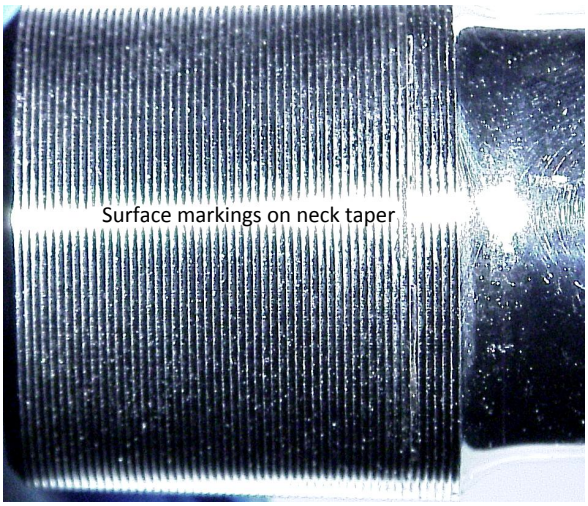

Figure 5-7: Photograph of an in-vitro neck taper after 10 million cycles showing the surface markings that have imprinted onto the head taper (magnification x5).

As well as being evident optically, these ridges could also be detected using surface profilometry (Figure 5-8).

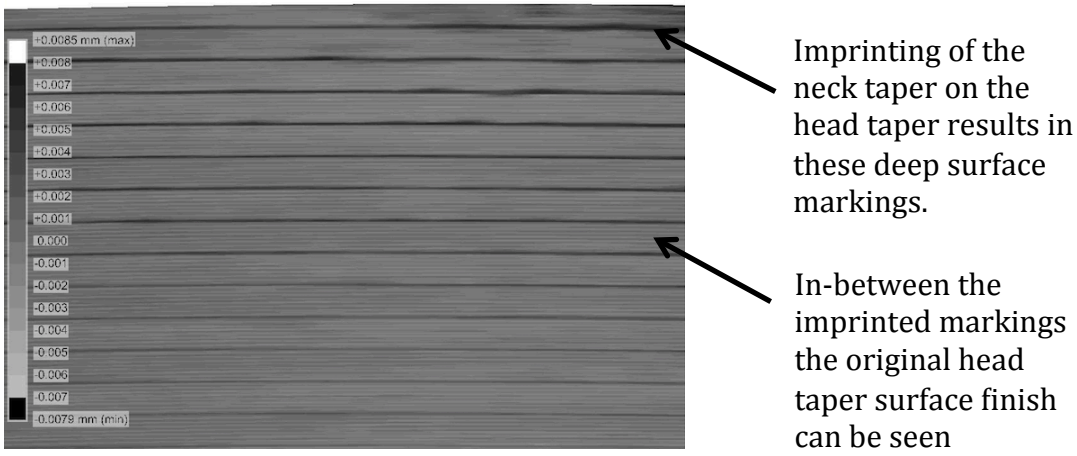

Figure 5-8: Close up of an in-vitro head taper using the Talyrond 365. The unidirectional deformation secondary to the imprinting of the rough neck taper surface on the head taper is evident.

The ridges seen were the result of loss of material and were more evident at the open/distal end of the head taper (Figure 5-9) where contact with the closed/proximal end of the neck taper took place evidenced by the deformation of the peaks and troughs on the surface of the neck taper in the closed/proximal region.

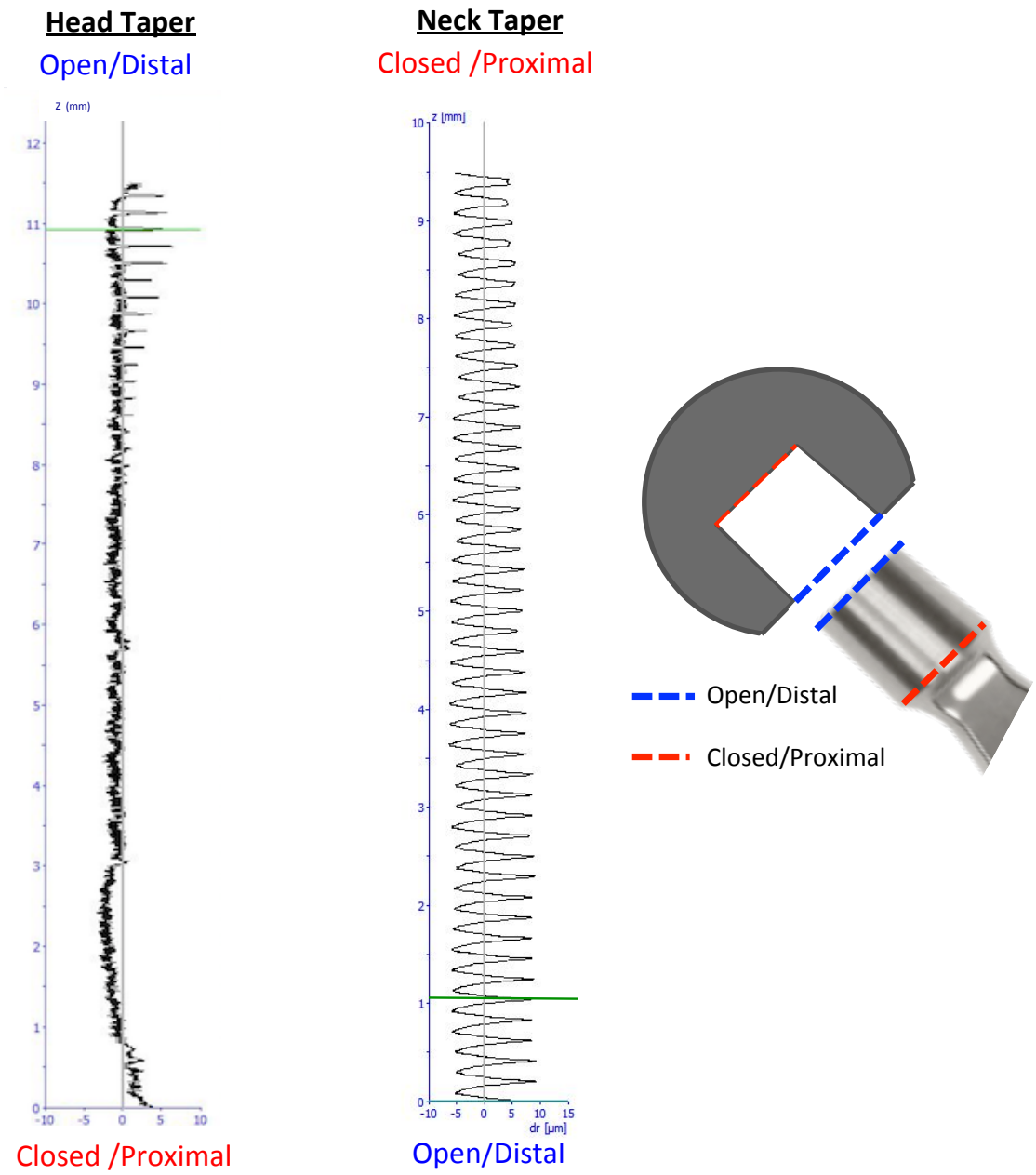

Figure 5-9: Single profile surface readings from in-vitro head and neck tapers in contact. The pronounced imprinting on the distal end of the head taper corresponds to the loss of roughness on the proximal end neck taper.

On the inferior surface of the head taper at the open/distal end a large gouge had developed and this was due to the bending which caused impingement and enhanced fretting and corrosion (Figure 5-10). In all six in-vitro cases, post 10 million cycles the

neck taper ridges were less pronounced and were more blunt at the closed/proximal end of the taper (Figures 5-9 and 5-10) and this is due to the neck taper contacting with the head in this region.

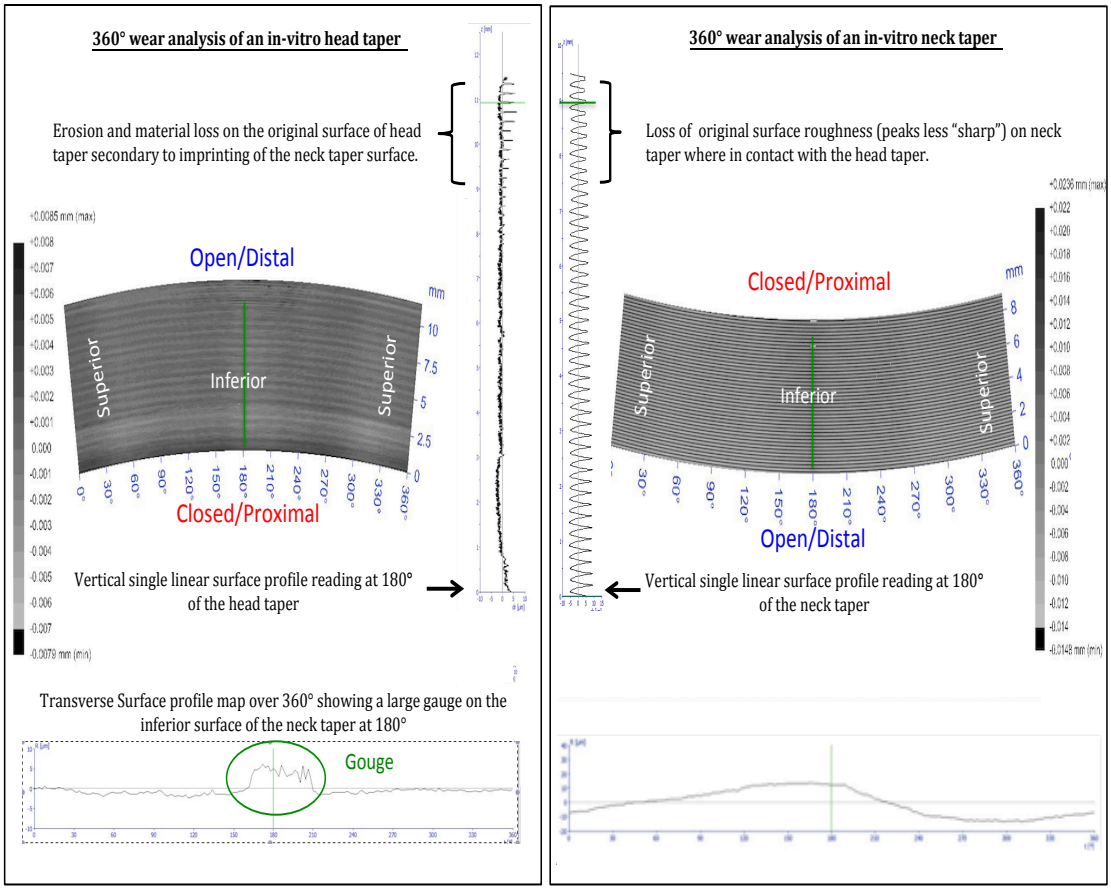

Figure 5-10: 360° wear analysis of an in-vitro head taper (left) and the corresponding neck taper (right) using the Talyrond 365.

Interferometry was used also to examine the surface topography of the same neck taper in the same position pre- and post- 10 million cycles loading. Their linear profiles are shown in Figure 5-11 noting that the surface R_a and R_z decreased after loading. However, this could also be associated with assembly impaction force and/or disassembly force.

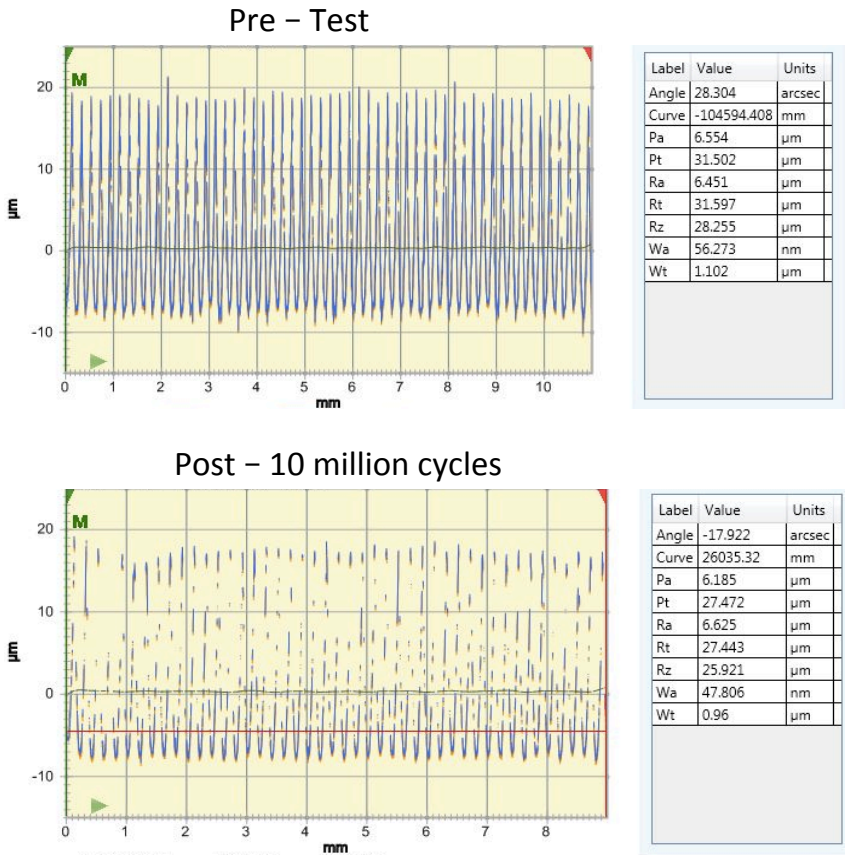

Figure 5-11: Surface profile measurements on the same neck taper showing the same line profile pre and post 10 million cycles of loading, identifying a smoothening of the neck taper of 2.33µm.

5.3.2.2. Retrievals

For the retrieved components, a comparison between their pre-implantation state and their condition after retrieval was not possible due to the lack of profilometry data before the initial surgery. Instead, the comparison was made between the unworn surfaces and the head-neck interface (Figure 5-12). The Goldberg score for retrievals is shown in Table 5-4.

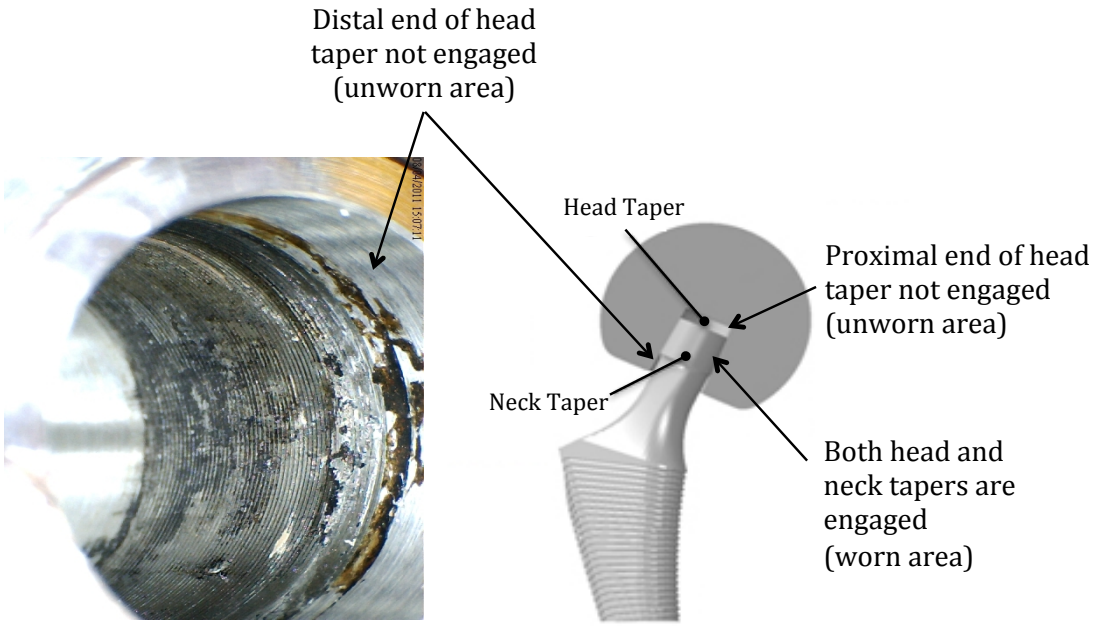

Figure 5-12: Close up photograph of a retrieved head taper and schematic diagram of the head-neck taper junction depicting a common situation where the entire neck taper is engaged with the head taper, whilst the latter has unworn areas. There are occasions where the most proximal portion of the neck taper is not fully engaged and can be used as a reference point for assessment of wear.

Case	Head Taper Corrosion Grading	Neck Taper Corrosion Grading
1	IV	II
2	III	II
3	IV	II
4	II	II
5	IV	II

Table 5-4: Analysis for corrosion using the Goldberg classification (Goldberg et al, 2002).

Figure 5-13 demonstrates the pattern of wear seen on a retrieval head taper. The close resemblance of the pattern of wear on this component to the one identified on the in vitro components (Figure 5-8 to 5-10) is clearly evident.

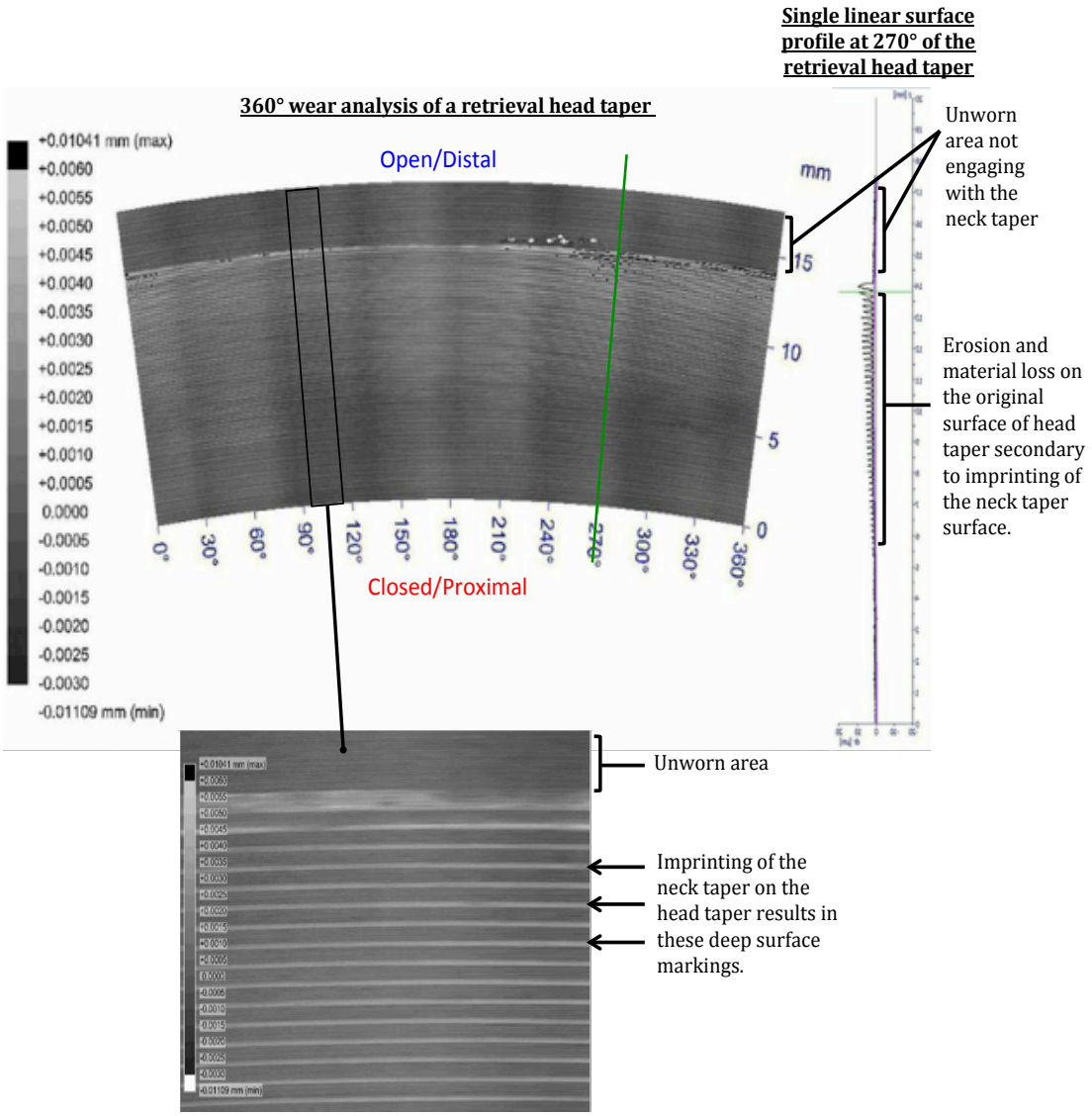

Figure 5-13: 360° wear analysis of a retrieval head taper showing evidence of wear similar to that seen in the in-vitro head tapers post 10 million cycles.

A similar pattern of wear was found in all the retrieved components, the only difference being the extent of the surface damage. Figure 5-14 shows two other retrieved head tapers where significant wear is evident. Interestingly, the retrieved components with the more extensive wear had been in situ longer than the ones damaged less.

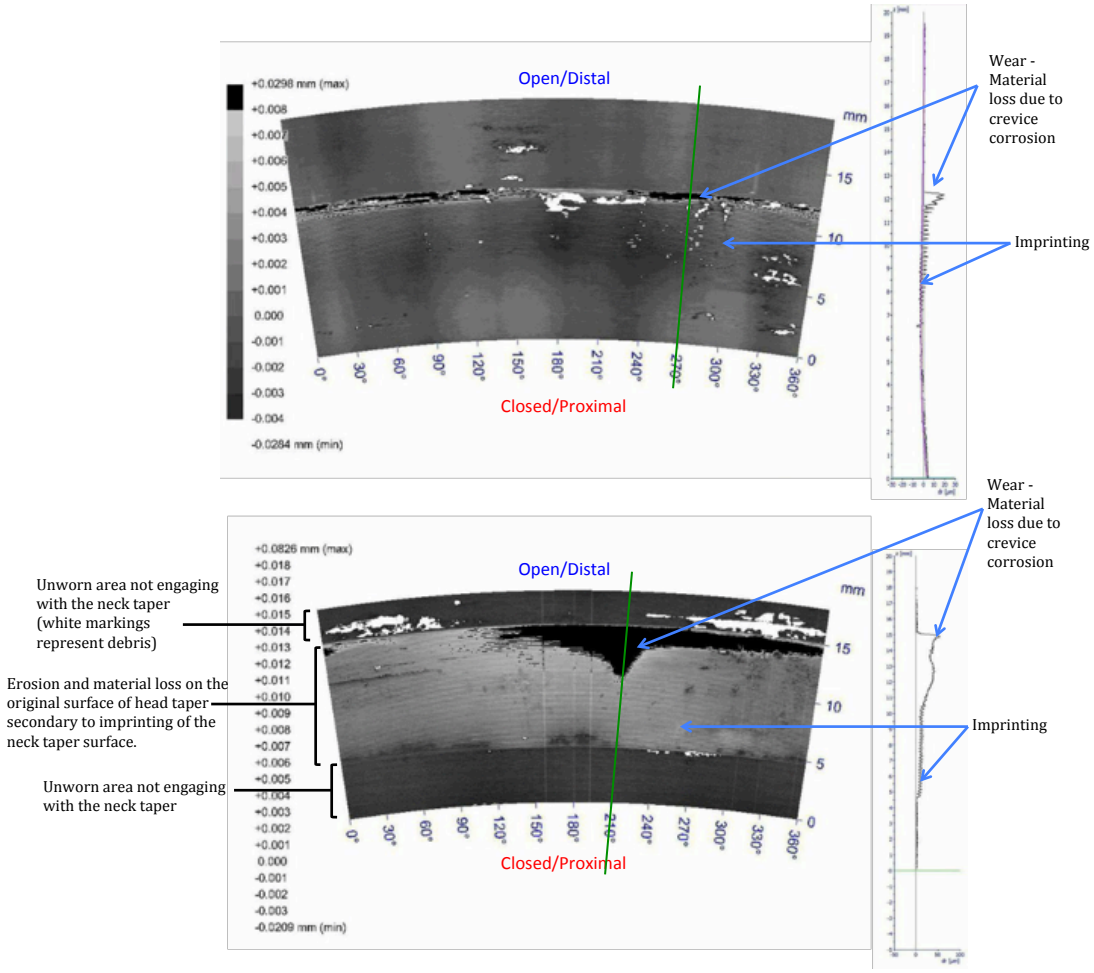

Figure 5-14: 360° wear analysis of two retrieved head tapers with significant evidence of surface damage.

5.3.3. Scanning Electron Microscopy Analysis

Evidence of imprinting was also evident on SEM analysis. Figure 5-15 depicts a clear demarcation between the edges of the in-vitro head taper (where the original machine finish can be clearly identified), and the imprinted area, which is more proximal.

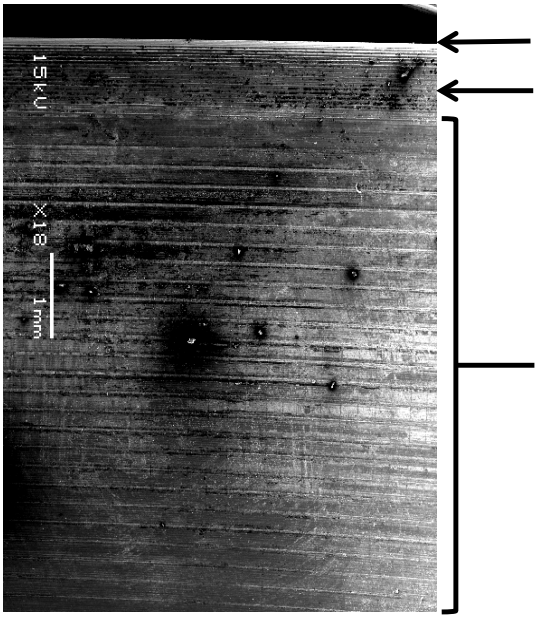

Edge of head taper

Unaffected area: displaying the original machine finish of the head taper.

Affected area: Surface finish of stem taper has imprinted onto the surface finish of the head taper.

Figure 5-15: Head taper SEM photograph showing a small unaffected zone close to the edge of the taper, where there was no contact with the neck taper, followed by the area of the interface, where there was extensive evidence of imprinting of the rough neck taper surface on the smooth head taper surface.

This pattern was evident both on the in-vitro and on the retrieved head tapers (Figure 5-16).

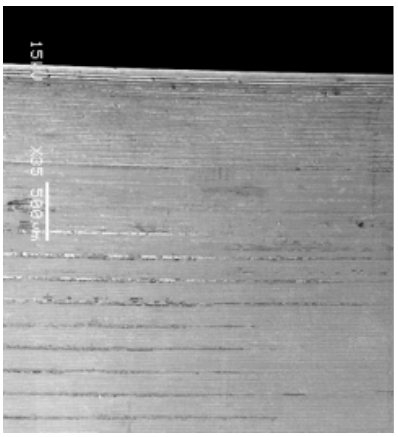

In Vitro Head Taper

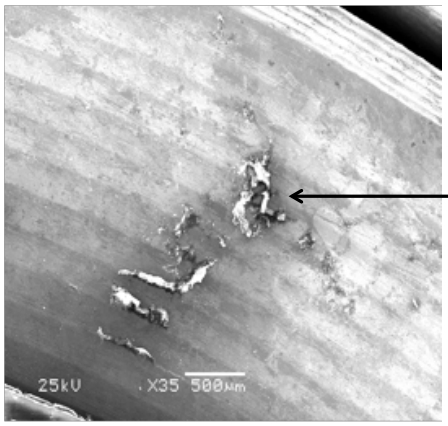

Wear Debris

Retrieval Head Taper

Figure 5-16: Head taper SEM photographs showing evidence of surface changes on the in-vitro and retrieved components (not matched for magnification). A small unaffected zone close to the edge of both tapers, where there was no contact with the neck taper, followed by the area of the interface, where there was extensive evidence of imprinting of the rough neck taper surface on the smooth head taper surface can be seen.

Contrary to the head, the neck taper was characterized by a rough surface as depicted in Figure 5-17. The predominant finding when examining the neck tapers, of both the in-vitro and retrieved components, was a pattern of increased damage with specific topographic characteristics; this type of damage was far more severe than the smoothening of the rough surface, which was uniformly observed.

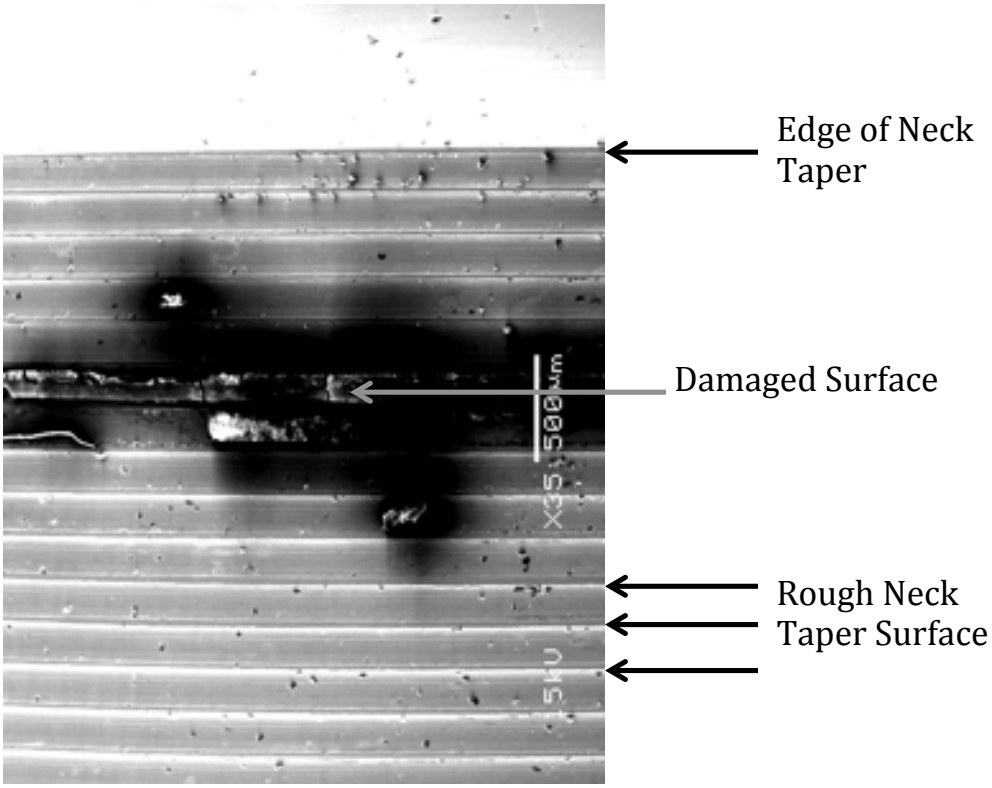

Figure 5-17: SEM photograph of an in-vitro neck taper showing evidence of localized, increased surface damage as well as the roughened surface, which is what imprints onto the neck taper.

This topographically characteristic area of surface damage on the neck taper was matched by corresponding surface damage on the head taper. Figures 5-18 and 5-19 depict the findings across the head taper under SEM and clearly identify an area of increased damage (purple circle). According to the markings on the in-vitro components, this area was at corresponding surfaces for the head and neck tapers. Similar findings

were noted on the retrieved components as well, although the exact topography was impossible to locate with precision.

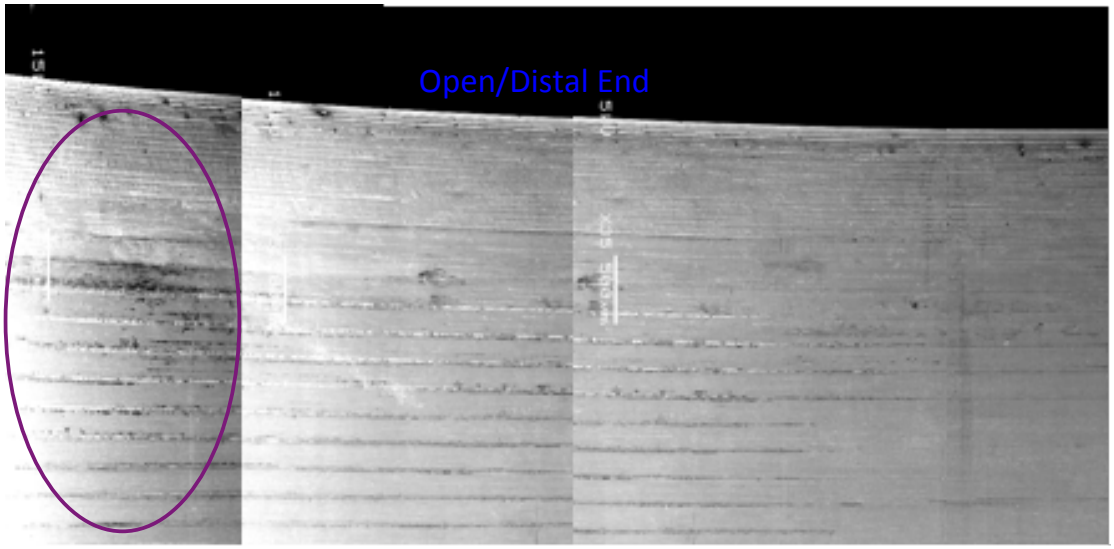

Figure 5-18: Panoramic view of an in-vitro head taper at small magnification under SEM, identifying an area of increased damage (purple circle), which matches the corresponding surface on the neck taper shown above in Figure 5-17. Also showing a circumferential transition from a more corroded region to a less corroded region that occurred on the open/distal inferior surface (from right to left) and associated possible with the toggling effect.

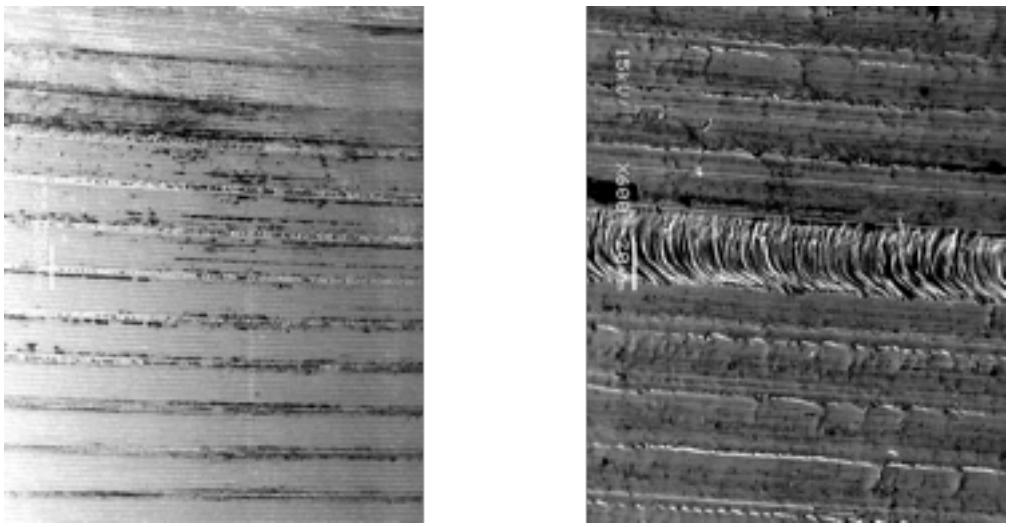

Figure 5-19: The same area shown above in Figure 5-18 (purple circle) under subsequently larger magnifications. The damage on the surface is evident.

5.3.4. Energy Dispersive X-ray Spectroscopy Analysis

Ti alloy is known to have different mechanical properties than CoCrMo alloy, such that transfer of Co and Cr from the head taper to the neck taper would be expected to be found at the modular junction. Both the in vitro and retrieved components were examined; specific areas were identified under SEM and further assessed with EDS. Titanium ions (Ti) were found at the rough surface of the neck tapers, as expected based on their chemical composition. At the same time, damaged neck taper areas were assessed with EDS and identified Co and Cr, implying transfer of material at the interface. The pattern of transfer of Co and Cr was identical for the in vitro and retrieved implants (Figure 5-20).

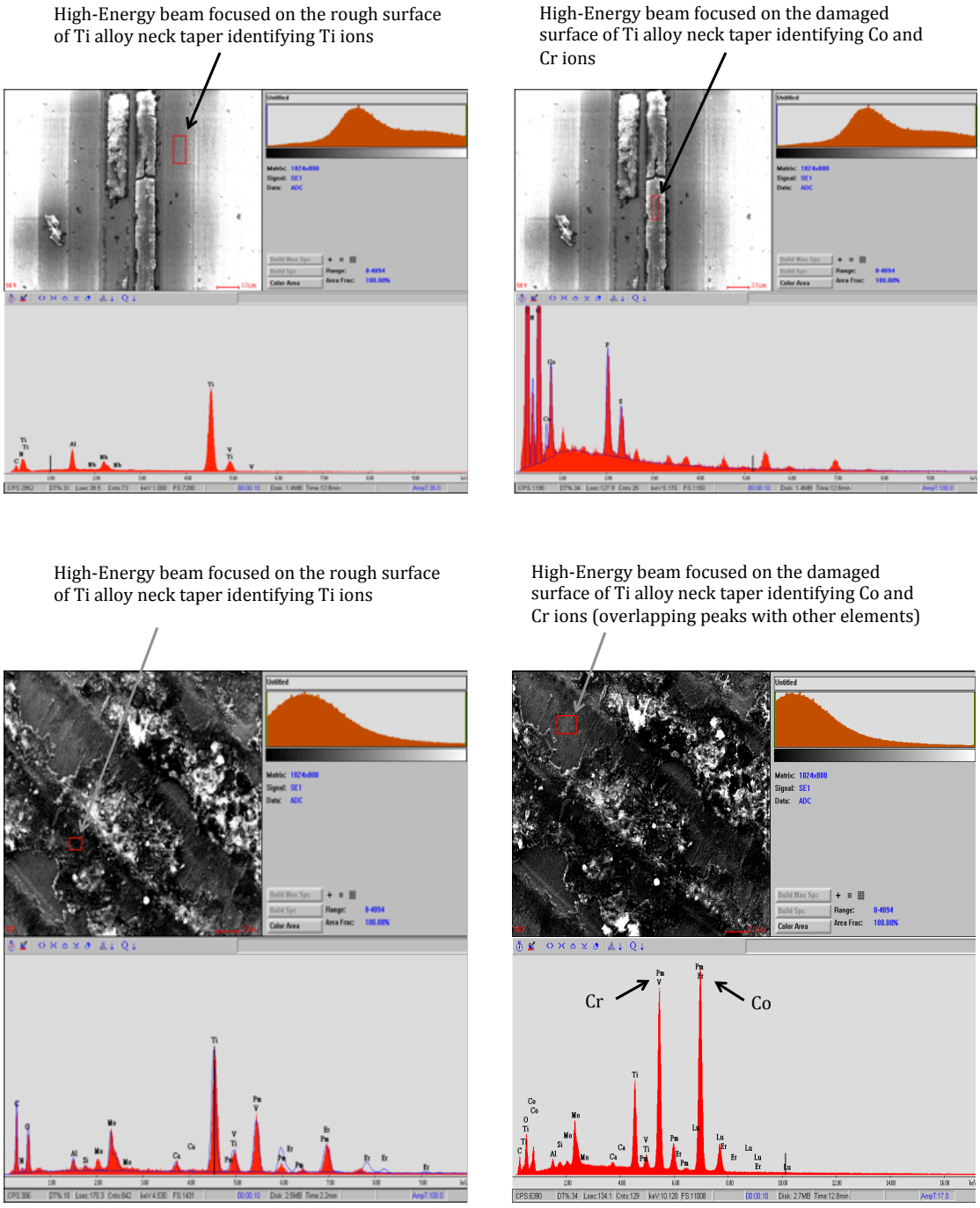

Figure 5-20: EDS at different regions of an in-vitro neck taper (top two images) and of a retrieved neck taper (bottom two images) (SEM magnification 15kv, x600) isolating the types of ions that were expected based on the implant composition and material transfer.

5.4. Discussion

5.4.1. Summary of Results

This study aimed to investigate the effect of bending moment on fretting corrosion and wear at the modular head-neck taper junction of MoM THRs. This involved an experimental component, where implants with a high-offset replicated conditions of increased bending moment, and an evaluation of the morphology of the taper junction from retrieved prostheses that allowed for comparative assessment.

Fretting corrosion was assessed in-vitro by measuring the fretting current during cyclic loading. The predominant observation was a pattern of increased mean maximal fretting current from the second to the third million cycles, which then remained high for four million cycles and subsequently reduced to lower levels from the sixth to the seventh million cycles. This was not believed to be due to technical error, as all components showed this trend and these changes were statistically significant. It is unknown why the fretting current reduced after six million cycles, but the belief is that this pattern was due to a sequence of events occurring at the modular head-neck taper junction. The initial impaction was sufficient in order to create a relatively stable, well-fixed interface. Subsequently the cyclic loading initiated a process of limited micromotion at the interface, with an almost uniform fretting current observed up to the third million cycles. At that point, it is possible that the local conditions allowed for increased micromotion and higher fretting currents to be recorded until the seventh million cycle, when deformation at the head-neck interface resulted in a better interlock, returning to a more "stable" condition with smaller fretting currents.

The second part of this study concentrated on identifying the pattern of wear at the in-vitro interface and comparing it to that of the retrieved components. Macroscopic

examination of the various components revealed obvious signs of wear on the implants, both the in-vitro ones and the retrievals. Profilometry data were then assessed. The in-vitro components had the same pattern of wear with the retrievals, mainly comprising of imprinting of the rough neck taper surface on the smooth head taper surface (Figures 5-8 and 5-13). The imprinting was uniformly present, irrespective of the extent of the observed surface damage. Indeed, even the retrieved implants that exhibited significant localized wear (Figure 5-14) had the same pattern of imprinting present.

Further to the above, the implants were also examined under SEM. Similar to the findings from profilometry extensive evidence of imprinting of the rough neck taper surface on the smooth head taper surface was identified. More importantly, on the in-vitro components there were areas of increased wear with a clear topographic orientation (Figures 5-18 and 5-19). Before the assembly of the in-vitro components, they had been marked to allow for orientation. As a result it was possible to "track" the surface damage on the head tapers and correlate it to corresponding areas on the neck tapers. Such an approach was impossible for the retrieved components and the heads were retrieved without the stems. As a result identifying the exact topography of the head taper surface wear and correlating it to a corresponding area on the neck taper was less reliable; but, the similarities between findings were too significant to be ignored. The appearance on the in-vitro samples was consistent with damage caused in bending and as this appearance was similar to that seen on retrieved samples I conclude that bending moment plays a significant role in taper damage.

Langton et al., (2012) described similar findings on retrieved components, which they attributed to a "toggle effect" secondary to increased bending moment. They suggested that; "the mechanical action causes damage to the taper surface and opens the junction

to the potential corrosive effects of physiologic fluids". Based on our findings, such an explanation is very plausible.

Following the assessment under SEM, we also used EDS. This further supported the previous findings; indicating material loss of CoCr alloy head through corrosion with the pattern of material transfer identical for the in-vitro and retrieved components.

The most prominent overall finding during our various assessments was the imprinting of the rough neck taper surface on the smooth head taper. This was more prominent in areas associated with increased bending moment and was often accompanied by evidence of extensive wear. At the same time, imprinting was also noted to a lesser degree on the rest of the CoCr alloy heads.

5.4.2. Study Limitations

This study has a number of limitations. To start with, in terms of the in-vitro components, the surface changes were not large enough to be statistically significant or provide reliably quantifiable data. The same was the case with some of the retrieved components. The rest of the retrieved components had surface changes that were large enough to be quantified reliably and exhibited statistical significance; the overall lack of data though meant that the assessment could largely be only observational. The lack of statistically significant, quantifiable data from the in-vitro profilometry is suggestive of the fact that this type of test may not have been sensitive enough to measure the extent of wear at 3Hz and after 10 million cycles. This might be an important finding for future corrosion testing, which should perhaps either be conducted over a longer period of time (<3Hz) or for more than 10 million cycles, the latter being the equivalent of five years in vivo. This could also have repercussions for the industry; manufacturers, who often test their components using 5 million cycles and possibly should adjust their protocols in

order to reliably, assess the relevant characteristics of their implants. Furthermore, the in vitro components were different to the retrieved ones, themselves being mostly dissimilar; however, interestingly, this did not appear to influence the findings.

5.4.3. Conclusions and Further Work

The long-term cyclic loading test was able to induce imprinting similar to that seen on retrieved implants. Both the head and the neck tapers are associated with fretting corrosion, but as with the retrievals this was more obvious on the head tapers than on the neck tapers. The head tapers showed the characteristic imprinting, which was particularly evident at the open/distal end of the taper. In this region deep grooves were evident and the periodicity of the imprinted circumferential grooves matched the finish on the neck taper. For the head taper the most damaged part was on the inferior distal surface and deep gouges were evident on the heads in this region.

Although less obvious, the neck tapers also showed evidence of fretting corrosion and the position of this mirrored that seen on the head tapers. After cyclic loading for 10 million cycles the proximally machined ridges on the neck taper reduced in height and were less sharp. At this point this could be down to corrosion due to the contact with the head taper, which appeared to occur more proximally or it could be due to deformation.

Although LH-MoM-THRs have been withdrawn from the market, conditions of increased bending moment can occur with implant combinations currently in wide use; simply by using a high offset CoCrMo head on a Ti-6Al-4V stem. To the best of my knowledge this is the first study that has shown the effect of high bending moment on fretting corrosion and wear at the modular head-neck junction. The clinical relevance of the findings is considerable; suggesting that surgeons should aim to avoid the use of high-offset CoCrMo heads particularly on Ti alloy stems where the necks have a high

inclination angle, by carefully planning and expertly performing their operations. It also suggests that the industry should reconsider some of the basic design principles of modular THR taper junctions. The next chapter will concentrate on the taper design factors and in particular the effect taper surface roughness and taper contact area have on the fretting corrosion at the modular junction.

Chapter 6 The Effect of Contact Area and Surface Topography on Corrosion at the Modular Junction

6.1. Introduction

* The need to increase the range of motion and prevent impingement in THRs has led manufacturing companies to develop shorter neck tapers or partially flattened taper/neck regions. Modern tapers are shorter with increased flexibility, making them more susceptible to corrosion than their predecessors (Porter et al., 2014). These designs, result in a reduced surface area at the junction, which may impact on the wear and corrosion process secondary to increased stress and concentration of bending force at the interface due to the use of large MoM heads. In a systematic review of components which were revised for symptomatic taper corrosion, the size of the taper was documented in 431 cases, of which all were 12/ 14, or smaller, in diameter (Carli et al., 2015).

In addition wide variation exists in the surface finish that manufacturers use for tapers in their attempts to improve fixation at the head-neck junction (Munir et al., 2015). The design of neck tapers was changed to incorporate increased roughness often with threaded surfaces to accommodate ceramic heads, which are less deformable than CoCrMo. In general this rough surface finish on the neck taper is the standard finish specified by some; for use with both ceramic and metal heads and is commonly used by a number of manufacturing companies. It should also be noted that 12/14 tapers from

* This chapter (Enhanced Wear And Corrosion in Modular Tapers In Total Hip Replacement Is Associated With The Contact Area And Surface Topography) was published in the Journal of Orthopaedic Research in July 2013.

different manufacturers might have differing angles and lengths, which can again alter the contact biomechanics.

Despite this, the literature is relatively deficient in identifying the importance of various parameters of taper geometry and the significance of surface topography in relation to corrosion at modular junctions is poorly understood.

The aims of this study therefore, were to investigate whether the use of neck tapers with reduced contact area resulted in enhanced wear and corrosion at the taper interface compared to standard neck tapers and if the surface finish of the modular components affected this.

6.2. Materials and Methods

6.2.1. Components

Neck tapers were manufactured using a conventional machine centre with a constant feed rate in Ti alloy (ASTM F136, 2013), and were machine finished. The neck tapers had a 12/14 taper with a cone angle between 5°37′30″ to 5°42′30″. The neck tapers with full length taper contact were termed 'standard' while tapers with reduced surface area were termed 'short' neck; they had a portion of the neck on either side reduced as two flats, which effectively reduced the contact area at the interface (Figure 6-1).

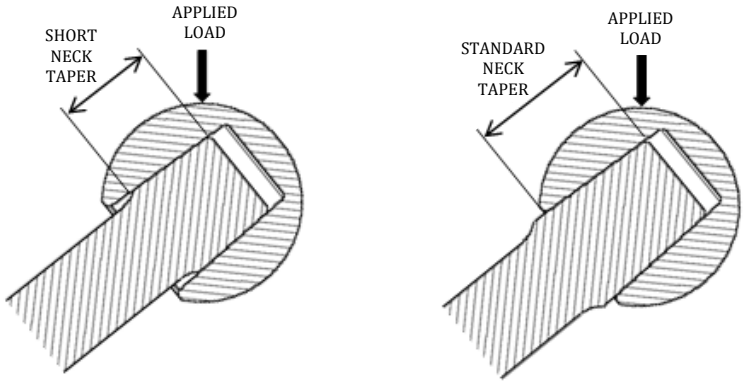

Figure 6-1: Diagram illustrating the difference in contact area between the short and standard neck tapers with the head tapers.

All heads were *'Metasul'* CoCrMo alloy (28mm diameter) from a single manufacturer (Zimmer, Inc. Warsaw, Indiana) with a cone angle 5°43'30". The heads were all +8 (long neck) to induce relatively high bending moment at the taper interface. For further details regarding component specifications refer to Chapter 3, sections 3.2.1.1 and 3.2.1.2, titled *Head and Neck Taper Coupons* and *Implants* respectively. Two tests were planned: in Test 1, rough short neck tapers were compared with rough standard neck tapers; in Test 2 rough short neck tapers were compared with smooth short neck tapers.

6.2.2. Surface Parameters

Surface profilometry as described in Chapter 3 was used to define the surface roughness of head and neck tapers pre and post-testing. Before the tests, the head tapers had an R_a value of 0.58 µm and R_z value of 2.8 µm. The R_a value for the rough short neck tapers was 2.73–2.79 µm, for the smooth short neck tapers 0.28–0.38 µm, and for the rough standard neck tapers 2.75–3.5 µm. In Test 1 measurements were made along a plane, which was the area adjacent to the non-articulating flats; in Test 2 measurements were taken along the same plane and at a plane that was 90° to it. Components were then passivated, cleaned and assembled as described in Chapter 3.

6.2.3. Mechanical Load Testing

Two cyclic load tests were prepared: In Test 1 rough short neck tapers (n=3) were compared with rough standard neck tapers (n=3). In Test 2 rough short neck tapers (n=3) were compared with smooth short neck tapers (n=3). The six assemblies for Test 1 were placed into their fixtures and mounted onto a purpose-built implant fatigue-testing machine (manufactured by R.D.P. Howden, Warwickshire, United Kingdom), used to apply load during testing (for a detailed description refer to Chapter 3, section 3.4.1, titled *Mechanical Load Testing)*. Following Test 1 the six other components of Test 2 were set up in a similar fashion. Examples of the experimental set up used in the anatomical configuration as per the ASTM F1875 – 98 Standard modified *Method I* for implant tapers are shown in Figures 3-9 and 3-10 respectively. The components were then sinusoidally loaded at 100 to 3100N for 10 million cycles, at 4Hz. The tests for each set of six components took 30 days to complete the 10 million cycles. The test fluid level was topped up just above the modular head-neck junction throughout testing. Electrochemical testing was not performed during the 10 million cycles for either Test 1 or Test 2.

6.2.4. Electrochemical Testing

To examine the electro-potential properties of the taper interface two of the test components that were previously used in the cyclic load test (Test 2) were chosen for the electrochemical tests: a rough short neck taper (R_a= 2.79μm) and a smooth short neck taper (R_a= 0.38μm). Application of electrical potential to the interface could induce additional corrosion compared with the remaining samples in both series. However as, the potentiostatic test for a relatively short time, the additional change in the surface texture associated with any corrosion was assumed negligible.

A cyclic load between 100 and 1500N (2x body weight) was used; this load is above that reported to initiate fretting corrosion in mixed alloys (Gilbert et al., 1993) and a frequency of 0.66 Hz was employed. The rest of the test set-up geometry and parameters were the same as those used for the mechanical load testing and electrochemical testing described in Chapter 3.

The protocol described below was used for short term loading tests to provide quantitative measures of fretting corrosion rates at the implant taper interface (head taper with rough short neck taper vs. head taper with smooth short neck taper) over 1600 cycles:

1. Each electrochemical cell was filled with 200mL of the pre-titrated test fluid (fluid level just above the modular head-neck junction).
2. The specimen was initially unloaded.
3. OCP was monitored for 1 hour and observed to settle to a steady potential.
4. A potentiodynamic cyclic polarisation scan was performed at a rate of 5 mV/sec starting at a cathodic potential of OCP-250mV to an anodic potential limit of 1V before reversing the potential at the same rate down to 0 mV.
5. OCP was again allowed to settle until a steady level was reached which took approximately one hour.
6. Sinusoidal load applied at 100 to 1500N at 0.66Hz was commenced.
7. A potentiostatic scan was performed at potential; OCP +200mV for 1600 seconds.
8. The sinusoidal load was initiated 50 seconds into the potentiostatic scan and terminated 1550 seconds into the scan giving sufficient time for the current to

settle pre & post loading. Sampling rate of 48 data points per second. With the test running at 0.66Hz this equates to 73 data points per cycle.

9. The specimen was then unloaded.
10. OCP was again allowed to settle for 1 hour.
11. A post-cyclic loading potentiodynamic cyclic polarisation scan was performed using the same parameters described in step (4).
12. Fluid was removed and the test cell was washed out.

6.2.5. Post Testing Preparation and Analysis

Damage to the modular taper was assessed at the end of the loading regime. The components were first set in resin to provide a stable mounting structure and then sectioned along the length of the taper in the sagittal plane using a diamond-bladed bone cutting saw to separate the head and neck without damaging the interface. The specimens were then washed in acetone in an ultrasonic bath for 1 h and cleaned with distilled water for 1h. Surface profilometry and SEMs were performed on all specimens.

6.2.6. Statistical Methods

The fretting current measurements were examined using the Shapiro-Wilk test for normality and found to be non-parametric. The Mann-Whitney U-test was therefore used to determine any significant differences in the measurements for the surface finishes between the rough short and rough standard neck tapers (Test 1) and the rough and smooth short neck tapers (Test 2). A p-value < 0.05 was considered statistically significant. All analyses were performed using Statistical package for the social sciences (SPSS) Statistics version 22 (Armonk, NY: IBM Corp.).

6.3. Results

6.3.1. Surface Measurements from Test 1 (Rough Short vs. Rough Standard Neck Tapers)

The surface profile of the head tapers changed with testing, more evidently on the heads with short neck tapers. R_a and R_z values for head tapers are summarized in Figure 6-2. Before the test the mean surface finish R_a of the head tapers in the short neck tapers and standard neck tapers groups averaged 0.58±0.06µm. After the test the head taper R_a values in both groups had increased which is an indication of physical change to the surface of the head taper. After cyclic load testing, the short neck taper group had significantly higher ($p=0.046$) head taper R_a values (mean 1.72µm) compared to the standard neck taper group (mean 0.98µm). Although the change in head taper R_a was less for the standard neck taper group it was significantly increased compared with the start of the test ($p=0.046$). The head taper R_z increased in both groups. The increase was significant ($p<0.05$) in the short group where the R_z values increased from 2.9 to 6.2 µm when compared to the standard neck taper group (mean = 4.5µm). The mean increase was 3.4±0.31µm in the short neck taper group and 1.7±0.65µm in the standard neck taper group as compared to pre-test values.

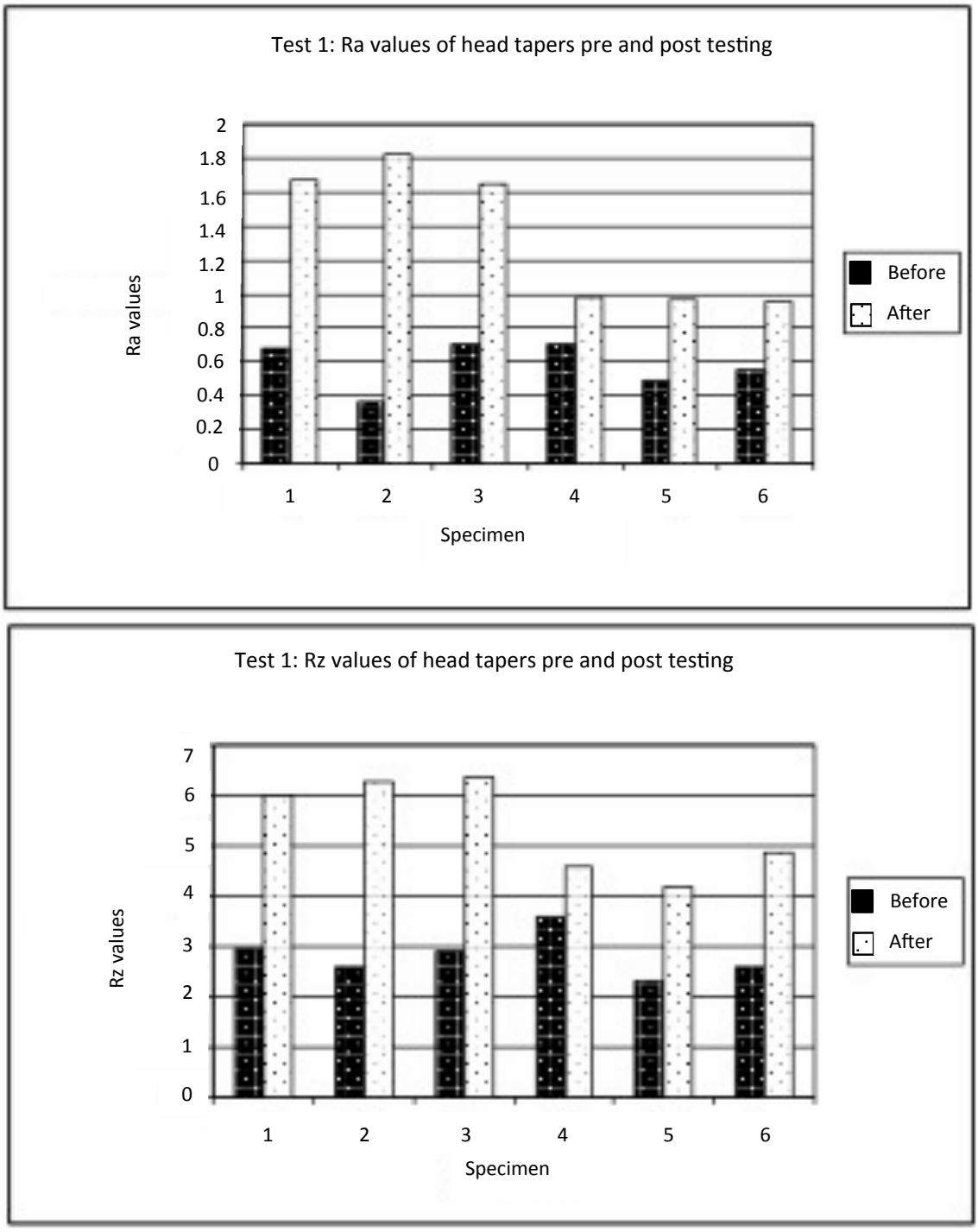

Figure 6-2: R_a and R_z values for head tapers for Test 1. Specimen 1, 2, and 3 were the rough short and 4, 5, and 6 were the rough standard neck taper groups.

The change in profile was most dramatic on all heads in the superior part. For heads coupled with the short neck tapers, an area adjacent to the distal cut out remained where the original surface profile and the machine marks of the head could be identified (Figure 6-3a). In the short group, the original surface profile and machine marks on the head tapers in the inferior region (the region not in contact with the short neck taper) could be identified in all specimens. On heads coupled with short neck tapers, a distinct change in the surface profile occurred superiorly from the original machine marks to a surface with circumferential grooves (Figure 6-3b). These grooves were more widely spaced and deeper than the original machine marks. There was loss of material with the coarser circumferential grooves, as shown by reduction in the height of the surface profile (Figure 6-3c). SEM also showed that the valleys of the grooves were corroded and pitted whereas the peaks demonstrated the original machine marks (Figure 6-3d). For the neck tapers in both designs, consistency was found within the groups. R_a values ranged from 2.73 to 2.79µm in the rough short group and 2.75– 3.5µm in the standard group. For the neck tapers, R_a and R_z values showed no differences before and after testing.

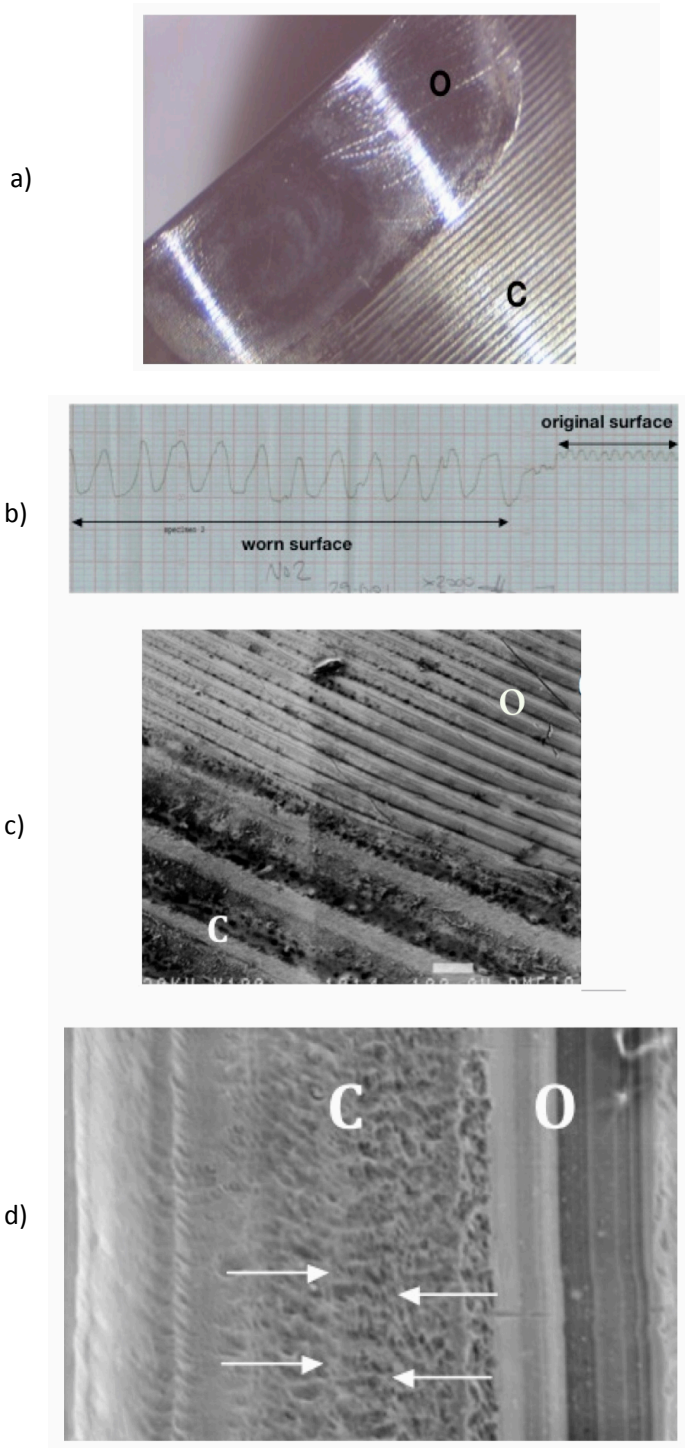

Figure 6-3: (a) Photograph of the internal bore of a head taper coupled with a rough short neck taper after cyclic loading in Test 1 showing the original surface finish (O) and the corroded area (C). (b) Superior surface profile traces for a head taper coupled with a mini neck taper showing the original machine marks and the new circumferential marks. (c) SEM showing the original finish (O) and broader grooves (C) associated with loss of material. Bar=100µm. (d) SEM of the circumferential marks (C) and the original surface finish (O). Pitting was seen in the circumferential grooves. Marks on the peaks were seen in the corroded area (arrows) retained from the original surface.

6.3.2. Surface Measurements from Test 2 (Rough vs. Smooth Short Neck Tapers)

R_a and R_z values for Test 2 for head taper pre and post testing are shown in Figure 6-4.

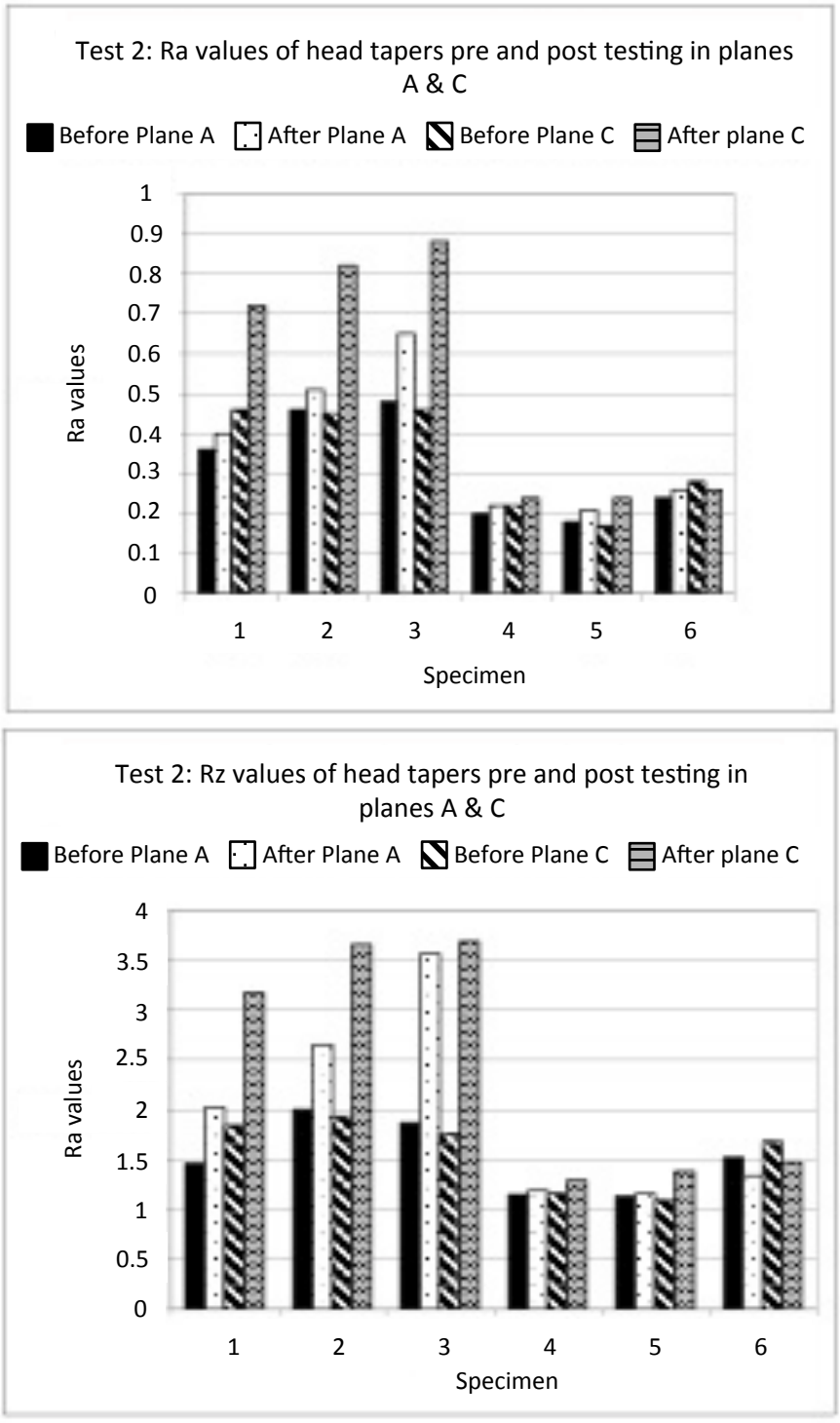

Figure 6-4: R_a and R_z values for head tapers of both designs in Test 2. Specimen 1, 2, and 3 were the rough and 4, 5, and 6 were the smooth short neck taper groups.

The head tapers coupled with rough short neck tapers had a mean R_a value of 0.45±0.04µm. After testing the greatest change was observed in the superior plane - (plane *C* - 0.35±0.08µm) (Figure 6-5). No significant change in the R_a values occurred on the head tapers with the smooth neck tapers. For the rough neck tapers R_a increased in plane *A*, but the increase was not significant; however, for this combination, a significant increase occurred in R_a in plane *C* ($p=0.04$, Figure 6-5). Plane *A* was at 90^0 to plane *C* and did not demonstrate as much change (Figure 6-5). This was expected, as the bending moments generated in plane *C* would be greater resulting in a greater contact pressure.

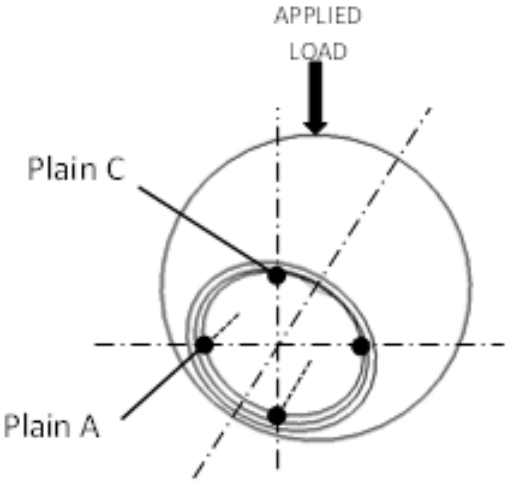

Figure 6-5: Diagram demonstrating plane *C* and plane *A* in the head tapers.

Analysis of the head tapers coupled with smooth short neck tapers showed that the mean R_a value was 0.22±0.04µm. There was no significant change in the R_a values after load testing along planes *A* and *C* (0.03±0.02µm). For R_z values there was no significant increase for the smooth short neck taper group. However, there was significant increase in R_z in the rough short neck taper group in plane *C* ($p<0.05$) compared with plane *A* where the difference was non significant ($p=0.07$). The surface profiles of the head tapers

coupled with the rough short neck taper group were similar to those in Test 1 with evidence of the original machine marks on the peaks of the coarse circumferential grooves. Examining the head taper surfaces under a light microscope showed debris on the head taper, which could not be removed by cleaning. This occurred in all smooth heads with less than 20% involvement of the surface area. For the neck tapers in both designs within the rough and smooth groups the R_a ranged from 2.73 to 2.79 μm and 0.28 to 0.38 μm respectively. All neck tapers showed negligible damage with R_a and R_z values showing no difference before and after testing.

6.3.3. Electrochemical Measurements

A notable difference was found between the two finishes when monitoring the OCP of the short neck taper before and after loading. The difference was significant ($p=<0.05$) after 1000 cycles. The OCP on the rough short neck taper decreased by 158±11.5 mV compared to 11±3.5mV for the smooth short neck taper combination, indicating that the oxide film on the rough short neck taper was being disrupted. The smooth short neck taper in comparison showed very little change. Potentiostatic tests reinforced this and showed that as the loading started an immediate spike in the current was observed on the rough short neck taper, which continued to fluctuate with each cycling load until the test was completed at 1600 cycles (Figure 6-6).

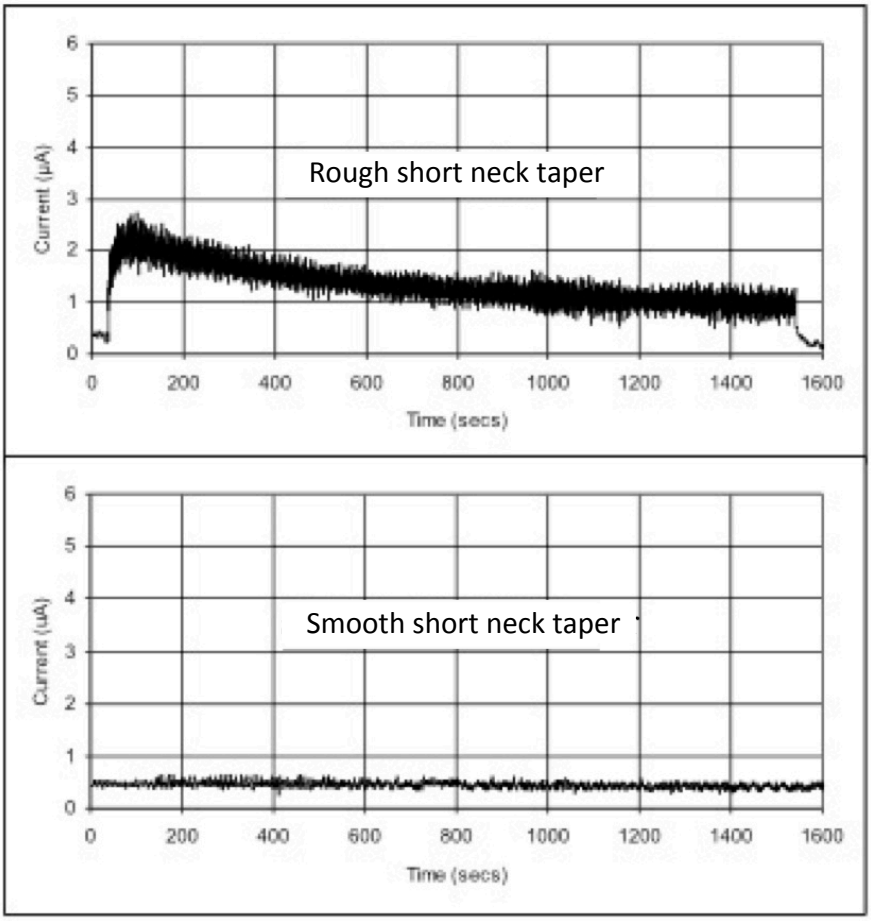

Figure 6-6: Potentiostatic scans showing current response to sinusoidal cyclic loading 100 to 1500kN at applied potential of OCP +200mV at 0.66 Hz over 1600 cycles.

Loading had no noticeable effect on the current for the smooth short neck taper. The current for the rough short neck taper generally decreased throughout the loading regime until levelling out towards the end of the test, indicating that the initial damage was greater but the rough short neck taper was able to recover (re-passivate) to a some degree. The magnitude of observed current decreased with respect to each new loading cycle, indicating a decrease in the damage caused by fretting the longer the rough short neck taper was loaded. To assess the effect of a low data acquisition rate, loading regimes of 10 cycles were applied at different speeds and the current was plotted against the induced load. Results showed that the current increased when load was applied and

decreased as the load diminished (Figure 6-7). Currents were also notably larger at the higher rate of loading showing the frequency dependence of fretting.

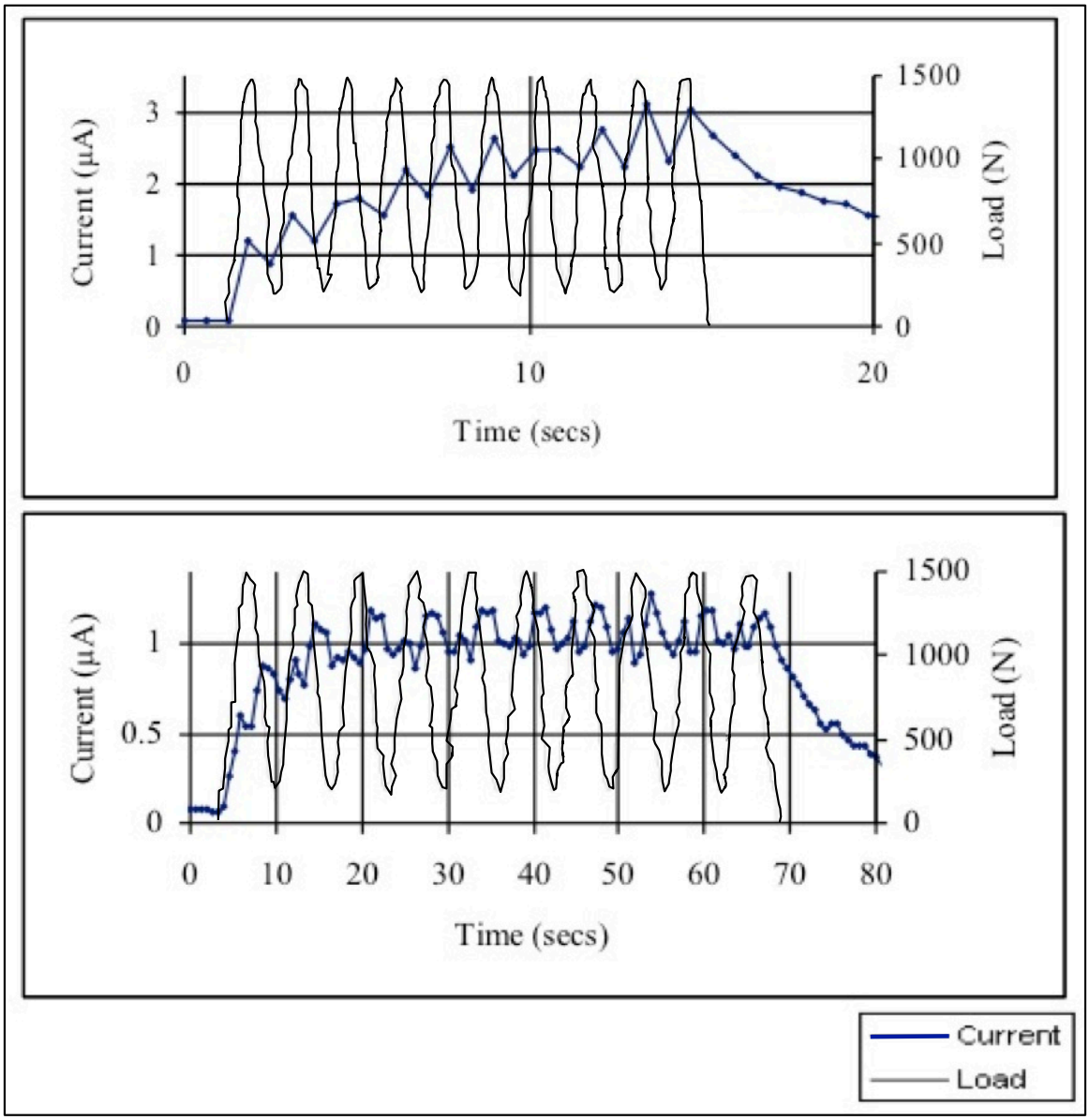

Figure 6-7: Current and load plots on a short neck taper for 10 cycles at 0.15 and 0.71 Hz.

Potentiodynamic scans were performed before and after loading for 1600 cycles and showed a change on both short neck tapers. However, the change was more evident in the rough short neck taper where a hysteresis loop was seen (Figure 6-8). It was noticed

that a lower potential was required for the current to diminish on the rough short neck taper. This difference was marginal, but provided evidence that the crevice environment for the rough short neck taper had become worse than with the smooth short neck taper and over a longer period of time an enlarged loop may be observed.

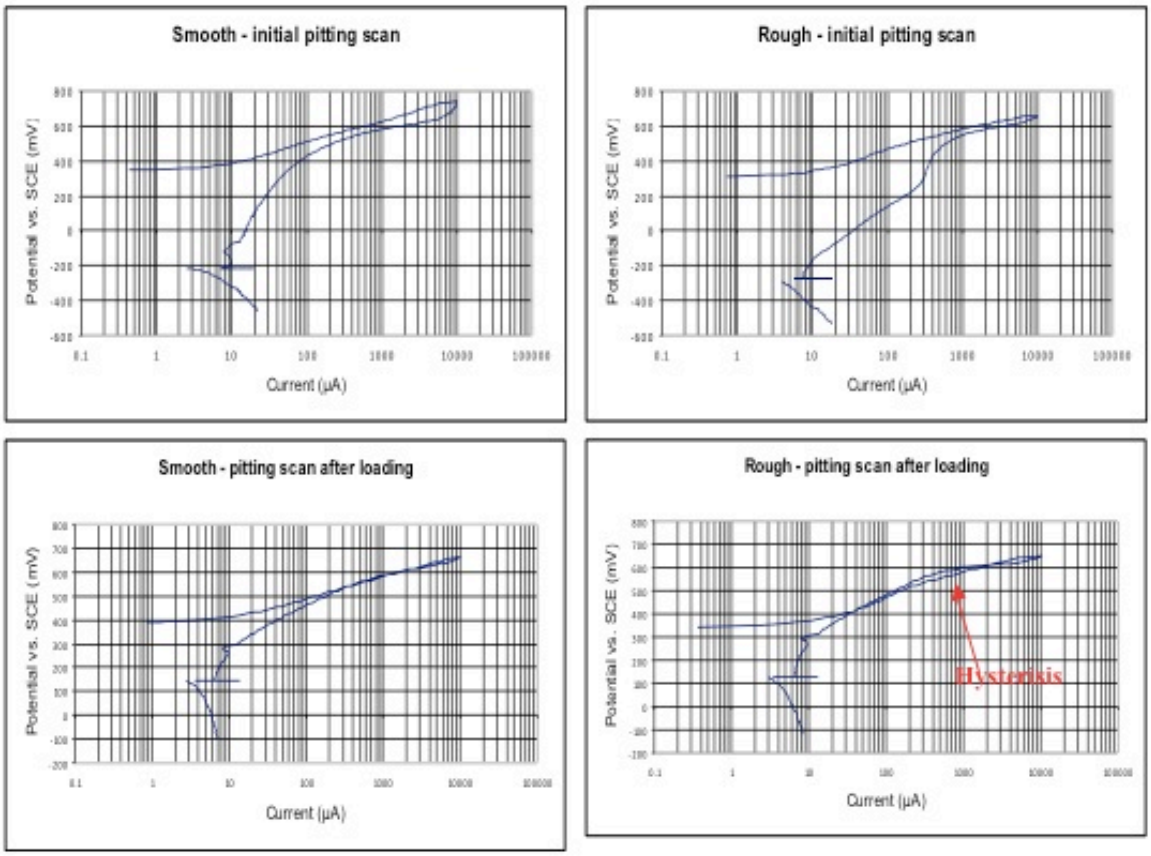

Figure 6-8: Potentiodynamic scans (pitting scans) for rough versus smooth short neck tapers pre- and post-loading for 1600 cycles.

6.4. Discussion

6.4.1. Summary of Results and Study Limitations

Head-neck modularity in THR typically consists of a metal-metal or a ceramic-metal conical junction with a tapered femoral trunnion that couples with a head that has a tapered bore. Corrosion in the crevice that is formed at this modular junction between the two component parts is a concern as corrosion can lead to the generation of debris and metal ions that lead to ARMD (Learmonth, 2000). Potential factors that govern taper corrosion include surface roughness, materials, cone diameter, cone-angles, tolerances, and the surface area of the taper contact (Krushell et al., 1991, Chmell et al., 1995, Hozack et al., 1996, Barrack et al., 1993). Manufacturers have developed different taper characteristics that may be important in promoting or reducing taper corrosion and it is important to ascertain the importance of such factors in the performance of the implant. My study sought to investigate the effect taper surface roughness and taper surface engagement area on the wear and corrosion at the taper junction.

In Test 1 the surface profile of the heads with both types of neck tapers showed a significant change between start and end of the test. These changes indicated that material from the CoCrMo head surface adjacent to the Titanium neck tapers had "eroded" and the surface texture of the neck taper had in fact imprinted onto the head taper. This imprinting of regular circumferential grooves on the head taper surface was identical to the circumferential grooves seen on the neck taper only in the contact region indicating that the original smooth surface of the head taper had now changed to a more roughened surface whilst the surface finish of the neck taper had remained the same. This was related to the loading on the head and the changes were most evident on the superior part of the head taper, which was the region of greatest bending forces. The

original surface can be clearly identified on these heads and the circumferential grooves approximate to the morphology of the neck taper surface (Figure 6-9). *Langton* (Langton et al., 2012) believe that this material loss is associated solely with a wear process. However material is lost in a manner that is difficult to interpret as being associated solely with a wear mechanism and in the past has been attributed to MACC (Gilbert et al., 1994, Goldberg et al., 1997a).

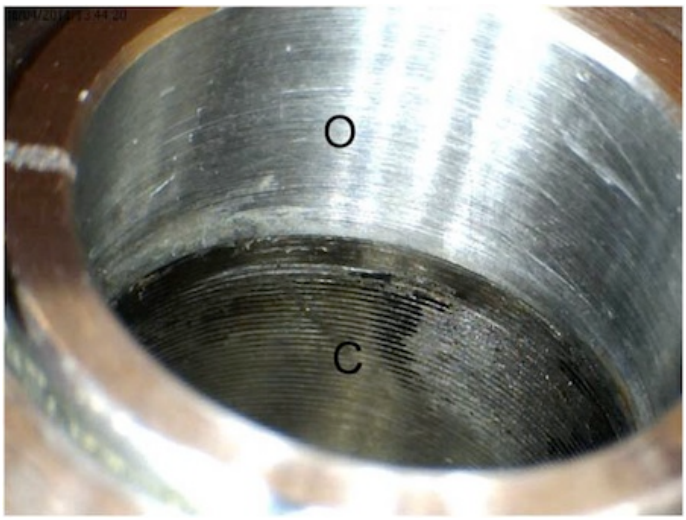

Figure 6-9: Photograph of a head taper that shows the circumferential patterning (C) and the original machine marks (O).

Bolland (Bolland et al., 2011) has reported a similar morphological change with black markings and deposits on the head taper modular interface in a retrievals study, and although my study reproduced the surface texture following in-vitro 10 million-cycle testing extensive material deposition was not seen. This morphological phenomenon which I also observed in Chapters 5 and 6 where the original CoCrMo surface has been replaced by a coarse circumferential grooved pattern similar to this study's findings was also observed in a number of retrieved heads from LH-MoM-THRs as described in Chapter 4. Both *Bolland* and *Langton* (Bolland et al., 2011, Langton et al., 2011) suggest that this appearance is enhanced by high torque and bending moments. It is

hypothesised that these morphological changes may be associated with the high torque placed on large heads leading to increased stresses at the taper interface. This study did not simulate torque but it noted that the circumferential pattern was accentuated by reducing the surface contact area of the neck taper and by using a rough surface finish which is used for many hip replacements and may be generating higher stresses especially those created by fictional torque in large heads.

Although surface topology showed significant material loss, it was difficult using these methods to accurately calculate the material that had been lost from the surface of the CoCrMo head. Dividing the taper junction post testing preserved the morphological features associated with mechanically assisted corrosion, but did not allow a volumetric analysis of the material lost. The head taper (CoCrMo) is harder with higher Young's modulus and is generally considered to be more wear resistant compared to the softer Ti alloy neck taper. Compared to Titanium alloy, CoCrMo is galvanically more susceptible to corrosion, so it may be expected that the loss of material is associated with corrosion rather than wear. However, the circumferential morphology of the CoCrMo head taper surface after testing was found only in regions associated with high loading caused by the large femoral head-offset resulting in larger bending moment. The fact that the morphology on the CoCrMo affected region was consistent with the machining marks on the Ti neck taper surface suggested that the rough finish enhanced crevice corrosion by allowing the ingress of fluid along the valleys. This was supported by the observation that the original machine marks were still evident in the affected region between the peaks created by the neck taper. The greatest degree of corrosion was seen at the interfaces where the highest bending movements were generated. This suggested that micromotion might have been a contributing mechanism to the corrosion process (Gilbert et al., 1993, Collier et al., 1991).

Fretting and corrosion are observed together in most cases. However, in some instances, corrosion is observed without evidence of fretting, most likely because the signs of the initial fretting damage are obscured by progressive corrosion (Goldberg et al., 2002). As fretting continues, electrochemically the OCP decreases into the active-passive transition region, the pH inside the crevice decreases and the crevice corrosion process is accelerated (as predicted by the model of mechanically assisted crevice corrosion). This acidic crevice environment will then reach the areas of the head where fretting scars were present, destroying the evidence of fretting. Recent in-vitro studies have shown that fretting initiated crevice corrosion in modular tapers can continue when fretting ceases, once the acidic crevice environment is established (Langton et al., 2011). In this study, crevice corrosion appeared to be the overriding mechanism. This was substantiated from the SEM examination of the corroded areas, which showed pitting, which is characteristic of crevice corrosion. It was difficult to ascertain whether both mechanisms were occurring in our specimens on just microscopic examination of the surfaces and therefore the electrochemical tests performed tried to clarify the exact mechanisms. The electrochemical tests supported the concept of fretting in the rough short neck taper samples because of the cyclic nature in the potentiostatic cyclically loaded tests and current spikes in the potentiostatic tests. The fact that pitting was more evident on the short neck tapers could be partly explained by the reduced contact area compared to that of the standard neck tapers. Forces may be concentrated and exceed the surface oxide fracture strains in the CoCrMo, leading to accelerated corrosion. Goldberg et al., 2002 showed the importance of neck stiffness on corrosion and concluded that larger diameter neck tapers had lower fretting corrosion rates (Goldberg et al., 2002). This could potentially be due to reduced contact pressures resulting from increased moment arm effectively reducing the bending moment at the interface. In the

short neck tapers the taper diameter was smaller and this may explain the greater extent of corrosion. Increasing contact area relative to the loading may reduce stresses and thus the fretting corrosion.

The principle of using a rougher surface finish was developed after its use with ceramic heads. It was then applied directly to the MoM articulation. In view of the results obtained from this study, rough finish may not be appropriate for large MoM combinations where the torque is believed to be higher on the taper and recommendations for a smoother finish should be sought. The electrochemical tests showed differences in the rough and the smooth neck tapers. When considering the OCPs, there was a large decrease in the rough compared to the relatively small change in the smooth neck tapers. Indicating that there was only a small amount of fretting in the smooth neck taper, and further testing showed that no noticeable fretting currents were observed, implying that there was minimal disruption to the oxide film. It must be noted that the tapers evaluated in this study had been through 10 million cycles and this may have influenced the results. Gilbert et al., 1993 showed that fretting corrosion reactions decreased over the period of a long- term test and suggested that the corrosion debris may act like a boundary lubricant between the two surfaces (Gilbert et al., 1993). Fretting evidenced by potentiostatic tests was greater in tapers, which were newly manufactured, compared with the tapers that were previously cyclically loaded. This adds weight to the theory that fretting is reduced when a hip is loaded for a long period of time (Bolland et al., 2011) and that the interface has properly bedded in. The data obtained on the newly manufactured tapers showed that the fretting current behaviours indicated less fretting with a taper that had a smooth finish, as compared to a rough finish. From the results it seems likely that the rough finish may not be suitable for the neck tapers.

6.4.2. Conclusions and Further Work

Modularity in hip replacements has many advantages and in order to optimise the modular junction in order to reduce ARMD associated with this interface it is necessary to understand the factors that contribute to MACC. This part of my study has identified enhanced fretting corrosion at the modular taper junction associated with roughened surface finish and short neck tapers and points to the overall concern associated with the use of modular taper connections in orthopaedic implants. In my study crevice corrosion is identified as the predominant mechanism, with evidence of pitting in all rough short neck tapers. The greatest wear and corrosion was in the plane where the greatest bending moments were generated, implicating fretting as a mechanism. The rough short neck tapers have a reduced surface area at the interface and ultimately bending forces are concentrated here. The next chapter will concentrate on the effects of frictional torque and bending moment on the modular junction.

Chapter 7 The Effect of Increased Frictional Torque and Bending on MACC at Modular Junctions of Different Material Combinations

7.1. Introduction

[*] In the last two decades, surgeons have favoured the use of larger femoral heads to increase stability and impingement-free range of movement, whilst promoting fluid film lubrication (Crowninshield et al., 2004 , Cuckler et al., 2004 , Mertl et al., 2010). Interestingly, a study by *Elkins* (Elkins et al., 2014) using FEA illustrated that increasing femoral head diameter did not increase stability beyond 40 mm diameter; a finding that was also supported by a clinical study that showed questionable improvement in function or range of movement with femoral heads whose diameter was > 36mm (Zijlstra et al., 2011).

The relationship between the diameter of the femoral head and corrosion has been scrutinised after the well-publicised failures of large head MoM THAs (Smith et al., 2012b, Langton et al., 2011, Bolland et al., 2011, National Joint Registry, 2012, Australian Orthopaedic Association National Joint Replacement Registry, 2012). Increasing the diameter of the femoral head in itself causes greater frictional torque forces, which are transmitted to the head-neck modular interface as rotational stresses (Witt et al., 2014). The reason why a larger head diameter increases torque is associated with the transmission of forces further away from the axis of rotation in comparison with smaller heads. Increasing stresses at the modular interface with increasing femoral head diameter was also illustrated by *Elkins* (Elkins et al., 2014) in their FEA study. It is

[*] This chapter (The Effect of Frictional Torque and Bending Moment on Corrosion at the Taper Interface: An In-Vitro Study) was published in the Bone Joint Journal in April 2015.

thought that these increased stresses transmitted to the head-neck junction result in increased micromotion, deterioration of the protective oxide film and mechanically assisted crevice corrosion (Dyrkacz et al., 2013). The high torque generated at the bearing surface however is not only a function of large head size; it is also amplified by abnormal wear and poor lubrication. An in-vitro study by *Bishop* (Bishop et al., 2013) showed a twofold increase in friction moments for 48 mm diameter metal bearings; translating to a joint friction moment of 11.8 Nm in dry conditions, which compares to 7 Nm in adequate lubrication. Poor lubrication may occur with edge loading and also on initiation of movement due to poor entrapment of lubricating fluid secondary to the absence of entraining velocity (Bishop et al., 2013, Nassut et al., 2003). With regards to component positioning, high inclination angles of the acetabular component are known to result in edge loading. High rates of wear during the run-in phase (Angadji et al., 2009), which occurs with hip resurfacing may also lead to higher friction (De Haan et al., 2008, Hart et al., 2008). The relationship with acetabular version is less clear, and it can be extrapolated that large femoral heads are more sensitive to malpositioning, particularly of the acetabular component, as a result of the increased frictional torque produced (Morlock et al., 2008, Lavigne et al., 2011).

In addition, as discussed previously in Chapter 5, increased bending moments acting at the modular junction may increase micromotion at the interface leading to enhanced corrosion. An increased bending moment may be associated with increased head-neck offset, increasingly varus neck shaft angles (Langton et al., 2012), heavier more active patients, increased bearing diameter (Figure 5-1) and an inappropriate relationship between the centre of the femoral head and its modular junction. The latter may be associated with 'overstuffing' of the joint or if a large femoral head is used and the femoral taper is not centrally placed (Langton et al., 2012). Analysis of retrieval

specimens has shown a pattern of material loss from the head CoCrMo taper that is consistent with either bending or torque, or a mixture of both. A pattern of bending has been shown to be associated with material loss on the inferior surface adjacent to the end of the head taper and on the superior surface at the opening of the head taper (Langton et al., 2012) (Langton et al., 2010). This pattern of material loss was also evident in the in-vitro long-term experiments outlined in Chapter 5 whereby implants with a high-offset were utilized to replicate conditions of increased bending moment.

Furthermore Chapter 6 alluded to the fact that not all tapers are the same and that their design varies between manufacturers. Retrieval and in-vitro studies have identified factors that may enhance fretting corrosion at the modular junction (Nassif et al., 2014, Panagiotidou et al., 2013); more specifically, rough surface finish and reduced contact area were found to be crucial variables as reported in Chapter 6.

One can now appreciate how the above-described factors may influence corrosion at the modular interface via mechanical action (fretting corrosion) and localised attack in crevices or cracks (crevice corrosion). Another factor that may influence corrosion of the modular interface is the use of dissimilar metals at that junction (galvanic corrosion) (Collier et al., 1991, Gilbert et al., 1993). Femoral head components typically, are manufactured from either CoCr alloy or ceramic due to their favourable wear properties at the bearing surface. In contrast, stems may be manufactured from CoCr, SS or Ti alloys. Retrieval and in-vitro studies have demonstrated that CoCr alloy couples (CoCr head with CoCr neck) are less susceptible to fretting corrosion than CoCr alloy coupled with either Ti or SS alloy (Cooper et al., 2012, Gilbert et al., 2009a). This is likely to be due to the effects of galvanic corrosion. However, CoCr alloy couples also have significantly lower pull-off forces and turn-off moments, indicating a weaker interface (Gilbert et al., 2009a, Rehmer et al., 2012). A recent retrieval study by *Kurtz* (Kurtz et al., 2013) showed

that corrosion and fretting were lower for neck tapers when ceramic femoral heads were used, suggesting that interfaces involving ceramic heads have a higher resistance to fretting; this finding was also suggested by other retrieval studies (Hallab et al., 2004). *Carli* (Carli et al., 2015) conducted a systematic review of published cases of revision THAs for symptomatic taper corrosion and found that only 5 out 776 cases did not involve a metal head. Whilst most cases (419) involved MoM interfaces and 352 involved a MoP interface.

A large head size therefore, in conjunction with the taper geometry and the combination of materials could potentially be the reason for the early failure of these modular THAs. The aims of this chapter were firstly, to quantify the effect of frictional torque and bending moment on the susceptibility to fretting and corrosion at the head–neck interface of MoM THAs using short-term in-vitro electrochemical tests and secondly, to investigate the susceptibility of head-neck taper combinations of different materials (CoCrMo head on CoCrMo neck, CoCrMo head on Ti alloy neck and ceramic head on CoCrMo neck) when subjected to increasing torque.

7.2. Materials and Methods

7.2.1. Application of Frictional Torque

Increasing the size of the femoral head causes increased frictional torque at the bearing surface; however, the direct impact of this on the head-neck modular interface is poorly defined. I therefore initially considered all the different head sizes available in the market as well as variable frictional conditions.

To analyze the amount of torsional force generated across a spectrum of increasing head sizes and coefficients of friction (μ), I used the formula shown in Figure 7-1.

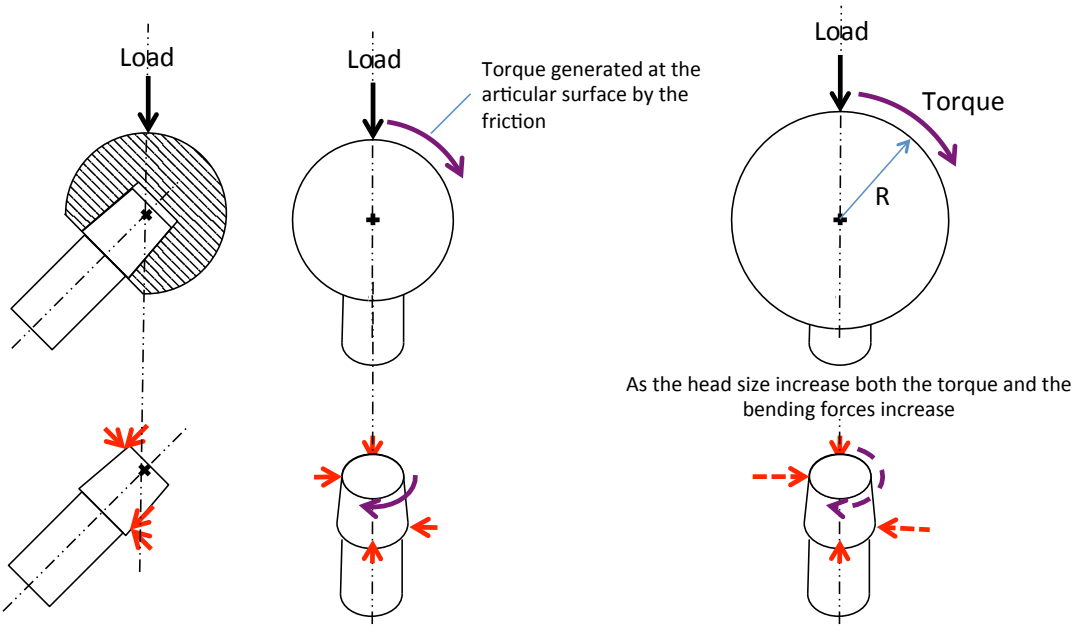

Figure 7-1: Schematic diagram showing the effect of frictional torque on the contact forces on the taper. Solid arrows: red representing bending, purple representing torque and dashed representing the increase in both torque and bending forces with increasing radius (R).

These calculations assume that the torque will be generated perpendicular to the resultant force on the acetabular component. For a set peak load of 2300 N (in accordance with the ASTM F1875 – 98 (2014) *'Standard Practice for Fretting Corrosion Testing of Modular Implant Interfaces: Hip Femoral Head- Bore and Cone Taper Interface'* (ASTM F1875-98(2014), 2014) the torsional force produced by each head size is shown in Table 7-1.

For applied load of 2300N			
	Torque (Nm)		
	Coefficient of Friction (μ)		
Head Size (mm)	0.1	0.2	0.3
35	4.0	8.1	12.1
40	4.6	9.2	13.8
45	5.2	10.4	15.5
50	5.8	11.5	17.3
55	6.3	12.7	19.0
60	6.9	13.8	20.7
65	7.5	15.0	22.4
70	8.1	16.1	24.2

Table 7-1: Table highlighting the measurements of torque with increasing head size at three levels of coefficients of friction (μ).

The μ of MoM THAs can be as low as 0.1, but where lubrication is not ideal then μ can be as high as 0.3. Assuming the likely range for the μ to be between 0.1 to 0.3 (Gilbert et al., 1993, Scholes and Unsworth, 2000), I predicted that the torsional force generated could vary between 4.0 Nm and 24.2 Nm. These figures are in line with the experimental work of Bishop et al., 2013 who showed frictional torques as high as 12Nm and 24Nm for Large head MoM and Ceramic bearings respectively in conditions of poor lubrication (Bishop et al., 2013). Changes in torque with increasing μ and increasing head size are also shown in Table 7-1.

In test 1 I, used a frictional torque equivalent of 0 Nm, 9 Nm, 14 Nm and 18 Nm by selecting increments of offset (d) of 0 mm, 4 mm, 6 mm and 8 mm in the anterior-posterior (AP) plane to the stem–neck axis for the load application (Figure 7-2).

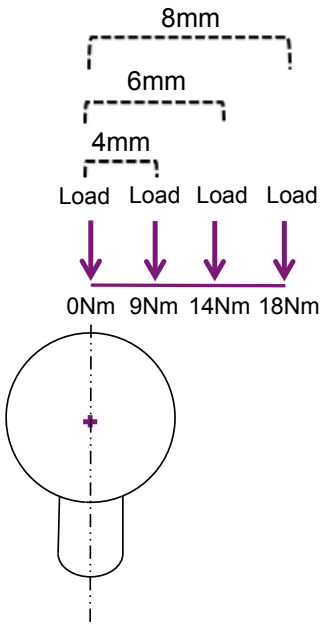

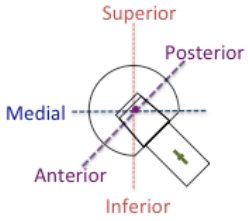

If (*d*) is the variable offset distance in the AP plane:

Torque = LOAD x (d)

In accordance with ASTM F1875-98 our peak LOAD was 2300N.

Therefore to apply 9Nm of torque the LOAD was offset by 4mm in the AP plane

(d) = 9/2300 = 0.004m = 4mm

Figure 7-2: Schematic diagram showing the calculation of the offset anterior-posterior (AP) distance to the neck-stem axis for the load application in order to achieve the desired torsional force.

In order to create accurately controlled, reproducible test conditions, a simplified solution was chosen, thereby eliminating the variability associated with the tribology of the bearing surfaces. In this configuration, the femoral head was fixed using bone cement and the axial peak load was applied at different AP offsets relative to the stem-neck axis, thus introducing torque to the modular junction. In this way and by using a single head size, I was able to introduce different amounts of torque that would otherwise be generated by different head sizes and tribological conditions.

Assuming μ, to be 0.3, torsional forces of 9 Nm, 14 Nm and 18 Nm were simulated (Table 7-1). A 0 Nm torsional force was used as a control by applying the load without an offset. Test samples consisted of three head-neck combinations of different materials. Each assembly was tested at its torque-allocated axial load offset and the sequence was then repeated until a total of three readings were achieved for each offset (Table 7-2).

Torque Generation (Nm)	Axial Load application offset in the AP plane (mm)	Modular Junction – Material Combination		
		Group 1	Group 2	Group 3
		CoCr head on CoCr neck	CoCr head on Ti neck	Ceramic head on CoCr neck
0	0	N=3	N=3	N=3
9	4	N=3	N=3	N=3
14	6	N=3	N=3	N=3
18	8	N=3	N=3	N=3

Table 7-2: Test samples investigated at different applications of frictional torque.

7.2.2. Application of Bending Moment

Bending has an obvious effect on the distribution of load on the taper. Positions of the taper, which are not in the centre of the femoral head, are subject to offset loading which increases the bending moment (Figure 7-3).

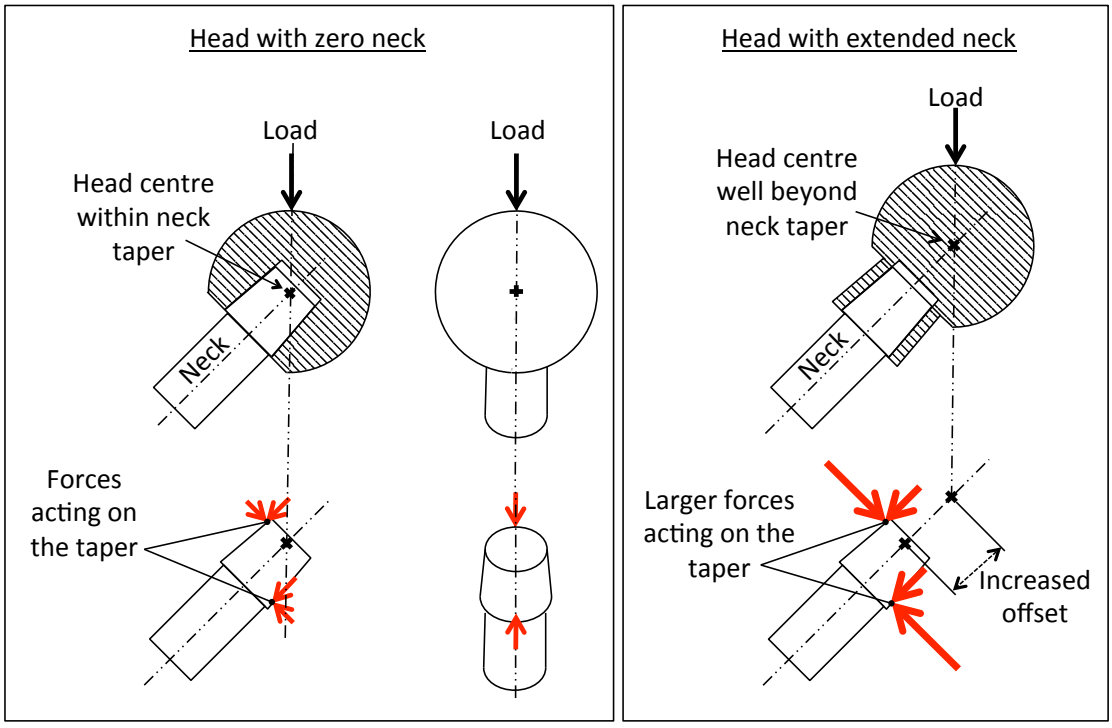

Figure 7-3: Schematic diagrams showing the effect of the head–neck length on the contact forces. As the head–neck length increases so will the bending forces.

In order to measure the effects of increasing the bending moment, components were loaded in a neutral position, but the load was offset in the mediolateral (ML) plane by the equivalent of using a 0 mm, 7 mm and 14 mm femoral head offset. Test 2 also consisted of three head-neck combinations of different materials. Each assembly was tested at its bending moment allocated axial load offset and the sequence was then repeated until a total of three readings were achieved for each bending offset (Table 7-3).

Head Offset	Axial Load application offset in the ML plane (mm)	Modular Junction – Material Combination		
		Group 1	Group 2	Group 3
		CoCr head on CoCr neck	CoCr head on Ti neck	Ceramic head on CoCr neck
+0	0	N=3	N=3	N=3
+7	4	N=3	N=3	N=3
+14	8	N=3	N=3	N=3

Table 7-3: Test samples investigated at different applications of bending moment.

7.2.3. Implants

Forty-two '*Metasul*' CoCrMo 36 mm femoral heads and twenty-one *'Biolox Delta'* ceramic 28mm femoral heads were used. All heads had a smooth finished 12/14 taper with a 0 neck offset and a cone angle of 5° 43' 30''. Forty-two '*CPT*' CoCrMo and twenty-one '*CLS Spotorno*' Ti6Al4V stems (Zimmer, Inc Warsaw, Indiana) were used. All stems had a 12/14 taper with the same surface finish, 0 offset and a neck angle of 135° (further details can be found in Chapter 3, section 3.2.1.2, titled *Implants*).

7.2.4. Mechanical Load and Electrochemical Testing

Implants were cleaned and assembled as described in Chapter 3. The assemblies were placed into their fixtures and then mounted onto a purpose-built implant fatigue-testing machine (manufactured by R.D.P. Howden, Warwickshire, United Kingdom), used to

apply load during testing (for a detailed description refer to Chapter 3, section 3.4.1, titled *Mechanical Load Testing)*. Examples of the experimental set up used in the anatomical configuration as per the ASTM F1875 – 98 Standard modified *Method I* for implant tapers are shown in Figures 3-7 and 3-10 respectively. The components were then sinusoidally loaded between 200 to 2300N at a frequency of 3Hz and during the loading regime the fretting current was measured by determining the amplitude of the oscillations and by the peak fretting current (Figure 3-12).

The protocol described below was used to provide quantitative measures of fretting corrosion rates at the implant taper interface (for each of the above described frictional torques, bending moments and material combinations) over 1000 cycles:

1. Each electrochemical cell was filled with 200mL of the pre-titrated test fluid (fluid level just above the modular head-neck junction).
2. The specimen was initially unloaded.
3. OCP was monitored for 1 hour and observed to settle to a steady potential.
4. Sinusoidal load applied at 200 to 2300N at 3Hz was commenced.
5. A potentiostatic scan was performed at potential; OCP +200mV for 1200 seconds.
6. The sinusoidal load was initiated 100 seconds into the potentiostatic scan and terminated 1100 seconds into the scan giving sufficient time for the current to settle pre & post loading. Sampling rate of 48 data points per second. With the test running at 3Hz this equates to 16 data points per cycle.
7. The specimen was then unloaded.
8. OCP was again allowed to settle for 1 hour.

9. Fluid was removed and the test cell was washed out.

10. The above procedure was repeated on separate specimens under different loading conditions as specified per Tables 7-2 and 7-3.

7.2.5. Statistical Methods

The fretting current measurements were examined using the Shapiro-Wilk test for normality and found to be non-parametric. The Mann-Whitney U-test was therefore used to determine any significant differences in the measurements in the generation of fretting current at the modular junction between the different torque applications, bending moments and material combinations. A p-value < 0.05 was considered statistically significant. All analyses were performed using Statistical package for the social sciences (SPSS) Statistics version 22 (Armonk, NY: IBM Corp.)

7.3. Results

7.3.1. Effects of Torque

Figure 7-4 shows the effect of increasing torque, applied in a cyclical fashion, on the monitored fretting currents. It can be seen that the fretting current lines for each of the torques induced have amplitude that is associated with each loading cycle. From 0 to 100 seconds and from 1100 seconds to the end of the test the specimens are not being loaded and since there is no movement to disrupt the passive layer the lines corresponding to each induced torque have no amplitude. This is because the fluctuating current is dependent on cyclical loading, which induces disruption and repassivation of the passive layer causing changes in the current with every loading cycle (Figure 3-12). The mean maximal fretting current and the amplitude of the line are measured from these

data. As the torque increases so does the fretting current, and the amplitude becomes wider.

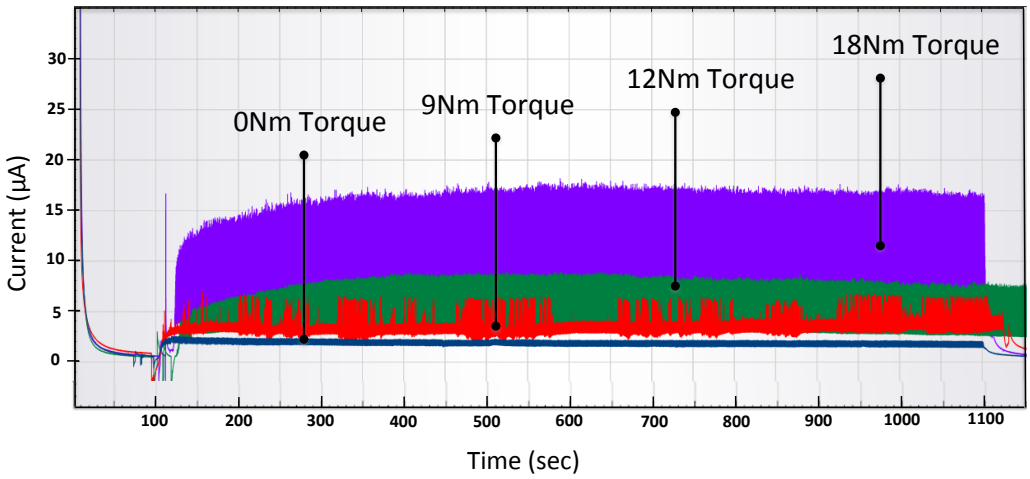

Figure 7-4: Graph showing the effect of increasing frictional torque on the corrosion current for a CoCrMo head with a titanium alloy neck.

After the start of loading, the amplitude and the fretting current were allowed to equilibrate for 100 cycles and were then quantified for 1000 cycles. The results of these two measurements with increasing torque and with different head–neck combinations are shown in Figures 7-4 and 7-5.

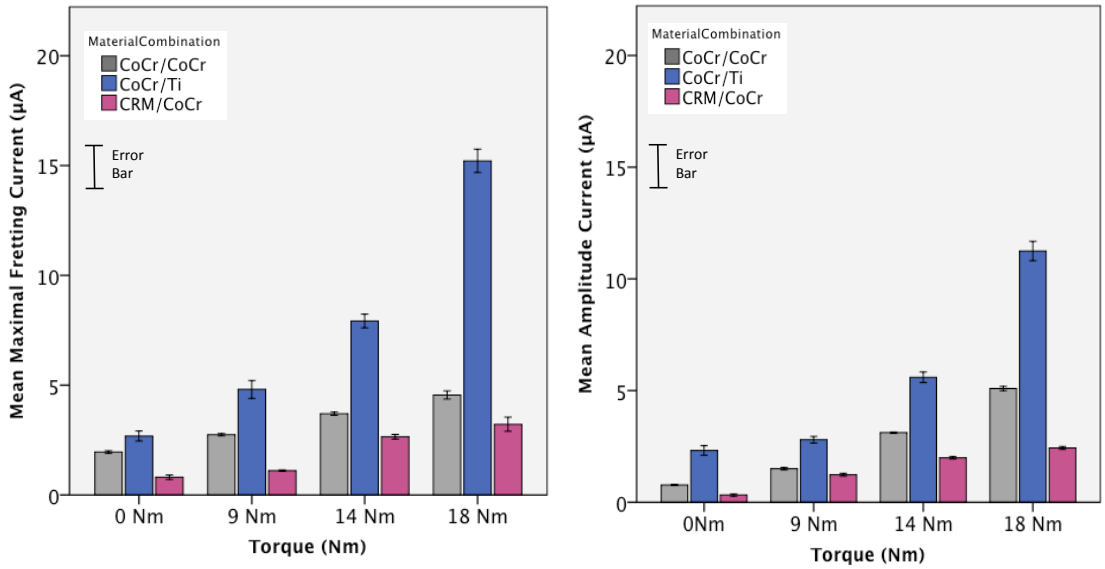

Figure 7-5: Histogram showing the effect of torque on the mean maximal fretting current and mean amplitude current of CoCr/CoCr, CoCr/ Ti and Ceramic/CoCr combinations.

Figure 7-5 shows that even when there is no imposed torque (Torque, 0 Nm) during sinusoidal loading, there is a fretting current, which differs depending on the material combinations of the taper. At 0 Nm torque CoCrMo heads on Ti alloy necks produce higher maximal fretting currents compared with CoCrMo heads on CoCrMo necks and Ceramic heads on CoCrMo necks (both $p \leq 0.001$). This pattern of response for the different combinations is similar even at the highest torques, with the difference in maximal fretting current between CoCrMo/Ti and the other combinations becoming more significant and more pronounced at higher torques. At the highest torque (18 Nm), the maximal mean fretting current for CoCrMo/Ti combination was just over 15 µA compared with 5 µA for the CoCrMo/ CoCrMo and < 3µA for the ceramic/CoCrMo combinations. A similar response was seen with the mean current amplitude (Figure 7-5) and all the combinations differed significantly from one another ($p \leq 0.001$). At higher torques the differences were not as great when the mean current amplitude was compared with the mean fretting current.

7.3.2. Effects of Bending

The bending moment associated with increasing the size of the femoral head leads to an increase in the mean maximal fretting current and the mean amplitude current (Figure 7-6). For the combination of CoCrMo/CoCrMo, under increasing bending moment, as in the response to torque, there is a cyclical response of the fretting current due to the disruption of the passive layer with each loading cycle (Figure 7-7). Even with no imposed bending, there was evidence of a fretting current on the junctions, which is due to the implant being under a small amount of torque associated with the offset in the AP plane. As with torque, the mean maximal fretting current increases, as does the amplitude of the response, with increased bending moment.

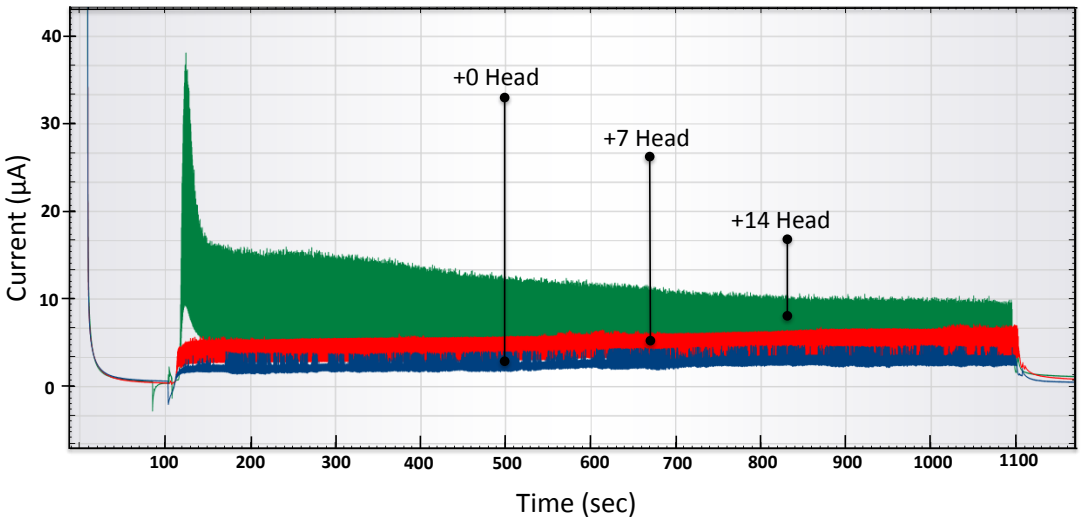

Figure 7-6: Graph showing the effect of increasing bending moment on the corrosion current for a CoCrMo head with a CoCrMo neck.

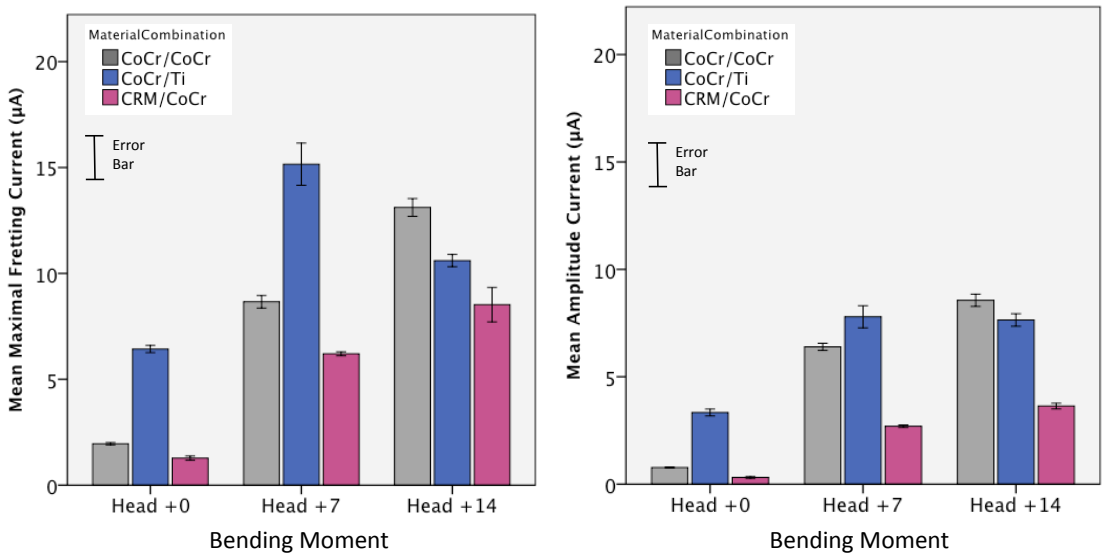

Figure 7-7: Histogram showing the effect of bending moment on the mean maximal fretting current and mean amplitude current of CoCrMo/ CoCrMo, CoCrMo/Ti and Ceramic/CoCrMo.

The highest fretting current (for CoCrMo/Ti) is with an equivalent of a +7 head. The highest levels of current were similar to those seen for the torque tests at around 15 µA. Larger bending moments than +7 were used in this test, however; the largest maximum fretting and mean amplitude currents were achieved by the CoCrMo/Ti combination with the bending moment induced by a +7 head. At higher bending moments (+14 mm) both of these currents decreased for the CoCrMo/Ti combinations and the reasons for this were unclear, however as expected they did increase for the other combinations (CoCrMo/CoCrMo & Ceramic/CoCrMo). So, at higher bending moments, CoCrMo/CoCrMo showed the highest mean maximal fretting and mean amplitude currents. In all instances, under bending, the Ceramic/CoCrMo combinations were again significantly better than other combinations ($p \leq 0.001$).

7.4. Discussion

7.4.1. Summary of Results

Corrosion has been a persistent challenge in orthopaedics. In practice, different metals are combined to improve the design of implants, which allows surgeons and patients the benefit of modularity. Evidence in retrieval analyses shows that crevice corrosion can lead to the conditions where active corrosion can occur inside the taper crevice. Many modes of failure are possible when this happens and active corrosion is as great a concern as material wear (Gilbert et al., 2012;). Any localised corrosion that is initiated during micromotion may continue to propagate and accelerate even after the micromotion is stopped. Several of the details of such a mechanism are explained in the model of crevice corrosion proposed by (Gilbert et al., 1993). Corrosion at the interface is due to a mixture of different modes of failure and it is often difficult to differentiate between them however, they are now generally attributed to MACC. This study quantified the corrosion associated with different material combinations and loading conditions by recording the fretting current directly linked to the frequency of loading. This fretting current is associated with MACC; which is a combination of fretting and crevice corrosion, with additional galvanic corrosion when dissimilar materials are used. Increasing frictional torque and bending have a significant effect on corrosion at the modular interface. Increased bending and torque probably act to enhance the removal of the passive layer, which then quickly reforms. The corrosion process is therefore mechanically assisted, but the imprinting effect seen on retrieved femoral heads (Matthies et al., 2013) (Chapter 4) and in long-term cyclically-loaded in-vitro tests (Panagiotidou et al., 2013) (Chapter 6) appears to develop into a regular pattern associated with the morphology of the surface of the taper, suggesting that only small amounts of movement (micromotion) are needed to enhance the process. Micromotion is

closely correlated to the head centre off-set as shown by *Donaldson* (Donaldson et al., 2014b) who in the their finite element simulation study reported on a 5μm increase in micromotion per 10mm increase in head offset.

Another effect, particularly of the bending moment, may be to open and close a crevice, thereby enhancing crevice corrosion. In this chapter study I showed that bending produced larger fretting currents than increases in torque. Modular tapers may be more sensitive to bending because this would lead to an opening and closing of the crevice enhancing corrosion. This may not happen with increasing torque.

In this study I monitored the amplitude and the peak fretting currents. These measurements indicated that the current needed to reform a passive layer once it had been disrupted by mechanical action. Although they were not a direct measurement of corrosion, for a given combination, changes in current associated with increasing torque and bending suggested increasing corrosion.

The fact that certain material combinations appeared to be more sensitive to increasing bending and torque indicated that these might be more susceptible to corrosion. In this study, the fretting current for the Ceramic/CoCr combination increased by 0.1 μA for every Nm of torque which compared to an increase of 0.7 μA for every Nm of torque for the CoCr/Ti and CoCr/ CoCr combinations. It appears that we may be seeing the effect of two other factors in addition to the mechanical effect (fretting); 1) the association of different material combinations and the subsequent effect of galvanic corrosion and 2) the association of different material moduli in the differential movement between the head and neck leading to crevice opening and closing. The superiority of ceramic as a material in terms of corrosion resistance and inability to conduct electricity may explain

the reduced currents seen during loading with increasing bending and torque (lack of galvanic corrosion).

7.4.2. Study Limitations

One of the limitations of this chapter is the short term testing of the combinations and ideally had time allowed I would have run the tests to 10 million cycles with analysis every 1 million cycles. However, the short-term results were replicated throughout the groups. In addition the reason as to why the CoCrMo/Ti combinations did not follow the expected trend and showed lower currents when bending was increased from +7 to +14 remained unexplained and could be investigated further by either increasing the number of cycles as mentioned above or by running the test at bending moments in between +7 and +14.

In this chapter I investigated Ti neck tapers with CoCrMo head tapers, CoCrMo neck tapers with CoCrMo head tapers and CoCrMo neck tapers with Ceramic head tapers. A combination that I would have liked to investigate in this chapter would have been Ti neck tapers with Ceramic head tapers. This combination has now become more common for younger patients whereby cementless stem fixation is used more routinely than cemented CoCrMo/SS stems.

Lastly in this study during simulation testing all parameters including lubrication where kept optimal and constant and thus, the Ceramic/CoCrMo combination faired the best under high bending and torsional moments. However a study by Bishop et al. (2012) has shown that if lubrication is not adequate then for large diameter and small diameter Ceramic bearings the amount of torque can increase by a ratio of 10.1 and 4.9 respectively (between serum and dry conditions) (Bishop et al., 2013). Their study

recorded a maximal moment force of 24.2Nm for large diameter Ceramic bearings in dry conditions, which compares to 11.8Nm for Metal bearings under the same conditions.

7.4.3. Conclusions and Further Work

This study was able to show that increasing the frictional torque significantly increased the resultant maximal fretting current and fretting amplitude in all material combinations. The Ti neck combinations showed the highest corrosion currents. In addition it showed that increased bending moments associated with using larger offset heads produced more corrosion; with Ti necks generally having performed worse than CoCr necks. Although the use of Ceramic heads did not prevent corrosion, it did appear to be significantly reduced in all loading configurations.

Therefore, when a large diameter head is required for stability one may avoid the severe corrosion associated with the increased torque by using a large diameter ceramic head.

Chapter 8 Taper Assembly Force and Interface Deformation

8.1. Introduction

[*] Modern THR designs are modular with a range of heads, which can be attached once the stem has been implanted. Advantages of head-neck modularity over the earlier 'monobloc' THR designs, with a one-piece femoral stem and head include; intra-operative selection of component size and type, freedom to customise the prosthesis to individual patient parameters, while at the same time reducing inventory and costs (Cook et al., 2013, Cameron, 1996, Barrack, 1994 , Yerby et al., 1996, McCarthy et al., 1997). Such benefits have made these prostheses very popular, a fact reflected by the prevalent use of modular hip replacements as recorded in the National Joint Registry (National Joint Registry, 2013).

A typical modular implant allows for self-locking and resistance to multidirectional loading between the head taper (head component) and neck taper (stem component) in total hip replacements. However, despite this geometry-specific locking mechanism, during cyclic loading, micromotion can occur between the interfaces (Jacobs et al., 1998), which facilitates MACC and fretting corrosion, leading to the production of wear debris and metal ion release (Gilbert et al., 1994, Goldberg et al., 1997a). Recognition of adverse effects of wear and failure of some tapers has led to greater scrutiny of their design features, optimal conditions for impaction and failure mechanisms.

There is a trend in the industry to manufacture the neck taper with circumferential ridges, which deform during assembly to provide compression and a tight interference fit with the smooth surfaced head taper, however there is variation in the design and

[*] This chapter (The Effect of Impact Assembly on the Interface Deformation and Fretting Corrosion of Modular Hip Tapers: An In Vitro Study) was published in the Journal of Orthopaedic Research in July 2017.

surface finish of the tapers used between different manufacturers but also within the same manufacturer. The recommendation by CeramTec for neck taper surface roughness to be used with a ceramic head is between 6μm and 20μm, and the majority of manufacturers have adopted this range for use in both ceramic and metal heads. With greater impaction, the interlock strength of the head-neck taper connection (disassembly force) increases linearly (Rehmer et al., 2012, Pennock et al., 2002, Yanoso-Scholl et al., 2017). As a result, the load required to initiate micromotion and fretting would increase, reducing the potential for MACC and production of wear debris (Goldberg et al., 1997a). Additionally, assembly under dry conditions is preferable to wet conditions, with implants assembled in serum or water behaving unpredictably compared to their dry counterparts (Pennock et al., 2002, Mroczkowski et al., 2006). Lavernia et al. (2009) also demonstrated that tapers contaminated with blood or fat had lower disassembly force than clean tapers (Lavernia et al., 2009).

Because moments generated at the bearing surface are transmitted to the head-neck interface, factors affecting taper interlock strength are important to understand. Such forces will increase with increasing head size as well as with poor lubrication, edge loading and suboptimal component placement during surgery (Angadji et al., 2009, Bishop et al., 2008). The interplay of these factors may result in premature failure of the implant if the impaction force is insufficient to create a taper interlock that is strong enough to sustain the moment acting on the taper. While there has been some work into the issues of corrosion, disassembly force and wear at this junction, there are very few studies that have aimed to demonstrate the effect of varying assembly loads on these phenomena. The relationship between force, number of impaction blows and pull-off strength has been explored (Rehmer et al., 2012, Pennock et al., 2002, Heiney et al., 2009, Schmidt et al., 1997).

However, It remains the case that *there are no official guidelines* for orthopaedic surgeons to follow with regard to the force they should impact modular heads during assembly. The purpose of this study therefore, was to investigate the effect of three different assembly loads (2kN, 4kN and 8kN) on the degree of deformation and amount of fretting corrosion of CoCrMo and Ti-6Al-4V neck tapers of different surface finish (smooth vs. rough) and engagement length (standard vs. short). I used the two different neck tapers to investigate the extremes of designs for current total hip replacements. These tapers were investigated previously and reported in Chapter 6 of my thesis and showed significantly different levels of corrosion under cyclic load. The hypothesis for this study was that increasing impact assembly load affects the deformation at the taper junction resulting in a stronger taper interlock that reduces MACC under high torsion and bending moments even for the taper designs that were more susceptible to corrosion.

8.2. Materials and Methods

8.2.1. Components' Surface Parameters and Specifications

All head and neck tapers were made to the following specifications: the R_z and R_a values for each component were assessed using a Talyrond 365 (Taylor Hobson, Leicester, UK) roundness instrument as previously described in Chapter 3. This study focuses on the metal taper junction (i.e. metal head with metal neck). In order to capture the two extreme ends of the neck taper roughness range the 'smooth' surfaces were within an R_z range of 3-6µm, while the 'rough' surfaces fell within a range of 16-20µm. The average R_z value of the smooth neck tapers used was 3.82µm, and for the rough neck tapers this was 16.58µm. The average R_a value of the smooth and rough neck tapers was 0.81µm and 4.14µm, respectively.

All head tapers were made from wrought CoCrMo alloy and had smooth taper finishes (R_a and R_z values 0.58 and 2.8µm respectively). All heads had a 36mm diameter and a +14mm neck offset to represent a high offset often seen at implantation and also with some large diameter head prostheses. Serrations were cut out of the bearing surface of each femoral head to prevent rotation within the cement mantle and since CoCrMo alloy is a relatively stiff material I, did not expect the serrations to interfere with the compliance of the head onto the neck taper. Furthermore, all head coupons used in this comparative study had the same configuration. Half of the neck tapers were CoCrMo and the others were Ti-6Al-4V alloy. For each material, the neck tapers were both a smooth finish and standard length or a rough finish and short length. Figure 3-1 illustrates the taper angles and locking zones along the tapers, the reference diameters of the head and neck tapers are not the same size and they are referenced at two separate points along the taper axis. What this means is that the taper engages much deeper in relation to the 12mm dimension mentioned. In fact, when fully impacted the large diameter of the short taper sits approximately 3.2mm inside the female bore which is reduced by 0.5mm due to the small chamfer in the female bore. Therefore, the total engagement length is 14.7mm and 12.0mm for long and short tapers respectively. This results in just over 18% difference in the amount of taper engaged.

Prior to the start of the test, all components were passivated and cleaned as described in Chapter 3.

8.2.2. Assembly of Components

Although it is common practice to use multiple blows for intraoperative head-neck assembly a study by Pennock et al. (2002) illustrated that when multiple impacts of varying force were utilised there was no difference in taper strength compared to a single blow of the strongest force (Pennock et al., 2002). Additionally when using

multiple impacts of the same force, 50% of the prostheses showed no difference in the taper strength between the first and subsequent impacts, whereas in the remaining 50% of their prostheses the first impact accounted for 90% of the overall taper strength and each additional impact contributed to a much lesser extent (Pennock et al., 2002). *Rehmer* (Rehmer et al., 2012) observed a similar relationship between dynamic and quasi-static assembly procedures therefore, combinations were assembled according to the ASTM F2009 at a loading rate of 0.05 mm/s in a materials testing machine to allow for reproducibility throughout the study.

In Test 1 (short term) each neck taper material and surface finish combination was impacted onto a CoCrMo head taper using an assembly force of 2kN, 4kN or 8kN (Table 8-1) in line with the taper. The rationale behind the choice of assembly forces was that *Heiney* (Heiney et al., 2009) demonstrated that the average impaction force applied by orthopaedic surgeons was a little over 4kN. Therefore, 2kN represented a light tap; 4kN represented a typical blow (Heiney et al., 2009) and finally 8kN represented a heavy blow. The 8kN impaction force was representative of the largest assembly forces measured in a study from 39 surgeons from German hospitals, which was up to 7848N (Nassutt et al., 2006).

In Test 2 (long term) the only combinations tested were of CoCrMo heads with Ti alloy rough/short neck tapers; n=3 were impacted at 4kN and n=3 impacted at 8kN (Table 8-1). Prior to testing, the samples underwent assessment using the Talyrond 365 where 180 traces were spaced 2° apart and provided a representative baseline volumetric measurement of the taper surface as described in Chapter 3.

CoCr Head Taper Assembly With:	**Test 1** - Short Term Loading Test (1000 cycles)			**Test 2** - Long Term Loading Test (5 million cycles)	
	IMPACTION FORCE				
	2kN	**4kN**	**8kN**	**4kN**	**8kN**
CoCr Rough Short Neck Taper	n=3	n=3	n=3		
CoCr Smooth Standard Neck Taper	n=3	n=3	n=3		
Ti Rough Short Neck Taper	n=3	n=3	n=3	n=3	n=3
Ti Smooth Standard Neck Taper	n=3	n=3	n=3		
TOTAL	**n=36**			**n=6**	

Table 8-1: Table showing an overview of tests performed.

8.2.3. Mechanical Load and Electrochemical Testing

Once impacted the assemblies were placed into their fixtures and then mounted onto a purpose-built implant fatigue-testing machine (manufactured by R.D.P. Howden, Warwickshire, United Kingdom), used to apply load during testing (for a detailed description refer to Chapter 3, section 3.4.1, titled *Mechanical Load Testing)*. An example of the experimental set up used in the anatomical configuration as per the ASTM F1875 – 98 Standard modified *Method I* for implant tapers is shown in Figure 3-8. The components were then sinusoidally loaded between 300N and 2300N at a frequency of 3Hz for both Test 1 (short term – 1000 cycles) and Test 2 (long term – 5 million cycles). During the loading regime the fretting current was measured by determining the amplitude of the oscillations, the peak fretting current and the average fretting current (Figure 3-12). Both CoCr alloy and Ti alloy spontaneously form a protective oxide layer on their surface, which acts as a semiconductor in the circuit and therefore, if this layer is damaged or removed, a spike in the current is observed (Figure 8-1).

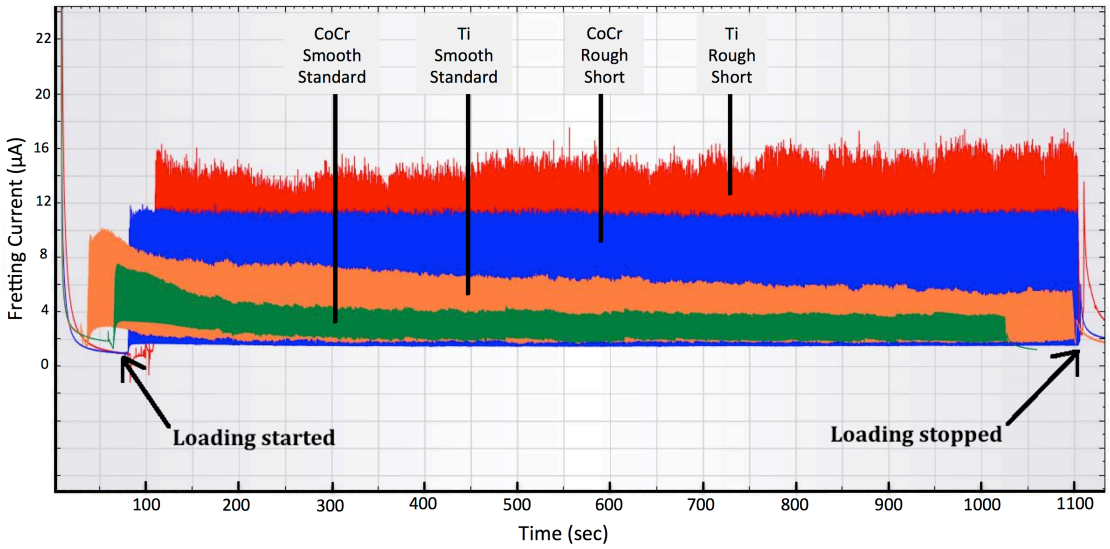

Figure 8-1: Example of fretting current measurements, superimposed on one another to demonstrate difference in current and amplitude. Red = Ti Rough Short neck taper, Blue = CoCr Rough short neck taper, Orange = Ti smooth standard neck taper, Green = CoCr smooth standard neck taper all coupled with CoCr head tapers. Each trace produced may be broken down into alternating peaks and troughs that directly correspond to the cyclic loading. As can be seen, the current rises immediately as loading begins, and drops back to the baseline when loading is stopped. Each peak represents the point where load is applied, fracturing the passive oxide film (depassivation) covering the taper and enabling current to flow across the interface. Each trough corresponds to the load being removed; at which point the film reforms (repassivation) and current can no longer flow freely across the interface. Thus, with cyclic loading a sinusoidal waveform of current is produced.

The protocol described below was used to provide quantitative measures of fretting corrosion rates at the implant taper interface for Test 1 over 1000 cycles:

1. Each electrochemical cell was filled with 200mL of the pre-titrated test fluid (fluid level just above the modular head-neck junction).

2. The specimen was initially unloaded.

3. OCP was monitored for 1 hour and observed to settle to a steady potential.

4. A potentiostatic scan was performed at potential; OCP +200mV for 1200 seconds.

5. Cyclic loading was initiated 100 seconds into the potentiostatic scan and terminated 1100 seconds into the scan giving sufficient time for the current to

settle pre & post loading. Sampling rate of 48 data points per second. With the test running at 3Hz this equates to 16 data points per cycle.

6. The specimen was then unloaded.
7. OCP was again allowed to settle for 1 hour.
8. Fluid was removed and the test cell was washed out.
9. The above procedure was repeated on separate specimens impacted at different assembly forces as specified in Table 8-1 (Test 1).

The protocol described below was used for Test 2 to provide quantitative measures of fretting corrosion rates at the implant taper interface over 5 million cycles:

1. Each electrochemical cell was filled with 200mL of the pre-titrated test fluid (fluid level just above the modular head-neck junction).
2. The specimen was initially unloaded.
3. OCP was monitored for 1 hour and observed to settle to a steady potential.
4. Sinusoidal load applied at 300 to 2300N at 3Hz was commenced.
5. After 1000 cycles a potentiostatic scan was performed at potential; OCP +200mV measuring the fretting current at the start of the sinusoidal load at a sampling rate of 48 data points per second.
6. The implants then continued to be loaded for 1 million cycles without any applied potential.

7. At the end of the 1 million cycles a potentiostatic scan was performed at potential; OCP +200mV for 1000 cycles at a sampling rate of 48 data points per second (whilst the implants continued to be sinusoidally loaded).

8. Each 1 million cycles at 3 HZ took 4 days to complete. The test fluid was topped up to the same starting level during these 4 days. At the end of each 1 million cycles and after the fretting current was recorded for 1000 cycles the load was briefly stopped for the 200mL of the test fluid to be changed and then the sinusoidal load was restarted.

9. This procedure was repeated at every 1 million cycles up to and including 5 million cycles. In total the experiment took 20 days to complete.

8.2.4. Post - Test Preparation and Analysis

Following 5 million cycles, two of the samples from test 2 (long term) were randomly selected and sectioned in the sagittal plane using a diamond-coated saw (Exact diamond-bladed bone cutting saw – Type 303) to allow disassembly without causing further deformation hence, the disengagement force was not measured. The two halves where then gently pealed apart thus, the surface furthest from the centreline would not be damaged due to shear. However, adhesive damage may be present but was assumed to be negligible. The head and neck tapers were examined under an optical microscope and scored using a previously published method (Goldberg et al., 2002) (Table 8-2) and SEM to assess the degree of corrosion seen at the interface, and provide an in-depth look at the taper surface. Following this, the remaining four samples were pulled apart in order to keep the taper in one piece, and then underwent volumetric wear analysis using the Talyrond 365 as described previously in Chapter 3. The deformation of the neck tapers at 5 million cycles was compared with the deformation immediately after assembly with 2, 4 and 8 kN.

Impaction Force (kN)	Head Taper (CoCr alloy) Corrosion Grading	Neck Taper (Ti alloy) Corrosion Grading
4	III	II
4	III	II
4	II	II
8	II	II
8	I	I
8	II	II

Table 8-2: Corrosion analysis using the Goldberg criteria (Goldberg et al., 2002) for head and neck tapers following 5 million cycles.

8.2.5. Statistical Analysis

Data was analysed with the aid of SPSS Statistics Version 22 (Armonk, NY: IBM Corp.). An initial data analysis on n=3 using Kolmogorov–Smirnov test was carried out showing that the data was non parametric. I, therefore carried out Kruskal-Wallis test followed by post hoc Mann – Whitney U test with Bonferroni correction to determine any significant differences ($p=<0.05$) in the generation of fretting current at the modular junction between the different impaction loads and material/surface finish combinations.

8.3. Results

8.3.1. Electrochemical Testing – Test 1 (Short Term)

All modular junctions assembled using 8kN of force showed significantly lower fretting currents than those assembled with either 2kN or 4kN assembly loads with the exception of CoCrMo smooth-standard neck tapers that showed a slightly higher amplitude fretting current when impacted with 8kN compared to 4kN (Table 8-3).

Impaction Force & Neck Taper Combination	Mean Current (± Standard Deviation)	
	Max Fretting Current (μA)	Amplitude Current (μA)
2kN Ti Rough-Short	**12.89** (±1.24)	**10.85** (±1.24)
2kN Ti Smooth-Standard	**16.31** (±1.54)	**10.05** (±1.43)
4kN Ti Rough-Short	**16.30** (±0.83)	**13.17** (±0.94)
4kN Ti Smooth-Standard	**6.75** (±0.74)	**5.02** (±0.70)
8kN Ti Rough-Short	**8.43** (±1.22)	**2.82** (±1.68)
8kN Ti Smooth-Standard	**5.22** (±1.45)	**3.76** (±1.20)
2kN CoCr Rough-Short	**10.33** (±1.35)	**7.72** (±1.18)
2kN CoCr Smooth-Standard	**14.08** (±3.25)	**9.41** (±3.55)
4kN CoCr Rough-Short	**14.03** (±1.20)	**12.18** (±0.88)
4kN CoCr Smooth-Standard	**4.23** (±0.89)	**2.50** (±0.36)
8kN CoCr Rough-Short	**7.00** (±0.94)	**3.42** (±0.43)
8kN CoCr Smooth-Standard	**6.88** (±0.49)	**5.58** (±0.44)

Table 8-3: Table showing the maximum fretting current and current amplitude values for each taper combination at three impaction loads (Test 1).

For both Ti-6Al-4V surface finishes and the CoCrMo rough-short taper, the lowest fretting current was observed in samples with the greatest force of impaction ($p<0.05$). At 2kN and 4kN impaction force, the fretting current measured for the CoCrMo/Ti-6Al-4V combination was significantly higher than CoCrMo/CoCrMo combination ($p<0.05$). However, at 8kN assembly load this effect was reversed and CoCrMo/Ti-6Al-4V showed lower fretting currents ($p<0.05$). Smooth-long tapers generated a significantly lower fretting current than rough-short tapers when impacted with 4kN of force ($p<0.05$). However, this was not the case when impacted at 8kN with the rough-short neck tapers performing better than their smooth-long counterparts when subjected to high impaction loads. This is, seen clearly on the graph for mean amplitude fretting current (Figure 8-2). However this effect was only seen on tapers impacted at 8kN and

did not occur when lower impaction forces were used. Statistical analysis for each short-term taper combination is shown in Table 8-4.

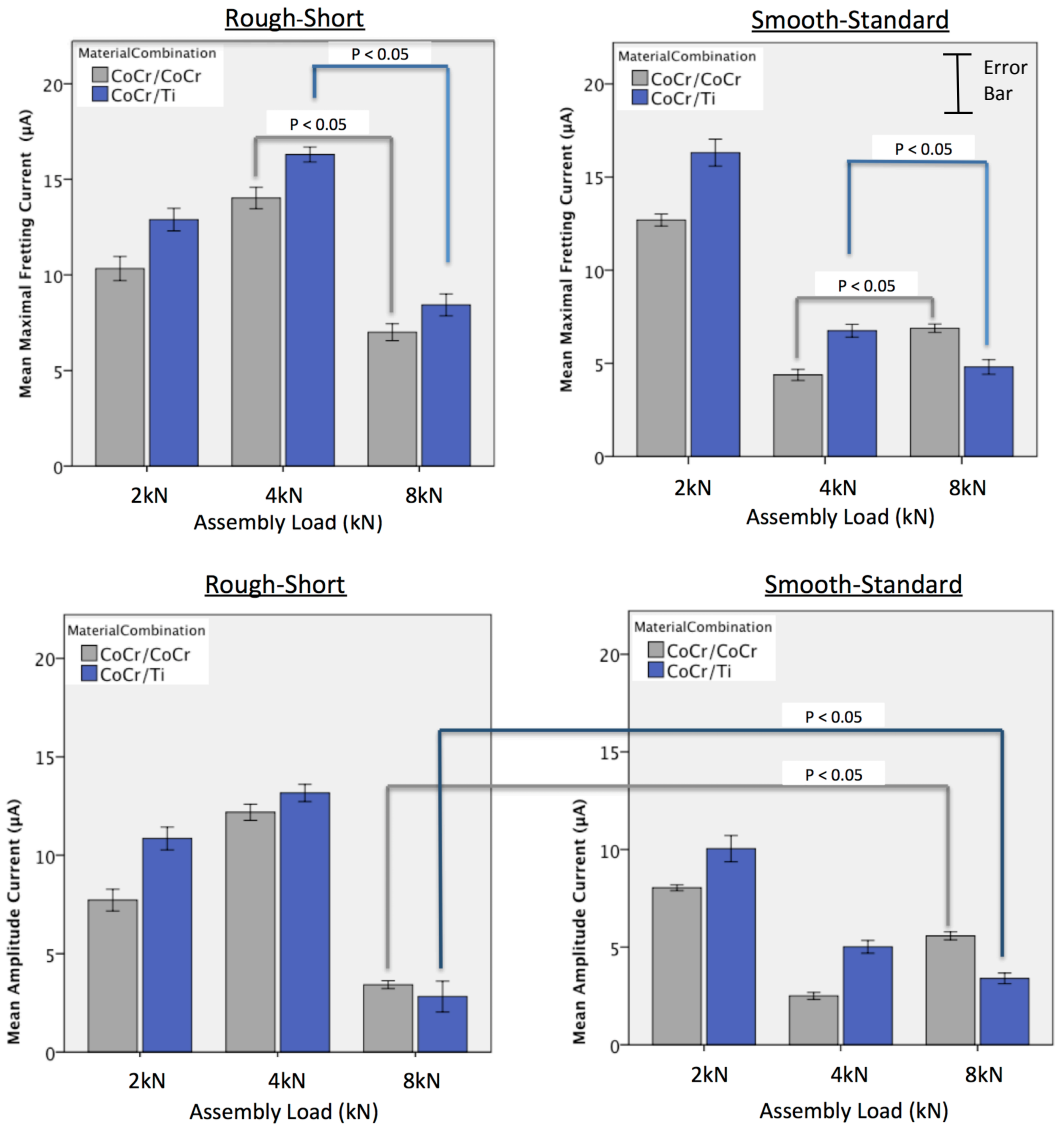

Figure 8-2: Short-term test results (Test 1). Bar graphs showing the mean maximal fretting and mean amplitude currents at three impaction assembly loads of the different head-neck combinations during 1000 cycles of sinusoidal loading.

Variable	Combination Compared, "A vs. B"	Difference in means, B – A (p-value)	
		Max Fretting Current (μA)	Amplitude Current (μA)
Surface Finish	Ti Rough-Short **vs.** Ti Smooth-Standard 2kN	**+3.42** (p = <0.001)	**-0.80** (p = 0.014)
	Ti Rough-Short **vs.** Ti Smooth-Standard 4kN	**-9.75** (p = <0.001)	**-8.15** (p = <0.001)
	Ti Rough-Short **vs.** Ti Smooth-Standard 8kN	**-3.21** (p = <0.001)	**+0.94** (p = 0.001)
	CoCr Rough-Short **vs.** CoCr Smooth-Standard 2kN	**+3.75** (p = <0.001)	**+1.69** (P = 0.019)
	CoCr Rough-Short **vs.** CoCr Smooth-Standard 4kN	**-9.80** (p = <0.001)	**-9.68** (p = <0.001)
	CoCr Rough-Short **vs.** CoCr Smooth-Standard 8kN	**-0.12** (p = NS)	**+2.16** (p = <0.001)
Impact Force	Ti Rough-Short 4kN **vs.** 8kN	**-7.87** (p = <0.001)	**-10.35** (p = <0.001)
	Ti Smooth-Standard 4kN **vs.** 8kN	**-1.53** (p = <0.001)	**-1.26** (p = <0.001)
	CoCr Rough-Short 4kN **vs.** 8kN	**-7.03** (p = <0.001)	**-8.76** (p = <0.001)
	CoCr Smooth-Standard 4kN **vs.** 8kN	**+2.65** (p = <0.001)	**+3.08** (p = <0.001)
Material	Ti Rough-Short **vs.** CoCr 4kN	**-2.27** (p = <0.001)	**-0.99** (p = 0.003)
	Ti Smooth-Standard **vs.** CoCr 4kN	**-2.52** (p = <0.001)	**-2.52** (p = <0.001)
	8kN Ti Rough-Short **vs.** CoCr	**-1.43** (p = <0.001)	**+0.60** (p = 0.001)
	8kN Ti Smooth-Standard **vs.** CoCr	**+1.66** (p = <0.001)	**+1.82** (p = <0.001)

Table 8-4: Table showing Comparison of maximum fretting current/amplitude according to taper characteristics (Test 1).

8.3.2. Electrochemical Testing – Test 2 (Long Term)

Both maximum fretting current and mean current amplitude decreased with time and the number of cycles (Table 8-5).

Ti RM Assembly Load & Cycles Completed	**Mean Current (± Standard Deviation) - Average of n=3**	
	Max Fretting Current (μA)	Current Amplitude (μA)
4kN – 1 million	**14.56** (±3.33)	**4.72** (±1.19)
4kN – 2 million	**9.71** (±3.22)	**3.07** (±0.86)
4kN – 3 million	**10.43** (±4.08)	**3.03** (±0.82)
4kN – 4 million	**7.06** (±2.14)	**2.03** (±0.56)
4kN – 5 million	**8.21** (±2.68)	**2.53** (±1.29)
8kN – 1 million	**7.15** (±6.09)	**2.74** (±1.88)
8kN – 2 million	**8.64** (±7.60)	**2.67** (±1.78)
8kN – 3 million	**5.41** (±3.50)	**2.71** (±1.53)
8kN – 4 million	**6.92** (±5.62)	**2.52** (±1.53)
8kN – 5 million	**3.48** (±2.75)	**1.72** (±0.90)

Table 8-5: Table showing Comparison of maximum fretting current/amplitude for each impaction force over 5 million cycles at 2 impaction loads (Test 2).

However, in the case of modular junctions impacted at 8kN this effect was far less pronounced and the fretting current seen after the first one million cycles was lower than those samples impacted at 4kN ($p<0.05$). For 4kN, there was a significant drop in maximum fretting current and amplitude between 1 million and 2 million cycles ($p<0.05$), but no such change between 2 million and 3 million cycles. The downward trend continued at 4 and 5 million cycles (Figure 8-3 and Table 8-6). At 8kN impaction force, there was no statistically significant difference in current between 1 million and 5 million cycles.

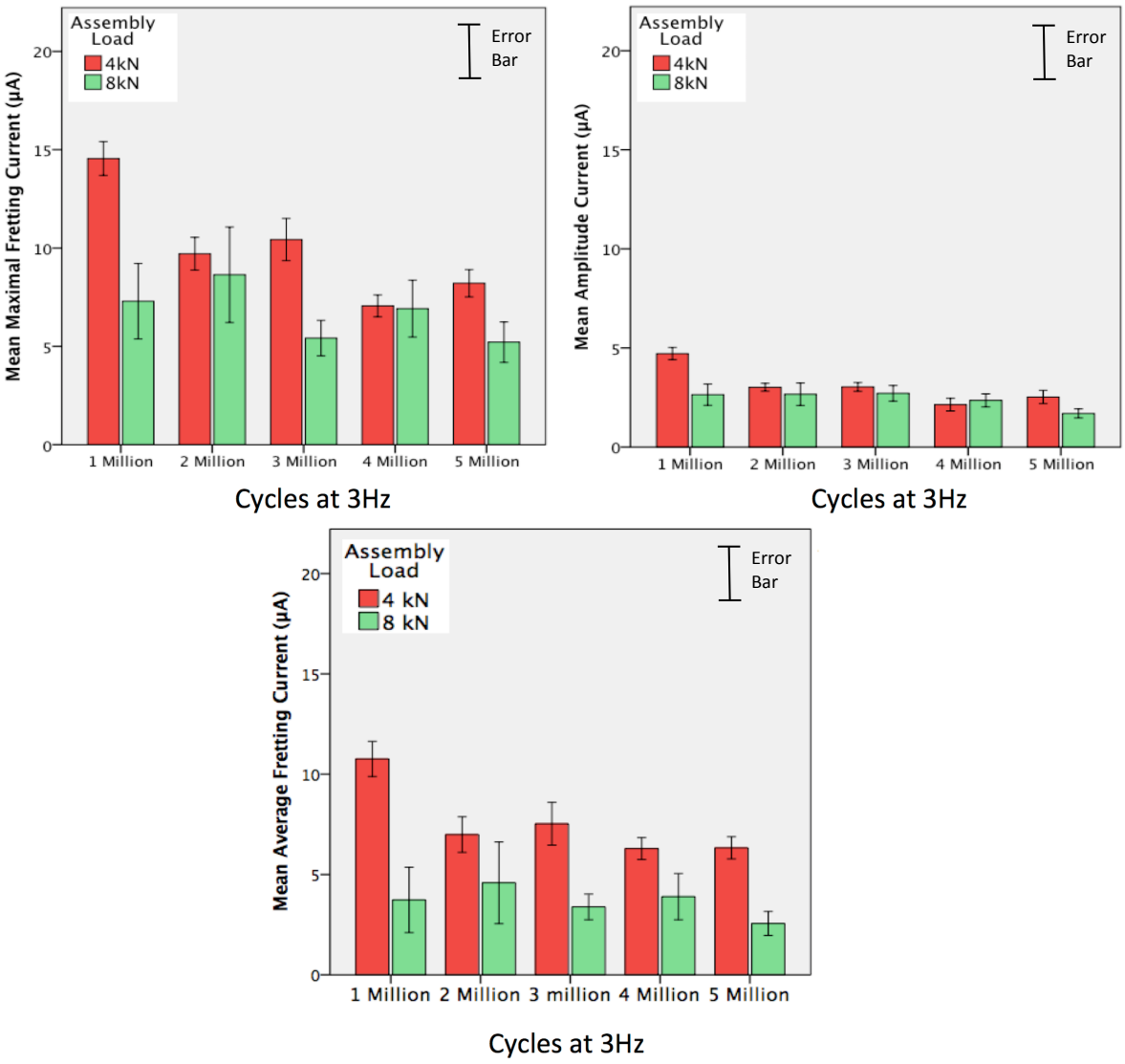

Figure 8-3: Long-term test results (Test 2). Bar graphs showing the mean maximal fretting current, the mean amplitude of current oscillation and average fretting current up to 5 million cycles, for 4kN and 8kN impaction forces in CoCrMo head taper with Ti-6Al-4V rough/short neck tapers.

Variable	Combination Compared, "A vs. B" (n=3 for each)	Difference in average means, B – A (p-value)	
		Max Fretting Current (μA)	Amplitude Current (μA)
Number of Cycles	4kN Ti Rough-Short 1 million **vs.** 2 million	**-4.85** (<0.001)	**-1.65** (<0.001)
	8kN Ti Rough-Short 1 million **vs.** 2 million	**+1.49** (NS)	**-0.07** (NS)
	4kN Ti Rough-Short 1 million **vs.** 5 million	**-6.35** (<0.001)	**-2.19** (<0.001)
	8kN Ti Rough-Short 1 million **vs.** 5 million	**-3.67** (0.039)	**-1.02** (0.002)
Impact Force	Ti Rough-Short 1 million 4kN **vs.** 8kN	**-7.41** (<0.001)	**-1.98** (<0.001)
	Ti Rough-Short 5 million 4kN **vs.** 8kN	**-4.73** (<0.001)	**-0.81** (0.002)

Table 8-6: Table showing Comparison of maximum fretting current/amplitude according to impaction force over 5 million cycles (Test 2).

8.3.3. Volumetric Wear Analysis – Test 2 (Long Term)

Measurement of surface roughness of the neck tapers at different impaction loads immediately after impaction showed evidence of deformation with flattening of the peaks at the apex in the area of engagement. Increased deformation of the ridges and increased area of taper engagement was seen with increasing impaction loads and was more prominent on neck tapers impacted at 8kN (Figure 8-4).

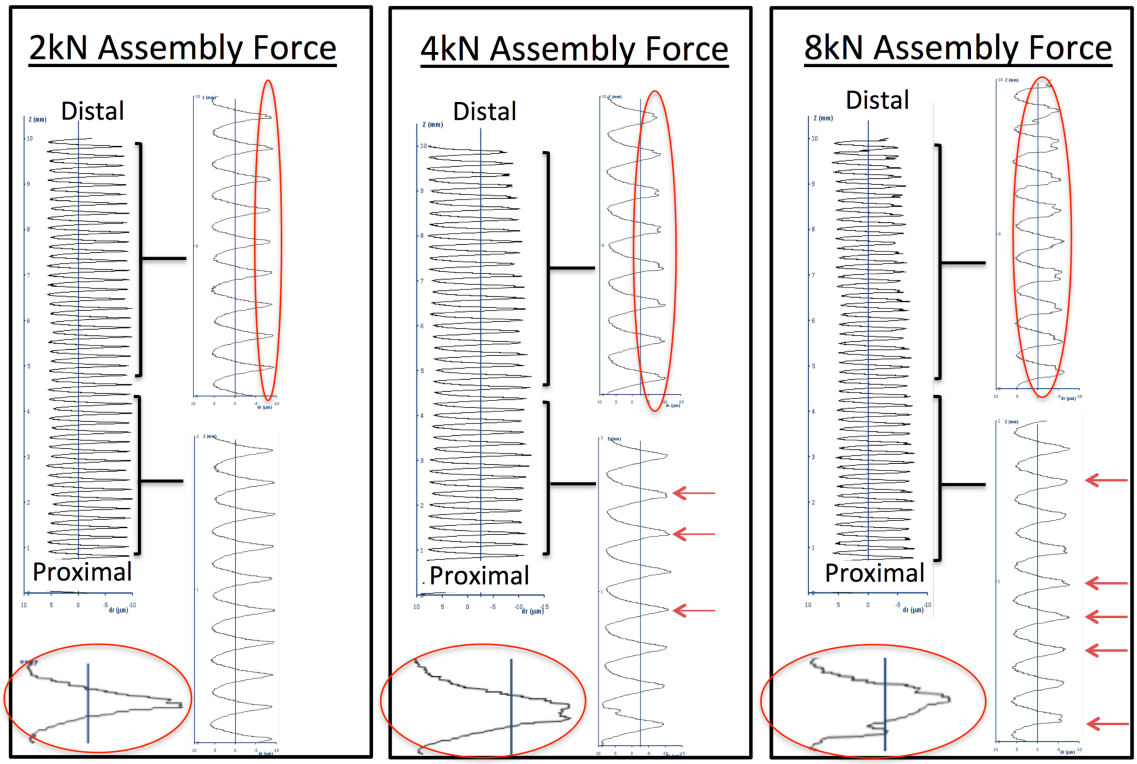

Figure 8-4: Single line profile measurements during volumetric wear analysis using Talyrond 365 of Ti-6Al-4V neck tapers immediately after impaction at 2, 4 and 8kN. Showing evidence of progressive increase in the deformation of the peaks with increase in impaction load (flattening of the peaks at the apex, area of maximal engagement). Also the greater the impaction force the greater the surface area of engagement with more of the proximal end of the taper engaging when impacted with 8kN compared to 4kN and 2kN.

The results showed that tapers become more impacted after cyclic loading. After 5 million cycles the deformation of the ridges on the male taper at both 4 and 8 kN was larger with more flattened peaks and there was evidence of greater taper engagement (Figure 8-5).

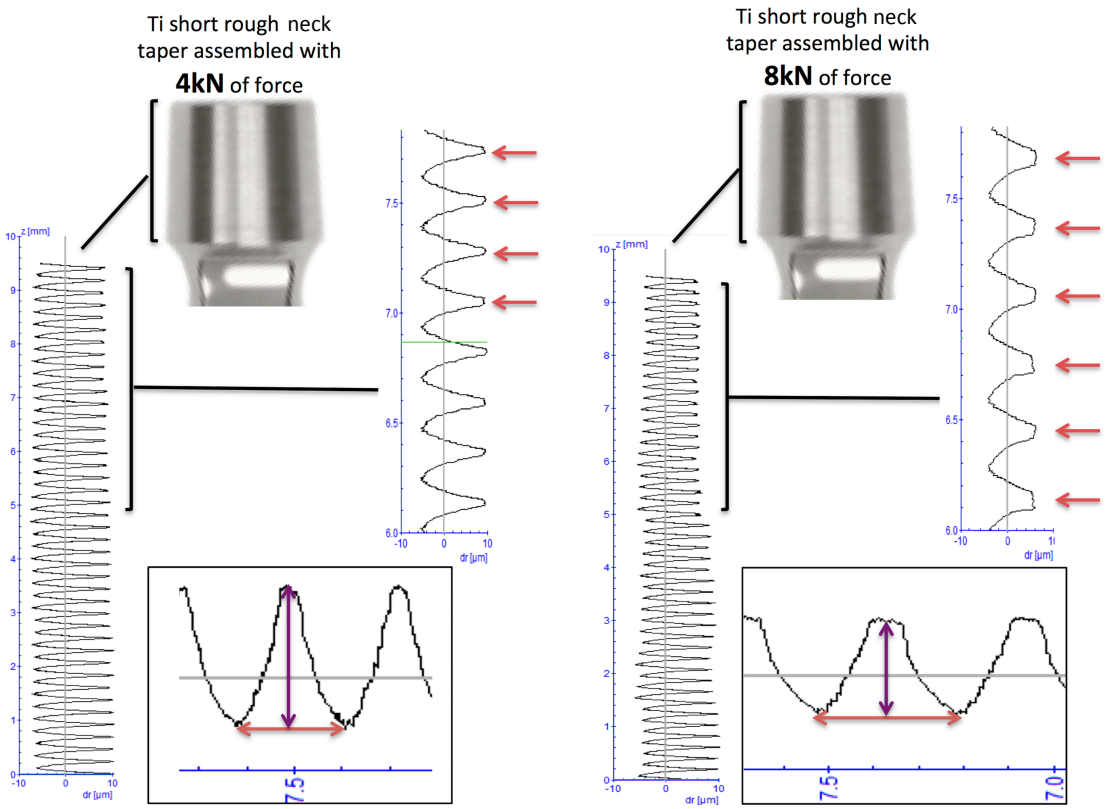

Figure 8-5: Single line profile measurements during volumetric wear analysis using Talyrond 365 of Ti-6Al-4V neck tapers impacted at 4kN and 8kN following 5 million cycles of loading. Showing evidence of increase in deformation with more flattened peaks and greater taper engagement with increasing number of cycles.

There was evidence of imprinting on tapers impacted with both 4kN and 8kN but this was more pronounced with the tapers impacted with 4kN (Figure 8-6). Volumetric assessment indicated no significant difference in volume loss between tapers impacted at 4kN and 8kN.

8.3.4. SEM – Test 2 (Long Term)

Fretting scars were seen to a greater extent on the 4kN than the 8kN assemblies (Figure 8-7). Tapers impacted with both of these loads showed corrosion occurring in areas, which was consistent with the large bending moment (Figure 8-8). This pattern was also evident on visual inspection and using optical microscopy (Figure 8-6). There was visual evidence corrosion with black deposits, as well as imprinting, on samples both at 4kN and 8kN assembly load (Figure 8-6).

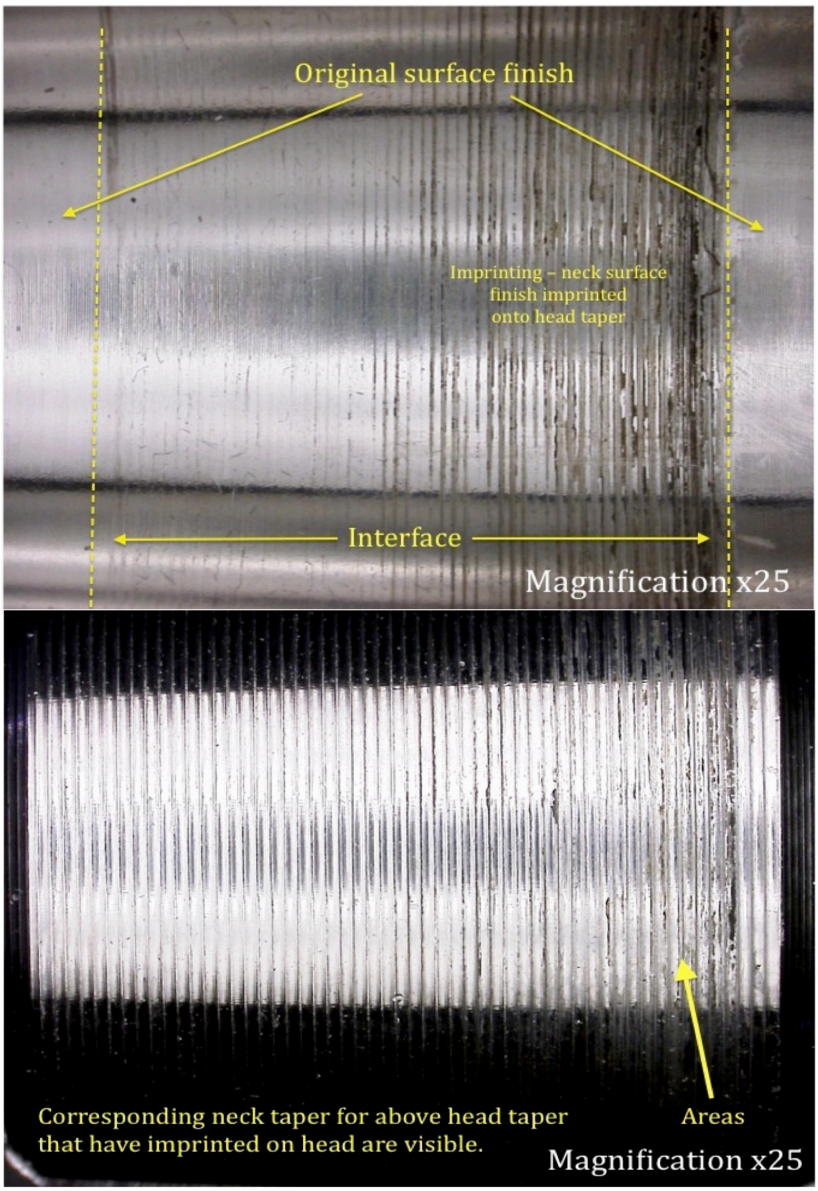

Figure 8-6: Light microscopy pictures of head taper (a) and neck taper (b) impacted at 4kN showing evidence of Goldberg Type 2 corrosion following 5 million cycles of sinusoidal loading. The surface finish of the neck taper is imprinted onto the head taper.

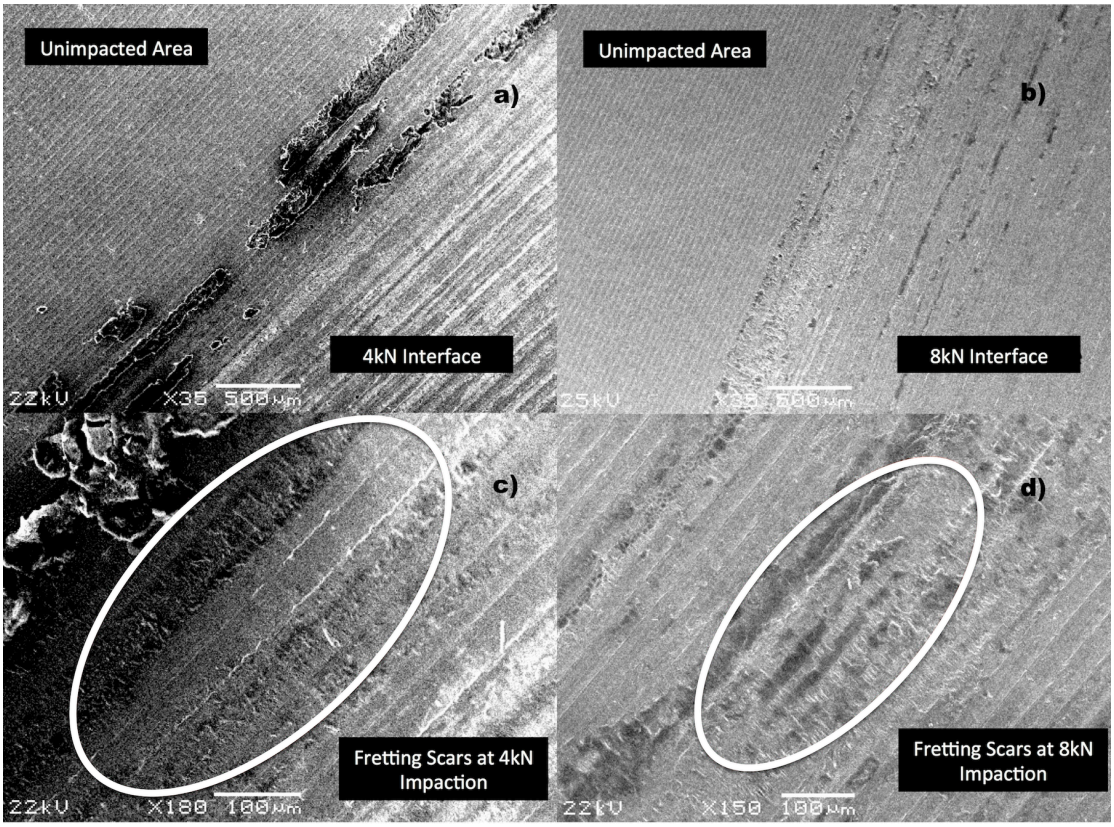

Figure 8-7: SEM images showing: a) An overview of the edge of the interface with 4kN assembly load. b) An overview of the edge of the interface with 8kN assembly load. c) Evidence of fretting scars near the interface edge with 4kN assembly load. d) Evidence of fretting scars near the interface edge with 8kN assembly load.

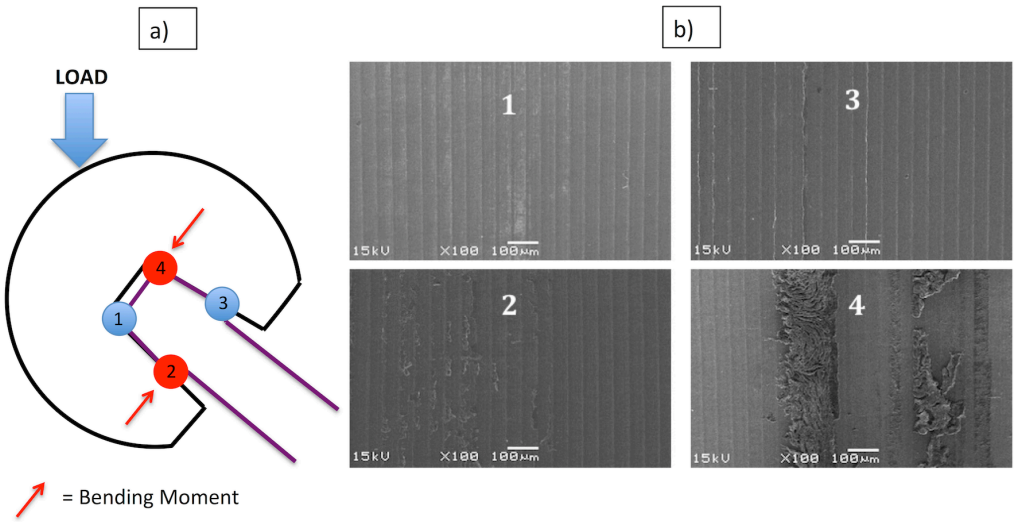

Figure 8-8: a) Diagram showing highest bending moment with a +14mm neck offset head. b) SEM pictures 1 and 3 show areas of little stress and therefore less corrosion/wear, pictures 2 and 4 show areas of high stress due to bending and evidence of high corrosion/wear.

8.4. Discussion

Studies indicate that surface finish, neck length, impaction load and manufacturing tolerances may contribute to the quality of interlock of the two tapers (Schmidt et al., 1997, Rehmer et al., 2012, Pennock et al., 2002, Mroczkowski et al., 2006), also that high frictional torque and bending stresses encountered with the use of large head diameters, exacerbated by improper alignment, may increase the amount of mechanical wear at the head-neck interface (Bolland et al., 2011, Langton et al., 2012, Panagiotidou et al., 2013). The degree of deformation of each surface is relevant as it determines the strength of the taper interlock. *Rehmer* (Rehmer et al., 2012) demonstrated that the quality of fixation increases with the amount of impaction force used to assemble the implant. This study aimed to investigate the effect of assembly load on the deformation and fretting corrosion of tapers used in hip replacements. Fretting corrosion was assessed by measurement of the fretting current during cyclic loading. The extent to which this occurs is an indication of micromotion at this junction and, ultimately, determines the rate of MACC. Each head-neck combination was impacted with 2kN (a light blow), 4kN (roughly the average force used) or 8kN (a large blow).

Results from the short-term cyclic loading test (Test 1) showed that for smooth-long neck tapers in both material combinations, 4kN impaction was preferable to 2kN with 8kN faring better than both ($p<0.05$). Interestingly however, rough-short neck tapers in both material combinations did not follow this trend, as impaction forces of above 2kN initially showed increased MACC whilst 8kN showed a significant reduction ($p<0.05$). The reason for this increase in MACC between 2 and 4kN in rough-short tapers is not clear. Although I did not investigate the causality of this unexpected result in this study I, suspect it may be due to the increased contact between the neck and head taper with higher impaction where reduction in motion is not alleviated by the increased force until 8 kN is used. The combination of interlock roughness and impaction force is complex

and one of the ways to investigate this further might be to investigate micromotion at the junction with increasing impaction.

Irrespective of material combination and surface finish the least fretting current is found in samples with the greatest assembly load with the exception of CoCrMo smooth-standard neck tapers that showed a slightly higher fretting current when impacted with 8kN compared to 4kN (Table 8-2). This may be explained by a result reported by *Rehmer* (Rehmer et al., 2012) where they showed that CoCrMo heads and necks had lower dissociation forces when combined together compared with CoCrMo heads with Ti alloy neck combinations. For both 2kN and 4kN impaction loads, the corrosion current was higher for Ti-6Al-4V necks compared with CoCrMo. However, when assembled with 8kN, Ti-6Al-4V generated lower corrosion currents than CoCrMo most likely due to greater deformation of this softer material resulting in a greater resistance to micromotion and MACC. In Chapter 6, I was able to demonstrate that tapers with a long neck and smooth finish are superior, in terms of fretting, to those with a short neck and rough surface finish (Panagiotidou et al., 2013). I investigated the fretting current seen with rough-standard vs. rough-short tapers, as well as rough-short vs. smooth-short, finding that short and rough tapers were subject to a greater degree of fretting and this may be "unsuitable for neck tapers". This study demonstrates that when impacted with 8kN of force, this is not the case and a well-impacted rough short taper performs equally well. However if a 2kN or 4kN load is used to impact the head then rough short tapers do corrode more than long smooth tapers. I was able to measure the effects of taper geometry on the corrosion current and subsequently how these effects can be reduced given the appropriate level of impaction. The clinical relevance of this finding is that the impaction force at the time of assembly is a key factor for taper corrosion and since the surgeons control impaction force intraoperatively, they have the potential to directly affect taper corrosion.

Following the results of the short-term tests, 4kN and 8kN impaction loads were compared through long-term cyclic loading in the rough-short group for the CoCrMo head and Ti-6Al-4V neck material combination. In doing so, the average force currently used was compared with the force that appeared to be the best option from the short-term tests. This study showed that as time and number of loading cycles increased, the fretting current decreased. This is important as the loads used were typically those for peak load during walking, indicating that these loads may lead to greater impaction and reduced corrosion over time. This decrease is larger in those samples impacted with 4kN. In samples assembled with 4kN of force there was a large fall in fretting current between 1 million and 2 million cycles ($p<0.05$). This is probably a direct result of the two tapers bedding into each other. This effect was seen in those impacted with 4kN, but impaction with 8kN provided a secure initial fixation with low corrosion currents measured from the start of the test. There was no statistically significant difference between fretting currents at 1 million and 2 million cycles for 8kN assemblies and these were lower than the first 1 million cycles when compared with tapers impacted with 4kN ($p<0.05$). For the remaining 4 million cycles the change in fretting current, particularly amplitude, was far less marked for the 8kN assemblies. We can therefore conclude that for both impaction loads over time the fretting corrosion processes seem to reach equilibrium, with seating loads mainly affecting the immediate post-seating fretting corrosion processes (between 1 and 2 million cycles). This difference is more noticeable in the group impacted at 4 kN.

After long-term testing (Test 2), imprinting was visible on the CoCrMo head taper. This imprinting of regular circumferential grooves on the head taper surface was identical to the circumferential grooves seen on the neck taper only in the contact region indicating that the original smooth surface of the head taper had now changed to a more roughened surface whilst the surface finish of the neck taper had remained the same.

This phenomenon was observed in all previous chapters in both retrieval and in-vitro sample analyses where the tapers were subject to long term cyclic loading. The amount of corrosion was greater in the samples impacted with only 4kN of force. As corrosion has been identified as a largely time-dependent process (Collier et al., 1992a) it is probable that more pronounced evidence of corrosion and imprinting would have been measured had either the number of cycles been increased or the frequency of loading increased. The localised position of crevice corrosion on the tapers seen in this in-vitro study is likely due to the imposed bending forces. MACC has been associated with other modular junctions such as the neck-stem junction as well as with more conventional MoP bearings. Additionally high torque and large bending moment at the head-neck junction associated with large diameter MoM heads can exacerbate MACC and may increase the risk of malfunction (Langton et al., 2012).

In this comparative study it has been shown that impaction force has an effect on MACC in-vitro and therefore I predict that impaction force will have an effect on MACC clinically. However the precise amount of force used clinically to alleviate MACC is not known. This study indicates that impaction force is important and that different taper configurations require different impaction levels in order to reduce MACC. The findings of this study suggest the benefit of impaction at 8kN. However it is possible that the bone condition of some patients undergoing THA will not allow for this amount of force to be imparted to an already inserted femoral stem without causing a fracture. It is also very difficult for the surgeon to assess the force required to impact with 8kN. However the results from this study demonstrate that greater impaction results in more deformation, that reduces fretting corrosion and surgeons should strive to achieve these. It may be that a change in practise is required where a surgeon assembles the hip replacement on the bench rather than in the patient and one can imagine that a tool could be developed to impact an in-line force on the taper in a controlled manner.

8.5. Conclusions

This study has shown that all tapers tested exhibited fretting corrosion however, I was able to identify that greater impaction force resulted in less fretting corrosion regardless of the engagement length, surface roughness or material combination. Long term testing over 5 million cycles illustrated a progressive improvement in resistance to fretting corrosion with an increase in the number of cycles for Ti-6Al-4V rough-short neck tapers. 8kN impaction force showed a better resistance to fretting corrosion for Ti-6Al-4V rough-short neck tapers compared to 4kN of impaction force. This may be associated with increasing deformation at the higher impaction loads and a stronger taper interlock. It would be advised that high impaction forces be used to assemble a taper as this may reduce MACC.

Chapter 9 Discussion

9.1. Overall Discussion

With the clinical success of total hip replacement recognised in the UK by a commemorative postage stamp and with the procedure recently described as 'The operation of the century' (Learmonth et al., 2007), the hip surgeons of today are the custodians of one of the most successful interventions in modern medicine (Manktelow et al., 2017).

Currently we are being faced with an ageing, yet increasingly active population, with high expectations. Meeting those aspirations and striving to ensure excellent outcomes with evidence-based choices in implant and bearing surface technology are amongst the challenges hip surgeons are presented with. With this in mind, if we are to continue to improve longevity and functional outcome, it is essential that surgeons are fully aware of the available options in surgical technique and implant design. It is important for surgeons, bioengineers and patients to understand the limitations of current designs. This understanding can be empirical, through experience gained with other implant designs, by carrying out preclinical tests, through clinical experience and by investigating failed prostheses. Often changes in implant design are incremental however the complexity of hip replacements means that small design changes can often cause quite large differences in clinical performance. For example the Exeter hip stem was initially polished and then the surface was changed to matte finish. This small change resulted in a much greater failure rate and the polished stem was reinstated (Howie et al., 1998). In this case what was perceived as a small change in design had much larger consequences. In my thesis what could be perceived as small taper design changes may have resulted in different levels of corrosion.

This chapter will conclude experimental and clinical findings and propose future work to be conducted.

The work in my thesis presents a systematic investigation into the factors influencing the rates and mechanisms of corrosion at the head-neck junction of modular THRs and thus, provides important insights into the patterns and determinants of their failure. By demonstrating that high frictional torque, increased bending moment (offset), neck taper surface roughness, neck taper contact surface area, taper assembly force and taper material composition contribute to the susceptibility of corrosion and wear at the head-neck modular junction of THRs, my thesis has addressed the questions raised in my introduction and has therefore, fulfilled its goal in identifying some of the ideal parameters for the creation of the "ultimate" taper. It is hoped that dissemination of the findings of this thesis can change the practice of those performing THRs. If more surgeons were to adopt the practices demonstrated to improve outcome, this would lead to a greater overall survival for patients undergoing THR, and would allow more patients to benefit from the advantages of THR in terms of function, morbidity and mortality.

My experimental findings, in this thesis, complement clinical data, with distinct similarities seen between the simulated and retrieved prostheses. Due to the number of findings and their complex nature, the conclusions associated with these have been split into sections.

9.1.1. Material Loss from Taper Junction

The study in Chapter 4 reports on a large series of revised LH-MoM-THRs and suggests that corrosion is likely to be the principle source of implant-derived material. Corrosion of the head taper was virtually universal (99 of 110 cases), and the presence of "imprinting" of the neck taper thread onto the head taper surface is highly suggestive of

galvanic corrosion, a process by which material is lost preferentially from the head taper. This axisymmetric pattern of regular and uniform circumferential grooves associated with material on the head taper likely represents uniform loss or transfer of material, supporting a mechanism involving corrosion rather than wear. This imprinting phenomenon was observed in all chapters for both retrieval and in-vitro sample analyses where the tapers were subject to long term cyclic loading. In Chapter 7 we also saw that the imprinting effect appeared to be more prominent in areas associated with increased bending moment where it was often accompanied by evidence of extensive wear. Furthermore studies by Langton et al. (2012) and Bolland et al. (2011) suggested that corrosion occurred secondary to a mechanical process (Langton et al., 2012) and high frictional torque associated with large diameter heads (Bolland et al., 2011).

Throughout my thesis corrosion associated with different material combinations, loading conditions, taper surface area, taper surface roughness and taper assembly force was quantified by recording the fretting current directly linked to the frequency of loading. This fretting current is associated with MACC; which is a combination of fretting and crevice corrosion, with additional galvanic corrosion when dissimilar materials are used. Increasing frictional torque and bending have a significant effect on corrosion at the modular interface. Increased bending and torque probably act to enhance the removal of the passive layer, which then quickly reforms. The corrosion process is therefore mechanically assisted, but the imprinting effect seen on retrieved femoral heads (Matthies et al., 2013) (Chapter 4) and in long-term cyclically-loaded in-vitro tests (Panagiotidou et al., 2013) (Chapter 6) appears to develop into a regular pattern associated with the morphology of the surface of the neck taper, suggesting that small amounts of movement are needed to enhance the process. Undoubtedly therefore, corrosion at the interface is due to a mixture of different modes of failure and it is often

difficult to differentiate between them however, they are now generally attributed to MACC.

Chapter 4 also demonstrated that similar to the trend observed for MoM hip resurfacings, in the group of retrieved MoM total hip replacements, bearing surface wear volumes were strongly correlated with blood metal ion levels. In contrast, the volumes lost from the MoM THR tapers were only weakly correlated with ion levels. Overall about 1/3rd of the total wear can be attributed to material loss at the taper. Since MoM THRs have a higher revision rate for failure this supports the theory that material loss from the taper junction is a significant source of implant-derived debris. Several studies have suggested that material loss at the taper is associated with a higher Co:Cr ratio in the blood steam and that as Co is believed to be more toxic then it has been postulated that this can lead to toxicity (Cooper et al., 2012). Another explanation for the higher revision rates of LH-MoM-THR is that these implants are subject to a higher total volume of material loss; a combination of material loss from the bearing and taper surfaces.

9.1.2. Effect of Taper Surface Topography

Chapter 6 demonstrated that the circumferential morphology (imprinting) on the CoCrMo head taper surface was accentuated by reducing the surface contact area of the neck taper and by using a rough surface finish. The fact that the morphology on the CoCrMo affected region was consistent with the machining marks on the Ti neck taper surface suggested that the rough finish enhanced crevice corrosion by allowing the ingress of fluid along the valleys (an effect also associated to bending moment due to the opening and closing of the crevice). The electrochemical tests further supported the concept of fretting corrosion in the rough short neck taper samples because of the cyclic nature in the potentiostatic cyclically loaded tests and current spikes in the potentiostatic

tests. The fact that pitting was more evident on the short neck tapers could be partly explained by the reduced contact area compared to that of the standard neck tapers. Forces may be concentrated and exceed the surface oxide fracture strains in the CoCrMo, leading to accelerated corrosion. *Goldberg* (Goldberg et al., 2002) showed the importance of neck stiffness on corrosion and concluded that larger diameter neck tapers had lower fretting corrosion rates. This could potentially be due to reduced contact pressures resulting from decreased area of contact or with tapers of lower stiffness with increased bending and micromotion at the junction leading to increased MACC.

9.1.3. Effect of Bending Moment, Torque and Material Combination

The study in Chapter 7 demonstrated the enhanced effect on corrosion at the taper junction secondary to increased frictional torque and bending moment. The use of large diameter heads will in itself increase the frictional torque and bending moment acting at the taper modular junction however other parameters need also be considered. Poor lubrication, high inclination angles and component positioning will also increase frictional torque through edge loading. In addition an increased head-neck offset, varus necks and heavier patients will also increase the bending moment acting at the modular taper junction.

A study by *Kotzar* (Kotzar et al., 1995) has shown that torque is not constant and that it will vary according to the position of the hip in the gait cycle associated with loading and movement. Both of these factors will affect the generation of fluid film and friction so torque at the taper junction is multifactorial and associated with more than just the radial offset. They reported the peak torques during stair ascent and during rising from a seated position to be 23 and 15 Nm, respectively, and the maximum value for torque measured in their study was 37 Nm during one attempt at single-limb stance (Kotzar et al., 1995). In my study I measured the effect of four different torsional forces, with the

maximal applied torque being 18Nm. The resulting fretting current seemed to increase from 0.1 μA for every Nm of torque for the Ceramic/CoCr combination to 0.7 μA for every Nm of torque for the CoCr/Ti and CoCr/ CoCr combinations with the CoCr/Ti combination showing the most susceptibility to MACC with a recorder max fretting current of 15 μA. Therefore, when considering that in-vivo THRs can be subjected to higher torsional forces one may assume that the effect MACC may be even greater than the one recorded in my study.

In this study the Ti alloy neck combinations showed the highest corrosion currents. In addition it showed that increased bending moments associated with using larger offset heads produced more corrosion; with Ti alloy necks generally having performed worse than CoCr alloy necks. Although the use of Ceramic heads did not prevent corrosion, they did appear to significantly reduce it in all loading configurations. The fact that certain material combinations appeared to be more sensitive to increasing bending and torque indicated that these might be more susceptible to corrosion. It appears that we may be seeing the effect of two other factors in addition to the mechanical effect (fretting); 1) the association of different material combinations and the subsequent effect of galvanic corrosion and 2) the association of different material moduli in the differential movement between the head and neck leading to crevice opening and closing. The superiority of ceramic as a material in terms of corrosion resistance and inability to conduct electricity may explain the reduced currents seen during loading with increasing bending and torque (lack of galvanic corrosion).

9.1.4. Effect of Assembly Load

The study in Chapter 8 has shown that impaction force has an effect on MACC in-vitro and therefore predicts that impaction force will have an effect on MACC clinically. Irrespective of material combination and surface finish the short term tests showed that

the least fretting current is found in samples with the greatest assembly load of 8 kN with the exception of CoCrMo smooth-standard neck tapers that showed a slightly higher fretting current when impacted with 8kN compared to 4kN. However, currently the majority of uncemented prostheses utilised in orthopaedic practice include a CoCrMo head with a Ti-6Al-4V stem and therefore, when this combination was assembled with 8kN, it generated lower corrosion currents than the CoCrMo/CoCrMo combination. This is most likely due to greater deformation of the softer Ti-6Al-4V material resulting in a greater resistance to micromotion and MACC. Following the results of the short-term tests, 4kN and 8kN impaction loads were compared through long-term cyclic loading in the rough-short group for the CoCrMo head and Ti-6Al-4V neck material combination. This study showed that as time and number of loading cycles increased, the fretting current decreased and this decrease was larger in those samples impacted with 4kN. In samples assembled with 4kN of force there was a large fall in fretting current between 1 million and 2 million cycles, which is probably a direct result of the two tapers bedding into each other. This effect was seen in those impacted with 4kN, but impaction with 8kN provided a secure initial fixation with low corrosion currents measured from the start of the test. Clinically the question remains, what does 8 kN represent? In the body the peak assembly force may be attenuated by the tissues and additionally imposing a blow of 8 kN on the head may lead to bone damage (e.g. in osteoporotic bone) assembly therefore, either outside the body after a trial reduction or by using specially designed tools may be appropriate.

It also important to note that in Chapter 6 we saw that tapers with a long neck engagement length and smooth finish were superior, in terms of fretting, to those with a short neck and rough surface finish (Panagiotidou et al., 2013). However, Chapter 8 demonstrated that when impacted with 8kN of force, this was not the case and that a well-impacted rough short taper performed equally well. However if a 2kN or 4kN load

was used to impact the head then rough short tapers did corrode more than long smooth tapers. The clinical relevance of this study being that the impaction force at the time of assembly is a key factor for taper corrosion and since surgeons control impaction force intraoperatively, they have the potential to directly affect taper corrosion.

9.2. Conclusions

- A significant volume of material is released at the taper junction and although the failure mechanism of MoM THRs remains unclear results from this thesis suggest that the mechanism of material loss is predominantly due to MACC.
- Lack of a significant correlation between taper material loss and either blood metal ion levels or incidence of pseudotumours has implications for the clinical surveillance of all patients with LH-MoM-THRs.
- Enhanced fretting corrosion at the modular taper junction is associated with roughened surface finish and short neck tapers and points to the overall concern associated with their current use in orthopaedic implants.
- Increased frictional torque and bending moment associated with large diameter heads (>36mm) and high offset increase the susceptibility of MACC at the taper junction particularly in the CoCrMo head Ti-4Al-4V neck combination which, is the commonest uncemented combination in current orthopaedic use.
- Ceramic heads did not prevent MACC, they did however, appear to significantly reduce it in all loading configurations.
- All head-neck taper junctions tested in this thesis exhibited evidence of MACC. However, it would appear that an assembly force of more than 4 kN reduces the amount of MACC regardless of the engagement length, surface roughness or material combination.

9.3. Study Limitations

Study limitations have been discussed in detail after each experimental chapter.

9.4. Future Work

When looking to improve the biomechanical properties of articulating implants and thus reduce the generation of wear debris and achieve lifetime longevity one must consider the exciting prospect surface coatings have to offer.

We saw how ceramic heads are less susceptible to corrosion of the taper than CoCrMo heads however the interface is weaker and subject to increased movement within normal loading conditions. The role of ceramic surface coatings and surface treatment such as Oxinium or Diamond Like Carbon (DLC) is a promising prospect that could offer increased resistance against corrosion, whilst allowing the material of the component to retain its biomechanical properties. Further research will be required to establish the efficacy and durability of coatings and surface treatments.

9.5. Closing Statement

From the evidence of this thesis it has been concluded that surgeons wishing to minimise head-neck corrosion should select components with smooth tapers and a large contact surface area. Manufacturers vary significantly in most aspects of taper design and this should be considered during the selection of components. The use of high-offset femoral heads and head diameters of > 36 mm should be avoided. If a large diameter head is required for stability one may avoid the severe corrosion associated with the increased torque by using a large diameter ceramic head. Where possible, increased femoral offset should be conferred by appropriate selection of the stem, rather than the femoral head.

Intra-operatively, components should be assembled dry using a single hammer strike with a high-impact load of > 4 kN.

Bibliography

AFFATAB, S. 2012. *Wear of orthopaedic implants and artificial joints.,* Cambridge, UK, Woohead Publishing

ALKIRE, R. C. & LOTT, S. E. 1985. Initiation of crevice corrosion on grade 304 stainless steel. *In: Extended Abstracts, Spring Meeting-Electrochemical Society,* 85-1 ed., 17.

ALVARADO, J., MALDONADO, R., MARXUACH, J. & OTERO, R. 2003. Biomechanics of hip and knee prostheses. *Applications of Engineering Mechanics in Medicine*.

ANGADJI, A., ROYLE, M., COLLINS, S. N. & SHELTON, J. C. 2009. Influence of cup orientation on the wear performance of metal-on-metal hip replacements. . *Proc Inst Mech Eng H* 223, 449–457.

ARCHARARD, J. F. 1980. Wear theory and mechanism. *In Peterson M.B and Winer, W.O (Eds) Wear control handbook. ,* New York, ASME.

ARTHRITIS RESEARCH UK 2014. *The Musculoskeletal Calculator*.

ASTM 2004. Standard Reference Test Method for Making Potentiostatic and Potentiodynamic Anodic Polarization Measurements. *G5-94.* http://www.astm.org: ASTM International.

ASTM 2009. Standard practice for Fretting Corrosion Testing of Modular Implant Interfaces: Hip Femoral Head-Bore and Cone Taper Interface. *F1875-98.* http://www.astm.org: ASTM International.

ASTM F86-13 2013. Standard Practice for Surface Preparation and Marking of Metallic Surgical Implants. http://www.astm.org: ASTM International.

ASTM F136 2013. Standard Specification for Wrought Titanium-6Aluminum-4Vanadium ELI (Extra Low Interstitial) Alloy for Surgical Implant Applications. http://www.astm.org: ASTM INternational.

ASTM F897 1998. Standard test method for measuring fretting corrosion of osteosynthesis plates and screws. *F897.* http://www.astm.org: ASTM International.

ASTM F1537 2011. Standard Specification for Wrought Cobalt-28Chromium-6Molybdenum Alloys for Surgical Implants. http://www.astm.org: ASTM International.

ASTM F1875-98(2014) 2014. Standard Practice for Fretting Corrosion Testing of Modular Implant Interfaces: Hip Femoral Head- Bore and Cone Taper Interface. http://www.astm.org: ASTM International.

ASTM F2009 2011. Standard Test Method for Determining the Axial Disassembly Force of Taper Connections of Modular Prostheses. http://www.astm.org: ASTM International.

ASTM F2129-08 Standard Test Method for Conducting Cyclic Potentiodynamic Polarization Measurements to Determine the Corrosion Susceptibility of Small Implant Devices. http://www.astm.org: ASTM International.

ASTM G5–94 2004. Standard Reference Test Method for Making Potentiostatic and Potentiodynamic Anodic Polarization Measurements. http://www.astm.org: ASTM International.

AUGUST, A. C., ALDAM, C. H. & PYNSENT, P. B. 1986. THE MCKEE-FARRAR HIP-ARTHROPLASTY - A LONG-TERM STUDY. *Journal of Bone and Joint Surgery-British Volume,* 68, 520-527.

AUSTRALIAN ORTHOPAEDIC ASSOCIATION NATIONAL JOINT REPLACEMENT REGISTRY 2012. *Annual report.*

BARGAR, W. L. 1989. Shape the Implant to the Patient A Rationale for the Use of Custom-Fit Cementless Total Hip Implants. *Clin Orthop Relat Res.,* 249**,** 73-78.

BARRACK, L. R., BURKE, D. W., COOK, S. D., SKINNER, H. B. & HARRIS, W. H. 1993. Complications related to modularity of total hip components. *J Bone Joint Surg Br* 75B**,** 688–692.

BARRACK, R. L. 1994 Modularity of prosthetic implants. . *J Am Acad Orthop Surg. ,* 2**,** 16-25.

BAUER, T. W., BROWN, S. A. & JIANG, M. 1992. Corrosion in Modular Hip Stems. . *Transactions of the orthopaedic research society.,* 17**,** 354.

BAUER, T. W., CAMPBELL, P. A., HALLERBERG, G. & GROUP., B. W. 2014. How have new bearing surfaces altered the local biological reactions to byproducts of wear and modularity? *Clin Orthop Relat Res* 472**,** 3687-3698.

BEAULE, P. E., KIM, P. R., HAMDI, A. & FAZEKAS, A. 2011. A prospective metal ion study of large-head metal-on-metal bearings: a matched-pair analysis of hip resurfacing versus total hip replacement. *Orthop Clin North Am* 42**,** 251-257.

BERRY, D. J., HARMSEN, W. S., CABANELA, M. E. & MORREY, B. F. 2002. Twenty-five-year survivorship of two thousand consecutive primary Charnley total hip replacements: factors affecting survivorship of acetabular and femoral components. *J Bone Joint Surg Am***,** 171-7.

BESONG, A. A., TIPPER, J. L., INGHAM, E., STONE, M. H., WROBLEWSKI, B. M. & FISHER, J. 1998. Quantitative comparison of wear debris from UHMWPE that has and has not been sterilised by gamma irradiation. *J. Bone Joint Surg.,* 80B**,** 340-344.

BHUSHAN, B. 1999. Definistion and history of tribology,. *Washington DC, LLC.*

BILLS, P. J., RACASAN, R., UNDERWOOD, R. J., CANN, P., SKINNER, S., HART, A. J. & BLUNT, L. 2012. Volumetric wear assessment of retrieved metal-on-metal hip prostheses and the impact of measurement uncertainty. *Wear,* 274**,** 212-219.

BISHOP, N. E., HOTHAN, A. & MORLOCK, M. M. 2013. High Friction Moments in Large hard-on-hard hip replacement bearings in conditions of poor lubrication. . *J Orthop Res* 807-813.

BISHOP, N. E., WALDOW, F. & MORLOCK, M. M. 2008. Friction moments of large metal-on-metal hip joint bearings and other modern designs. *Med. Eng. Phys.,* 30**,** 1057-1064.

BLOOMFIELD, M. R., ERICKSON, J. A., MCCARTHY, J. C., MONT, M. A., MULKEY, P. P., C.L., PIVEC, R. & M.S., A. 2014. Hip pain in the young, active patient: surgical strategies. . *Instr Course Lect,* 63**,** 159-176.

BOEHLER, M., PLENK, H. & SALZER, M. 2000. Alumina ceramic bearings for hip endoprostheses.the austrian experiences. *Clin Orthop,* 379**,** 85-93.

BOLLAND, B., CULLIFORD, D. J., LANGTON, D. J., MILLINGTON, J. P. S., ARDEN, N. K. & LATHAM, J. M. 2011. High failure rates with a large-diameter hybrid metal-on-metal total hip replacement CLINICAL, RADIOLOGICAL AND RETRIEVAL ANALYSIS. *Journal of Bone and Joint Surgery-British Volume,* 93B**,** 608-615.

BOURNE, R. B., BARRACK, R. L., RORABECK, C. H., SALEHI, A. & GOOD, V. 2005. Arthroplasty options for the young patient: Oxinium on cross-linked polyethylene. *Clin Orthop Rel Res,* 441**,** 159-167.

BRIGHAM, R. J. 1992. *Corros. Sci,* 33**,** 799.

BROSSIA, C. S. & KELLY, R. G. 1999. *Corros. Sci.*

BROWN, S. A., ABERA, A., D'ONOFRIO, M. & FLEMMING, C. 1997. Modularity of orthopaedic implants. *STP 1301***,** 189-198.

BROWN, S. A., FLEMMING, C. A. C., KAWALEC, J. S., PLACKO, H. E., VASSAUX, C., MERRITT, K., PAYER, J. H. & KRAAY, M. J. 1995. Fretting corrosion accelerates crevice corrosion of modular hip tapers. *Journal of Applied Biomaterials,* 6**,** 19-26.

BROWN, S. R., DAVIES, W. A., DEHEER, D. H. & SWANSON, A. B. 2002. Long term survival of McKee Farrar total hip prostheses. *Clin Orthop Rel Res,* 402**,** 157-63.

BRUSIC, V. 1972. Oxides and Oxide films. *J.W. Diggle and Marcel Deckker New York* 1**,** 1.

BURSTEIN, G. T. & MATTIN, S. P. 1995. Critical factors in localised corrosion II. *The electrochemical society proceedings series,* 95-15**,** 1.

CAMERON, H. U. 1996. Modularity in Primary Total Hip Arthroplasty. *J. Arthroplasty.,* 11**,** 332–334.

CAMPBELL, P., EBRAMZADEH, E., NELSON, S., TAKAMURA, K., SMET, K. D. & AMSTUTZ, H. C. 2010. Histological Features of Pseudotumor-like Tissues From Metal-on-Metal Hips. *Clin Orthop Relat Res,* 468**,** 2321-2327.

CARLI, A., POLITIS, A., ZUKOR, D., HUK, O. & ANTONIOU, J. 2015. Clinically significant corrosion at the head-neck taper interface in total hip arthroplasty: a systematic review and case series. *Hip Int* 25**,** 7-14.

CHAN, F. W., BOBYN, J. D., MEDLEY, J. B., KRYGER, J. J. & TANZEN, M. 1999a. Wear and lubrication of metal-on-metal hip implants. *clin orthop,* 369**,** 10-24.

CHAN, F. W., BOBYN, J. D., MEDLEY, J. B., KRYGIER, J. J. & TANZER, M. 1999b. Wear and lubrication of metal-on-metal hip implants. *Clin. Orthop. ,* 369**,** 10-24.

CHAO, C. Y., LIN, L. F. & MACDONALD, D. D. 1981. *J. Electrochem. Soc. ,* 128**,** 1187.

CHARNLEY, J. 1970. Total hip replacement by low-friction arthroplasty. *Clin Orthop Relat Res.,* 72**,** 7-21.

CHARNLEY, J. 1979. Low friction arthroplasty of the hip. *Springer-Verlag,* Berlin.

CHEN, A., GUPTE, C., AKHTAR, K., SMITH, P. & COBB, J. 2012. The Global Economic Cost of Osteoarthritis: How the UK Compares. *Arthritis,* 2012**,** 698709.

CHMELL, M. J., RISPLER, D. & POSS, R. 1995. The impact of modularity in total hip arthroplasty. *Clin Orthop* 319**,** 77–84.

COLLIER, J. P., MAYOR, M. B., JENSEN, R. E., SURPRENANT, V. A., SURPRENANT, H. P. & MACNAMAR, J. L. 1992a. Mechanisms of failure of modular prostheses. *Clin Orthop Relat Res.,* 285**,** 129-139.

COLLIER, J. P., SURPRENANT, V. A., JENSEN, R. E., MAYOR, M. B. & SURPRENANT, H. P. 1992b. Corrosion between the components of modular femoral hip prostheses. 74**,** 511-517.

COLLIER, J. P., SURPRENANT, V. A., ROBERT, E. J. & MAYOR, M. B. 1991. Corrosion at the interface of Cobalt-Alloy Heads on Titanium-Alloy Stems. *Clin Orthop Relat Res,* 271**,** 305-12.

COOK, R. B., BOLLAND, B. J., WHARTON, J. A., TILLEY, S., LATHAM, J. M. & WOOD, R. J. 2013. Pseudotumour formation due to tribocorrosion at the taper interface of large diameter metal on polymer modular total hip replacements. *The Journal of bone and joint surgery (Am).* 94**,** 1655–1661.

COOK, S. D., BARRACK, R. L., BAFFES, G. C., CLEMOW, A. J., SEREKIAN, P., DONG, N. & KESTER, M. A. 1994a. Wear and Corrosion of Modular Interfaces in Total Hip Replacements. *Clin Orthop Relat Res,* 298**,** 80-88.

COOK, S. D., BARRACK, R. L. & CLEMOW, A. J. 1994b. corrosion and wear at the modular interface of uncemented femoral stems. *J Bone Joint Surg. Br.,* 76-B**,** 68-72.

COOPER, H. J., DELLA VALLE, C. J., BERGER, R. A., TETREAULT, M., PAPROSKY, W. G., SPORER, S. M. & JACOBS, J. J. 2012. Corrosion at the Head-Neck Taper as a Cause for Adverse Local Tissue Reactions After Total Hip Arthroplasty. *J. Bone Joint Surg. Am.,* 19**,** 1655-1661.

COTTRELL, A. 1995. *An Introduction to Metallurgy,* Cambridge, The Institute of Materials.

CRAIG, B. & POHLMAN, S. L. 1987. Forms of corrosion. *ASM Handbok,* 13**,** 77-45.

CROWNINSHIELD, R. D., MALONEY, W. J., WENTZ, D. H., HUMPHREY, S. M. & BLANCHARD, C. R. 2004 Biomechanics of large femoral heads what they do and don't do. *Clin Orthop Relat Res. ,* 429**,** 102-7.

CUCKLER, J. M., MOORE, K. D., LOMBARDI, A. V. J., MCPHERSON, E. & EMERSON, R. 2004 Large versus small femoral heads in metal-on-metal total hip arthroplasty. *J Arthroplasty,* 19**,** 41-4.

DAVIS 1998. *Metals, Handbook,* United States, ASM International,.

DE HAAN, R., PATTYN, C., GILL, H. S., MURRAY, D. W., CAMPBELL, P. A. & DE SMET, K. 2008. Correlation between inclination of the acetabular component and metal ion levels in metal-on-metal hip resurfacing replacement. *J Bone Joint Surg [Br]* 90**,** 1291–1297.

DONALDSON, F. E., COBURN, J. C. & SIEGEL, K. L. 2014a. Total hip arthroplasty head-neck contact mechan-ics: a stochastic investigation of key parameters. *J Biomech Eng,* 47**,** 1634-1641.

DONALDSON, F. E., COBURN, J. C. & SIEGEL, K. L. 2014b. Total hip arthroplasty head–neck contact mechanics: A stochastic investigation of key parameters. *Journal of Biomechanics,* 47**,** 1634–1641.

DONELL, S. T., DARRAH, C. & NOLAN, J. F. 2010. Early failure of the Ultima metal-on-metal total hip replacement in the presence of normal plain radiographs. *J Bone Joint Surg (Br),* 92-B**,** 1501-1508.

DOORN, P. F., MIRRA, J. M., CAMPBELL, P. A. & AMSTUTZ, H. C. 1996. Tissue reaction to metal on metal total hip prostheses. *Clin Orthop Relat Res.,* 329 Suppl**,** 187-205.

DOWSON, D. 2003. the relationship between steady-state wear rate and theoretical film thickness in Metal on Metal total replacement hip joints. *Procedings of the 29th Leeds-Lyon symposium on Tribology,* 41**,** 273-280.

DOWSON, D., HARDAKER, C., FLETT, M. & ISAAC, G. H. 2004. A hip joint simulator study of the performance of metal-on-metal joints. *The Journal of Arthroplasty,* 19**,** 124-130.

DUFFY, R. K. & SHAFRITZ, A. B. 2011. Bone cement. *The Journal of Hand Surgery,* 36**,** 1086–1088.

DUNSTAN, E., LADON, D., WHITTINGHAM-JONES, P., CARRINGTON, R. & BRIGGS, T. W. 2008. Chromo-somal aberrations in the peripheral blood of patients with metal-on-metal hip bear-ings. . *J Bone Joint Surg (Am),* 90-A.

DYRKACZ, R. M., BRANDT, J. M., OJO, O. A., TURGEON, T. R. & WYSS, U. P. 2013. The influence of head size on corrosion and fretting behaviour at the head-neck interface of artificial hip joints. *J Arthroplasty,* 28**,** 1036-1040.

EKLUND, G. S. 1976. *J. Electrochem. Soc.,* 123**,** 170.

ELKINS, J. M., CALLAGHAN, J. J. & BROWN, T. D. 2014. Stability and trunnion wear potential in large-diameter metal-on-metal total hips: a finite element analysis. . *Clin Orthop Relat Res* 472**,** 529–542.

ENDO, M., BARBOUR, P., BARTON, D. & AL., E. 2001. Comparative wear and wear debris under three different counterface conditions of crosslinked and non-crosslinked ultra high molecular weight polyethylene. *Biomed. Mater. Eng.*

11**,** 23-35.

FISHER, J. & DOWSON, D. 1991. Tribology of total artificial joints. *Proc. Inst. Mech. Eng. J. Eng. Med.,* 205**,** 73-79.

FISHER, J., FIRKINS, P., ATKINSON, J. R., DOWSON, D., KENNEDY, P. D. & SMITH, M. R. 1995. the influence of scratches to metallic counterfaces on the wear of ultra-high molecular weight polyethylene. *Proc. Instn Mech. Engrs, Part H: J. Engineering in Medicine,* 209**,** 263-264.

FLEMING, C., BROWN, S. A. & PAYER, J. H. 1994. Biomaterials mechanical properties. *ASTM international STP 1173*, 156-166.

FONTANNA, M. G. & GREENE, N. D. 1967. Corrosion Engineering. *Mc Graw-Hill, New York*.

FRANKEL, G. S. 1998. Pitting Corrosion of Metals. *J. Electrochem. Soc,* 145, 2186-2198.

FRICKA, K. B., HO, H., PEACE, W. J. & ENGH, C. A. J. 2012. Metal-on-Metal local tissue reaction is associated with corrosion of the head taper junction. *J. Arthroplasty. ,* 27, 26-31.

FRICKER, D. C. & SHIVANATHAN, R. 1990. Fretting corrosionstudies of universal femoralhead prostheses and cone taper spigots. *Biomaterials,* 11, 495-500.

GALVELE, J. 1989. *set,* 21, 221.

GARBUZ, D. S., TANZER, M., V. GREIDANUS, N. V., MASRI, B. A. & DUNCAN, C. P. 2010. The John Charnley Award Metal-on-Metal Hip Resurfacing versus Large-diameter Head Metal-on-Metal Total Hip Arthroplasty. *Clin Orthop Relat Res,* 468, 318-325.

GEETHA, M., SINGH, A. K., ASOKAMANI, R. & GOGIA, A. K. 2009. Ti based biomaterials, the ultimate choice for orthopaedic implants–A review. *Progress in Materials Science,* 54, 397-425.

GILBERT, J. L. 2012. Mechanically assisted corrosion of metalic biomaterials. *Materials for medical devices,* 23.

GILBERT JL & SACHIN, A. M. 2012. *Degradation of implant materials,* New York, Springer Science.

GILBERT, J. L., BUCKLEY, C. A. & JACOBS, J. J. 1993. In vivo corrosion of modular hip prosthesis components in mixed and similar metal combinations. The effect of crevice, stress, motion, and alloy coupling. *J. Biomed Mat Res,* 27, 1533-1544.

GILBERT, J. L., BUCKLEY, C. A., JACOBS, J. J., BERTIN, K. C. & ZERNICH, M. R. 1994. Intergranular corrosion-fatigue failure of cobalt-alloy femoral stems. *J. Bone Joint Surg. Am. ,* 76, 110-115.

GILBERT, J. L., MALI, S., URBAN, R. M., SILVERTON, C. D. & JACOBS, J. J. 2012;. In vivo oxide-induced stress corrosion cracking of Ti-6Al-4V in a neck stem modular taper: emergent behavior in a new mechanism of in vivo corrosion. . *J Biomed Mater Res B Appl Biomater* 100, 584–594.

GILBERT, J. L., MEHTA, M. & PINDER, B. 2009a. Fretting crevice corrosion of stainless steel stem-CoCr femoral head connections: comparisons of materials, initial moisture, and offset length. *J Biomed Mater Res B Appl Biomater,* 88, 162-73.

GILBERT, J. L., MEHTA, M. & PINDER, B. 2009b. In-vitro fretting crevice corrosion of stainless steel-cobalt chrome modular hip stems: effect of material, assembly and offset. *J. Biomed Mater Res,* 88B, 162-173.

GOLDBERG, J. 2004. The electrochemical and mechanical behavior of passivated and TiN/AlN-coated CoCrMo and Ti6Al4V alloys. *Biomaterials,* 25, 851-864.

GOLDBERG, J. R., BUCKLEY, C. A., JACOBS, J. J. & GILBERT, J. L. 1997a. Modularity of orthopaedic implants *ASTM STP 1301 Corrosion testing of modular hip implants* 157-176.

GOLDBERG, J. R. & GILBERT, J. L. 2003. In vitro corrosion testing of modular hip tapers. *Journal of Biomedical Materials Research Part B-Applied Biomaterials,* 64B, 78-93.

GOLDBERG, J. R. & GILBERT, J. L. 2004. The electrochemical and mechanical behaviour of passivated TiN/AIN coated CoCrMo and Ti6Al4V alloys. *Biomaterials,* 25, 851-864.

GOLDBERG, J. R., GILBERT, J. L., JACOBS, J. J., BAUER, T. W., PAPROSKY, W. & LEURGANS, S. 2002. A multicenter retrieval study of the taper interfaces of modular hip prostheses. *Clin Orthop Relat Res,* 401, 149-61.

GOLDBERG, J. R., LAUTENSCHLAGER, E. P. & GILBERT, J. L. 1997b. Electrochemical response of CoCrMo to high speed fraction of its metal oxide using an electrochemical scratch test method. *J. Biomed. Mater. Res.,* 37**,** 421-433.

GREEN, T. R., FISHER, J., STONE, M. H., WROBLEWSKI, B. M. & INGHAM, E. 1998. Polyethylene particles of a critical size are necessary for the induction of cytokines by microphages in vitro. *Biomaterials,* 19**,** 2297-2302.

GRIFFITH, M. J., SEIDENSTEIN, M., WILLIAMS, D. & CHARNLEY, J. 1978. Socket wear in Charnley low friction arthroplasty of the hip. *Clin Orthop Relat Res,* 137.

GUPTA, S., HAWKER, G. A., LAPORTE, A., CROXFORD, R. & COYTE, P. C. 2005. The economic burden of disabling hip and knee osteoarthritis (OA) from the perspective of individuals living with this condition. *Rheumatology (Oxford),* 44**,** 1531-7.

H.H., S. 1984. *Proc. – Int.Congr. Met. Corros,* 2**,** 99.

HADDAD, F. S., THAKRAR, R. R., HART, A. J., SKINNER, J. A., NARGOL, A. V., NOLAN, J. F., GILL, H. S., MURRAY, D. W., BLOM, A. W. & CASE, C. P. 2011. Metal-on-metal bearings: the evidence so far. *J Bone Joint Surg Br.,* 93**,** 572-579.

HALLAB, N. J., MESSINA, C., SKIPOR, A. & JACOBS, J. J. 2004. Differences in the fretting corrosion of metal-metal and ceramic-metal modular junctions of total hip replacements. *Journal of Orthopaedic Research,* 22**,** 250-259.

HART, A. J., BUDDHDEV, P., WINSHIP, P., FARIA, N., POWELL, J. J. & SKINNER, J. A. 2008. Cup inclination angle of greater than 50 degrees increases whole blood concentrations of cobalt and chromium ions after metal-on-metal hip resurfacing. . *Hip Int* 18**,** 212–219.

HART, A. J., MATTHIES, A., HENCKEL, J., ILO, K., SKINNER, J. & NOBLE, P. C. 2012. Understanding why metal-on-metal hip arthroplasties fail: a comparison between patients with well-functioning and revised Birmingham hip arthroplasties. *J Bone Joint Surg [Am]* 94.

HEINEY, J., BATTULA, S., VRABEC, G. A., PARIKH, A., BLICE, R., SCHOENFELD, A. J. & NJUS, G. O. 2009. Impact magnitudes applied by surgeons and their importance when applying the femoral head onto the Morse taper for total hip arthroplasty. *Arch. Orthop. Trauma Surg.,* 129**,** 793-796.

HELSON, J. A. & BREME, H. J. 1998. Metals as Biomaterials. *Wiley*

HENCH, L. L. & WILSON, J. P. Introduction to bioceramics. World Scientific, 1993 Singapore.

HERNIGOU, P., QUEINNEC, S. & LACHANIETTE, C. 2013. One hundred and fifty years of history of the Morse taper: from Stephen A Morse in 1864 to complications related to modularity in hip arthroplasty. *Int Orthop,* 37**,** 2081-2088.

HIGGS, B., HANZLIK, J. A., MACDONALD, D. W., GILBERT, J. L., RIMNAC, C. M. & KURTZ, S. M. 2013. Is Increased Modularity Associated With Increased Fretting and Corrosion Damage inMetal-On-Metal Total Hip Arthroplasty Devices? A Retrieval Study. *Journal of Arthroplasty,* 28**,** 2-6.

HIGUCHI, F., INOUE, A. & SEMLITSCH, M. 1997. Metal-on-metal CoCrMo McKee-Farrar total hip arthroplasty: Characteristics from a long-term follow-up study. *Archives of Orthopaedic and Trauma Surgery,* 116**,** 121-124.

HOUDE, M. & SCHREIBER, H. P. 1992. *J Appl Polym Sci,* 46**,** 2049.

HOWIE, D. W., MIDDLETON, R. G. & COSTI, K. 1998. Loosening of matt and polished cemented femoral stems. *J Bone Joint Surg Br. ,* 80**,** 573-576.

HOZACK, W. J., MESA, J. J. & ROTHMAN, R. H. 1996. Head/neck modularity for total hip arthroplasty. Is it necessary? *J. Arthroplasty* 11**,** 397–400.

HRYNIEWICZ, T., ROKOSZ, K. & ROKICKI, R. 2008. Electrochemical and XPS studies of AISI 316L stainless steel after electropolishing in a magnetic field. . *Corrosion Science* 50**,** 2676-81.

HUBER, M., REINISCH, G. & TRETTENHAM, G. 2009. Presence of corrosion products and hypersensitivity associated reactions in periprosthetic tissue after aseptic loosening of total hip replacements with metal bearing surfaces. *Acta Biomater,* 5.

INGHAM, E. & FISHER, J. 1995. preliminary study of the effect of aging following irradiation on the wear of UHMWPE. *J. Arthroplasty.,* 10**,** 689-692.

ISO/CD 4287 1997. Geometrical Product Specifications (GPS) -- Surface texture: Profile method -- Terms, definitions and surface texture parameters. http://www.iso.org: ISO.

J.W. SCHULTZE, J. W. & LOHRENGEL, M. M. 2000. *Electrochim. Acta.,* 45**,** 2499.

J.WILLIAMS, J. 1994. Engineering Tribology, 2nd ed. *Cambridge University Press*.

JACOBS, J. J., GILBERT, J. L. & URBAN, R. M. 1998. Corrosion of metal orthopaedic implants. *Journal of Bone and Joint Surgery-American Volume,* 80A**,** 268-282.

JACOBS, J. J., URBAN, R. M., GILBERT, J. L., SKIPOR, A. K., BLACK, J., JASTY, M. & GALANTE, J. O. 1995. Local and distant products from modularity. . *Clin. Orthop. Relat. Res. ,* 319**,** 94-95.

JACOBS, J. J. S. A. K. 1998. Metal release in patients who have had a primary total hip arthroplasty. a prospective, controlled, longitudinal study. *jbjs (br)*.

JACOBSSON, S.-A., DJERF, K. & WAHLSTR√∂M, O. 1996. 20-Year Results of McKee-Farrar Versus Charnley Prosthesis. *Clinical Orthopaedics and Related Research,* 329**,** S60-S68.

JIN, Z., DOWSON, D. & FISHER, J. 1996. Analysis of fluid film lubrication in artificial hip joint replacements with surfaces of high elastic modulus. *Proc. Instn Mech. Engrs, Part H: J. Engineering in Medicine,* 211**,** 247-256.

JONES, D. L., VIGNA, F. & BARRACK, R. L. 2001. The use of modularity in revision total hip replacement. *Am J Orthop (Belle Mead NJ),* 30**,** 297-302.

KHAN, M. A., WILLIAMS, R. L. & WILLIAMS, D. F. 1996. In-vitro corrosion and wear of titanium alloys in the biological environment. *Biomaterials,* 17**,** 2117-2126.

KOCIJA, A., MILOSEV, I. & PIHLAR, B. 2004. Colbalt-based alloys for orthopeadic applications studied by electrochemical and XPS analysis. . *Journal of Materials Science: Materials in Medicine,* 15**,** 643-50.

KOP, A. M., KEOGH, C. & SWARTS, E. 2012. Proximal Component Modularity in THA-At What Cost?: An Implant Retrieval Study. *Clinical Orthopaedics and Related Research,* 470**,** 1885-1894.

KOP, A. M. & SWARTS, E. 2009. Corrosion of a Hip Stem With a Modular Neck Taper Junction A Retrieval Study of 16 Cases. *Journal of Arthroplasty,* 24**,** 1019-1023.

KOTZAR, G. M., DAVY, D. T., BERILLA, J. & GOLDBERG, V. M. 1995. Torsional Loads in the Early Postoperative Period Following Total Hip Replacement. *Journal of Orthopaedic Research,* 13**,** 945-955.

KOWALCZYK, P. 2001. Design Optimization of Cementless Femoral Hip Prostheses Using Finite Element Analysis. *J. of Biomechanical Engineering,* 123**,** 396.

KRUGER, J. 1988. *Inter. Mater. Res.,* 33**,** 113.

KRUSHELL, R. J., BURKE, D. W. & HARRIS, W. H. 1991. Range of motion in contemporary total hip arthroplasty. The impact of modular head–neck components. *J. Arthroplasty* 6.

KURTZ, S., MOWAT, F., ONG, K., CHAN, N. & LAU, E. 2005. Prevalence of primary and revision total hip and knee arthroplasty in the United States from 1990 through 2002. *Journal of Bone and Joint Surgery; American volume,* 87**,** 1487-1497.

KURTZ, S., ONG, K., LAU, E., MOWAT, F. & HALPERN, M. 2007. Projections of primary and revision hip and knee arthroplasty in the United States from 2005 to 2030. *J Bone Joint Surg Am,* 89**,** 780-5.

KURTZ, S. M., KOCAGO˙Z, S. B., HANZLIK, J. A., UNDERWOOD, R. J., GILBERT, J. L., MACDONALD, D. W., LEE, G., MONT, M. A., MATTHEW, J. & RIMNAC, C. M. 2013. Do ceramic femoral heads reduce taper fretting corrosion in hip arthroplasty? a retrieval study. *Clin Orthop Relat Res,* 471**,** 3270-86.

KWON, Y. M., OSTLERE, S. J., MCLARDY-SMITH, P., ATHANASOU, N. A., GILL, H. S. & MURRAY, D. W. 2011. "Asymptomatic" Pseudotumors After Metal-on-Metal Hip Resurfacing Arthroplasty. *Journal of Arthroplasty,* 26**,** 511-518.

LANGTON, D., SIDAGINAMALE, R., LORD, J., JOYCE, T., NATU, S. & NARGOL, A. 2013. Metal debris release from taper junc-tions appears to have a greater clinical impact than debris released from metal on metal bearing surfaces. *Bone Joint J,* 95-B(Supp1).

LANGTON, D. J., JAMESON, S. S., JOYCE, T. J., GANDHI, J. N., SIDAGINAMALE, R., MEREDDY, P., LORD, J. & NARGOL, A. V. F. 2011. Accelerating failure rate of the ASR total hip replacement. *Journal of Bone and Joint Surgery-British Volume,* 93B**,** 1011-1016.

LANGTON, D. J., JAMESON, S. S., JOYCE, T. J., HALLAB, N. J., NATU, S. & NARGOL, A. V. F. 2010. Early failure of metal-on-metal bearings in hip resurfacing and large-diameter total hip replacement A CONSEQUENCE OF EXCESS WEAR. *Journal of Bone and Joint Surgery-British Volume,* 92B**,** 38-46.

LANGTON, D. J., SIDAGINAMALE, R., LORD, J. K., NARGOL, A. V. F. & JOYCE, T. J. 2012. Taper junction failure in large-diameter metal-on-metal bearings. *Bone and Joint Research,* 1**,** 56-63.

LAVERNIA, C., BAERGA, L., BARRACK, R. L., TOZAKOGLOU, E., COOK, S. D., LATA, L. & ROSSI, M. D. 2009. The Effects of Blood and Fat on Morse Taper Disassembly Forces. *J. Bone Joint Surg. Am* 38**,** 187-190.

LAVIGNE, M., BELZILE, E. L., ROY, A., MORIN, F., AMZICA, T. & VENDITTOLI, P.-A. 2011. Comparison of Whole-Blood Metal Ion Levels in Four Types of Metal-on-Metal Large-Diameter Femoral Head Total Hip Arthroplasty: The Potential Influence of the Adapter Sleeve. *J Bone Joint Surg Am.,* 93-A**,** 128-136.

LAYCOCK, N. J., STEWART, J. & NEWMAN, R. C. 1997. The initiation of crevice corrosion in stainless steels. *Corrosion Science* 39**,** 1791-809.

LEARMONTH, I. D. 2000. Clinical implications of component modularity in total hip replacement. *In:* LEARMONTH, I. D. (ed.) *Interfaces in Total hip arthroplasty.* Springer London.

LEARMONTH, I. D., YOUNG, C. & RORABECK, C. 2007. The operation of the century:total hip replacement. *Lancet,* 370**,** 1508-1519.

LEVINE, D. L. & STAEHLE, R. W. 1977. Crevice corrosion in orthopedic implant metals. *Journal of biomedical materials research,* 11**,** 553-561.

LIEBERMAN, J. R., RIMNAC, C. M., GARVIN, K. L., KLEIN, R. W. & SALVATI, E. A. 1994. An analysis of the head-neck taper interface in retrieved hip prostheses. *Clin Orthop Relat Res. ,* 300**,** 162-167.

LINDGREEN, J. U., BRISMAR, B. H. & WIKSTROM, A. C. 2011. Adverse reaction to metal release from a modular metal-on-polyethylene hip prosthesis. *J Bone Joint Surg [Br]* 93**,** 1427-1430.

MAHYUDIN, F., WIDHIYANTO, L. & HERMAWAN, H. 2016. Biomaterials in Orthopaedics. *In:* MAHYUDIN, F. & HERMAWAN, H. (eds.) *Biomaterials and medical devices.* Switzerland: Springer International Publishing.

MALONEY, W. J. & SMITH, R. L. 1996. Periprosthetic osteolysis in total hip arthroplasty: the role of particulate wear debris. . *Instr Course Lect* 45**,** 171.

MALVIYA, A. & HOLLAND, J. P. 2009. Pseudotumours associated with metal-on-metal hip resurfacing: 10-year Newcastle experience. *Acta Orthop Belg. ,* 75**,** 477-483.

MALVIYA, A., RAMASKANDHAN, J. R., BOWMAN, R., KOMETA, S., HASHMI, M., LINGARD, E. & HOLLAND, J. P. 2011. What advantage is there to be gained using large modular metal-on-metal bearings in routine primary hip replacement? A PRELIMINARY REPORT OF A PROSPECTIVE RANDOMISED CONTROLLED TRIAL. *Journal of Bone and Joint Surgery-British Volume,* 93B**,** 1602-1609.

MANKTELOW, A. R. J., GEHRKE, T. & HADDAD, F. S. 2017. Hip surgery - state of the art. *Bone Joint J,* 99-B**,** 1-2.

MAO, X., WONG, A. A. & CRAWFORD, R. W. 2011. Cobalt toxicity--an emerging clinical problem in patients with metal-on-metal hip prostheses? . *Med J Aust* 194**,** 649-651.

MARLOWE, D. E., PARR, J. E. & M.B., M. 1997. Modularity of orthopaedic Implants. *West Conshohocken, PA: American Society for Testing and Materials***,** 189–198.

MATHEISEN, E. B., LINDGREN, J. U., BLOMGREN, G. G. & REINHOLT, F. P. 1991. Corrosion of modular hip prostheses. *J. Bone Joint Surg. Br,* 73-B**,** 569-575.

MATTHIES, A., UNDERWOOD, R., CANN, P., ILO, K., NAWAZ, Z., SKINNER, J. & HART, A. J. 2011. Retrieval analysis of 240 metal-on-metal hip components, comparing modular total hip replacement with hip resurfacing. *J Bone Joint Surg [Br],* 93**,** 307-314.

MATTHIES, A. K., RACASAN, R., PAUL BILLS, P., LIAM BLUNT, L., CRO, S., PANAGIOTIDOU, A., BLUNN, G., SKINNER, J. & HART, A. J. 2013. Material Loss at the Taper Junction of Retrieved Large Head Metal-on-Metal Total Hip Replacements. *J Orthop Res,* 31**,** 1677-85.

MATTHIES, A. K., SKINNER, J. A., OSMANI, H., HENCKEL, J. & HART, A. J. 2012. Pseudotumors are common in well-positioned low-wearing metal-on- metal hips. *Clin Orthop Relat Res* 470**,** 1895–1906.

MCCAFFERTY, E. Introduction to corrosion science. *Spinger science + Bussiness media LLC New York USA,* 1st Ed.

MCCARTHY, J. C., BONO, J. V. & O'DONNELL, P. J. 1997. Custom and modular components in primary total hip replacement. *Clin Orthop Relat Res. ,* 344**,** 162-171.

MCKELLOP, H., PARK, S. H., CHIESA, R., DOORN, P., LU, B., NORMAND, P., GRIGORIS, P. & AMSTUTZ, H. 1996. in vivo wear of metal-on-metal hip prostheses during two decades of use. *Clin Orthop,* 329S**,** 128-140.

MCMINN, D., TREACY, R., LIN, K. & PYNSENT, P. 1996. Metal-on-metal surface replacement of the hip. Experience of the McMinn prosthesis. *Clin Orthop Rel Res,* 329S**,** 89-98.

MERTL, P., BOUGHEBRI, O., HAVET, E., TRICLOT, P., LARDANCHET, J. F. & GABRION, A. 2010. Large diameter head metal-on-metal bearings total hip arthroplasty: Preliminary results. *Orthopaedics & Traumatology: Surgery & Research,* 96**,** 14-20.

MEYER, H., MUELLER, T., GOLDAU, G., CHAMAON, K., RUETSCHI, M. & LOHMANN, C. H. 2012. Corrosion at the Cone/Taper Interface Leads to Failure of Large-diameter Metal-on-metal Total Hip Arthroplasties. *Clin Orthop and Relat Res. ,* 470**,** 3101–3108.

MHRA. 2012. *Medical Device Alert* [Online].

MILLER, P. D. & HOLLADAY, J. W. 1958. Friction and wear properties of titanium. *Wear,* 2**,** 133-140.

MILOSÍEV, I. & REMSKAR, M. 2009. Production of nanosized metal wear debris formed by tribochemical reaction as confirmed by high-resolution TEM and XPS analyses. . *Journal of Biomedical Materials Research: Part A,* 91A**,** 1100-10.

MITTELMEIER, H. 1984. Ceramic prosthetic devices. *Hip Int***,** 146-160.

MORLOCK, M. M., BISHOP, N. & ZUSTIN, J. 2008. Modes of imlplant failure after hip resurfacing: morphological and wear analysis of 267 retrieval specimens. . *J Bone Joint Surg (Am),* 90-A**,** 89-95.

MROCZKOWSKI, M. L., HERTZLER, J. S., HUMPHREY, S. M., JOHNSON, T. & BLANCHARD, C. R. 2006. Effect of impact assembly on the fretting corrosion of modular hip tapers. *Journal of Orthopaedic Research,* 24**,** 271-279.

MUNIR, S., WALTER, W. L. & WALSH, W. R. 2015. Variations in the trunnion surface topography between different commercially available hip replacement stems. . *J Orthop Res* 33**,** 98-105.

NAG, S., SAMUEL, S., PUTHUCODE, A. & BANERJEE, R. 2009. Characterization of novel borides in Ti–Nb–Zr–Ta + 2B metal-matrix composites. *Materials Characterization,* 60**,** 106-113.

NASSIF, N. A., NAWABI, D. H., STONER, K., ELPERS, M., WRIGHT, T. & PADGETT, D. E. 2014. Taper Design Affects Failure of Large-head Metal-on-metal Total Hip Replacements. *Clin Orthop Relat Res,* 472**,** 564-571.

NASSUT, R., WIMMER, M. A., SCHNEIDER, E. & MORLOCK, M. M. 2003. The influence of resting periods on friction in the artificial hip. . *Clin Orthop Relat Res* 407**,** 127–138.

NASSUTT, R., MOLLENHAUER, I., KLINGBEIL, K., HENNIG, O. & GRUNDEI, H. 2006. Relevance of the insertion force for the taper lock reliability of hip stem and ceramic femoral head. . *Biomed Tech. (Berl),* 52**,** 103-109.

NATIONAL JOINT REGISTRY 2012. *NJR 9th Annual Report*.

NATIONAL JOINT REGISTRY 2013. NJR 10th Annual Report.

NAVARRO, M., MICHIARDI, A., CASTAÑO, O. & PLANELL, J. A. 2008. Biomaterials in orthopaedics. *J R Soc Interface.,* 5**,** 1137–1158.

NYRÉN, O., MCLAUGHLIN, J. K., GRIDLEY, G., EKBOM, A., JOHNELL, O., FRAUMENI, J. F. & ADAMI, H. O. 1995. Cancer risk after hip replacement with metal implants: a population-based cohort study in Sweden. *J Natl Cancer Inst,* 87**,** 28-33.

OLDFEILD, J. W. & SUTTTON, W. H. 1979. New Technique for Predicting the Performance of Stainless Steels in Sea Water and other Chloride-containing Environments. . *British Corrosion Journal* 15.

OLDFIELD, J. W. & SUTTON, W. H. 1978. Crevice Corrosion of Stainless Steel I-A Mathematical Model. *Brit. Corrosion journal* 13**,** 13-22.

OMBARDI, A. V., MALLORY, T., VAUGHAN, B. K. & DROUILLARD, P. 1989. Aseptic Loosening in total hip arthroplasty secondary to osteolysis induced by wear debris from titanium-alloy modular femoral heads. *J. Bone Joint Surg[Am]* 71-A.

OSMAN, K., PANAGIOTIDOU, A., KHAN, M., BLUNN, G. & HADDAD, F. S. 2016. Corrosion at the head-neck interface of current designs of modular femoral components. *Bone Joint J* 98-B.

PANAGIOTIDOU, A., MESWANIA, J., HUA, J., MUIRHEAD-ALLWOOD, S., HART, A. & BLUNN, G. 2013. Enhanced Wear and Corrosion in Modular Tapers in Total Hip Replacement Is Associated with the Contact Area and Surface Topography. *J Orthop Res,* 12**,** 2032-2039.

PATEL, N. R. & GOHIL, P. P. 2012. A review on biomaterials: Scope, applications & human anatomy significance. *International Journal of Emerging Technology and Advanced Engineering,* 2**,** 91-101.

PENNOCK, A. T., SCHMIDT, A. H. & BOURGEAULT, C. A. 2002. Morse-Type Tapers Factors That May Influence Taper Strength During Total Hip Arthroplasty. *The Journal of Arthroplasty,* 17**,** 773.

PICKERING, H. W. 1989. The significance of the local electrode potential within pits, crevices and cracks. . *Corrosion Science* 29**,** 325-341.

PICKERING, H. W. 1990. Advances in Localized Corrosion. *NACE, Houston, TX*

PICKERING, H. W. 1995. The role of electrode potential distribution in corrosion processes. . *Mat. Sci. and Eng part A,* 198**,** 213-223.

PIVEC, R., JOHNSON, A. J., MEARS, S. C. & MONT, M. A. 2012. Hip arthroplasty. *The Lancet,* 380**,** 1768-1777.

POLYZOIS, I., NIKOLOPOULOS, D., MICHOS, I., PATSOURIS, E. & THEOCHARIS, S. 2012. Local and systemic toxicity of nanoscale debris particles in total hip arthroplasty. *J Appl Toxicol. ,* 32**,** 254-269.

PORTER, D. A., URBAN, R. M., JACOBS, J. J., GILBERT, J. L., RODRIGUEZ, J. A. & COOPER, H. J. 2014. Modern trunnions are more flexible: a mechanical analysis of THA taper designs. *Clin Orthop Relat Res* 472**,** 3963–3970.

RAMSDEN, J. J., ALLEN, D. M., STEPHENSON, D. J., ALCOCK, J. R., PEGGS, G. N., FULLER, G. & GOCH, G. 2007. The Design and Manufacture of Biomedical Surfaces. *CIRP Annals - Manufacturing Technology,* 56**,** 687-711.

RASQUINHA, V. J., RANAWAT, C. S. & WEISKOPF, J. 2006. Serum metal levels and bearing surfaces in total hip arthroplasty. . 21**,** 47-52.

REHMER, A., BISHOP, N. E. & MORLOCK, M. M. 2012. Influence of assembly procedure and material combination on the strength of the taper connection at the head-neck junction of modular hip endoprostheses. *Clinical Biomechanics,* 27**,** 77-83.

REVIE, R. W. 2000. Thermodynamics:corrosion tendancy and electrode potentials. In: Corrosion and corrosion control. *John Wiley and Sons, ,* 1ed**,** 22-66.

RING, P. A. 1989. *Press-fit prosthesis: clinical experience. In: Osteoarthritis and the young adult hip - options for surgical management*, Churchill-Livingstone.

RODRIGUES, D. C., URBAN, R. M., JACOBS, J. J. & GILBERT, J. L. 2009. In vivo severe corrosion and hydrogen embrittlement of retrieved modular body titanium alloy hip-implants. . *J Biomed Mater Res B Appl Biomater* 88**,** 206-219.

ROWE, C. N. 1980. Lubricated Wear. In: Wear Control Handbook. *Peterson, M.B. and W.O. Wine (Eds.). ASME., New York*.

SAITO, S., SHII, T., MORI, S., HOSAKA, K., OOTAKI, M. & TOKUHASHI, Y. 2010. Long-term results of metasul metal-on-metal total hip arthroplasty. *Orthopaedics,* 33.

SATO, N. 1971. *Electrochim. Acta.,* 16**,** 1683.

SAWATARI, C. & MASTUO, M. 1987. *Polym J,* 19**,** 1365.

SCHMIDT, A. H., LOCH, D. A., BECHTOLD, J. E. & KYLE, R. F. 1997. Assessing morse taper function: The relationship between impaction force, disassembly force and design variables. . ASTM Special Technical Publication: American Society for Testing and Materials.

SCHMIDT, M., WEBER, H. & SCHON, R. 1996. Cobalt chromium molybdenum metal combination for modular hip prostheses. *Clin Orthop,* 329S**,** 35-47.

SCHOLES, S. C., GREEN, S. M. & UNSWORTH, A. 2001. The wear on metal-on-metal total hip prostheses measured in a hip simulator. *Proc. Instn Mech Engrs, H: J. Engineering in Medicine,* 215**,** 523-530.

SCHOLES, S. C. & UNSWORTH, A. 2000. Comparison of friction and lubrication of different hip prostheses. *Proc Inst Mech Eng H,* 214**,** 49-57.

SCULLY, J. R. & TAYLOR, W. D. 1987. Laboratory Testing, ASM Handbook. *Corrosion,* 13**,** 212-228.

SEMLITSCH, M., STREICHER, R. M. & WEBER, H. 1989. The wear behavior of capsules and heads of CoCrMo casts in long-term implanted all-metal hip prostheses. *Orthopade,* 18**,** 377-381.

SHAREEF, N. & LEVINE, D. 1996. Effect of manufacturing tolerances on the micromotion at the Morse taper interface in modular hip implants using the finite element technique. *Biomaterials,* 17**,** 623–630.

SHAW, B. A., MORAN, P. J. & GARTLAND, P. O. 1991. *Corros. Sci,,* 32**,** 707.

SKINNER, J., GIE, G. & KAY, P. 2012. Metal on Metal Hip Replacement and Hip Resurfacing Arthroplasty: what does the MHRA Medical Device Alert mean? http://www.britishhipsociety.com/pdfs/ BHS_MOM_THR.pdf. *British Orthopaedic Association*.

SMITH, A. J., DIEPPE, P., PORTER, M. & BLOM, A. W. 2012a. Risk of cancer in first seven years after metal-on-metal hip replacement compared with other bearings and general population: linkage study between the National Joint Registry of England and Wales and hospital episode statistics. . *BMJ,* 344**,** 2383.

SMITH, A. J., DIEPPE, P., VERNON, K., PORTER, M. & ASHLEY, W. B. 2012b. Failure rates of stemmed metal-on-metal hip replacements: analysis of data from the National Joint Registry of Englandand Wales. *Lancet,* 379**,** 1199-1204.

SMITH, J., LEE, D., BALI, K., RAILTON, P., KINNIBURGH, D., FARIS, P., MARSHALL, D., BURKART, B. & POWELL, J. 2014. Does bearing size influence metal ion levels in large-head metal-on-metal total hip arthroplasty? A comparison of three total hip systems. *J Orthop Surg Res* 9.

SOCHART, D. H. & PORTER, M. L. 1997. The long-term results of Charnley low-friction arthroplasty in young patients who have congenital dislocation, degenerative osteoarthrosis, or rheumatoid arthritis. *J Bone Joint Surg Am,* 79**,** 1599-617.

SRIDHAR, N. & DUNN, J. 1997. *Electrochem. Soc., ,* 140**,** 643.

STANSBURY, E. & BUCHANAN, R. 2000. ASM International. *Fundamentals of electrochemical corrosion, Ohio*.

SUTULA, L. C., COLLIER, J. P., SAUM, K. A., CURRIER, B. H. & AL, E. 1995a. Impact of gamma sterilization on clinical performance of polyethylene in the hip. *Clin. Orthop.,* 319**,** 28-40.

SUTULA, L. C., COLLIER, J. P., SAUM, K. A., CURRIER, B. H., CURRIER, J. H., SANFORD, W. M., MAYOR, M. B. & SURPRENANT, B. A. 1995b. Impact of Gamma Sterilization on Clinical Performance of Polyethylene in the Hip *Clin Orthop,* 319**,** 28-40.

TALMO, C. T., SHARP, K. G. & MALINOWSKA, M. 2014. Spontaneous modular femoral head dissociation complicating total hip arthroplasty. . *Orthopedics,* 37**,** 592–595.

TAMBOLI, S. M., MHASKE, S. T. & KALE, D. D. 2004. Crosslinked polyethylene. *Indian Journal of Chemical Technology,* 11**,** 853-864.

UHLIG, H. H. 1950. Adsorbed and reaction-product films on metals. *J. Electrochem. Soc.,* 97**,** 215.

URBAN, R. B., JACOBS, J. J., GILBERT, J. L., RICE, S. B., JASTY, M., BRAGDON, C. R. & GALANTE, J. O. 1997. Characterisation of solid products of corrosion generated by modular-head femoral stems of different designs and materials. *Modularity of orthopaedic implants ASTM STP* 1301**,** 33-44.

URBAN, R. M., JACOBS, J. J., GILBERT, J. L. & GALANTE, J. O. 1994. Migration of corrosion products from modular hip prostheses. Particle microanalysis and histopathological findings. *J Bone Joint Surg (Am),* 76**,** 1345-13559.

URBAN, R. M., JACOBS, J. J., TOMLINSON, M. J., GAVRILOVIC, J., BLACK, J. & PEOC'H, M. 2000. Dissemination of wear particles to the liver, spleen, and abdominal lymph nodes of patients with hip or knee replacement. . *J Bone Joint Surg (Am),* 82-A**,** 457–476.

VENUGOPALAN, R., WEIMER, J. J., GEORGE, M. A. & LUCAS, L. C. 2000. *Biomaterials,* 21**,** 1669-1677.

VISURI, T. 1987. Long-term results and survivorship of the McKee-Farrar total hip prosthesis. *Archives of Orthopaedic and Trauma Surgery,* 106**,** 368-374.

WALKER, P. S. & GOLD, B. L. 1971. The tribology (friction, lubrication and wear) of all-metal artifisial hip joints. *Wear,* 17**,** 285-299.

WALKER, P. S., SALVATI, E. & HOTZLER, R. K. 1974. WEAR ON REMOVED MCKEE-FARRAR TOTAL HIP PROSTHESES. *Journal of Bone and Joint Surgery-American Volume,* A 56**,** 92-100.

WATERHOUSE, R. B. 1972. Fretting Corrosion: International series of monographs on materials science and technology. *Pergamon press*.

WEBB, J. C. & SPENCER, R. F. 2007. The role of polymethylmethacrylate bone cement in modern orthopaedic surgery. *Journal of Bone and Joint Surgery British,* 89**,** 851-857.

WEBER, B. G., FREY, O., SEMLITSCH, M. & DÖRRE, E. 1977. Assorted aluminium-oxide ceramic heads for prostheses of the hip-joint. A preliminary communication. *Zeitschrift fur Orthopadie und ihre Grenzgebiete,* 115**,** 305–309.

WHITEHOUSE, M. R., ENDO, M., ZACHARA, S., NIELSEN, T. O., GREIDANUS, N. V., MASRI, B. A., GARBUZ, D. S. & DUNCAN, C. P. 2015. Adverse local tissue reactions in metal-on-polyethylene total hip arthroplasty due to trunnion corrosion: the risk of misdiagnosis. . *Bone Joint J,* 87-B**,** 1024-30.

WILLERT, H., BROBACK, L., BUCHHORN, G., P.JEMSEN, P., KOSTER, G., LANG, I., OCHSNER, P. & SCHENK, R. 1996a. Crevice corrosion of cemented titanium alloy stems in total hipreplacements. *Clin Orthop Relat Res* 333**,** 333-351.

WILLERT, H. G., BUCHHORN, G. H., GOBEL, D., KOSTER, G., SCHNAFFNER, S., SCHENK, R. & SEMLITSCH, M. 1996b. Wear behaviour and histopathology of classic metal-on-metal hip endoprostheses. *Clin Ortop Rel Res,* 329 Suppl**,** 187-205.

WILLERT, H. G. & SEMLITSCH, M. 1977. Reactions of the Articular Capsule to Wear Products of Artificial Joint Prostheses. *J. Biomed. Mat. Res. Part B-Appl. Biomat,* 11**,** 157-164.

WITT, F., BOSKER, B. H., BISHOP, N. E., ETTEMA, H. B., VERHEYEN, C. C. & MORLOCK, M. M. 2014. The relation between titanium taper corrosion and cobalt-chromium bearing wear in large-head metal-on-metal total hip prostheses: a retrieval study. *J Bone Joint Surg Am,* 96**,** e157.

WRIGHT, T. M. & MAHER, S. A. 2008. *Orthopaedic basic science, foundations of clinical practice.*, American Academy of Orthopaedic Surgeons.

WROBLEWSKI, B. M., SINEY, P. D. & FLEMING, P. A. 2009. The principle of low frictional torque in the Charnley total hip replacement. *Journal of Bone and Joint Surgery-British Volume,* 91B**,** 855-858.

Y. YAN, Y., NEVILLE, A. & DOWSON, D. 2007. Biotribocorrosion of CoCrMo orthopaedic implant materials: assessing the formation and effect of the biofilm. . *Tribology International* 40**,** 1492-9.

YAN, Y., NEVILLE, A. & DOWSON, D. 2007. Tribo-corrosion properties of cobalt-based medical implant alloys in simulated biological environments. *wear,* 263**,** 1105-1111.

YANOSO-SCHOLL, L., PIERRE, D., LEE, R., AMBROSI, M., SWAMINATHAN, V., FAIZAN, A. & TENHUISEN, K. 2017. Influence of impaction force and support compliance on initial taper stability. . *Bone Joint J,* 99-B**,** 106.

YERBY, S. A., TAYLOR, J. K., PARK, J. & SHACKELFORD, J. F. 1996. Corrosion at the interface. A possible solution to cobalt-chrome heads on titanium alloy stems. *The Journal of arthroplasty,* 11**,** 157-162.

YU, S., O'GRADY, W. E., RAMAKER, D. E. & NATISHAN, P. M. 2000. *J Electrochem. Soc.* , 147**,** 2952.

ZHU, M. & WINDLER, M. 2003. Stainless steel for medical and surgical applications. *STP 1438 ASTM International***,** 235-248.

ZIAEE, H., DANIEL, J., DATTA, A. K., BLUNT, S. & MCMINN, D. J. W. 2007. Transplacental transfer of cobalt and chromium in patients with metal-on-metal hip arthroplasty: a controlled study. *J Bone Joint Surg (Br),* 89-B**,** 301-305.

ZIJLSTRA, W. P., VAN DEN AKKER-SCHEEK, I., ZEE, M. J. M. & VAN RAAY, J. J. 2011. No clinical difference between large metal-on-metal total hip arthroplasty and 28-mm-head total hip arthroplasty? *Int Orthop* 35**,** 1771–1776.

ZWEYMÜLLER, K., ZHUBER, K. & LOCKE, H. 1977. A metal-ceramic composite endoprosthesis for total hip replacement *Wiener klinische Wochenschrift,* 89**,** 548–551.

Appendix Publications Associated with this Thesis

Matthies AK, Racasan R, Bills P, Cro S, Panagiotidou A, Blunn G, Skinner J, Hart A. Material loss at the taper junction of retrieved large head metal-on-metal total hip replacements. *J Orthop Res 2013;*N*ov;31(11):1677-85.*

Panagiotidou A, Meswania J, Hua J, Muirhead-Allwood S, Hart A, Blunn G. Enhanced wear and corrosion in modular tapers in total hip replacement is associated with the contact area and surface topography. *J Orthop Res 2013 Dec;31(12):2032-9.*

Whittaker R, Hexter A, Hothi H, Panagiotidou A, Bills P, Skinner J, Hart A. Component size mismatch of metal on metal hip arthroplasty: an avoidable event. *J Arthroplasty 2014 Aug;29(8):1629-34.*

Panagiotidou A, Meswania J, Osman K, Bolland B, Latham J, Skinner J, Haddad FS, Hart A, Blunn G. The effect of torque and frictional bending moment on corrosion at the taper interface: an in-vitro study. *Bone Joint J 2015 Apr;97-B(4):463-72.*

Osman K, Panagiotidou A, Khan M, Blunn G, Haddad FS. Corrosion at the head-neck interface of current designs of modular femoral components: essential questions and answers relating to corrosion in modular head-neck junctions. *Bone Joint J 2016 May;98-B(5):579-84.*

Panagiotidou A, Cobb T, Meswania J, Skinner J, Hart A, Haddad FS, Blunn G. Effect of impact assembly on the interface deformation and fretting corrosion of modular hip tapers: an in-vitro study. *J Orthop Res 2017 May.*